“Solid Phase Synthesis of Thiazole Orange Labeled Peptide Nucleic Acids for Homogeneous Detection of Single Base Mutation in DNA”

Dissertation

zur Erlangung des akademischen Grades

d o c t o r r e r u m n a t u r a l i u m

(Dr. rer. nat.)

im Fach Chemie

eingereicht an der

Mathematisch-Naturwissenschaftlichen Fakultät I

der Humboldt-Universität zu Berlin

von M. Sc. Dilip Venkatrao Jarikote

geboren am 01.04.1977 in Digrass-Nanded, Maharashtra (INDIA)

Präsident der Humboldt-Universität zu Berlin

Prof. Dr. C. Markschies

Dekan der Mathematisch-Naturwissenschaftlichen Fakultät I

Prof. Dr. C. Limberg

Gutachter: 1. Prof. Dr. Oliver Seitz

2. Prof. Dr. Beate Röder

3. Prof. Dr. Ronald Micura

Tag der mündlichen Prüfung:23. 02. 2007

Die vorliegende Arbeit wurde im Arbeitskreis von Prof. Dr. H. Waldmann unter der Betreuung von Dr. Oliver Seitz in der Zeit von Dezember 2002 am Institut für Organische Chemie der Universität Dortmund und am Max-Planck-Institut für molekulare Physiologie sowie ab Juni 2003 bis Oktober 2006 im Arbeitskreis von Prof. Dr. Oliver Seitz am Institut für Chemie im Fachinstitut für Organische und Bioorganische Chemie der Humboldt-Universität zu Berlin angefertigt.

To my youngest brother Umakant.

I. Zusammenfassung

Interkalatorfarbstoffe wie Thiazolorange (TO) wurden an Stelle einer internen Nucleobase in PNA eingebaut. Solche Konjugate werden als FIT-Sonden (*F*orced *I*ntercalation of *T*hiazole Orange) bezeichnet. Bei Hybridisierung interkaliert Thiazolorange in unmittelbarer Nachbarschaft zu einem *mismatch* Basenpaar in einen PNA·DNA-Duplex (Abbildung I).

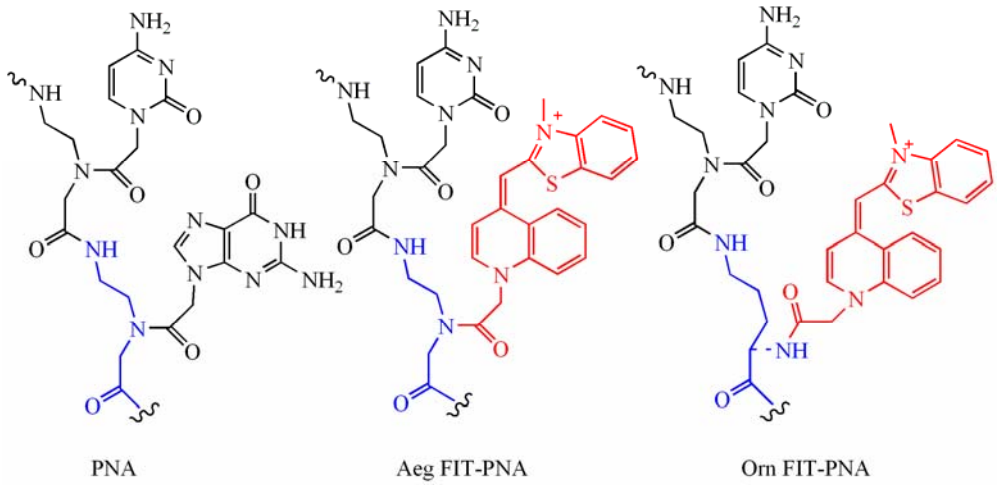

Abbildung I: Einzelstrang von PNA (links), Aeg-FIT-PNA (mitte) und Orn-FIT-PNA (rechts).

I.I Synthese

Diese Arbeit befasste sich zunächst mit der Entwicklung einer linearen Strategie für die Festphasensynthese von PNA. Dafür musste ein neuer Thiazolorange-Monomer-Baustein hergestellt werden. Der neue Baustein Fmoc-Aeg(TO)-OH sowie die rückgratmodifizierten Derivate Fmoc-L- bzw. Fmoc-D-Orn(TO)-OH wurden mittels Kupplung von Thiazolorange-Carbonsäure mit den Fmoc/Allyl-geschützten Bausteinen **2b** und **22b** synthetisiert. Die anschließende Pd(0)-katalysierte Abspaltung der Allylgruppe ergab die gewünschten TO-Bausteine **3b** und **24b** mit 73% und 65% Ausbeute (Schema I). Die neuen Monomere wurden bei der linearen Festphasensynthese von FIT-PNA-Oligomeren wie den TO-Sonden **10** oder **38** eingesetzt. Zunächst wurde der erste Teil der Sequenz am Harz (Schema II) aufgebaut. Bei der anspruchsvolleren Kupplung der TO-Monomere wurde PPTS zugesetzt, um deren Löslichkeit zu erhöhen. Anschließend wurde der lineare Aufbau des PNA-Oligos fortgesetzt.

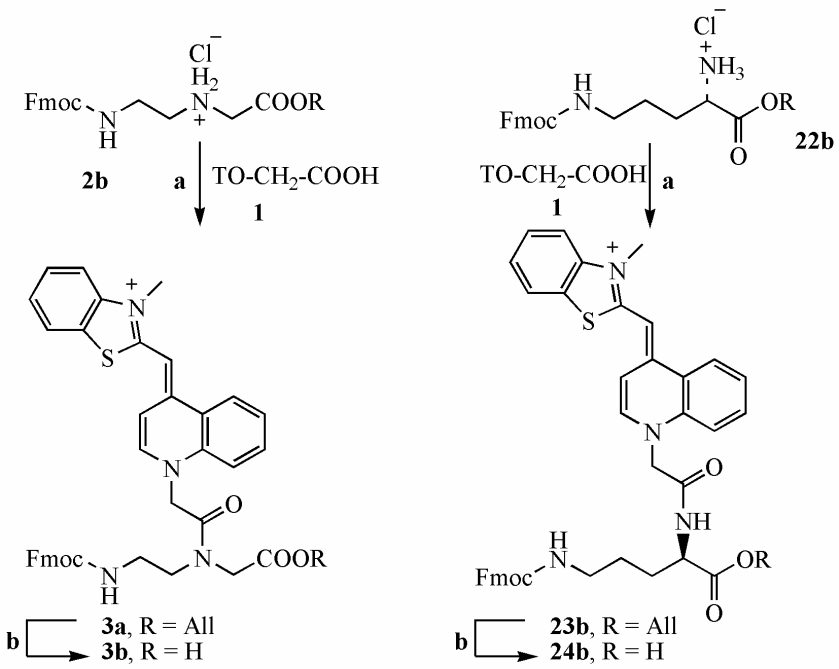

Schema 1: a) TO-CH_2COOH (**1**), **2b** oder **22b**, PyBOP, PPTS, NMM, DMF; b) [$Pd(PPh_3)_4$], $PhNHCH_3$, THF.

Die erhaltenen TO-PNA-Konjugate wurden mittels TFA von der festen Phase abgespalten. Der Reinheitsgrad der Rohprodukte war höher als der der auf dem Wege der divergenten Festphasensynthese hergestellten Produkte. Nach diesem Protokoll wurden die TO-PNA-Oligomere mit Gesamtausbeuten von 7.8-9.4% synthetisiert.

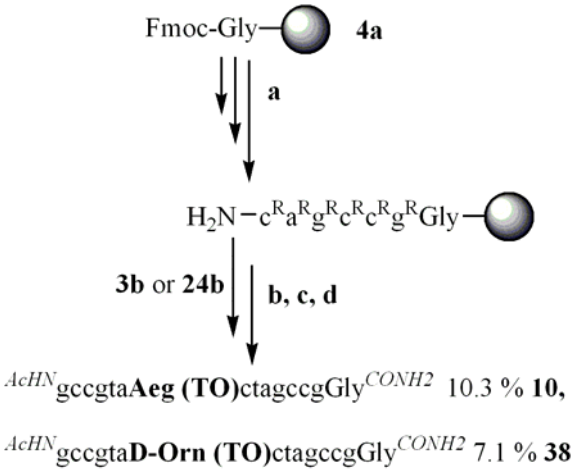

Schema 2: Lineare PNA-Synthese: a) und c) Synthesezyklus mit 1) Piperidin/DMF; 2) Fmoc-B (Bhoc)-OH, NMM, PyBOP, DMF; 3) Ac_2O/Pyridin, DMF; b) Synthesezyklus mit 1) Piperidin/DMF; Fmoc-Aeg (TO)-OH **3b** oder Fmoc-D-Orn (TO)-OH **24b**, NMM, PyBOP, PPTS, DMF; 3) Ac_2O/Pyridin, DMF; d) TFA, m-Kresol, H_2O, L-Cys-OMe.

I.II Nachbarschaftseffekte

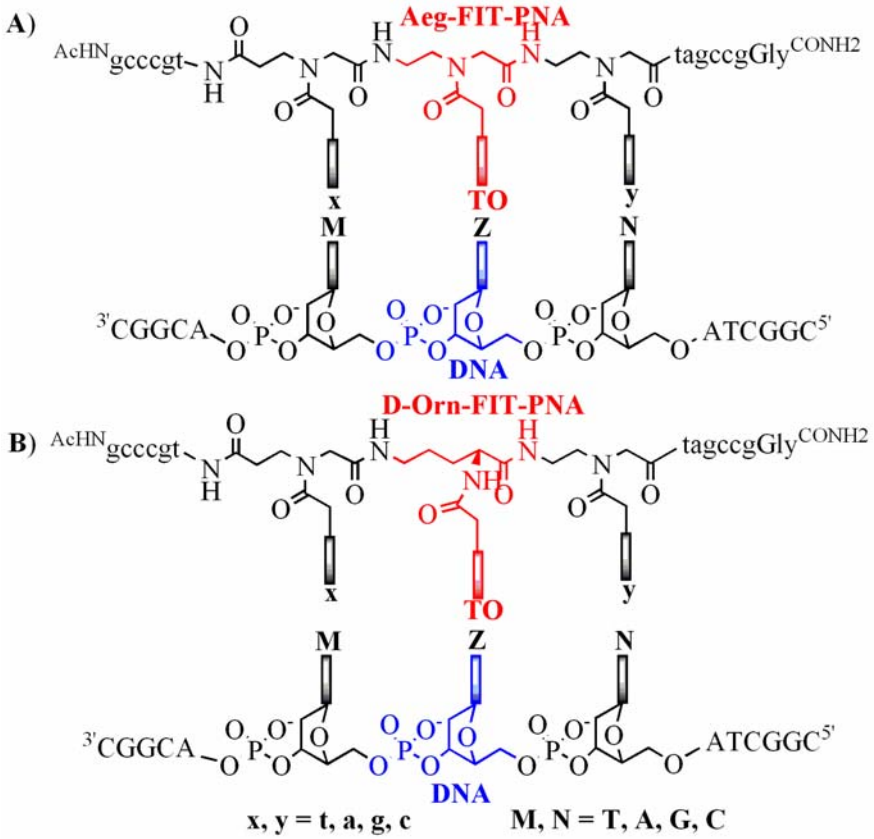

Abbildung II: Untersuchte Bibliothek von A) Aeg-FIT-PNA und B) D-Orn-FIT-PNA mit perfekt komplementärer oder einzelbasenfehlpaarender DNA.

Um den Einfluss der *stacking*- und *pairing*-Partner von Thiazolorange auf Stabilität und optische Eigenschaften der entsprechenden PNA•DNA-Duplexe zu untersuchen, wurden sowohl N-terminal (x) als auch C-terminal (y) benachbarte Basen von TO in Aeg-TO- und D-Orn-TO-Oligomeren variiert. (Abbildung II) Sechzehn verschiedene Sonden wurden mit den Oligonucleotiden **5´-20´MZN** in der Weise hybridisiert, dass TO sich gegenüber Base Z des Targetstrangs und in unmittelbarer Nachbarschaft jedes möglichen Basenpaares befand.

Thermische Stabilität

Schmelzkurvenanalysen zeigten, dass eine GC-reiche Umgebung von TO (T_M = 77°C) zu einer höheren Duplexstabilität führt als eine AT-haltige Nachbarschaft, in der sich TO zwischen zwei Thyminen, zwei Adeninen oder einem Adenin und einem Thymin (T_M = 69 - 73°C) befindet. Perfekte (*match*) Duplexe waren stets stabiler als einzelbasenfehlgepaarte (*mismatch*) Duplexe. Die Daten aus Abschnitt **2.4** belegen, dass die Hybridisierung von FIT-PNA ausnahmslos

sequenzselektiv ist. Aus Schmelzanalysen geht außerdem hervor, dass alle vier Nucleobasen A, C, G und T als Paarungspartner von TO toleriert werden. Interessanterweise ist die thermische Stabilität der Duplexe um T_M = 3°C höher, wenn sich gegenüber TO keine Nucleobase befindet verglichen mit Duplexen, in denen T als Paarungspartner von TO fungiert. Scheinbar erfolgt die Interkalation des TO-Farbstoffs besonders leicht, wenn die sterische Hinderung durch eine gegenüberliegende Nucleobase reduziert ist. Wird dagegen eine zum interkalierenden TO benachbarte Base entfernt, verringert sich die Duplexstabilität wahrscheinlich auf Grund fehlender Stapelungswechselwirkung um 9°C.

Absorptions-Untersuchungen

Für Einzelstrang-FIT-PNAs liegt der Extinktionskoeffizent ε_{max} zwischen 16100 und 59300 $M^{-1}cm^{-1}$(Abbildung III), in Doppelsträngen ist ε_{max} um 22–53 % höher. Die Absorption von TO sowohl in einzel- als auch in doppelsträngigen FIT-PNAs ist stark von seiner unmittelbaren Nachbarschaft abhängig. Zum Vergleich wurde die Bindung des freien Farbstoffs TO-PRO1 an die Komplexe DNA•DNA bzw. PNA•DNA untersucht. Die Anlagerung an die entsprechenden Doppelstränge führt zu einer Verringerung von ε_{max} um 23% bzw. 33%.

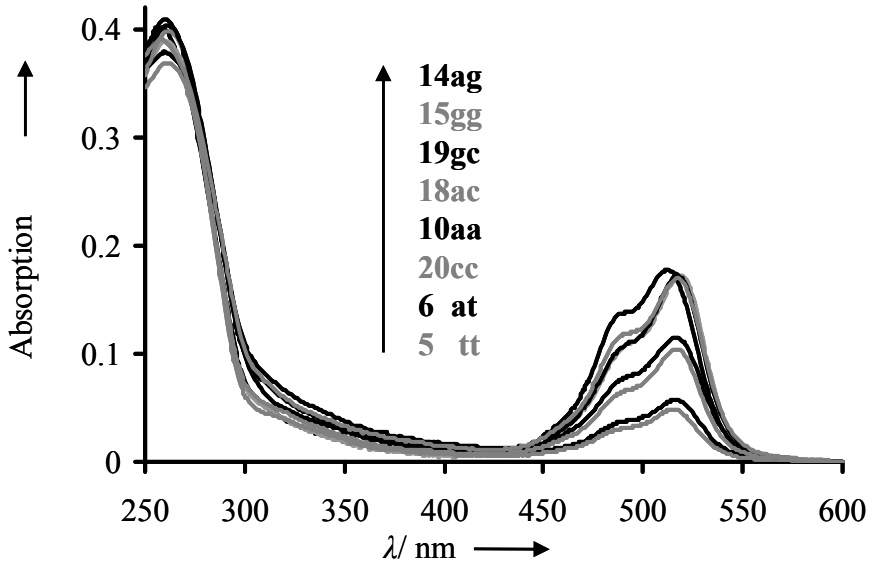

Abbildung III: Absorptionsspektren von Einzelstrang-PNA-TO-Konjugaten (**5-20xy**). Die Absorption wurde entsprechend dem Wert bei 600 nm korrigiert, die Absorptionskurven wurden mit dem berechneten Wert für ε_{260} kalibriert.

Fluoreszenz-Studien

In Abbildung IV ist die Fluoreszenzerhöhung von Aeg-TO-PNA (grau) und D-Orn-TO-PNA (schwarz) nach Bildung perfekter Duplexe mit komplementären Oligonucleotiden dargestellt. TO wurde dabei mit allen vier Nucleobasen gepaart.

o = Aeg/D-Orn (TO), x; y = t, a, g und c
M, Z, N = T, A, G and C

x	Z	y	$(F_{ds\ (match)}/\ F_{ss})^a$
a	**T**	a	29 / 24
a	**T**	c	32 / 20
t	**T**	a	20 / 19
t	**T**	t	19 / 16
a	**T**	g	16 / 16
a	**T**	t	27 / 14
g	**T**	a	22 / 13
a	**G**	a	6 / 11
c	**G**	g	2 / 10
a	**A**	a	11 / 9
t	**G**	a	3 / 9
a	**G**	c	14 / 8
a	**A**	c	10 / 8
a	**A**	g	6 / 8
c	**T**	g	7 / 7
a	**C**	a	10 / 7
t	**A**	a	3 / 7
t	**T**	g	4 / 6
t	**T**	c	9 / 6
t	**C**	t	2 / 6
t	**C**	a	3 / 6
g	**A**	a	5 / 6
g	**T**	c	16 / 6
g	**T**	t	3 / 5
a	**G**	t	9 / 5
t	**A**	t	3 / 5
c	**A**	g	3 / 5
g	**T**	g	9 / 5
a	**C**	c	9 / 5
c	**T**	c	10 / 4
g	**G**	a	7 / 4
g	**C**	a	7 / 4
c	**T**	a	24 / 4
g	**G**	c	11 / 4
a	**A**	t	9 / 4
a	**C**	g	4 / 4
c	**G**	a	7 / 4

o = Aeg/D-Orn (TO), x; y = t, a, g und c
M, Z, N = T, A, G and C

x	Z	y	($F_{ds\ (match)}$/ F_{ss})[a]
t	**G**	t	7 / 4
a	**C**	t	6 / 4
a	**C**	g	2 / 4
g	**A**	c	7 / 4
g	**C**	g	5 / 3
c	**G**	c	6 / 3
t	**A**	g	1 / 3
g	**G**	g	2 / 3
t	**G**	c	7 / 3
c	**C**	a	4 / 3
g	**G**	t	2 / 3
t	**C**	c	4 / 3
c	**A**	c	5 / 3
t	**C**	g	1 / 3
c	**A**	a	8 / 2
g	**C**	t	1 / 2
g	**A**	g	2 / 2
t	**A**	c	4 / 2
t	**G**	g	1 / 2
c	**T**	t	5 / 2
c	**C**	c	2 / 2
g	**C**	g	3 / 2
g	**A**	t	1 / 2
a	**G**	g	7 / 2
c	**C**	t	1 / 1
c	**G**	t	1 / 1
c	**A**	t	1 / 1

Abbildung IV: Fluoreszenzintensivierung der PNA-Sonden **5-20** (grau) und **25-40** (schwarz) bei 530 nm nach Ausbildung perfekter Duplexe, Paarungspartner für TO ist jeweils Thymin, Adenin, Guanin oder Cytosin. 25°C, Puffer. [[a] F_{ds}/F_{ss} = Quotient aus Fluoreszenzintensität der FIT-PNA nach und vor Zugabe von DNA bei 530 nm]

Aeg-TO-PNA

1) ≥8 fache Fluoreszenzerhöhung in 14 Duplexen (22%).

2) ≥4 fache Fluoreszenzerhöhung in 42 Duplexen (66 %) .

3) <4 fache Fluoreszenzerhöhung in 22 Duplexen (34 %).

D-Orn-PNA

1) ≥8 fache Fluoreszenzerhöhung in 22 Duplexen (34 %).

2) ≥4 fache Fluoreszenzerhöhung in 42 Duplexen (66 %).

3) <4 fache Fluoreszenzerhöhung in 22 Duplexen (34 %).

4) Die Fluoreszenz steigt im Durchschnitt um das 6,9 fache, wenn ein AT-Basenpaar als *stacking*-Partner fungiert und um das 4,9 fache mit einem GC-Basenpaar.

5) Die durchschnittliche Fluoreszenz steigt um den Faktor 10,4; 4,3; 4,7 bzw. 3,7, wenn sich gegenüber von TO ein T, A, G bzw. C befindet.

6) Die durchschnittliche Fluoreszenz-intensivierung beträgt 8,8 mit Adenin als Innerstrang-Stapelungspartner von TO und 4,4; 4,6 bzw. 5,5 mit c, g bzw. t.

7) Die Fluoreszenzerhöhung bleibt konstant oder nimmt zu bei steigender Temperatur. Bei Temperaturen um den T_M-Wert nimmt die Duplexfluoreszenz rapide ab.

8) Von allen 384 untersuchten einzelbasenfehlgepaarten Duplexen zeigen 80% eine niedrigere Fluoreszenz im Vergleich zu perfekten Duplexen .

9) 25% der Sonden zeigen eine *match/mismatch* Diskriminierung von ≥ 3 bei 25°C.

10) Die durchschnittliche Fluoreszenz-erhöhung aller Aeg-TO-markierten Oligomere in allen perfekten Duplexen beträgt 5,8 bei 25°C.

4) Die Fluoreszenz steigt im Durchschnitt um das 6,6 fache, wenn ein AT-Basenpaar als *stacking*-Partner fungiert und um das 6,7 fache mit einem GC-Basenpaar.

5) Die durchschnittliche Fluoreszenz steigt um den Faktor 15,6; 5,0; 5,4 bzw. 4,8, wenn sich gegenüber von TO ein T, A, G bzw. C befindet.

6) Die durchschnittliche Fluoreszenz-intensivierung beträgt 12,0 mit Adenin als Innerstrang-Stapelungspartner von TO und 7,5; 5,6 bzw. 5,4 mit c, g bzw. t.

7) Die Fluoreszenzerhöhung bleibt konstant oder nimmt zu bei steigender Temperatur. Bei Temperaturen um den T_M-Wert nimmt die Duplexfluoreszenz rapide ab.

8) Von allen 384 untersuchten einzelbasenfehlgepaarten Duplexen zeigen 92% eine niedrigere Fluoreszenz im Vergleich zu perfekten Duplexen .

9) 41% der Sonden zeigen eine *match/mismatch* Diskriminierung von ≥ 3 bei 25°C.

10) Die durchschnittliche Fluoreszenz-erhöhung aller D-Orn-TO-markierten Oligomere in allen perfekten Duplexen beträgt 7,8 bei 25°C.

I.III Bindungsverhalten von Thiazolorange

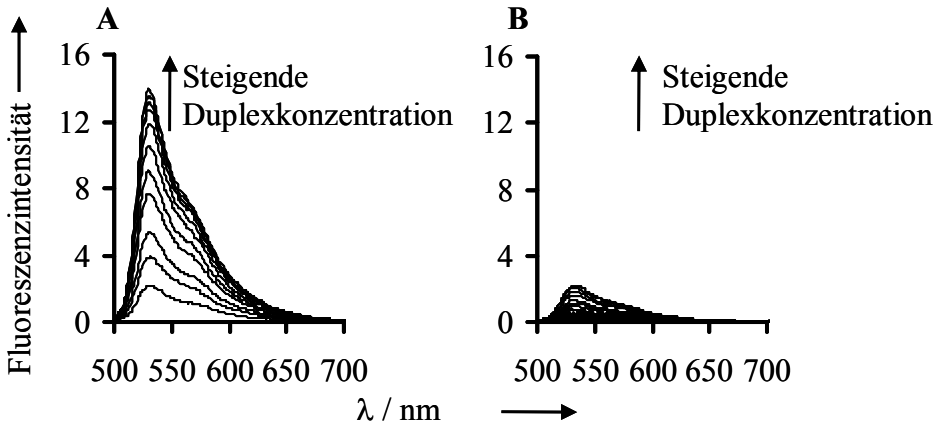

Abbildung V: Fluoreszenzemission von TO-PRO1 vor und nach Zugabe von A) DNA•DNA duplex **4'AT•4'TA** (0.1, 0.2, 0.3, 0.5, 0.7, 1.0, 1.5, 2.0, 2.5, 3.0 and 4.0 µM) und B) PNA•DNA duplex **4at•4'TA** (0.1, 0.2, 0.3, 0.5, 0.7, 1.0, 1.5, 2.0, 2.5, 3.0, 4.0, 5.0, 6.0, 8.0, 10.0, 12.0 und 14.0 µM).

Die Ergebnisse dieser Arbeit zeigen, dass die Fluoreszenz von TO ansteigt, wenn der freie Farbstoff TO-PRO1 an PNA•DNA-Duplexe (**4at•4´TA**) (Quantenausbeute $\Phi_{em} = 0{,}02$) bzw. an DNA-Doppelstränge (**4AT•4´TA)** ($\Phi_{em} = 0{,}21$) gebunden ist. Die Fluoreszenztitrationsanalyse ergab eine niedrigere Affinität für die Bindung von TO-PRO1 an PNA•DNA ($K_{app} = 7{,}3 \pm 0{,}4$ µM pro Basenpaar) verglichen mit der Bindung an DNA•DNA ($K_{app} = 134 \pm 20$ µM pro Basenpaar).

Bei zeitaufgelösten Fluoreszenzuntersuchungen [durchgeführt von Nils Krebs und Sebastian Tannert im Arbeitskreis von Prof. Beate Röder (Institut für Physik, Humboldt-Universität zu Berlin, Newtonstr. 15, D-12489 Berlin, Deutschland)] von TO-PRO1 in DNA•DNA- und PNA•DNA-Duplexen sowie von FIT-PNA-Komplexen wurden vier verschiedene Abkling je nach Umgebung von TO gefunden: 1) ein sehr schneller Prozess (0,04 - 0,07 ns), der verschwindet, wenn FIT-PNA an DNA bzw. TO-PRO1 an doppelsträngige DNA bindet, der jedoch detektierbar bleibt, wenn TO-PRO1 an PNA•DNA bindet; 2) ein schneller Prozess (0,22 – 0,48 ns), der stark von der Existenz benachbarter *mismatch*-Basenpaare abhängt; 3) ein vergleichsweise unempfindlicher mittlerer Abklingprozess (1,05 – 1,54 ns) und 4) ein langsamer Prozess (2,33 – 3,95 ns), der allgemein durch Hybridisierung oder den Austausch einer benachbarten Nucleobase in FIT-PNA•DNA-Duplexen beeinflusst wird. Der sehr schnelle Prozess kann einer für Wasser zugänglichen TO-Spezies zugeordnet werden. TO-PRO1 im PNA•DNA-Komplex **4at•4TA** hat demnach Kontakt mit

Wasser der Pufferlösung. Im Gegensatz dazu scheint ein solcher kontakt beider Assoziation von TO-PRO1 an doppelsträngiger DNA oder von TO in FIT-PNA•DNA-Duplexen.

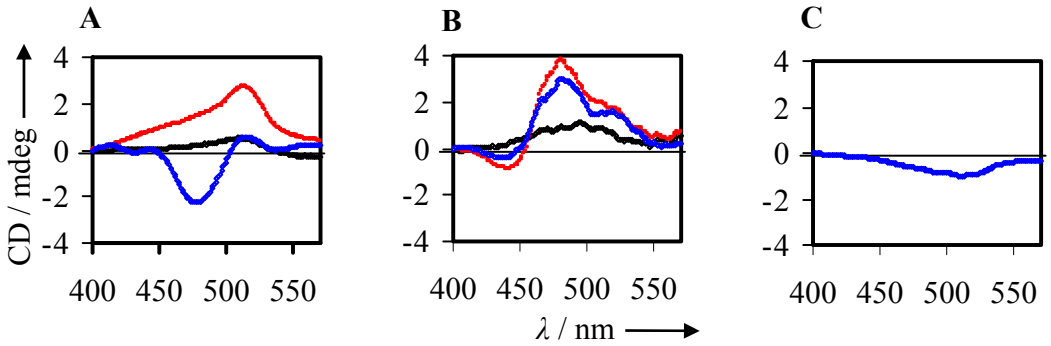

Abbildung VI: CD-Spektren von TO-PRO1 und A) DNA•DNA-Duplex **4´AT4´AT** und B) PNA•DNA-Duplex **4´at•4´TA** jeweils im Verhältnis Farbstoff:Basenpaare von 1:10 (schwarz), 1:4 (rot) und 1:2,5 (blau). C) CD-Spektrum des Komplexes FIT-PNA•DNA **19gc•16´CTG**. Die Spektren wurden entsprechend dem Wert bei 400 nm korrigiert.

Der induzierte Circular dichroisms von TO-PRO1, gebunden an DNA•DNA und PNA•DNA ist bei niedrigem Farbstoff-Basenpaar-Verhältnis positiv (Abbildung VI). Bei hohem Farbstoff-Basenpaar-Verhältnis treten zwei Banden mit verschiedenem Vorzeichen auf. Eine solche Struktur kann auf einer überlagerten Exciton-Kopplung beruhen, induziert durch Farbstoff-Farbstoff-Wechselwirkungen in der kleinen Furche. Im PNA•DNA-Duplex wird das CD-Couplet bei niedrigerem Farbstoff-Basenpaar-Verhältnis (1:4) als im DNA•DNA-Komplex (1:2,5) beobachtet. Eine Assoziierung von TO-PRO1 in der kleinen Furche von PNA•DNA scheint demnach für die untersuchten Sequenzen bei niedrigeren Farbstoffkonzentrationen stattzufinden als in der kleinen Furche von DNA•DNA.

Das Chromophor TO im FIT-PNA•DNA-Hybrid **19gc•16´CTG** zeigt eine negative Bande mit einem Maximum bei 518 nm (Abbildung VI), das mit den Absorptionsbanden übereinstimmt. Da negative Banden auf Interkalation hinweisen [1, 2, 3, 4], wird TO im FIT-PNA•DNA-Duplex **19•16´** vorzugsweise ins Innere des Komplexes interkalieren. Im Gegensatz dazu ist die Art der Bindung von TO-PRO1 an DNA•DNA und PNA•DNA weniger eindeutig.

Die vergleichsweise niedrige Affinität von TO-PRO1 zu PNA•DNA, die Wasserzugänglichkeit der gebundenen TO-Spezies sowie die CD-Spektren lassen

vermuten, dass TO-PRO1 im PNA•DNA-Duplex bevorzugt eine extrahelikale Bindungsstelle einnimmt. Demmach ist in FIT-PNA•DNA-Duplexen die Interkalation von TO offensichtlich ein erzwungener Bindungsmodus, da der freie Farbstoff TO-PRO1 in PNA•DNA-Duplexe nicht interkaliert. Diese Ergebnisse werden durch die umgebungssensitiven Fluoreszenzeigenschaften von TO in FIT-PNA bestätigt. Die Quantenausbeuten waren in Duplexen mit Adenin-Thymin-Basenpaaren als *stacking*-Partner von TO am höchsten und mit benachbarten Guanin-Cytosin-Paaren am geringsten. Diese Daten stimmen nicht mit früheren Beobachtungen überein, wonach TO und TO-PRO1 eine höhere Fluoreszenz-Quantenausbeute aufweisen, wenn sie mit GC-reichen Duplexen wechselwirken verglichen mit AT-reichen Duplexen. Diese Ergebnisse sowie die deutliche Sensibilität des Extinktionskoeffizienten ε_{260} weisen darauf hin, dass TO in FIT-PNA•DNA-Duplexen in eine Art angebandenist welche die elektronische Kopplung zu benachbarten Nucleobasen erleichtert.

Die durchgeführten Studien belegen, dass das Thiazolorange-Basensurrogat seine Fluoreszenzintensität bei Hybridisierung am stärksten ändert, wenn es von zwei Adenin-Bausteinen flankiert wird. Der bevorzugte Paarungspartner für hohe Emissionsanstiege mit *match* DNA und für hohe *match/mismatch* Diskriminierungsfähigkeit ist Thymin. Die Mehrzahl der FIT-Sonden zeigte in Komplexen mit perfekt komplementärer DNA deutlich höhere Fluoreszenzanstiege als mit einzelbasenfehlpaarender DNA. Dadurch ist es möglich, *mismatch* DNA von *match* DNA sogar unterhalb des T_M-Wertes vom *mismatch* Sonden-Target-Komplex zu unterscheiden. Zusätzlich können die Vorteile der selektiven Hybridisierung der FIT-Sonden genutzt werden. So zeigten die untersuchten *mismatch* Duplexe stets eine geringere thermische Stabilität als die entsprechenden *match* Duplexe. Mittels FIT-PNA-Oligomeren ist es somit möglich, bei Temperaturen unterhalb des T_M des perfekten Duplexes und oberhalb des T_M vom *mismatch* Duplex, alle einzelbasenmutierten DNA-Targets von perfekt komplementärer DNA zu unterscheiden.

Die D-Orn-TO-markierten PNAs sind ähnlich umgebungssensitiv in Bezug auf benachbarte Basen, Paarungs- und Stapelungspartner von TO. Bemerkenswerterterweise wurden hier noch höhere Fluoreszenzanstiege in perfekten Duplexen und eine ausgeprägtere *match/mismatch* Diskriminierung erreicht als mit Aeg-TO-markierten PNAs.

I.IV FIT-PNA im Vergleich zu *Light-up*-PNA

Light-up-Sonden unterscheiden sich von FIT-Sonden (Abbildung VII) durch die Art der TO-Verknüpfung. In *Light-up*-Sonden ist TO über einen flexiblen Linker mit dem N-oder C-Terminus des Oligomers verbunden, in FIT-Sonden ist eine Base durch TO ersetzt. Beide Varianten wurde in Hybridisierungsexperimenten miteinander verglichen.

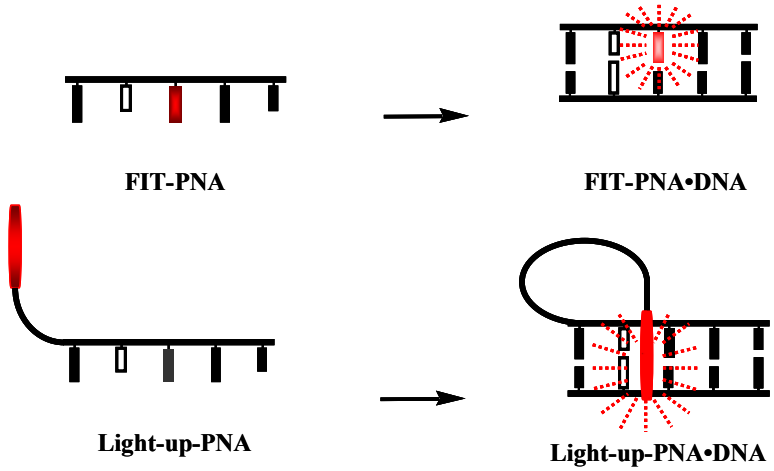

Abbildung VII: Schematische Darstellung von FIT-PNA und *Light-up*-PNA.

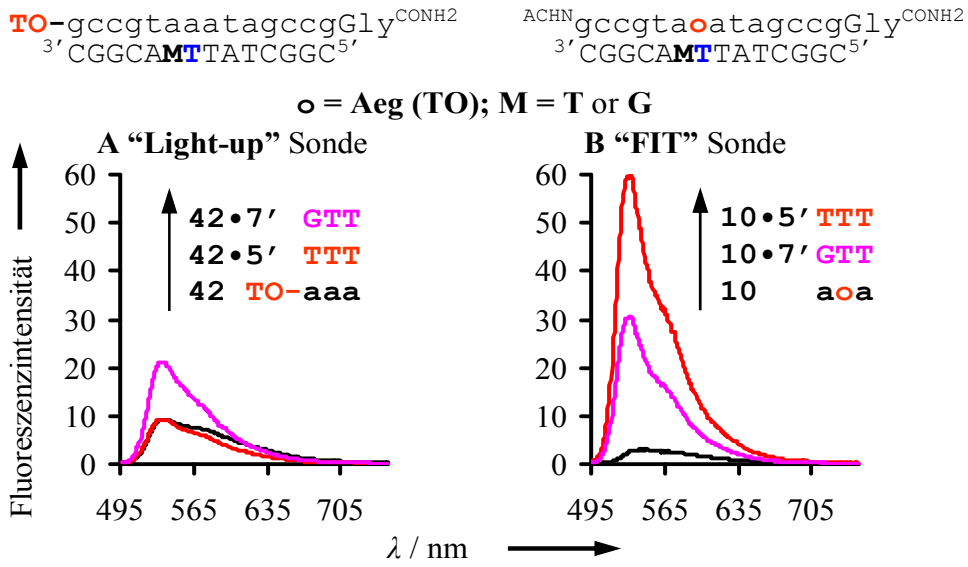

Abbildung VIII: Fluoreszenz-Emissionsspektren vor (schwarz) und nach Zugabe äquimolarer Mengen *match* DNA **5′TTT** (rot) sowie *mismatch* DNA **7′GTT** (margenta) für A) *Light-up*-Sonde **42**, B) FIT-Sonde **10** bei 25°C.

Die Daten aus UV/VIS-Untersuchungen, CD- sowie Fluoreszenzmessungen (Abbildungen VIII und IX) machen deutlich, dass das Basensurrogat TO der FIT-PNAs ortsspezifisch in PNA•DNA-Duplexe interkalieren kann, für das TO der

Light-up-PNAs gibt es jedoch keine entsprechenden Hinweise. Gebunden an *match* DNA stieg die Fluoreszenz der FIT-Sonden um das 16-24fache, die der *Light-up*-Sonden **42** und **45** dagegen kaum an. Einzelbasenfehlgepaarte Duplexe der FIT-PNAs **10** und **46** fluoreszieren weniger stark als perfekte Duplexe. Die *Light-up*-Sonde **42** zeigte dagegen eine erhöhte Fluoreszenz nach Hybridisierung mit *mismatch* DNA.

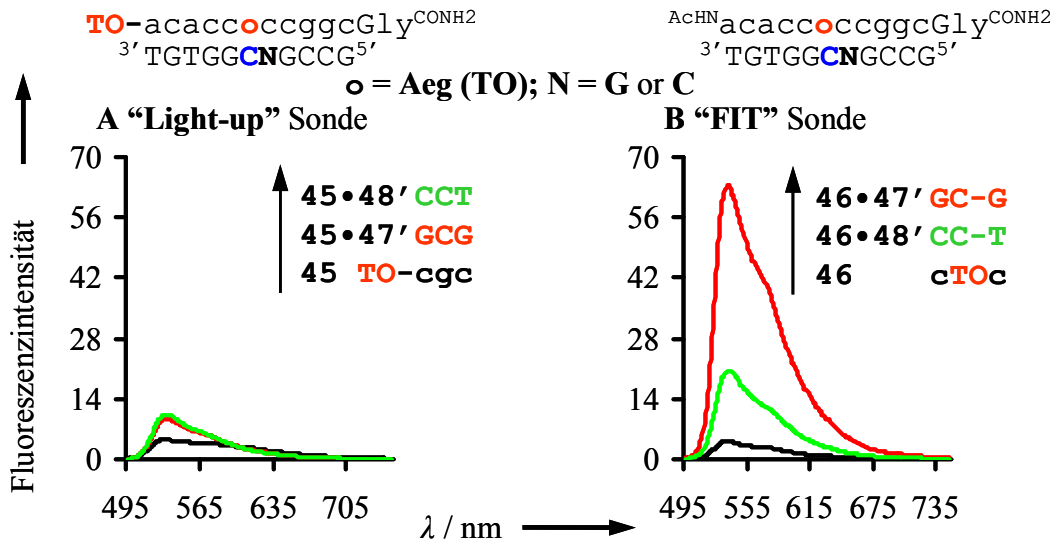

Abbildung IX: Fluoreszenz-Emissionsspektren vor (schwarz) und nach Zugabe äquimolarer Mengen *match* DNA **47′CGC** (rot) sowie *mismatch* DNA **48′GCT** (grün) für A) *Light-up*-Sonde **45**, B) FIT-Sonde **46** bei 25°C.

In zeitaufgelösten Fluoreszenzmessungen wurde ein sehr schneller Relaxationsprozess beobachtet, der verschwindet, sobald die FIT-Sonden mit DNA hybridisieren, bei Doppelstrangbildung der *Light-up*-Sonden bleibt er unverändert. Ebenso zeigten die Absorptionsspektren deutliche Unterschiede. Der Extinktionskoeffizient liegt für die FIT-PNA bei $\varepsilon_{max} = 38200\ M^{-1}cm^{-1}$ und für die *Light-up*-PNA bei $\varepsilon_{max} = 85800\ M^{-1}cm^{-1}$. Ursache dafür sind die verschiedenen Wechselwirkungen zwischen TO und den Nucleobasen. Betreffend selektiver Hybridisierung, Fluoreszenzanstieg und *match/mismatch* Diskriminierung zeigten sich die FIT-PNAs den *Light-up*-PNAs überlegen.

I.V Doppelt markierte FIT-PNA

Mittels doppelt markierter FIT-PNA-Oligos, in denen zwei TO-Bausteine eine Einzelbasen-Mutationsstelle flankieren, wurde die Möglichkeit eines TO-TO-Kontakts untersucht (Abbildung X).

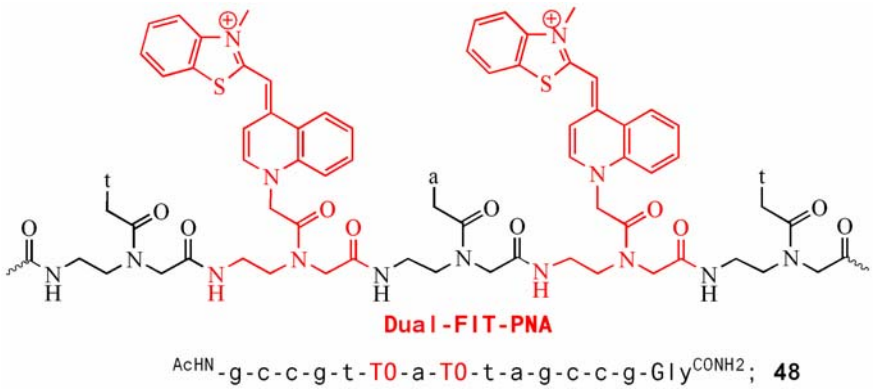

Abbildung X: Struktur doppelt markierter FIT-PNA.

Der Fluoreszenzanstieg von $(TO)_2$-PNA bei Hybridisierung ist höher als der von FIT-PNA. Interessanterweise ist die Schulter bei 577 nm im Fluoreszenzspektrum der *mismatch* Duplexe stärker ausgeprägt. Das kann ein Hinweis auf eine Wechselwirkung zwischen beiden TO-Chromophoren über das *mismatch* Basenpaar hinweg sein.

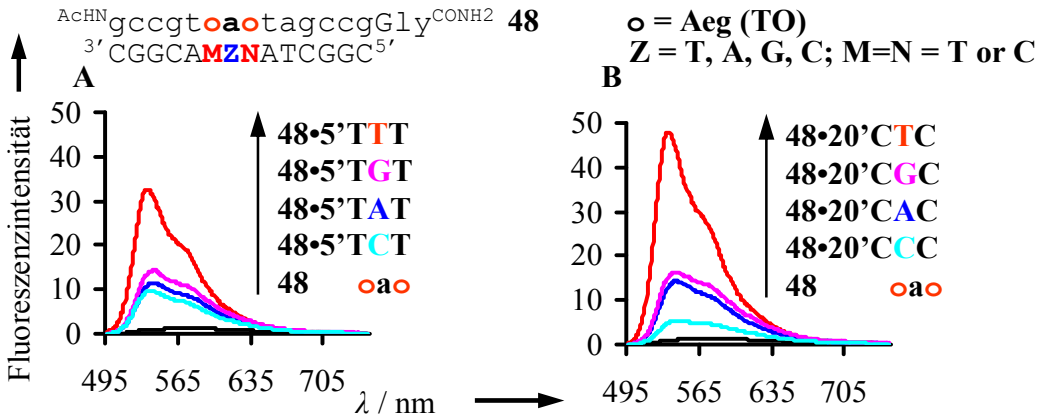

Abbildung XI: Fluoreszenz-Emissionsspektren der PNA-Sonde **48** vor (schwarz) und nach Zugabe äquimolarer Mengen von A) *match* DNA **5´TTT** (rot), *mismatch* DNA **5´TAT** (blau), DNA **5´TGT** (margenta) und **5´TCT** (cyan); B) *match* DNA **20´CTC** (rot), *mismatch* DNA **20´CAC** (blau), DNA 20´**CGC** (margenta) und **20´CCC** (cyan).

Die höchsten Fluoreszenzanstiege wurden mit Pyrimidin-Basen als Paarungspartner von TO gemessen. Die T_M-Analyse ergab jedoch, dass die zwei TO-Chromophore die Spezifität der Hybridisierung reduzieren und daher solche Sonden

für die PCR keinen Vorteil gegenüber FIT-Sonden aufweisen. Dennoch ist die *match/mismatch* Diskriminierung bei Raumtemperatur höher als für FIT-PNAs.

I.VI Pyridin-benzothiazol als Basensurrogat

Um Einzelbasen-Polymorphismen noch besser detektieren zu können, ist ein Farbstoff, spezifisch für die Wildtypsequenz, und ein zweiter, spezifisch für die Mutante erforderlich. Als zusätzlicher Farbstoff wurde BO gewählt, bei dem der Chinolinring im TO durch einen Pyrimidinring ersetzt ist.

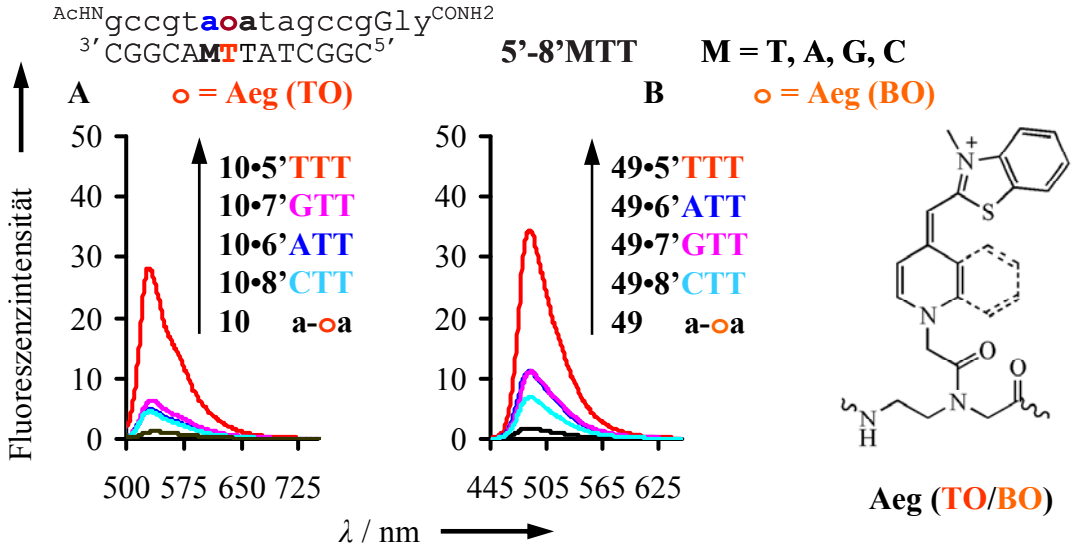

Abbildung XII: Fluoreszenz-Emissionsspektren von A) TO-PNA-Konjugat **10** und B) BO-PNA-Konjugat **48** vor (schwarz) und nach Zugabe äquimolarer Mengen DNA **5´TTT** (rot), **6´ATT** (blau), **7´GTT** (margenta) und **8´CTT** (cyan) bei 60°C.

Die hybridisierungsinduzierte Fluoreszenzverstärkung in Gegenwart von BO ist weniger ausgeprägt als mit TO. Bei erhöhten Temperaturen (60°C), die vor allem für PCR-Applikationen interessant sind, konnten jedoch Emissionsanstiege um bis zu Faktor 18 erreicht werden (Abbildung XII). Schmelzanalysen ergaben für perfekte Duplexe höhere T_M-Werte als für einzelbasenfehlgepaarte Duplexe. Die Sensitivität der BO-Fluoreszenz gegenüber einer benachbarten *mismatch* Nucleobase ist bei hohen Temperaturen ähnlich der von TO-Derivaten. Es sollte demnach möglich sein, ein DNA-Target von seiner Einzelbasenmutante mittels BO-markierten FIT-Sonden zu unterscheiden.

CONTENTS

1. Introduction

1.1 Introduction

The structure of DNA was first described by James Watson and Francis Crick in 1953.[5] Watson and Crick proposed that adenine forms a so-called base pair with thymine and similarly guanine with cytosine (Figure 1). This mutual recognition of the nucleobase interaction is an important natural process.

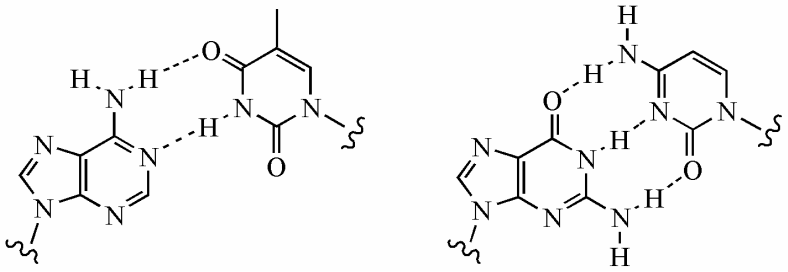

Figure 1: Watson Crick base pairings between the complementary nucleobases adenine/ thymine (left) and guanine/ cytosine (right).

On the molecular level base pairing of the nucleic acids is one of the most important natural recognition processes. Gene mutations can arise through many different processes. Spontaneous mutations can result from replication errors or from spontaneous lesions, such as those generated by deamination or depurination. Mutagens can increase the frequency of mutations. Some of these act by mimicking a base and then mispairing in DNA replication. Others alter bases in the DNA and convert them into derivatives that mispair. A third class of mutagens, which includes most carcinogens, damages DNA in such a way that replication is blocked. The activation of an enzymatic pathway, termed the SOS system, is required to replicate past the blocking lesions. This results in mutations that arise across from the blocking lesion. Repair enzymes present in living cells greatly minimize genetic damage, thus averting many mutations.

Various diseases, such as Tay Sachs disease, Huntington's disease, Alzheimer's disease, cystic fibrosis, familial hypercholesterolemia, and even cancer can be caused by gene mutations.[6] A "point mutation" (a single nucleotide base change in the DNA) can be sufficient to introduce the disease state. DNA-targeted diagnostic methods play an important role in various clinical settings and may offer the

possibility of detecting a developing disease such as cancer before symptoms begin to appear.

1.2 Single Base Polymorphisms in DNA

Developments in DNA sequencing now make it easy to look for allelic versions of a gene by sequencing samples of the gene taken from different members of a population (or from a heterozygous individual). Alleles whose sequence reveals only a single changed nucleotide are called single nucleotide polymorphisms or SNPs. By definition SNPs have a frequency of at least 1 % of the population. A change in a single base can cause SNPs in coding or regulatory DNA, where incorporation of a "wrong" amino acid can take place in a protein upon translation. Single base polymorphism is responsible for a multiplicity of further inherited illnesses, like asthma, high blood pressure and migraine.[7, 8] Hence, beyond doubt early diagnosis of mutation damage is very important.

The specificity of most DNA detection methods is governed by the selectivity of binding of a designed probe to the DNA target. Considerable research efforts have been made to improve the DNA binding characteristics of nucleic acids.[9, 10, 11, 12] Minor structural changes in oligonucleotides for example the replacement of an oxygen atom by sulphur (phosphorothioates) or by a neutral methyl group (methyl phosphonates) have resulted in decreases of binding affinity.[13, 14, 15] A dramatically alteration of backbone structure is found in peptide nucleic acids (PNA). PNA’s are nucleic acid mimetic with higher binding-affinity to complementary DNA and RNA compared to unmodified oligonucleotides. The remarkable binding properties of PNAs have sparked a rapid expansion of a new field of research which aims of taking advantage of the properties of PNA in DNA diagnostics and biotechnology.

1.3 Peptide Nucleic Acid (PNA)

Peptide nucleic acids (PNAs) developed by Peter E. Nielsen, Michael Egholm, Rolf H. Berg and Ole Buchardt[16] are a remarkable example of a simple DNA-analogous base pairing system which in terms of molecular recognition properties has surpassed most other attempts to mimic the native nucleic acid structures (Figure 2).[17] Peptide nucleic acid is a chemical structure similar to DNA or RNA but differing in the composition of its "backbone". DNA and RNA have a ribose sugar backbone, whereas PNA's backbone is composed of repeating units of N- (2-aminoethyl)-glycine linked by peptide bonds. The various purine and pyrimidine bases are linked to the backbone by methylene carbonyl bonds.[18]

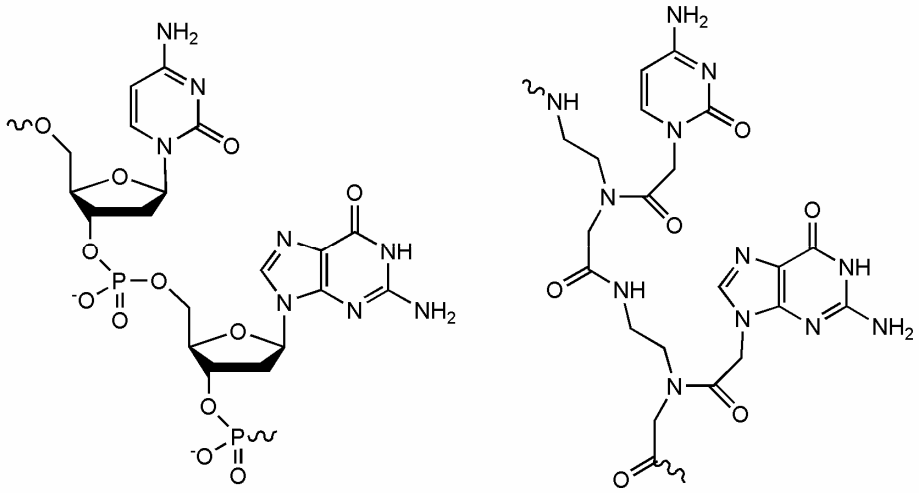

Figure 2: Diagram DNA single strand (left) and PNA single strand (right)

Since the backbone of PNA contains no charged phosphate groups, the binding between PNA and DNA strands is stronger than between DNA and DNA strands due to the lack of charge repulsion.[19] Early experiments with homopyrimidine strands (strands consisting of only one repeated pyrimidine base) have shown that the T_M ("melting" temperature) of a 6-base thymine PNA/ adenine DNA double helix ($^{N'}$ttttt$^{C'}$ and $^{3'}$AAAAAA$^{5'}$) was 31°C in comparison to an equivalent 6-base DNA/ DNA duplex that denatures at a temperature less than 10°C.[20] Mixed base PNA molecules are true mimics of DNA molecules in terms of base-pair recognition. Synthetic peptide nucleic acid oligomers have been used in recent years in molecular biology procedures, diagnostic assays, and antisense therapies. Due to their higher

binding strength it is not necessary to design long PNA oligomers for use in these roles, which usually require oligonucleotide probes of 20-25 bases. The main concern of the length of the PNA-oligomers is to guarantee the specificity. PNA oligomers also show greater specificity in binding to complementary DNAs, with a PNA-DNA base mismatch being more destabilizing than a similar mismatch in a DNA-DNA duplex. This binding strength and specificity also applies to PNA-RNA duplexes. PNAs are not recognized by either nucleases or proteases,[21] making them resistant to enzyme degradation. PNAs are also stable over a wide pH range.

1.3.1 Solid Phase Synthesis of PNA

Solid phase peptide synthesis protocols can be easily applied to the synthesis of oligomeric PNAs. As in the case with solid phase peptide synthesis, PNA synthesis is also done conveniently from the 'C' terminus to the 'N' terminus. For this, the monomeric units must have their amino functions suitably protected, and their carboxylic acid functions free. The most commonly used N-protecting groups for solid phase peptide synthesis are the *tert*-butyloxycarbonyl (Boc) and the 9-flurorenylmethoxycarbonyl (Fmoc) groups.

1.3.1.1 Boc Strategy:

The Boc-protection strategy uses, PNA-monomers in which the primary amino group is protected by the Boc-group (Scheme 1). The coupling of the free carboxyl group to a resin-bound amine can be achieved by using HBTU and HOBt as activating agents. Solid-phase synthesis typically is performed by using Merrifield resin as the solid polymeric matrix onto which the oligomers are built.[22] The PNA oligomers are synthesized using repetitive cycles, each comprising the following steps: (a) Deprotection of the N-protecting Boc-group using 50 % TFA in DCM. (b) Coupling of the free amine with the free carboxylic acid group of the incoming monomer. The coupling reaction should be carried out in DMF/ NMP/ DMSO with coupling reagent in the presence of base. (c) The unreacted amino groups are capped using acetic anhydride in pyridine: DCM.[23, 24, 25]

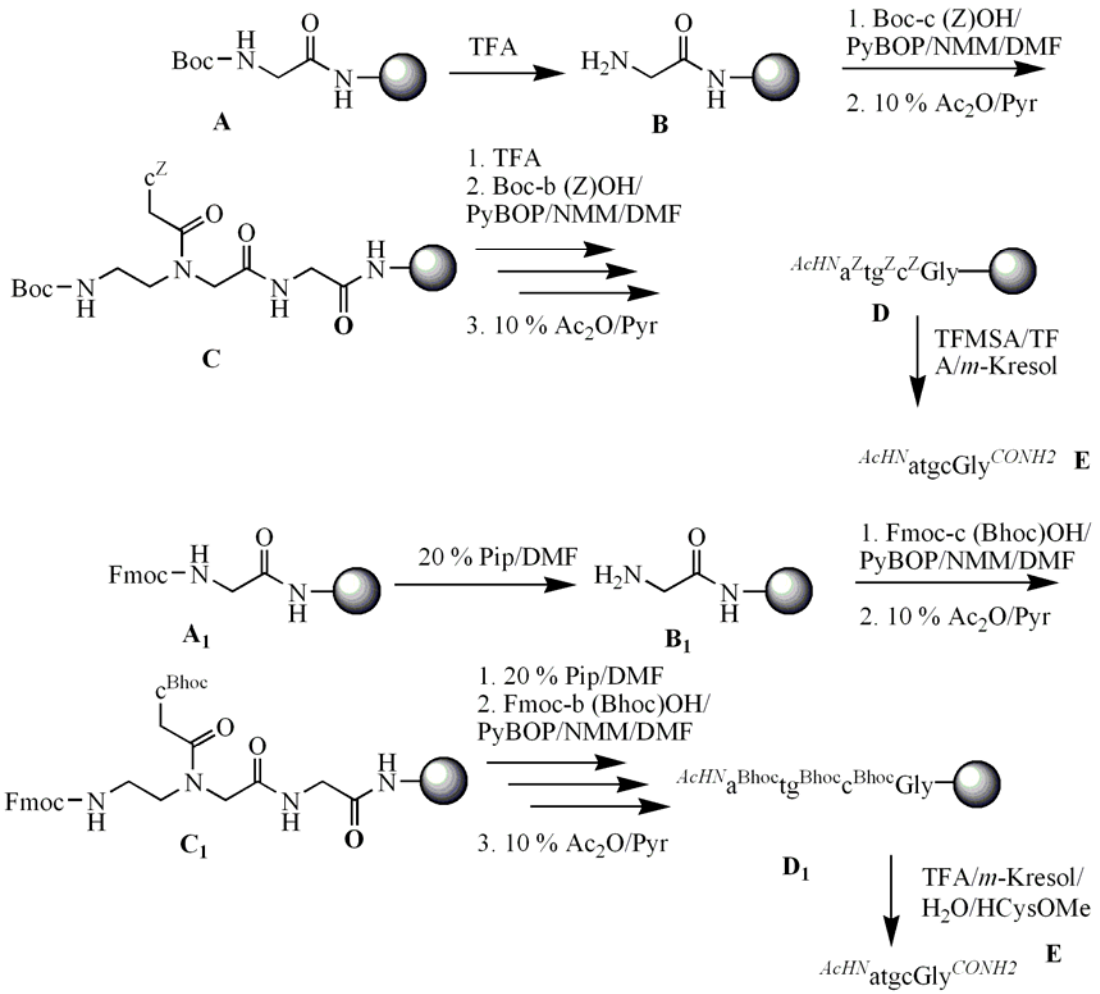

Scheme 1: Standard solid-phase synthesis of PNA-Oligomer for Boc/ Z-Strategy (top) and Fmoc/ Bhoc-Strategy (bottom).

1.3.1.2 Fmoc Strategy:

The Fmoc-protection strategy uses an Fmoc-protected amino function of the monomers as the corresponding Fmoc-derivative and the carboxylic acid function is free to enable coupling with the resin-linked monomer. This procedure requires Fmoc-protected amino acid attached with nucleic acids derivatives (Fmoc-Aeg (B)-OH, B = T, A, G, C) for PNA synthesis. The PNA oligomers can be synthesized using repetitive cycles, each comprising the following steps: (a) Deprotection of the N-protecting Fmoc-group using piperidine in dimethylformamide (20 %) (b) Coupling of the free amine with the free carboxylic acid group of the incoming monomer. The coupling reaction should be carried out in DMF or NMP with coupling reagent in the presence of base. The deprotections of the *N*-Fmoc protecting group can be monitored by measuring UV absorption of the released

fluorene adduct. (c) Capping of noncoupled amino acids by using Ac_2O/ Pyridine (10 %) to avoid elongation of failure sequences. After washing with DMF, DCM, and DMF the next cycle can be performed. After, completion of the desired oligomer the desired PNA is liberated by treatment with TFA: m-cresol: L-cystine methyl ester: water.[26]

1.3.2 Structure of PNA

The three-dimensional structures of four PNA complexes have been determined. The PNA•RNA[27] and PNA•DNA[28] duplex structures were determined by NMR methods, while the structures of a PNA2•DNA triplex[29] and a PNA•PNA duplexes[30] were solved by X-ray crystallography. Several general conclusions can be drawn from these structural studies. In general the PNA is able to adapt to a great extent to its partner. In the PNA•RNA and PNA•DNA duplexes the oligonucleotide adopts close to its natural A-conformation and B-conformation, respectively, in terms of sugar puckering, while the helix parameters have both A and B-form characteristics. The PNA however does, prefer a unique, different helix form, the P-form, which is taking over already in the PNA2•DNA triplex and is fully developed in the PNA•PNA duplex. This helix is very wide (28 Å diameter) and has a very large pitch (18 base pairs). In terms of base pair conformations it is a very regular helix, and the base pairs are virtually perpendicular to the helix axis.

1.4 Detection of Single Base Mutation

DNA-targeted analyses play a very important role and are used in various clinical settings. The binding of a probe molecule to the complementary nucleic acid target is the molecular basis for most of the current methods in DNA-based diagnostics.[31] In principal there are two different approaches, heterogeneous and homogeneous formats. Heterogeneous assays rely on an immobilization of either the target strand or the probe molecule to a solid- or gel-phase, which facilitates the removal of unbound binding partners (Figure 3).

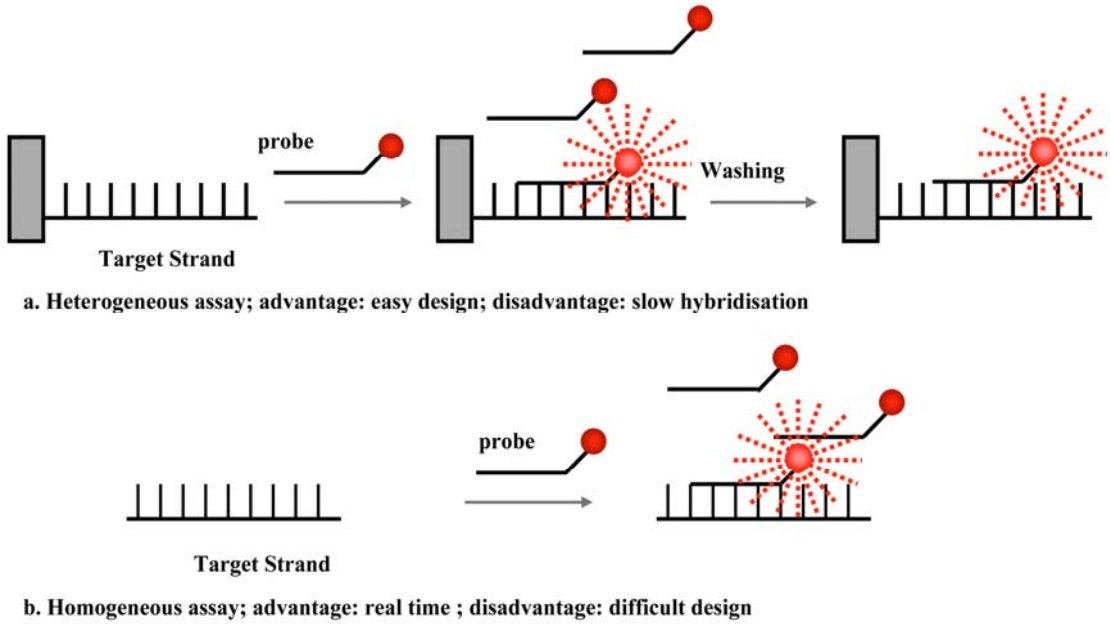

Figure 3: a. Heterogeneous assay and b. Homogeneous assay

Areas in which binding had occurred are detectable by means of a reporter-group that is usually appended to the soluble binder. In contrast, homogeneous assays are comprised of only a solution phase and separation of unbound from bound molecules is not possible. One of the advantages of homogeneous DNA-detection is that nucleic acid hybridisation can be monitored in real-time even within a living cell. Furthermore, single closed-tube assays are feasible which reduces the contamination risk and speeds up analysis.

1.4.1 Homogeneous Detection

Homogeneous detection procedures bear higher conceptional expenditures than heterogeneous. Due to the fact that both bound and non-bound probes are present, it is necessary that a measurable characteristic of a reporter group changes upon the transition from the single to the double strand. However, once a homogeneous detection system has been put in to practice, it offers the reward of real time detection. The interest in the real time detection strategies has grown. One reason is the advent of quantitative PCR, a technique, in which the amplified DNA is quantified during the PCR process itself. This approach reduces the number of the work procedures and is thus, more effectively and less error-prone thereby. Common design principles of homogeneous detection methods are summarised below.

Adjacent probes

Most detection chemistry takes advantage of fluorescence resonance energy transfer (FRET) between two chromophores. FRET occurs due to the interaction between the electronic excited states of two dye molecules. The excitation is transferred from one (the donor) dye molecule to the other (the acceptor) dye molecule without emission of a photon. This is distance-dependent, that is the donor and the acceptor dye must be in close proximity. FRET has been used for investigating a variety of biological phenomena that produce changes in molecular proximity. FRET probes are a pair of fluorescent probes placed in close proximity. Fluorophores are chosen such that the emission spectrum of one overlaps significantly with the excitation spectrum of the other. During FRET, the donor fluorophore excited by a light source, transfers its energy to an acceptor fluorophore when positioned in the direct vicinity of the former. The acceptor fluorophore emits light of a longer wavelength, which is detected in specific channels. The light source must not excite the acceptor dye.

The adjacent probe hybridisation system consists of two oligonucleotides labeled with fluorescent dyes.[32] The hybridisation probe pair is designed to hybridize to adjacent regions on the target DNA. Each probe is labeled with a different marker dye. Interaction of the two dyes can only occur when both are bound to their target (Figure 4). The donor probe is labeled with a fluorophore at the 3'- end and the acceptor probe at the 5'- end. During PCR, the two different oligonucleotides

hybridize to adjacent regions of the target DNA such that the fluorophores, which are coupled to the oligonucleotides, are in close proximity in the hybrid structure. The donor fluorophore (F_1) is excited by an external light source, and then passes part of its excitation energy to the adjacent acceptor fluorophore (F_2). The excited acceptor fluorophore (F_2) emits light at a different wavelength which can then be detected and measured.

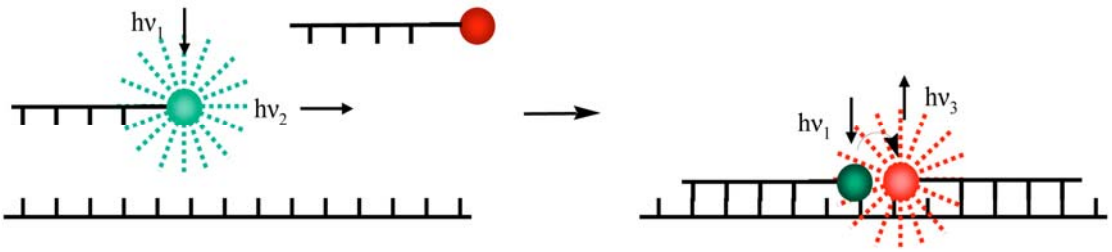

Figure 4: Intermolecular FRET in adjacent/ kissing probes.

Molecular Beacon

Molecular beacons are hairpin-shaped oligonucleotide probes that report the presence of specific nucleic acids in homogenous solutions.[33, 34] When they bind to their targets they undergo a conformational reorganization that restores the fluorescence of an internally quenched fluorophore (Figure 5). Their hairpin conformation enables the use of a wide variety of differently colored fluorophores. Use of several molecular beacons, each designed to recognize a different target and each labeled with a different fluorophore, demonstrated that multiple targets can be distinguished in the same solution, even if they differ from one another by as little as a single nucleotide. A comparison of "hairpin probes" with corresponding "linear probes" confirms that the presence of the hairpin stem in molecular beacons significantly enhances their specificity.

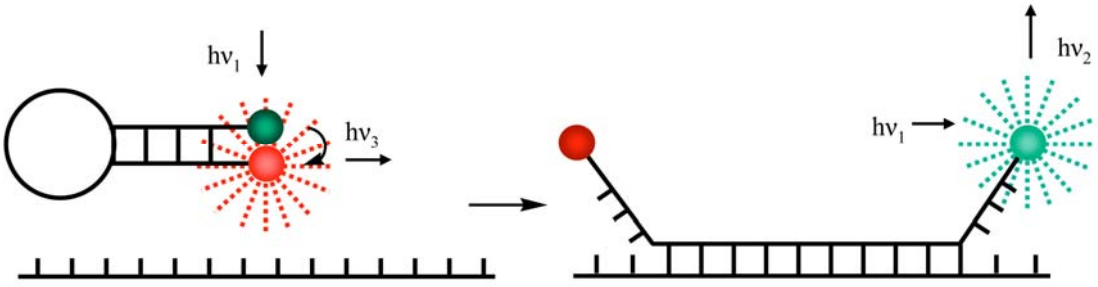

Figure 5: Schematic showing molecular beacons.

Magi probe

In so-called magi probes an intercalator is used as fluorescence acceptor.[35] The fluorophore (**F**) and intercalator (**I**) are positioned internally in the oligonucleotide probe (Figure 6). In this structure, the distance between the fluorophore and intercalator must be close enough to permit direct energy transfer, and the fluorescence of Magi Probe is quenched by the intercalator in the absence of a target sequence. Upon hybridisation, however the probe emits higher fluorescence due to the interference in quenching by intercalation. In addition to the homogeneous assay format for the detection of specific sequences, Magi Probe discriminates single base alterations because its intercalation is less stable with a one-base mismatched duplex than with a perfect matched one, in which the mispair is located close to the intercalator. As a result, the fluorescence intensity in the one-base mismatched duplex is less than that in the perfect matched duplex

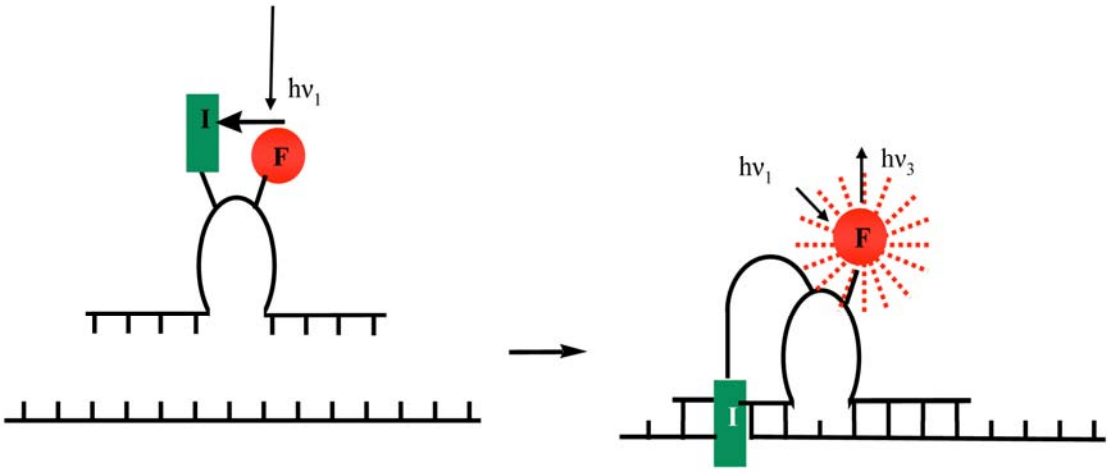

Figure 6: Schematic showing for intercalation of magi probe.

TaqMan assay

TaqMan[36] indicates the probe used to detect specific sequences in PCR products by employing the 5'-->3' exonuclease activity of *Taq* DNA polymerase. The TaqMan probe (generally 20-30 bp), disabled from extension at the 3'- end, and consists of a site-specific sequence labeled with a fluorescent reporter dye and a fluorescent quencher dye (Figure 7). During PCR the TaqMan probe hybridizes to its complementary single strand DNA sequence within the PCR target. When amplification occurs the TaqMan probe is degraded due to the 5'-->3' exonuclease

activity of *Taq* DNA polymerase, thereby separating the quencher from the reporter during extension. Due to the release of the quenching effect on the reporter, the fluorescence intensity of the reporter dye increases. During the entire amplification process this light emission increases exponentially.

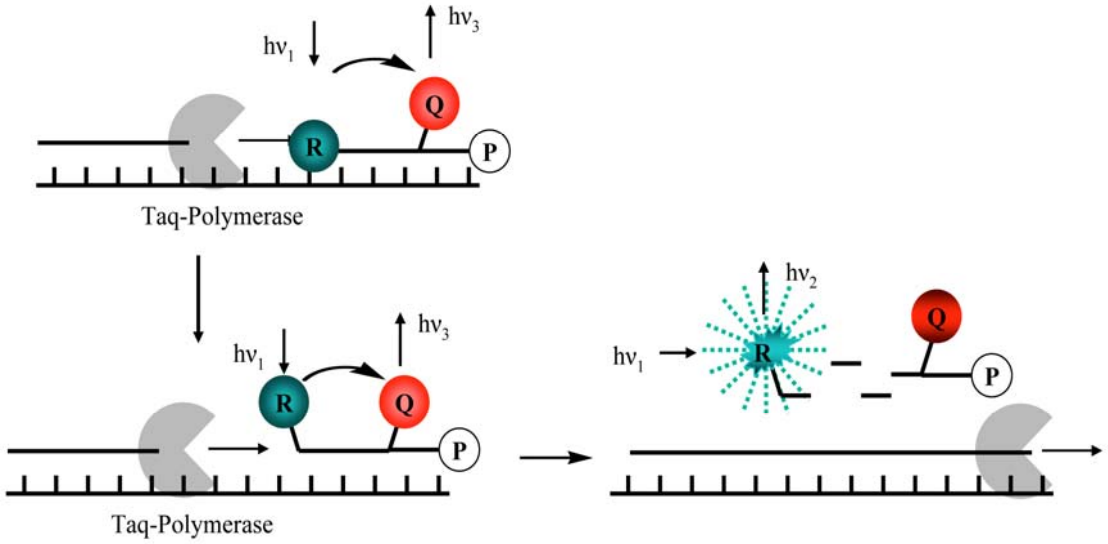

Figure 7: Schematic showing for TaqMan assay.

Scorpion primers

Scorpion primers[37] are bi-functional molecules in which a primer is covalently linked to a probe. The molecules also contain a fluorophore and a quencher (Figure 8). In the absence of the target, the quencher nearly absorbs the fluorescence emitted by the fluorophore. During the PCR reaction, in the presence of the target, the fluorophore and the quencher separate which leads to an increase in the fluorescence emitted. The fluorescence can be detected and measured in the reaction tube. The Scorpion primer carries a probe element at the 5'- end. The probe is a self-complementary stem sequence with a fluorophore at one end and a quencher at the other. The primer sequence is modified at the 5'- end. It contains a PCR blocker at the start of the hairpin loop (Usually HEG monomers are added as blocking agent). In the initial PCR cycles, the primer hybridizes to the target and extension occurs due to the action of polymerase. Scorpion primers can be used to examine and identify point mutations by using multiple probes. Each probe can be tagged with a different flourophore to produce different colours. After one cycle of PCR extension completes, the newly synthesized target region will be attached to the same strand as the probe. Following the second cycle of denaturation and annealing, the probe and the target

hybridize. The denaturation of the hairpin loop requires less energy than the new DNA duplex produced. Consequently, the hairpin sequence hybridizes to a part of the newly produced PCR product. This results in the separation of the fluorophore from the quencher and causes emission.

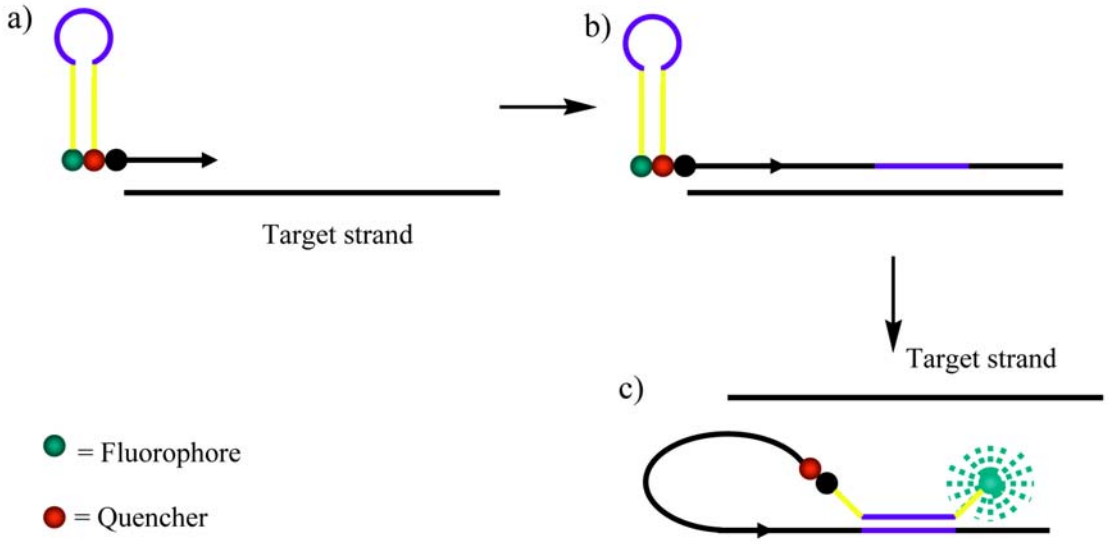

Figure 8: Schematic showing for Scorpion-Primer.

Invader assay

The Invader DNA[38, 39] assay enables simultaneous detection of two different alleles in a bi-allelic system in a non-PCR based assay. Two oligonucleotide probes (an allele specific primary probe and an Invader probe) hybridise in tandem to the target DNA to form a specific overlapping structure. The 5'-end of the primary probe contains a 5'-Flap that is non-complementary to the target DNA and so is unable to hybridise to the target sequence. The 3'-end of the bound Invader probe overlaps the primary probe by a single base this is the site of the allelic variant or SNP.

A cleavase enzyme (Flap endonuclease I) recognises the overlapping structure and cleaves the 5'-Flap on the primary probe at the base of the overlap releasing it as a target specific product. If the probe does not hybridise perfectly at the site of interest no overlapping structure is formed and no cleavage occurs and the target specific product is not released. The reaction consists of two primary probes and two invader probes that are specific to either allele 1 or allele 2 of a bi-allelic system meaning two target specific products are generated. The target specific 5'-Flap oligos's are involved in a secondary reaction where they act as Invader probes on a fluorescent resonance energy transfer (FRET) cassette leading to the formation of an overlapping

structure that is recognised by the cleavase enzyme. When the FRET cassette is cleaved a fluorophore is released form a quencher on the FRET generating a fluorescence signal. There are two signal fluorophores attached to two different FRET cassettes (FRET 1 and FRET 2) that are spectrally distinct and specific to either allele of the bi-allelic system (Figure 9). The ratios of the two fluorescent signals then allow a genotype to be assigned.

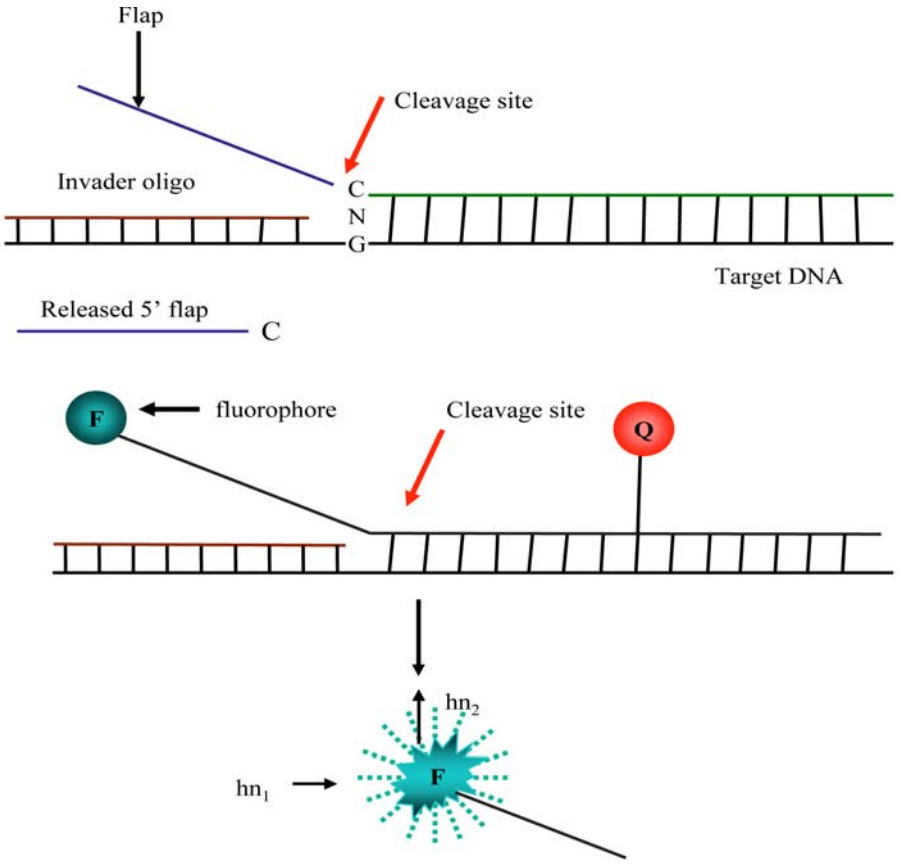

Figure 9: Schematic for Invader assay.

HyBeacons

Hybridisation of HyBeacons[40, 41, 42] to complementary DNA target sequences results in a measurable elevation of probe fluorescence emission. The single nucleotide difference may be discriminated by measuring the T_M of various perfectly matched and single base mismatched duplexes (Figure 10). The FAMCAP (fluorescein-5(6)-amidocaproic acid) was used as fluorophore. The fluorescein was connected to the linker moiety at position 5. The increased fluorescence on hybridization is due to disruption of quenching interactions in the single-stranded probe DNA between the fluorophore and nucleobases. Hybridization leads removing the fluorophore from the immediate vicinity of the DNA bases.

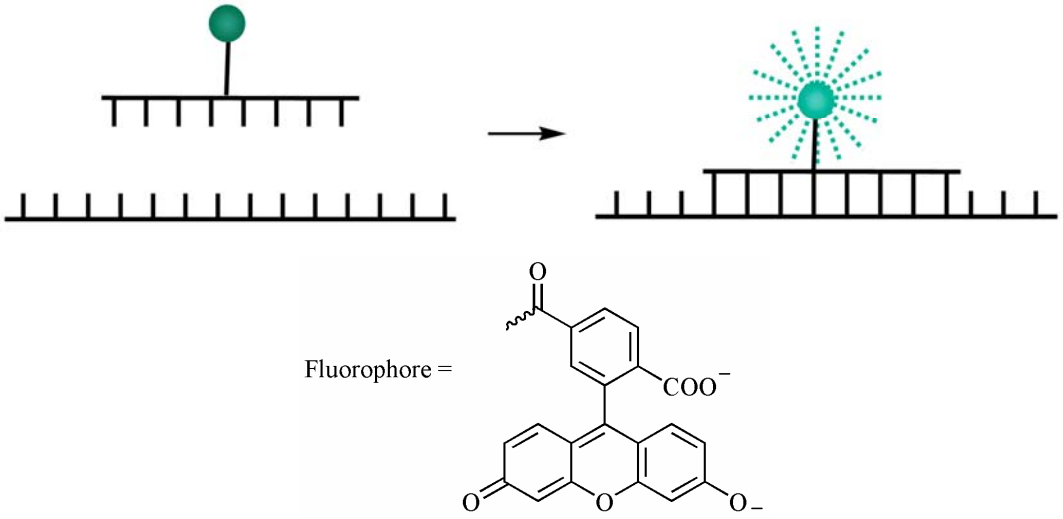

Figure 10: Schematic for HyBeacons probes and structure of attached fluorophore.

Pyrene labelled fluorescent DNA probes

Pyrene labelled base discriminating DNA has been proposed by Isao Saito and co-workers.[43, 44] They developed ^{Py}U and ^{Py}C, which contain pyrenecarboxyamide chromophore connected by a propargyl linker (Figure 11). The fluorophore should be extruded to the outside of the groove, a highly polar aqueous phase, due to base pairing with A/G (matched) exhibiting a strong A/G-base selective fluorescence opposite to ^{Py}U and ^{Py}C. In contrast, when the pyrene fluorophore is intercalated into a DNA duplex due to the lack of base-pairing (mismatched), the labelled base would exhibit no emission due to the location of the fluorophore at a highly hydrophobic site in the groove.

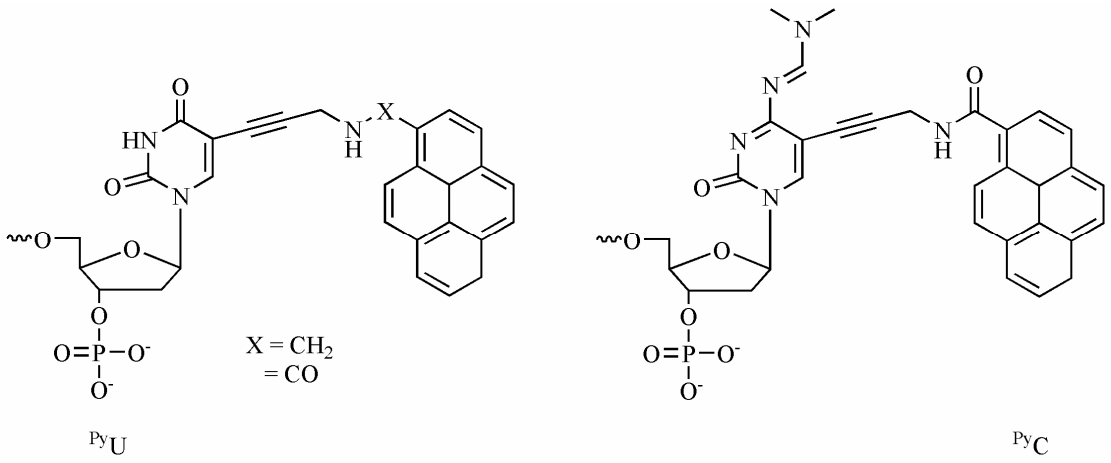

Figure 11: Structure of pyrene labelled ‘U’ and ‘C’ DNA monomer.

Phenanthridinium as an artificial DNA base

Phenanthridinium as artificial DNA base together with DNA-mediated charge transfer process for the detection of base mismatch and abasic site has been reported by Wagenknecht and co-workers.[45] The fluorescence of phenanthridinium moiety is influenced minorly by opposite DNA base as well as the adjacent duplex environment (Figure 12). In this DNA system, base mismatches do enhance the CT efficiency. Changes of fluorescence in this method are not limited to the directly adjacent bases and thus allow scanning a sequence of two base pairs.

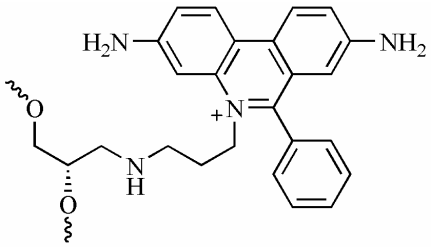

Figure 12: Structure of phenanthridinium labelled DNA monomer.

γ-Substituted PNAs

Synthesis of γ-substituted peptide nucleic acids attached with fluorescent group has been proposed by Daniel H. Appella. The attachment of fluorene labeled thymine PNA residue gives modest increase in fluorescence signals upon binding with complementary DNA (Figure 13). The PNA sequences used are short length and the fluorescent enhancement is poor (4 fold).[46]

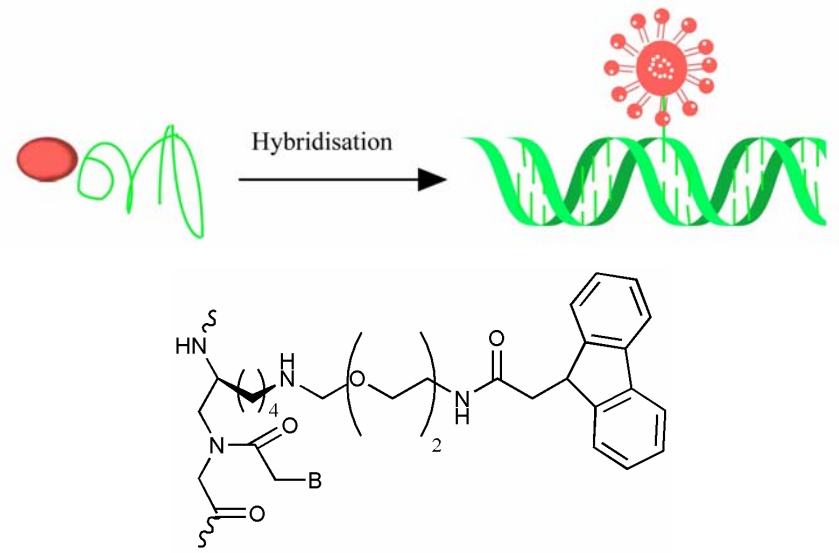

Figure 13: Structure of γ-lysine PNA.

Light-up Probes

The Light-up probes are peptide nucleic acids (PNA) to which the asymmetric cyanine dye thiazole orange (TO) is appended (Figure 14). It combines good hybridisation properties of PNA and the large fluorescence enhancement of TO upon binding to DNA.[47, 48, 49, 50, 51] Free probes have low fluorescence, which is increased upon addition to complementary nucleic acid.

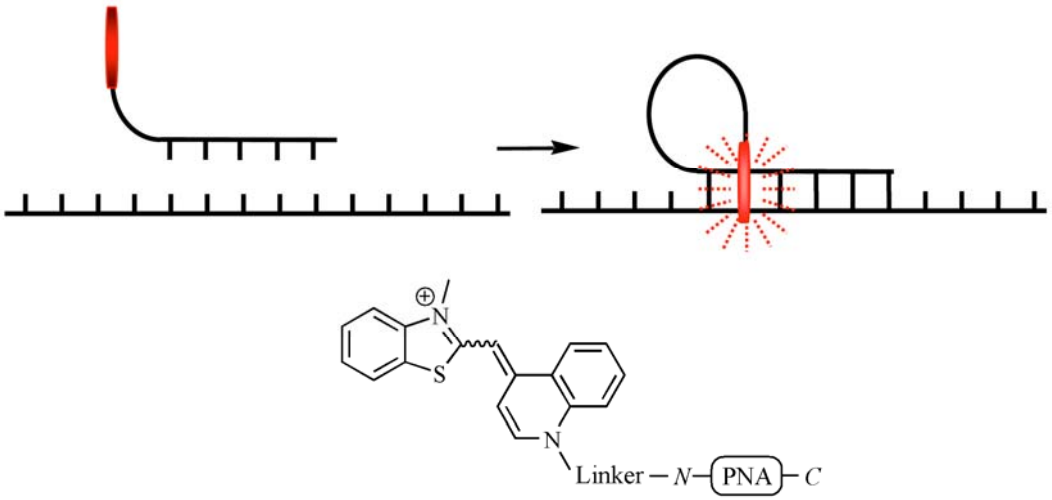

Figure 14: Schematic for Thiazole orange linked Light-up Probes.

Thiazole orange labelled DNA probes

Very recently Ulysse Asseline and co-workers[52, 53] has reported thiazole orange labelled design of terminal-mismatch discriminating fluorescent oligonucleotides. The method is based on the use of sets of oligo-2'-deoxyribonucleotide probes linked *via* their 5'-ends varying-sized flexible polymethylene chains to thiazole orange derivative (Figure 15). The linker is attached to the benzothiazole moiety. Such type of probes upon their hybridization with the target sequence shows good fluorescence discrimination between the matched and the mismatched duplexes. These probes produces high fluorescence with the mismatched duplexes compared to the perfectly matched one. Overall low enhancement of fluorescence upon double strand formation is major disadvantage of these probes.

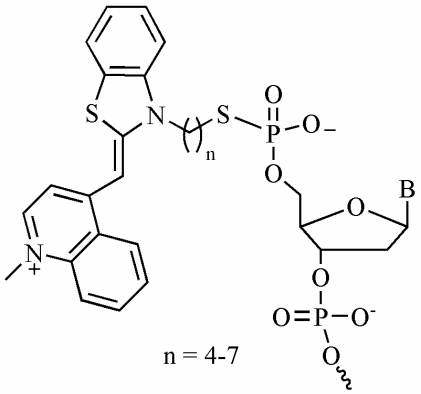

Figure 15: Structures of the linkage and thiazole orange derivative connected to oligo-2'-deoxyribonucleotide conjugates.

FIT-probes

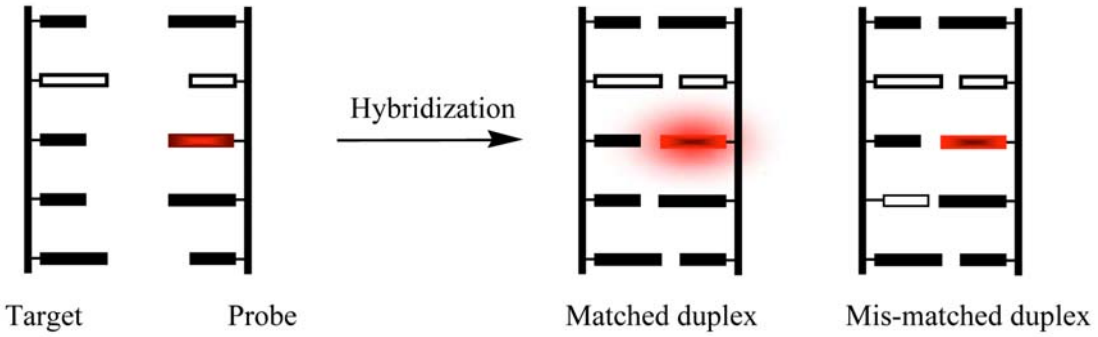

Figure 16: The intercalator dye serves as a base surrogate that is forced to intercalate adjacent to the expected mutation site. The specific positioning renders the fluorophore responsive to matched and mismatched hybridization.

In general above probes contain fluorescent labels that are attached to nucleic acids by linking them through a flexible tether. The linkers are designed to not interfere with the hybridization process. The dyes can adapt to structural changes upon local alterations of duplex structure, such as formation of mismatched base pair. The replacement of central nucleobase of PNA by thiazole orange affords FIT-PNA (Forced Intercalation of Thiazole orange) FIT-probes (Figure 16). Thiazole orange in FIT-probes due to the use as base surrogate is restricted in its conformational flexibility. Such probes are found useful for the homogeneous analysis of single-base mutations. FIT probes are specific probes which fluoresce upon hybridisation with matched DNA and gives attenuated fluorescence with mismatched DNA (Figure 16). Previous work by Olaf Köhler[54] exposed the importance of linker length and mode of attachment of TO-derivative to PNA backbone.[55] He found that PNA in which thiazole orange was linked as a base surrogate through an acetyl tether to the

quinoline ring exhibited a superior fluorescence behavior when compared with other studied linkers.

Lars Röglin in his work towards diploma thesis has replaced the aminoethylglycine backbone by both L- and D-ornithine.[56] He synthesised backbone modified FIT-PNA by divergent synthesis using Fmoc/Alloc-protected L- or D-ornithine building block (Figure 17). The ornithine FIT-PNA was also successful to discriminate matched and mismatched DNA with added advantage of confirming higher fold fluorescence enhancements and higher match/mismatch discrimination than Aeg FIT-PNA.

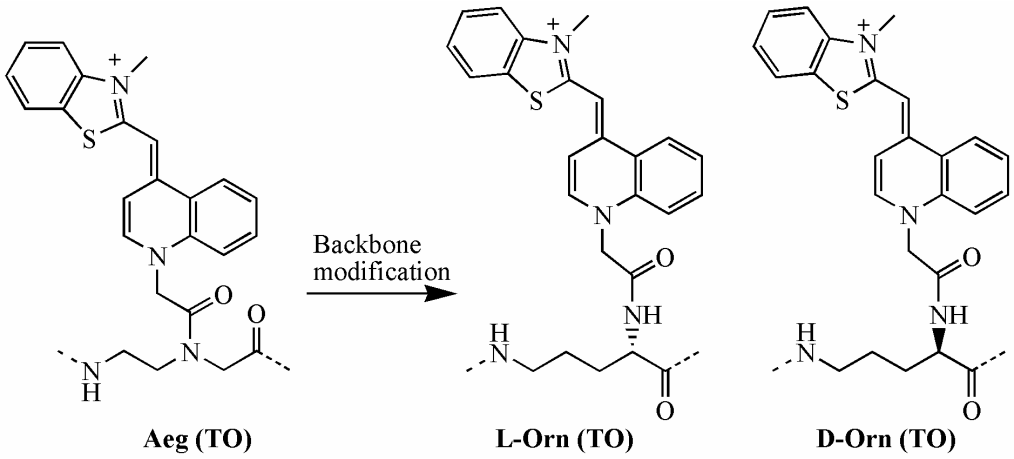

Figure 17: Structure of modified backbone of Aeg (TO)

1. 5 Objectives

This thesis was undertaken to explore the suitability of thiazole orange labelled PNA as tool in mutational analysis. The primary objectives of this work were:

1) Development of a convenient and fast synthetic route for PNA containing thiazole orange coupled as base surrogates to aminoethylglycine and ornithine backbones.

2) The screening for favoured and disfavoured TO pairing partners and preferred adjacent bases to obtain high hybridisation induced fluorescence enhancements and high fluorescence based match/mismatch discrimination.

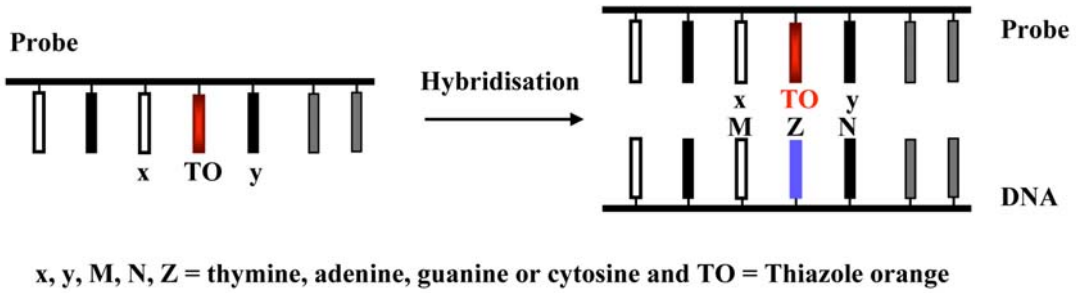

Figure 18: FIT-PNA before and after hybridisation varying stacking and pairing bases for thiazole orange.

3) To explore other cyanine dyes of the thiazole orange family as PNA base surrogate in order to extend the repertoire of colours.

4) To explore dual labelling of two thiazole orange dyes as PNA base surrogates. Dual labelled PNA may improve fluorescence signalling if two dyes are placed adjacent to the base mismatches. Two chromophores may come in contact in the single stranded form and in mismatched duplexes resulting in changes of fluorescence properties which could enable higher match/mismatch fluorescence discrimination than FIT-PNA.

5) In order to investigate the difference between terminal labelling via flexible tethers and internal labelling by means of base surrogate, it was decided to compare FIT-PNA with Light-up PNA.

2. Solid-phase synthesis and evaluation of PNA containing thiazole orange as fluorescent base surrogate attached to aminoethylglycine.

Many intercalator dyes have fluorescence properties that allow distinction between the presence of single stranded and double stranded DNA.[57] Oligonucletotide probes linked *via* a flexible spacer to intercalator dyes have been shown to signal hybridisation and are therefore suitable for homogeneous DNA-detection.[48, 58, 59] Previous studies in our group have shown probes in which an intercalator dye is linked by replacing an internal nucleobase rather than by hanging from a flexible tether. These PNA-based FIT-probes profit from the added advantage of being responsive to structural perturbations such as those imposed by single base mismatches.[54]

2.1 Synthesis

PNA synthesis is performed by employing solid-phase strategies that allow the automation of the repetitive process of protecting group removal and building block coupling. Most commonly, the Fmoc group is used as temporary protecting group while the acid-labile benzyhydryloxycarbonyl (Bhoc) group is used for permanent protection of the exocyclic amino groups of nucleobases. There are two different approaches for the synthesis of TO-PNA, divergent and linear solid-phase synthesis.

2.1.1 Divergent solid phase synthesis

Divergent solid-phase synthesis was considered as useful for accelerating the identification of a suitable thiazole orange derivative since one polymer bound oligomer can be subjected to coupling reactions with different chromophores. It was decided to use the Fmoc/Alloc protected building block Fmoc-Aeg (Alloc)-OH. Previous work by Olaf Köhler[55] has shown that the Alloc-group can be removed on resin. The liberated secondary amino group in (Scheme 2) serves to introduce the

thiazole orange chromophore (Scheme 2). Mild acidolysis release the desired PNA-TO conjugate **4**.

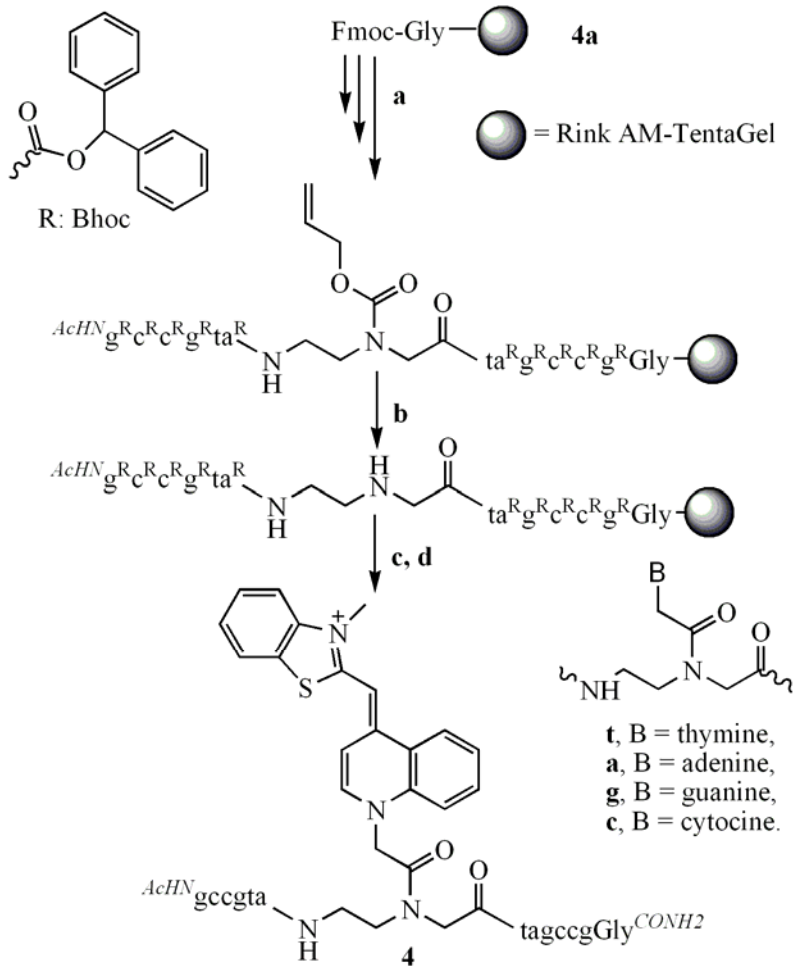

Scheme 2: a) Cycle of 1) piperidine/ DMF; 2) Fmoc–B (Bhoc)–OH or Fmoc-Aeg (Alloc)-OH, NMM, PyBop, NMP; 3) Ac_2O/ lutidine, DMF; b) $[Pd(PPh_3)_4]$, $Me_2NH{\cdot}BH_3, CH_2Cl_2$; c) TO-$CH_2$-COOH, PyBOP, PPTS, NMM, DMF (double coupling); d) TFA, m-cresol, H_2O, L-Cys-OMe, 8.8 % overall yield.

2.1.2 Linear solid phase synthesis

After a suited dye had been identified[55] it was considered more convenient to apply preformed TO-containing monomers in standard linear solid phase synthesis. This protocol is easier to automate than the divergent synthesis. The linear route is explored by employing Fmoc-Aeg (TO)-OH monomer **3b** (see Scheme 3) as preformed building block in the synthesis of PNA–TO conjugate **4**.

2.1.3 Synthesis of Fmoc-Aeg (TO)-OH

Synthesis of PNA monomer **4** containing TO **3b** as fluorescent base surrogate is shown in Scheme 3. It was first attempted to couple TO derivative **1** to the free amino group of reported Fmoc-AegO*t*Bu[60] **2a**. Neither the pivaloyl chloride[61] mediated coupling used in standard PNA monomer synthesis nor the optimized PyBOP[62] coupling protocol gave access to product **3b**. However, the difficult coupling succeeded in 62 % yield after replacement of the *t*Bu ester by the sterically less demanding allyl ester in **2b** and usage of PyBOP as coupling reagent. Finally, the allyl protecting group in **3a** was removed by Pd(0)-catalyzed allyl transfer to *N*-methyl aniline[63] which afforded the TO–PNA monomer **3b** in 73 % yield.

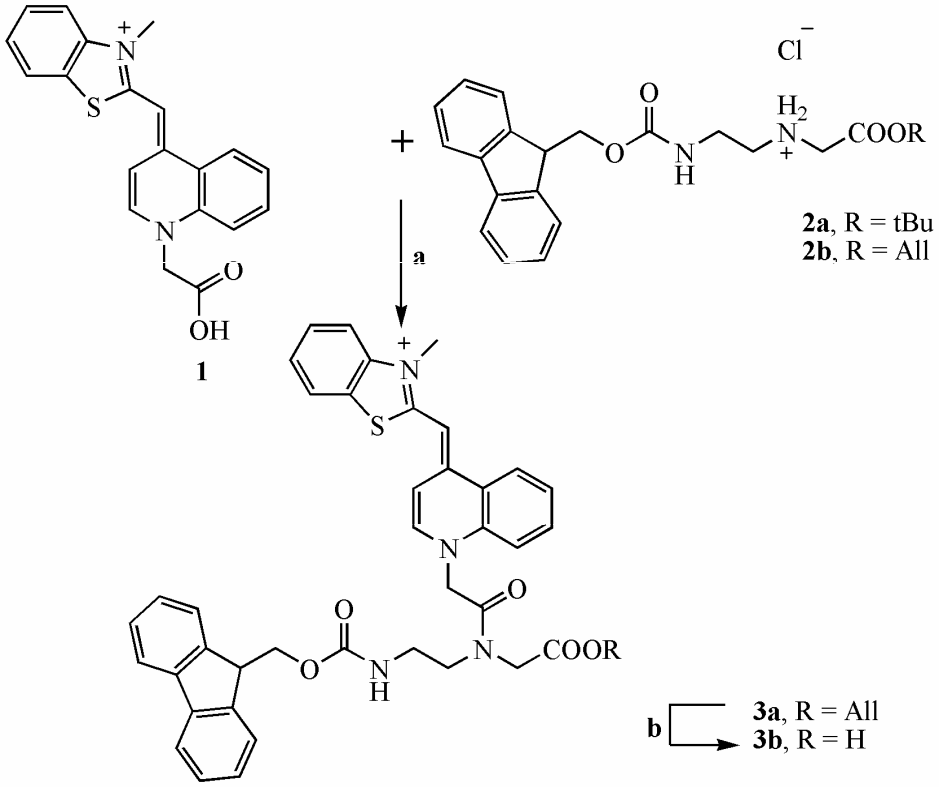

Scheme 3: a) 1, PyBOP, PPTS, NMM, DMF, 62 %; b) [Pd (PPh_3)$_4$], $PhNHCH_3$, THF, 73 %.

The linear solid-phase synthesis was performed with an automated synthesizer. The Fmoc-protected PNA resin **4a** was assembled first by using 4 eq. of PNA monomer and HCTU (3.8 eq.) as coupling reagent in the presence of *N*-methyl morpholine (8 eq.) in NMP as solvent (Scheme 4). For the introduction of the Fmoc-Aeg (TO)-OH monomer **3b** as well as for the subsequent building block double

couplings were performed. PPTS (Pyridinium-*p*-toluolsulfonic acid) was added to the coupling mixture to increase the solubility[64] of **3b**. After completion of the linear building block assembly, a final TFA treatment liberated PNA–TO conjugate **4**.

HPLC analysis of crude **4** and comparison with material obtained by the divergent approach (Figure 19) suggests that the purity of crude PNA–TO samples produced by the linear solid phase synthesis is higher than the purity of crude material furnished by the divergent solid-phases synthesis. As a result, purification was easier to perform. The overall yields achieved by linear solid-phase synthesis were comparable to the yields reached in the divergent synthesis (9 % in linear synthesis vs. 8 % in divergent synthesis). HPLC traces and MALDI-TOF mass spectrometry[65] of purified material attested to the purity and molecular mass of **4** (Figure 19).

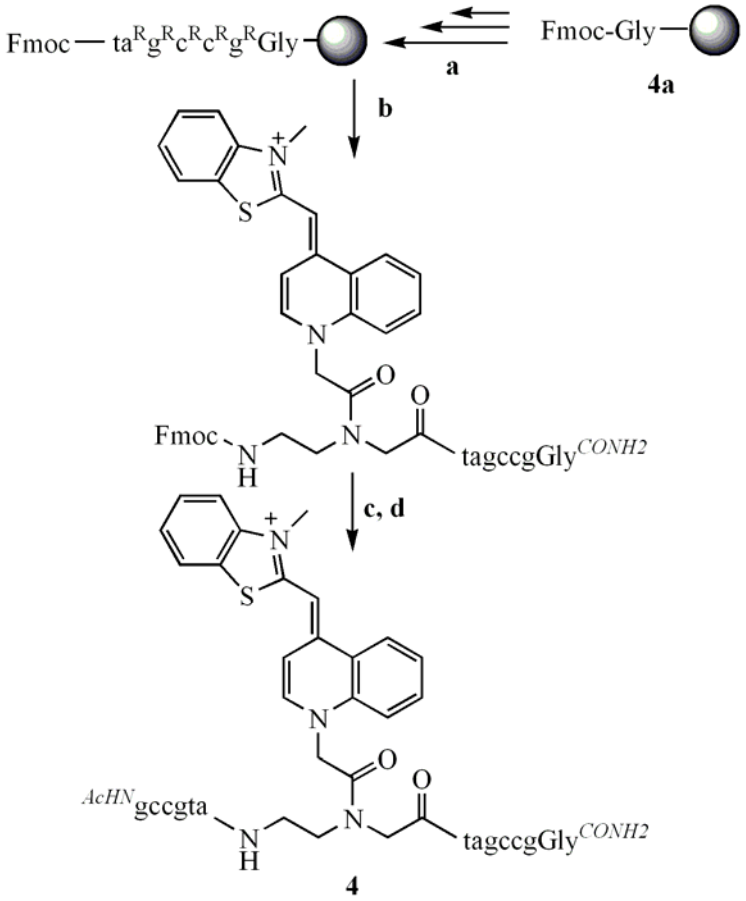

Scheme 4: a) Cycle of 1) piperidine/ DMF; 2) Fmoc-B (Bhoc)-OH, NMM, HCTU, NMP; 3) Ac_2O/ lutidine, DMF; b) cycle of 1) piperidine/ DMF; 2) Fmoc-Aeg (TO)-OH, HCTU, NMM, PPTS, NMP (double coupling); 3) Ac_2O/ lutidine, DMF; c) cycle of 1) piperidine/ DMF; 2) Fmoc-B (Bhoc)-OH, NMM, HCTU, NMP; 3) Ac_2O/ lutidine, DMF; d) TFA, m-cresol, H_2O, L-Cys-OMe, 9 % overall yield.

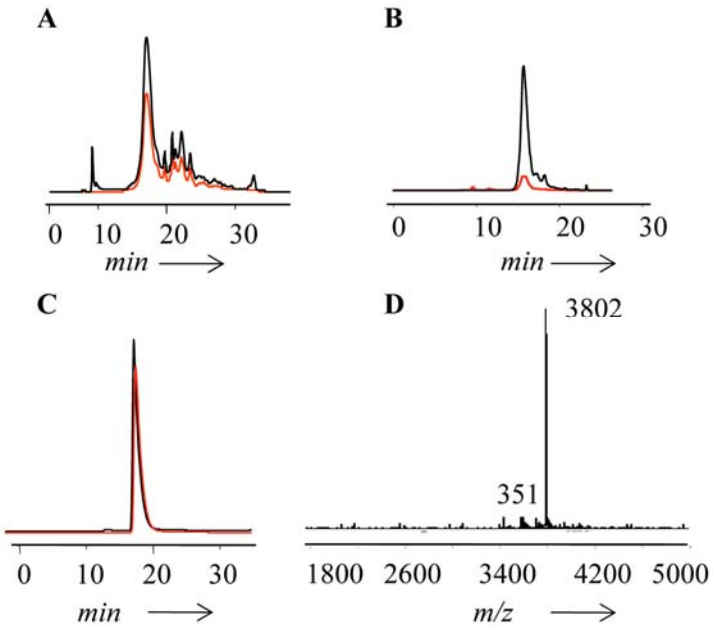

Figure 19: Crude HPLC traces of probe **4** obtained by A) divergent solid-phase synthesis, B) linear soild-phase synthesis; and C) clean HPLC trace of probe **4** obtained by linear solid-phase synthesis and D) MALDI-TOF-MS of purified probe **4** [HPLC conditions: flow: 6 mL/ min; gradient: 0–1 min: 3 % MeCN (0.1 % TFA) in H_2O (0.1 % TFA); 1-25 min: 3-30 % MeCN (0.1 % TFA) in H_2O (0.1 % TFA)].

In the comparison to the divergent solid-phase synthesis the linear approach was found to bear advantages as far as the rapidity of synthesis is concerned. Furthermore, the linear solid-phase synthesis provided crude materials of higher purity. Linear solid-phase protocols are easier to automate. The synthesis of preformed Fmoc-Aeg (TO)-OH monomer enables routine access to PNA oligomers containing TO as fluorescent universal base.

2.2 Fluorescence and Melting Study of PNA-TO

Thiazole orange has low fluorescence in free form[66] but is rendered highly fluorescent upon intercalation into DNA. Köhler and Seitz have found that hybridisation of TO-PNA probes also results in TO fluorescence enhancements that could enable homogeneous DNA detection.[54] The TO-PNA **4** (a-TO-t) was hybridised to perfectly matched and single base mismatched oligonuclotides.

2.2.1 Fluorescence Study

Figure 20 shows fluorescence spectra of TO-PNA **4** before and after hybridisation with matched and single base mismatched DNAs **4ZY'** (**TT, TA, TG** and **TC**). It became apparent that duplex formation was accompanied by a shift of the emission maximum from 533 nm to 527 nm. Such hypsochromic shifts have been observed in other intercalation experiments.[67] The binding event led to substantial increases in fluorescence intensity.

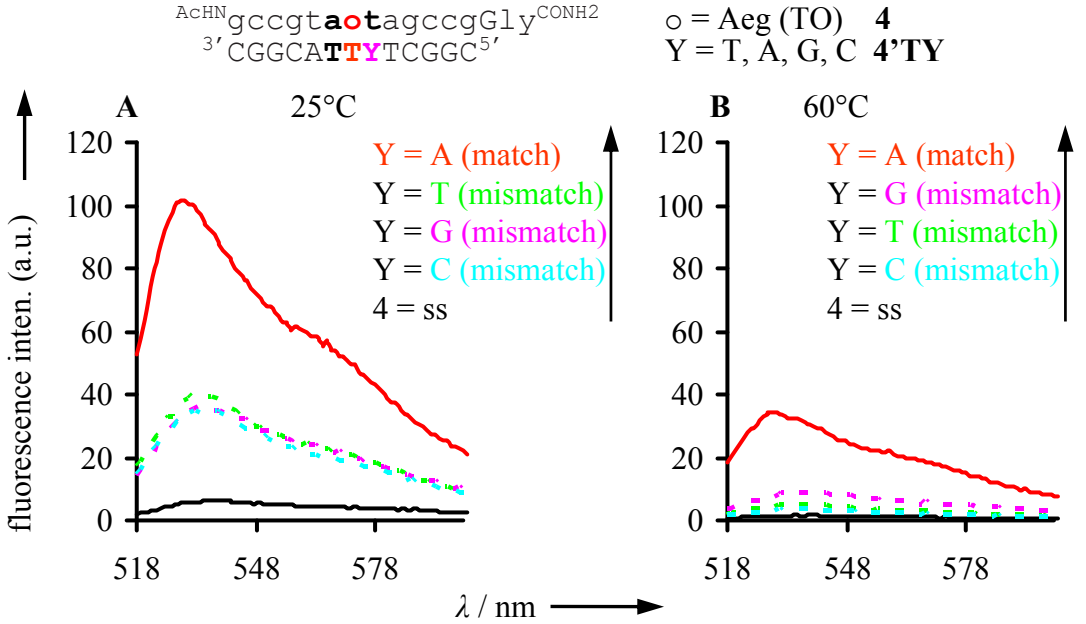

Figure 20: Fluorescence spectra of PNA probe **4** A) 25°C, B) 60°C before (black) and after addition of matched and mismatched DNA [red = matched, dotted lines = mismatched towards C-side. (Y = T green, G pink and C turquoise) with thymine as pairing partner for Aeg-TO]. Measurement conditions: Ex. 510 nm, Em. 518-600 nm. Ex. Slit: 5 nm and Em. Slit: 2.5 nm.

Figure 21 presents fluorescence enhancement of probe **4** upon hybridisation to DNA featuring varying pairing partners and stacking partners of embedded TO. The emission of duplexes **4•4'GA** and **4•4'TA** in which TO was paired against guanine and thymine was 14 and 19 fold higher than the emission of the single stranded probe **4**. Binding opposite to adenine **4•4'AA** and cytosine **4•4'CA** increased TO fluorescence by factors of 11 and 12 fold, respectively. The TO fluorophore is located at a specific site within the **TO-PNA•DNA** duplex. Hence, it is possible that the TO fluorescence is responsive to localised perturbations of the duplex structure such as

imposed by an adjacent base mismatch. Indeed, the emission of duplexes (**4•4'TY,** Y = T, G and C) that contained t-T, t-G and t-C mismatches was 3.1, 3.0 and 2.6 fold lower than emission of matched duplex (**4•4'TA**) when measured at 25°C. The TO-PNA fluoresces 14 fold (match, **4•4'AY**) and 5.8, 7.8, 4.9 fold higher when t-T, t-G and t-C (mismatch), respectively, than single stranded PNA when adenine is opposite to TO.

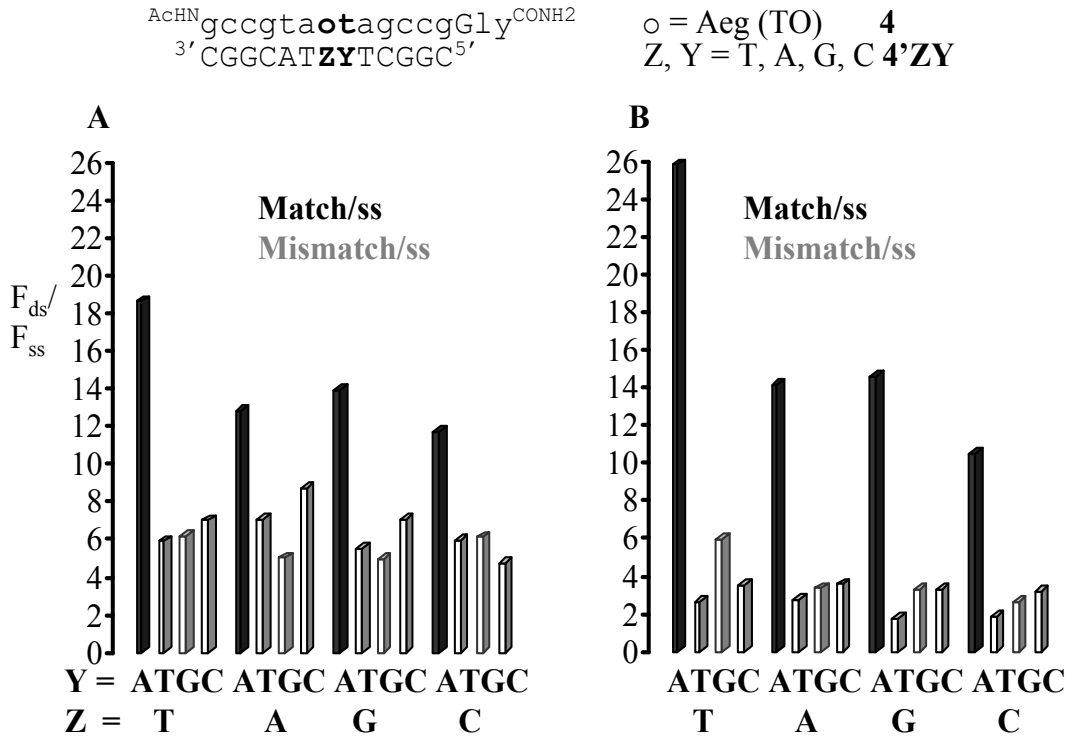

Figure 21: Fluorescence enhancement F_{ds}/F_{ss} of PNA probe **4** measured at 530 nm after formation of match duplexes (black columns) and mismatch duplexes (white columns) at A) 25°C and B) 60°C. F_{ss} = fluorescence intensity of the PNA single strand, F_{ds} = fluorescence intensity after addition of DNA **4' (TY, AY, GY** or **CY)**. [Measurement conditions: 1µM probe and DNA in buffer (100 mM NaCl, 10 mM NaH_2PO_4, pH 7), excitation: 510 nm].

Figure 21B shows the results of fluorescence measurement at 60°C. Matched hybridisation at elevated temperature (60°C) was accompanied by almost unchanged (Z = C, G) or even increased fluorescence enhancement (Z = A, T) in comparison to the results obtained for hybridisation at 25°C. At 60°C hybridisation to **4•4'TA** increased the fluorescence by factor of 26 as opposed to 19 fold fluorescence enhancement at 25°C. In contrast, increases of temperature led to reduced fluorescence enhancement upon mismatched hybridisation. As a result, hybridisation

at elevated temperature allowed better discrimination between matched and single mismatched targets. For example, the fluorescence emission of probe **4** in the presence of the single mismatched target **4'CT** (Figure 21), as opposed to a threefold stronger fluorescence enhancement upon matched hybridisation at 25°C. This enhanced match/mismatch discrimination can be explained by the reduced thermal stability of the mismatched duplex which is 11°C lower when compared with the T_M value of the matched duplex (Table 1).

2.2.2 Thermal analysis:

Figure 22 shows absorbance curves vs. temperature of the perfectly matched DNA•DNA (**4'AT•4'TA**) duplex (black), PNA•DNA (**4at•4'TA**) duplex (grey), and TO-PNA•DNA (**4•4'TA**) duplex (red). The melting curves showed sigmoidal behaviour in all cases which indicates co-operative base pairing. In PNA•DNA duplexes **4•4'ZA** (**Z = T, A, G, C**) TO was paired against each of the four nucleobases. The DNA•DNA duplex shows 53°C T_M. The FIT-PNA•DNA duplex shows T_M = 68°C. The T_M = 69°C provided by PNA•DNA duplex **4at•4'TA** reveals that the replacement of adenine by TO reduces duplex stability by only 1°C.

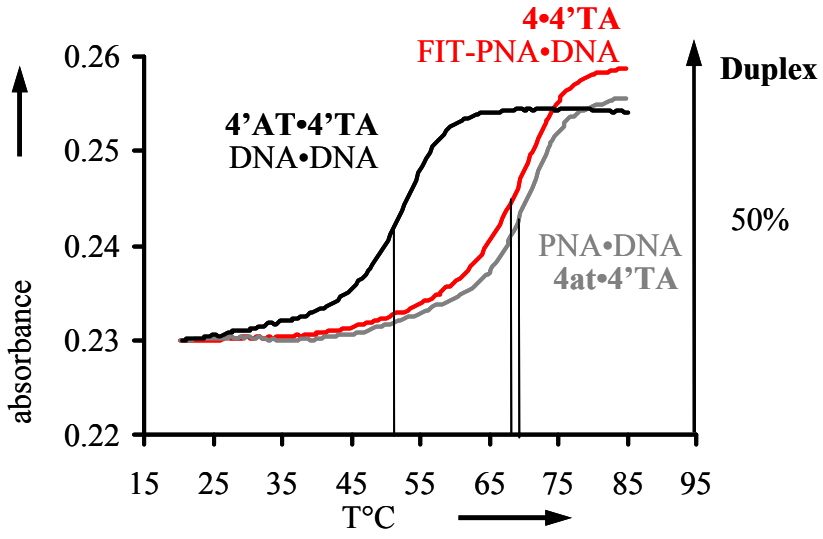

Figure 22: Melting curves of a DNA•DNA (black), PNA•DNA (grey) and FIT-PNA•DNA (red) double strand. (**4** = ^{AcHN}gccgta**TOt**agccgGly^{CONH2}, **4at** = ^{AcHN}gccgta**at**agccgGly^{CONH2}, **4'AT** = $^{5'}$CGGCAT**TA**T CGGC$^{3'}$ and **4'TA** = $^{3'}$GCCGTA**AT**AGCCG$^{5'}$).

This suggests that within studied sequence **4,** pairing of TO against T, A, G and C is almost as efficient in duplex stabilisation as pairing of A against T. The decreased T_M values (ΔT_M = 11, 9, 11 and 14°C, respectively) observed with duplexes **4•4'TC, 4•4'AC, 4•4'GC,** and **4•4'CC** revealed that probe hybridisation was sequence selective irrespective of the identity of the TO pairing partner (Table 1). The ΔT_M value of 15°C determined when comparing the thermal stability of matched and mismatched duplexes **4at•4'TA** and **4at•4'TC** suggested that hybridisation of unchanged PNA **4at** is slightly more selective than hybridisation of TO-containing PNA **4**.

Table 1: T_M data of thiazole orange containing PNA•DNA duplexes

^{AcHN}gccgtaotagccgGly^{CONH2} $^{3'}$CGGCAT**ZY**TCGGC$^{5'}$	o = Aeg (TO), 4'**Z**Y = **T**A/ C, **A**A/ C, **G**A/ C, **C**A/ C				
o-ZY	TO-TA	TO-AA	TO-GA	TO-CA	A-TA
T_M/ °C[a]	68	67	68	68	69
o -ZY	TO-TC	TO-AC	TO-GC	TO-CC	A-TC
T_M/ °C[a]	57	58	57	54	54

[a] Measured as denaturation curves at 1 μM concentration in a buffered solution (100 mM NaCl, 10 mM NaH_2PO_4, pH = 7).

In conclusion, thiazole orange is able to confer universal PNA–DNA base pairing while maintaining duplex stability. The replacement of a central nucleobase with thiazole orange afforded a PNA probe that fluoresced upon hybridisation. The sensitivity of thiazole orange fluorescence to a neighbouring base mismatch suggests that it might be possible to distinguish a DNA target from its single base mutant by avoiding the usual need for stringent hybridisation conditions.

2.3 Sequence Dependent Fluorescence of Aeg-TO-PNA (dye-nucleic acid conjugates)

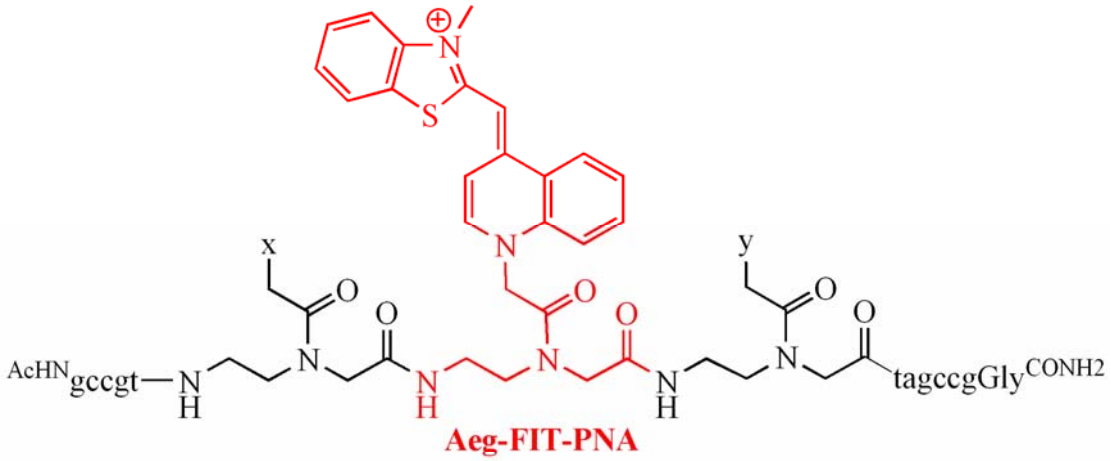

5;[x:y] = tt, 6;[x:y] at, 7;[x:y] = gt, 8;[x:y] ct,
9;[x:y] = ta, 10;[x:y] aa, 11;[x:y] = ga, 12;[x:y] ca,
13;[x:y] = tg, 14;[x:y] ag, 15;[x:y] = gg, 16;[x:y] cg,
17;[x:y] = tc, 18;[x:y] ac, 19;[x:y] = gc, 20;[x:y] cc.

Scheme 5: Structure of Aeg (TO)-OH labeled peptide nucleic acids library.

The interesting fluorescence properties of the 'thiazole orange base' called for a more detailed analysis of fluorescence in different sequence contexts. To explore the influence of thiazole orange stacking and pairing partners, sixteen PNA-probes were produced by linear or divergent synthesis. The bases (x) on the N'-terminal and the bases (y) on the C'-terminal side of thiazole orange were varied (Scheme 5). The 16 probes were hybridised to oligonucleotide **5'-20'MZN** such that TO was paired against base Z of the target strand and flanked by each possible base pairs. Fluorescence emission at 25°C was recorded. The stability of each of possible match duplex was measured. Accordingly, TO in between all possible bases and with all possible opposite targets was studied. This investigation exposed the influence of opposite TO partner bases and stacking partners on the fluorescence properties of TO.

Scheme 6: Aminoethylglycin-TO-PNA probes **5-20** and DNA's **5'-20'** (MZN) which were allowed to hybridise with differing by pairing partner, stacking partners to N-side and C-side of thiazole orange.

2.3.1 Matched Hybridization

Figure 23 shows the fluorescence enhancement of TO-PNA conjugates after formation of matched duplexes with complementary oligonucleotides in which thiazole orange was paired against all four DNA bases (Z = T, A, G and C).

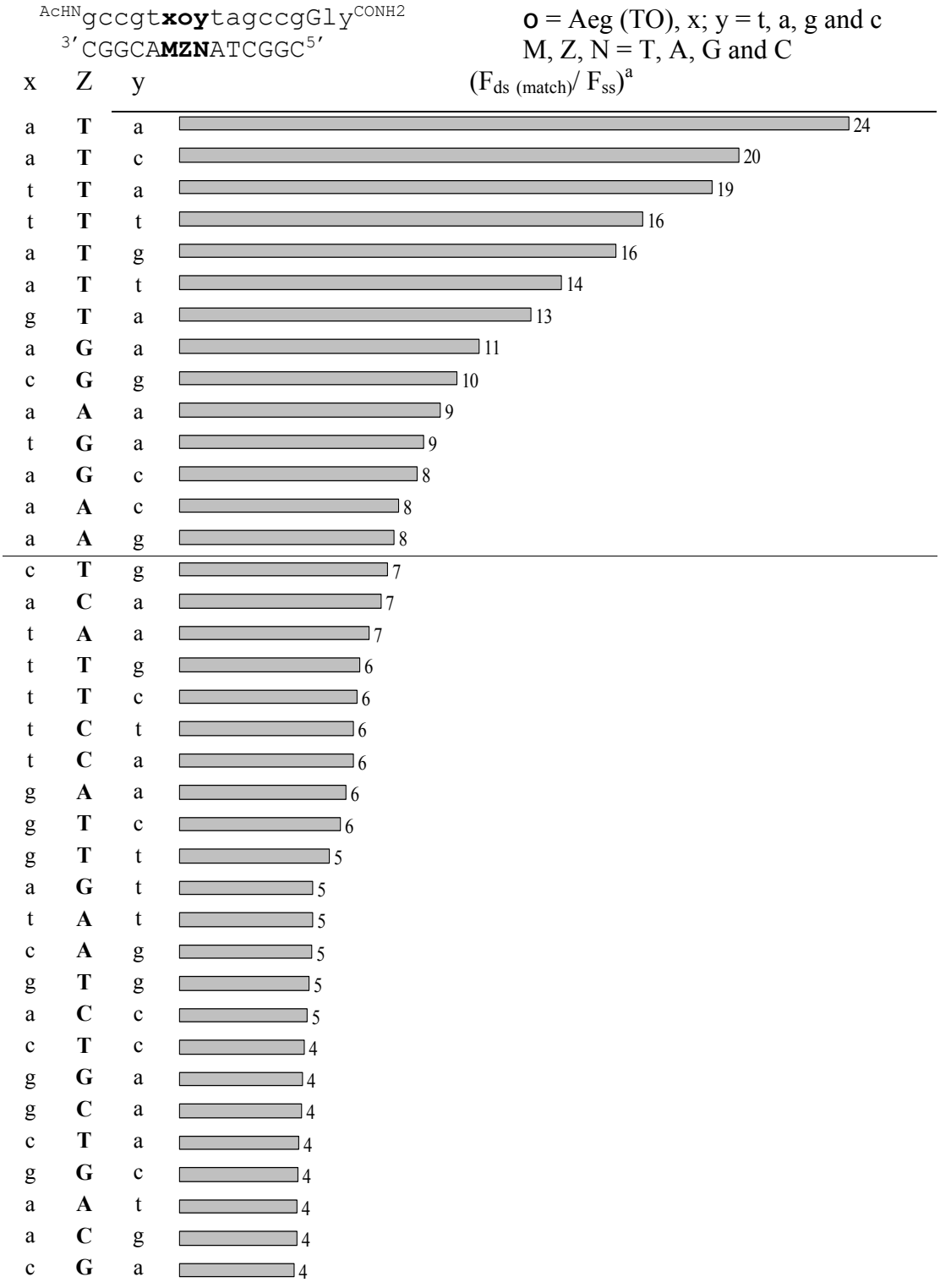

^{AcHN}gccgt**xoy**tagccgGly^{CONH2}
$^{3'}$CGGCA**MZN**ATCGGC$^{5'}$

o = Aeg (TO), x; y = t, a, g and c
M, Z, N = T, A, G and C

x	Z	y	($F_{ds\ (match)}$/ F_{ss})[a]
t	**G**	t	4
a	**C**	t	4
a	**C**	g	4
g	**A**	c	4
g	**C**	g	4
c	**G**	c	3
t	**A**	g	3
g	**G**	g	3
t	**G**	c	3
c	**C**	a	3
g	**G**	t	3
t	**C**	c	3
c	**A**	c	3
t	**C**	g	3
c	**A**	a	2
g	**C**	t	2
g	**A**	g	2
t	**A**	c	2
t	**G**	g	2
c	**T**	t	2
c	**C**	c	2
g	**C**	g	2
g	**A**	t	2
a	**G**	g	2
c	**C**	t	1
c	**G**	t	1
c	**A**	t	1

Figure 23: Fluorescence enhancement of PNA probes **5-20,** measured at 530 nm after formation of matched duplexes, when TO was paired against thymine, adenine, guanine and cytosine at 25°C in buffer. [^{a} F_{ds}/ F_{ss} = Ratio between fluorescence intensities of FIT-PNA after and before addition of DNA at 530 nm. Measurement conditions: 1µM probe and DNA in buffer (100 mM NaCl, 10 mM NaH_2PO_4, pH 7), excitation: 510 nm].

Discussion

The sequence dependent fluorescence of Aeg-TO-PNA conjugates after formation of matched duplexes shows interesting fluorescence effects depending upon TO neighbouring, stacking and pairing bases. Figure 23 shows relative fluorescence increase upon formation of matched duplex in descending order (top-bottom). The letters x and y are for adjacent nucleobases for TO in PNA probe from N'-side to C'-side respectively. Thiazole orange was forced to intercalate between all possible nucleobases. The M and N are complementary DNA bases to neighbouring

nucleobases (x-y) of forced thiazole orange. Among 64 matched duplexes highest fluorescence enhancement (23.8 fold) was measured for probe **10** (a-TO-a) upon duplex formation with DNA when thymine was acting as pairing partner for TO. No change in fluorescence was recorded for three duplexes of probe **8** (c-TO-t) after addition of match DNA with adenine, guanine or cytosine as pairing partner for TO. The FIT-PNA probes can be classified into good probes ≥ 8 fold, mediocre probes ≥4 to <8 fold and modest probes < 4 fold. It is important to note that the results of this study are valid only with the given sequence.

The probe **10** (a-TO-a) was found best as far as fluorescence enhancement is concerned. Altering pairing partners of TO as thymine, adenine and guanine after formation of matched duplex with probe **10** produces, 23.8, 9.3 and 10.6 fold fluorescence enhancements, respectively. The second best base pair environment was seen in probe **18** (a-TO-c), which gives 19.9 fold fluorescence enhancements with match DNA when thymine acts as pairing partner for TO.

In this library 14 duplexes (22 % probes) are able to produce fluorescence enhancement greater or equal to 8 fold. All but one of these probes place TO between AT base pairs. That means 93 % of well performing probes have at least one A or T as TO stacking partner. 50 % within this probe section have T as a TO pairing partner. C as pairing partner is not found in the good category.

More than four fold and less than 8 fold fluorescence enhancement at 530 nm was achieved in 28 duplexes (44 %). Less than 4 fold fluorescence enhancement was observed in 22 (34 %) hybridisation experiments. Virtually no fluorescence enhancement was seen in probes that featured TO between c and t. All modest probes have at least one GC pair as TO stacking partner. Only one provides A as intrastrand TO stacking partner. Thymine, which was identified as preferred pairing partner in probes providing high fluorescence enhancement occurred in seven duplexes in the modest "< 4 fold enhancement" category.

The collected data from fluorescence spectroscopy at 25°C showed that highest fluorescence enhancements are obtained upon formation of duplexes that contain at least one a-T base pair as TO stacking partner. Thymine and guanine seem to be the preferred TO pairing partners. Only one duplex gives less than 4 fold fluorescence enhancement when thymine was pairing partner for TO.

Average fluorescence increase with one adenine as intrastrand TO stacking partner is 8.8 fold. Enhancement of 4.4 fold, 4.6 fold and 5.5 fold were obtained with c, g and t

respectively, as stacking partner. Average fluorescence increase when at least one AT base pair acts as stacking partner for TO was measured 6.9 fold. It was recorded 4.9 fold if at least one GC base pair acts as TO stacking partner. The average fluorescence increase when TO is against T, A, G or C was measured 10.4, 4.3, 4.7 and 3.7 fold, respectively. It hence, appears that for the studied sequence context both TO pairing partner and stacking partner are important for achieving high hybridisation-induced fluorescence enhancements.

2.3.2 Fluorescence vs. Temperature study upon hybridization with matched oligonucleotides

In applications hybridisation experiments will be performed at various temperatures. For example live cell imaging will be performed between 20-40°C. DNA detection in real time PCR is done during the annealing step between 50-70°C. It is, hence, important to study the response of TO fluorescence as a function of temperature.

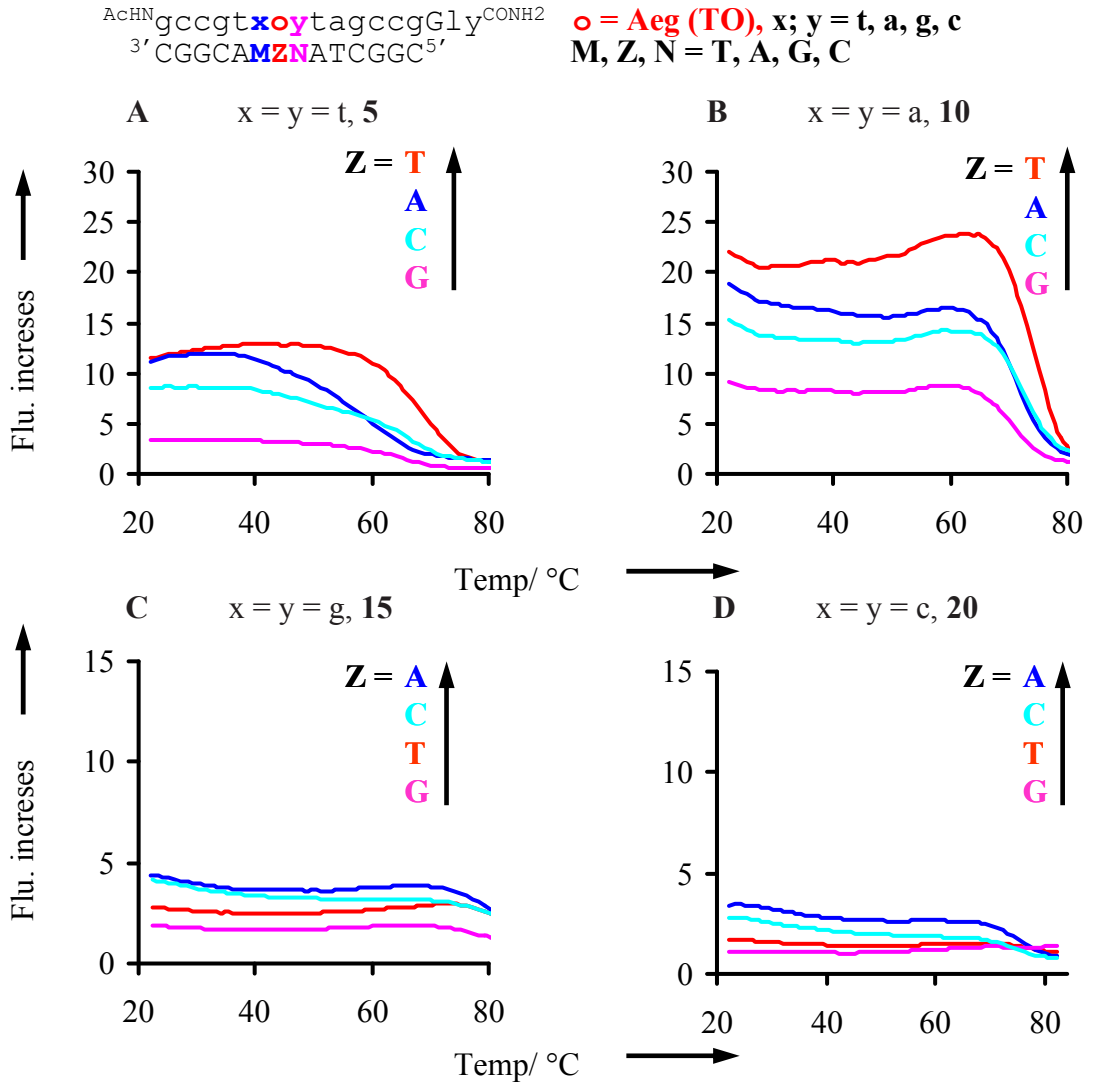

Figure 24: Fluorescence enhancement vs. temperature of FIT-PNA upon hybridization with matched DNA (TO vs T = red, TO vs A = blue, TO vs G = pink and TO vs C = turquoise). M and N are always complementary to x and y, A) **5** (t-TO-t), B) **10** (a-TO-a), C) **15** (g-TO-g) and D) **20** (c-TO-c). [Measurement conditions: 1 µM FIT-PNA or 1 µM FIT-PNA•DNA duplex in degassed buffer (100 mM NaCl, 10 mM NaH_2PO_4 at pH 7.0, Ex. 510 nm, Em. 530 nm, rate of heating 1°C/ min.)].

Figure 24 shows the fluorescence enhancement vs. temperature of TO-PNA upon hybridization with matched oligonucleotides. The fluorescence emission of FIT-PNA and its matched duplexes decreases upon increase in temperature (See experimental section). Fluorescence enhancement is constant or even increased upon increases of temperatures. This is in contrast to molecular beacons that show decreases of fluorescence enhancements at elevated temperature.[68] At temperature around the T_M fluorescence of the duplex strand rapidly decreases as expected. For example, probe **10** (a-TO-a) gives 21 fold fluorescence enhancement at 25°C and it is 14.3 fold at 73°C upon hybridization with matched DNA **5'TTT** (Figure 24B). In contrast, hybridization of probe **10** with matched DNA that contained varying TO pairing partner A, G, C gives lower fold fluorescence enhancement at elevated temperature than at 25°C.

The fluorescence study vs. temperature shows different fluorescence enhancements than recorded at constant temperatures. However, the measurement conditions are different. At constant temperature full spectra were recorded whereas fluorometric measurements at constant emission wavelength were performed in the fluorescence vs. temperature experiments. Figure 25 shows the fluorescence enhancement at optimal temperature.

^{AcHN}gccgt**xoy**tagccgGly^{CONH2}
$^{3'}$CGGCA**MZN**ATCGGC$^{5'}$

o = Aeg (TO), x; y = t, a, g and c
M, Z, N = T, A, G and C

x	Z	y	T°C[a]	$(F_{ds\ (match)}/\ F_{ss})^a$
a	**T**	a	63	24
a	**A**	a	59	17
a	**T**	t	44	16
g	**A**	a	25	16
a	**C**	a	59	14
a	**A**	g	52	14
t	**T**	t	47	13
t	**A**	t	32	12
g	**T**	a	25	12
a	**T**	g	64	12
g	**C**	a	25	11
t	**A**	a	35	11
t	**C**	a	37	10
t	**T**	a	45	10
a	**A**	t	32	9
a	**G**	a	59	9
t	**C**	t	32	9
a	**C**	t	32	8
t	**C**	c	25	8
t	**A**	g	25	8
a	**C**	g	25	7
c	**C**	a	25	7
t	**C**	g	25	7
t	**A**	c	25	6
a	**A**	c	45	6
c	**A**	g	25	6
g	**T**	t	55	6
t	**T**	c	25	5
a	**G**	t	32	5
a	**T**	c	25	5
t	**T**	g	59	5
g	**C**	t	32	5
c	**C**	g	25	5
c	**A**	a	25	5
g	**A**	c	63	5
g	**C**	c	25	4
g	**C**	g	25	4
g	**A**	t	32	4
g	**G**	a	25	4
t	**G**	a	43	4
g	**A**	g	64	4
c	**A**	c	25	4
t	**G**	t	32	3
g	**T**	c	69	3
a	**C**	c	45	3
c	**T**	a	25	3

^{AcHN}gccgt**xoy**tagccgGly^{CONH2}
$^{3'}$CGGCA**MZN**ATCGGC$^{5'}$

o = Aeg (TO), x; y = t, a, g and c
M, Z, N = T, A, G and C

x	Z	y	T°C[a]	($F_{ds\ (match)}$/ F_{ss})[a]
g	**T**	g	69	3
c	**C**	c	25	3
t	**G**	c	25	3
c	**G**	g	69	3
g	**G**	t	32	3
c	**C**	t	70	3
a	**G**	c	47	2
c	**T**	g	59	2
c	**T**	t	70	2
g	**G**	c	25	2
g	**G**	g	66	2
c	**A**	t	68	2
c	**G**	a	25	2
c	**T**	c	25	2
t	**G**	g	59	2
c	**G**	c	25	2
a	**G**	g	52	1
c	**G**	t	70	1

Figure 25: Fluorescence enhancement at optimal temperature of PNA probes **5-20,** measured at 530 nm after formation of matched duplexes, when TO was paired against thymine, adenine, guanine and cytosine. [[a] T = Temperature at which high fluorescence enhancement was recorded. [b] F_{ds}/ F_{ss} = Ratio between fluorescence intensities of FIT-PNA after and before addition of DNA at 530 nm. Measurement conditions: see caption of Figure 24].

Discussion

Highest fluorescence enhancement (24 fold) was again achieved for hybridisation of probe **10** (a-TO-a) at 63°C. Of the 64 studied hybridisation experiments 20 were accompanied by ≥ 8 fold fluorescence enhancement. All of the duplexes contained at least one AT base pair as TO stacking partner. One noticeable observation is that the preference for T as TO pairing partner is less pronounced. This suggests that the influence of the TO pairing partner is decreased at elevated temperatures.

Not a single probe was able to produce high fluorescence enhancement when either two guanines or two cytosines or one guanine and one cytosine were adjacent bases for thiazole orange. Mediocre 4 fold to 8 fold fluorescence enhancement at 530 nm was obtained in 22 hybridisation experiments. This category also contains two duplexes in which guanine acts as pairing base for TO. Almost 66 % of duplex formations produced modest to good fluorescence enhancement.

2.3.3 Match/ mismatch discrimination

In FIT-PNA, TO plays the role of a base surrogate. TO is thus, in intimate contact with adjacent base pairs. As result TO responds to changes of the stacking environment. For example, mismatched base pairs perturb duplex structure which influences the TO fluorescence properties. This behaviour should be of interest in applications where it is difficult to select stringent hybridisation conditions, such as in real-time PCR[69] and self-reporting arrays.[70] It has previously been shows that TO fluorescence remains low upon forced intercalation next to a mismatched base pair.[54] In this study the generality of this phenomenon is explored.

^{AcHN}gccgt**xoy**tagccgGly^{CONH2}
$^{3'}$CGGCA**MZN**ATCGGC$^{5'}$

o = Aeg (TO), x; y = t, a, g and c
M, Z, N = T, A, G and C

x	Z	y	$[F_{ds\ (match)} - F_{ss}]/[F_{ds\ (mismatch)} - F_{ss}]^a$	$F_{ds\ (match)}/F_{ds\ (mismatch)}^b$
c•G	T	**t•C**	32.9	1.7
a•C	A	c•G	15.8	5.5
t•G	C	c•G	14.8	2.3
c•T	G	c•G	13.9	2.8
a•C	G	c•G	12.3	5.3
a•A	A	g•C	12.1	4.9
c•A	G	c•G	8.5	2.6
a•A	A	c•G	8.3	4.3
a•C	C	c•G	8.3	3.2
c•C	G	c•G	8.1	2.6
a•C	A	g•C	7.4	4.0
g•C	G	**t•T**	7.3	2.2
g•C	T	**t•C**	6.8	3.3
g•C	C	**t•T**	6.7	1.8
a•C	C	a•T	6.4	3.6
g•C	C	**a•C**	6.3	2.8
c•G	C	**a•C**	6.3	2.2
t•A	T	**t•C**	6.2	4.7
a•C	G	t•A	6.2	3.0
t•A	T	**t•T**	6.1	4.6
a•A	A	a•T	6.0	3.9
a•A	G	c•G	6.0	3.8
a•C	A	t•A	5.9	2.7
a•A	G	t•A	5.8	2.9
c•G	A	**a•C**	5.8	1.8
a•A	G	a•T	5.6	3.9
g•T	G	g•C	5.5	2.2
t•A	T	t•G	5.4	4.3
g•C	G	**t•C**	5.4	2.1

^{AcHN}gccgt**xoy**tagccgGly^{CONH2}
$^{3'}$CGGCA**MZN**ATCGGC$^{5'}$

o = Aeg (TO), x; y = t, a, g and c
M, Z, N = T, A, G and C

x	Z	y	$[F_{ds\ (match)} - F_{ss}]/[F_{ds\ (mismatch)} - F_{ss}]^a$	$F_{ds\ (match)}/F_{ds\ (mismatch)}^b$
t•C	G	t•A	5.3	2.5
a•T	T	**t•G**	5.3	4.0
a•A	A	t•A	5.2	2.6
a•C	G	a•T	5.2	3.7
a•C	C	t•A	5.0	2.1
t•A	G	**c•T**	5.0	2.5
t•G	T	a•T	4.9	4.1
a•T	C	**a•C**	4.9	3.2
c•A	C	a•T	4.9	2.1
t•A	C	**t•C**	4.8	3.0
t•A	C	**t•T**	4.8	3.0
a•A	T	c•G	4.6	3.9
g•C	T	**t•G**	4.5	2.7
a•T	G	**c•A**	4.4	3.2
c•G	G	**c•A**	4.4	2.2
a•T	T	**t•C**	4.3	3.5
a•A	T	t•A	4.3	3.5
c•A	T	a•T	4.3	2.4
c•G	G	**c•T**	4.3	2.1
c•G	G	**c•C**	4.3	2.1
t•G	T	t•A	4.3	3.6
g•C	C	**t•G**	4.2	1.7
a•C	A	a•T	4.1	3.1
a•C	C	g•C	4.1	2.3
t•T	C	c•G	4.0	1.9
g•C	T	**t•T**	4.0	2.5
a•C	T	t•A	3.9	3.2
g•G	A	c•G	3.9	2.1
t•A	T	**a•C**	3.8	3.3
t•A	G	**c•C**	3.7	1.9
t•A	G	**c•A**	3.7	1.9
g•A	G	a•T	3.7	2.3
g•C	A	**a•C**	3.7	2.5
g•G	A	a•T	3.7	2.5
t•C	T	a•T	3.7	3.2
a•T	T	**t•T**	3.6	3.0
c•A	A	a•T	3.6	1.7
t•A	C	a•C	3.6	2.5
a•A	C	a•T	3.6	2.6
a•T	G	**c•T**	3.6	2.8
g•C	C	**t•C**	3.6	1.6
a•T	G	**a•C**	3.5	2.8
g•G	T	a•T	3.5	2.9
g•C	G	**t•G**	3.5	1.8
t•C	C	c•G	3.4	1.8
t•A	C	**t•G**	3.4	2.5

^{AcHN}gccgt**xoy**tagccgGly^{CONH2}
$^{3'}$CGGCA**MZN**ATCGGC$^{5'}$

o = Aeg (TO), x; y = t, a, g and c
M, Z, N = T, A, G and C

x	Z	y	$[F_{ds\ (match)} - F_{ss}]/[F_{ds\ (mismatch)} - F_{ss}]^a$	$F_{ds\ (match)}/F_{ds\ (mismatch)}^b$
c•G	G	**a•C**	3.4	2.1
g•A	A	g•C	3.3	1.6
a•T	G	**c•C**	3.3	2.6
t•G	C	a•T	3.3	2.4
t•G	T	c•G	3.2	2.4
c•A	A	c•G	3.2	1.7
c•T	A	c•G	3.2	1.7
a•T	A	**a•C**	3.2	2.6
a•C	T	c•G	3.2	2.9
t•T	T	a•T	3.2	2.8
t•T	T	t•A	3.2	2.8
g•G	G	a•T	3.2	2.1
g•A	G	g•C	3.1	1.8
c•G	T	**a•C**	3.1	2.1
t•G	G	t•A	3.1	2.0
t•T	G	t•A	3.1	2.0
a•A	C	g•C	3.1	2.0
g•G	T	t•A	3.1	2.2
t•T	C	t•A	3.0	2.3
t•C	T	t•A	3.0	2.7
a•A	C	t•A	2.9	2.0
a•A	C	c•G	2.9	2.0
g•A	A	a•T	2.9	2.2
t•G	T	g•C	2.9	2.2
t•C	G	c•G	2.9	1.7
t•G	A	c•G	2.9	1.5
c•G	G	**a•G**	2.8	1.2
c•C	C	t•A	2.8	1.2
a•T	G	**t•G**	2.8	2.0
c•G	G	**g•A**	2.8	2.4
t•G	C	t•A	2.7	2.1
a•T	C	**t•C**	2.7	1.9
a•T	C	**c•C**	2.7	2.0
t•A	G	**a•C**	2.6	2.2
g•C	T	**a•C**	2.6	2.3
t•A	T	**a•A**	2.6	2.4
a•G	T	t•A	2.6	2.3
g•T	G	t•A	2.6	1.6
a•T	T	**c•A**	2.6	2.4
t•C	C	**t•A**	2.5	2.0
c•G	T	**a•A**	2.5	1.9
c•T	T	a•T	2.5	1.9
t•T	T	c•G	2.5	2.0
g•T	A	a•T	2.5	2.0
a•T	C	**t•T**	2.4	1.8
a•T	G	**a•A**	2.4	2.1

^{AcHN}gccgt**xoy**tagccgGly^{CONH2}
$^{3'}$CGGCA**MZN**ATCGGC$^{5'}$

o = Aeg (TO), x; y = t, a, g and c
M, Z, N = T, A, G and C

x	Z	y	$[F_{ds\ (match)} - F_{ss}]/[F_{ds\ (mismatch)} - F_{ss}]^a$	$F_{ds\ (match)}/F_{ds\ (mismatch)}^b$
a•T	A	**g•T**	2.4	2.0
c•C	A	c•G	2.4	1.5
c•G	A	**c•C**	2.4	1.5
a•T	T	**a•C**	2.4	2.3
g•C	G	**a•C**	2.4	1.8
g•T	G	a•T	2.4	1.8
a•A	T	a•T	2.4	2.2
t•A	T	**a•G**	2.4	2.2
g•A	T	t•A	2.3	1.9
a•T	G	**t•C**	2.3	1.8
a•T	G	**t•T**	2.3	1.8
t•T	A	c•G	2.3	1.4
g•T	A	c•G	2.3	1.7
g•C	C	**a•G**	2.3	1.8
a•T	T	**a•G**	2.2	2.1
a•T	G	**a•G**	2.2	2.0
c•C	A	a•T	2.2	1.4
c•T	C	c•G	2.2	1.4
a•G	A	a•T	2.2	1.9
c•G	G	**a•A**	2.2	1.7
c•G	T	**a•G**	2.2	1.7
a•T	T	**a•A**	2.2	2.1
g•G	G	g•C	2.2	1.5
t•C	A	c•G	2.1	1.4
g•C	G	**c•A**	2.1	1.7
g•C	T	**c•A**	2.1	1.8
g•T	T	c•G	2.1	1.8
a•G	T	a•T	2.1	2.0
c•G	C	**t•T**	2.1	1.2
c•A	G	a•T	2.1	1.7
c•A	A	g•C	2.1	1.7
t•A	A	t•G	2.1	1.7
c•T	C	a•T	2.1	1.5
c•A	T	c•G	2.1	1.7
a•T	C	**t•G**	2.1	1.6
a•T	A	**c•C**	2.0	1.8
a•T	A	**c•A**	2.0	1.8
g•G	T	c•G	2.0	1.7
a•T	T	**c•C**	2.0	1.9
t•A	G	**a•G**	2.0	1.8
c•G	T	**t•T**	1.9	1.3
t•G	C	g•C	1.9	1.4
c•A	C	c•G	1.9	1.3
t•A	C	**a•G**	1.9	1.7
c•T	A	a•T	1.9	1.4
g•T	A	t•A	1.9	1.2

^{AcHN}gccgt**xoy**tagccgGly^{CONH2}
$^{3'}$CGGCA**MZN**ATCGGC$^{5'}$

o = Aeg (TO), x; y = t, a, g and c
M, Z, N = T, A, G and C

x	Z	y	$[F_{ds\ (match)} - F_{ss}]/[F_{ds\ (mismatch)} - F_{ss}]^a$	$F_{ds\ (match)}/F_{ds\ (mismatch)}^b$
a•T	A	**a•G**	1.9	1.7
a•T	A	**a•A**	1.9	1.7
t•A	A	**t•C**	1.9	1.6
c•C	G	t•A	1.9	1.1
g•G	C	c•G	1.9	1.5
g•C	T	**a•G**	1.9	1.7
g•C	T	**a•A**	1.9	1.7
g•A	T	a•T	1.9	1.7
t•A	C	**c•C**	1.8	1.4
a•T	C	**a•G**	1.8	1.6
t•G	A	a•T	1.8	1.6
t•G	G	c•G	1.8	1.4
g•C	G	**c•C**	1.8	1.5
t•A	A	**a•C**	1.8	1.6
t•A	T	**c•A**	1.8	1.6
t•C	C	a•T	1.8	1.6
t•T	C	a•T	1.8	1.6
a•G	A	t•A	1.7	1.5
t•A	T	**c•C**	1.7	1.6
c•C	G	a•T	1.7	1.5
a•G	G	a•T	1.7	1.6
t•G	A	t•A	1.7	1.5
g•C	G	**g•T**	1.7	1.4
g•C	G	**c•T**	1.7	1.5
c•C	T	a•T	1.7	1.5
a•T	T	**c•T**	1.7	1.6
a•T	C	**a•A**	1.7	1.5
c•A	T	g•C	1.7	1.5
a•T	A	**t•G**	1.7	1.4
t•T	G	**c•G**	1.7	1.3
g•A	G	t•A	1.7	1.2
g•G	A	t•A	1.7	1.3
c•C	C	c•G	1.7	1.3
g•C	A	**a•G**	1.7	1.5
g•G	A	g•C	1.7	1.3
g•G	G	t•A	1.6	1.3
g•C	C	**c•C**	1.6	1.4
c•T	C	**t•A**	1.6	1.1
c•T	A	g•C	1.6	1.4
t•A	G	**a•A**	1.6	1.5
a•T	C	**c•A**	1.6	1.4
c•G	G	**t•T**	1.6	1.1
t•A	C	**a•A**	1.6	1.5
t•A	A	**a•A**	1.6	1.5
g•A	A	c•G	1.6	1.4
t•A	A	**c•C**	1.6	1.2

^{AcHN}gccgt**xoy**tagccgGly^{CONH2}
$^{3'}$CGGCA**MZN**ATCGGC$^{5'}$

o = Aeg (TO), x; y = t, a, g and c
M, Z, N = T, A, G and C

x	Z	y	$[F_{ds\ (match)} - F_{ss}]/[F_{ds\ (mismatch)} - F_{ss}]^a$	$F_{ds\ (match)}/F_{ds\ (mismatch)}^b$
c•C	C	a•T	1.6	1.3
g•C	T	**c•C**	1.6	1.4
t•A	A	**a•G**	1.6	1.4
g•C	A	**a•A**	1.6	1.4
c•G	T	**t•G**	1.5	1.2
c•T	G	a•T	1.5	1.4
c•G	C	a•G	1.5	1.8
g•T	T	t•A	1.5	1.4
c•G	T	**c•C**	1.5	1.4
c•G	G	**g•G**	1.5	1.4
g•T	C	c•G	1.5	1.3
t•C	A	t•A	1.5	1.3
t•T	A	t•A	1.5	1.3
c•A	C	g•C	1.5	1.3
c•G	C	t•C	1.5	1.1
c•T	C	g•C	1.5	1.3
g•C	A	**t•C**	1.5	1.1
a•C	T	a•T	1.5	1.4
a•T	A	**c•T**	1.4	1.4
c•C	A	g•C	1.4	1.3
t•C	T	c•G	1.4	1.3
t•C	C	g•C	1.4	1.2
g•G	G	c•G	1.4	1.3
g•T	G	c•G	1.4	1.3
t•C	T	g•C	1.4	1.3
t•T	T	g•C	1.4	1.3
c•G	T	**c•T**	1.4	1.3
t•A	A	**g•G**	1.4	1.2
t•T	A	a•T	1.4	1.3
c•G	T	**c•A**	1.4	1.3
a•T	A	**t•C**	1.4	1.3
g•C	A	**c•T**	1.4	1.3
c•G	A	**g•T**	1.4	1.3
t•T	C	g•C	1.4	1.2
c•G	A	**a•G**	1.4	1.5
c•G	C	**a•A**	1.4	1.2
g•T	C	t•A	1.4	1.2
c•T	T	c•G	1.4	1.3
g•C	C	**c•A**	1.4	1.2
g•C	C	**c•T**	1.4	1.2
t•G	G	a•T	1.4	1.3
c•G	G	**g•T**	1.3	1.3
a•G	A	g•C	1.3	1.3
g•C	A	**t•T**	1.3	1.1
g•T	T	a•T	1.3	1.3
c•G	T	**g•T**	1.3	1.3

^{AcHN}gccgt**xoy**tagccgGly^{CONH2}
$^{3'}$CGGCA**MZN**ATCGGC$^{5'}$

o = Aeg (TO), x; y = t, a, g and c
M, Z, N = T, A, G and C

x	Z	y	$[F_{ds\ (match)} - F_{ss}]/[F_{ds\ (mismatch)} - F_{ss}]^a$	$F_{ds\ (match)}/F_{ds\ (mismatch)}^b$
g•C	T	**c•T**	1.3	1.2
g•C	A	**g•T**	1.3	1.1
g•T	A	g•C	1.3	1.1
c•G	C	**c•C**	1.3	1.1
g•A	C	t•A	1.3	1.1
g•C	G	**a•G**	1.3	1.2
c•G	A	**c•T**	1.3	1.1
a•T	C	**c•T**	1.3	1.2
t•C	G	a•T	1.3	1.2
t•C	A	a•T	1.2	1.2
a•G	G	t•A	1.2	1.2
g•G	T	g•C	1.2	1.2
a•G	T	c•G	1.2	1.2
c•T	T	g•C	1.2	1.2
g•G	C	t•A	1.2	1.1
g•C	C	**a•A**	1.2	1.1
a•T	A	**t•T**	1.2	1.1
a•G	C	c•G	1.2	1.1
c•G	A	**a•A**	1.2	1.1
g•C	G	**g•G**	1.2	1.1
g•C	A	**c•A**	1.2	1.1
g•C	G	**a•A**	1.1	1.1
a•T	T	**g•T**	1.1	1.1
g•C	A	**t•G**	1.1	1.0
t•G	G	g•C	1.1	1.0
g•C	T	**g•T**	1.1	1.1
g•T	T	g•C	1.1	1.1
c•C	C	g•C	1.1	1.0
t•A	A	**t•T**	1.1	1.0
g•A	C	c•G	1.0	1.0
t•A	C	c•T	1.0	1.0
g•A	G	c•G	1.0	1.0
c•G	G	**t•G**	1.0	1.0
g•A	T	g•C	1.0	1.0
c•G	C	**c•T**	1.0	1.0
g•C	G	**g•A**	0.9	1.0
a•G	C	a•T	0.9	1.0
t•A	G	t•G	0.9	0.9
t•T	G	a•T	0.9	0.9
a•T	A	**g•A**	0.9	0.9
a•G	C	t•A	0.9	0.9
a•T	A	**g•G**	0.9	0.9
c•G	C	**g•G**	0.9	0.9
a•G	A	c•G	0.9	0.9
t•A	A	**g•T**	0.8	0.9
c•G	A	**c•A**	0.8	0.9

^{AcHN}gccgt**xoy**tagccgGly^{CONH2}
$^{3'}$CGGCA**MZN**ATCGGC$^{5'}$

o = Aeg (TO), x; y = t, a, g and c
M, Z, N = T, A, G and C

x	Z	y	$[F_{ds\ (match)} - F_{ss}]/[F_{ds\ (mismatch)} - F_{ss}]^a$	$F_{ds\ (match)}/F_{ds\ (mismatch)}^b$
c•C	T	**c•G**	0.8	0.9
a•G	T	g•C	0.8	0.8
c•G	C	**t•G**	0.8	0.9
c•G	A	**g•G**	0.8	0.9
g•C	A	**c•C**	0.8	0.9
t•A	A	**c•A**	0.8	0.9
g•A	T	c•G	0.8	0.8
g•A	A	t•A	0.8	0.9
a•T	T	**g•G**	0.8	0.8
t•A	T	**g•A**	0.8	0.7
t•A	A	**g•A**	0.8	0.9
c•G	T	**g•G**	0.8	0.8
t•A	C	**c•A**	0.8	0.9
t•A	T	**g•G**	0.8	0.8
a•A	T	g•C	0.8	0.8
c•G	T	**g•A**	0.7	0.8
a•G	G	c•G	0.7	0.7
c•G	A	**g•A**	0.7	0.7
a•T	T	**g•A**	0.7	0.7
t•A	G	**g•T**	0.7	0.8
t•A	T	**g•T**	0.7	0.7
c•C	T	g•C	0.6	0.7
c•G	C	g•T	0.6	0.7
t•A	A	**c•T**	0.6	0.8
t•G	A	g•C	0.6	0.7
t•T	G	g•C	0.6	0.7
g•C	A	**g•G**	0.6	0.7
c•A	G	g•C	0.6	0.6
g•C	T	**g•A**	0.5	0.6
t•A	T	**c•T**	0.5	0.6
g•G	C	a•T	0.5	0.6
a•T	C	**g•G**	0.5	0.6
a•G	C	g•C	0.5	0.6
t•A	G	**g•G**	0.5	0.7
t•C	G	g•C	0.5	0.7
g•C	A	**g•A**	0.5	0.7
c•G	C	**g•A**	0.5	0.6
a•G	G	g•C	0.5	0.7
c•T	G	g•C	0.5	0.5
g•T	C	a•T	0.5	0.6
g•C	C	**g•G**	0.5	0.7
a•C	T	g•C	0.5	0.5
g•C	T	**g•G**	0.5	0.5
t•A	G	**g•A**	0.4	0.8
t•T	A	g•C	0.4	0.5
g•A	C	a•T	0.4	0.5

^{AcHN}gccgt**xoy**tagccgGly^{CONH2}
$^{3'}$CGGCA**MZN**ATCGGC$^{5'}$

o = Aeg (TO), x; y = t, a, g and c
M, Z, N = T, A, G and C

x	Z	y	$[F_{ds\ (match)} - F_{ss}]/[F_{ds\ (mismatch)} - F_{ss}]^a$	$F_{ds\ (match)}/F_{ds\ (mismatch)}^b$
t•A	C	**g•T**	0.4	0.5
c•C	G	g•C	0.4	0.4
c•G	C	c•A	0.4	0.5
t•C	A	g•C	0.4	0.5
t•A	C	**g•G**	0.4	0.5
t•A	G	**t•C**	0.4	0.4
t•A	G	**t•T**	0.3	0.4
t•A	C	**g•A**	0.3	0.5
g•C	C	**g•T**	0.3	0.4
g•T	C	g•C	0.3	0.4
a•T	C	**g•A**	0.2	0.3
a•T	C	**g•T**	0.2	0.3
g•C	C	**g•A**	0.2	0.3
g•G	C	g•C	0.2	0.3
a•T	G	**g•T**	0.1	0.3
g•A	C	g•C	0.1	0.2
a•C	G	g•C	0.1	0.2
a•A	G	g•C	0.1	0.2
a•T	G	**g•G**	0.1	0.2
a•T	G	**g•A**	0.1	0.2
c•T	A	**t•A**	0.0	2.1
c•G	A	**t•G**	0.0	2.0
c•C	A	t•A	0.0	1.4
c•G	A	**t•T**	-0.1	1.2
c•G	A	**t•C**	-0.1	1.2
c•A	A	t•A	-0.1	1.2
c•A	G	t•A	-0.5	3.2
c•T	G	t•A	-1.8	1.5
c•T	T	t•A	-4.1	2.1
c•A	T	t•A	-5.7	2.0
c•A	C	t•A	-6.1	1.5
c•G	G	**t•C**	-8.6	1.3
c•C	T	t•A	-10.2	1.9

Figure 26: Match/mismatch fluorescence discrimination of PNA probes **5-20,** measured at 530 nm, when TO was paired against thymine, adenine, guanine and cytosine at 25°C in buffer. $^a[F_{ds\ (match)} - F_{ss}]/[F_{ds\ (mismatch)} - F_{ss}]$ = Ratio between fluorescence intensities of FIT-PNA after formation matched duplex-single strand fluorescence/mismatched duplex-single strand fluorescence at 530 nm. $^b[F_{ds\ (match)}/F_{ds\ (mismatch)}]$ = Ratio between fluorescence intensities of FIT-PNA after formation matched duplex-mismatched duplex at 530 nm. Measurement conditions: 1µM probe and DNA in buffer (100 mM NaCl, 10 mM NaH_2PO_4, pH 7), excitation: 510 nm.

Discussion

Figure 26 shows match/mismatch fluorescence discrimination of probes **5-20** at 25°C that means at temperatures where both match and mismatched duplexes form. The fluorescence match/mismatch discrimination is presented in two forms. 1) $[F_{ds\ (match)} - F_{ss}]/[F_{ds\ (mismatch)} - F_{ss}]$, this type of discrimination is (bars in Figure 26) very important in application studies like real time PCR. In this the background signals of fluorescent probe are subtracted and then measurements are carried out. 2) $[F_{ds\ (match)}/F_{ds\ (mismatch)}]$ this type of discrimination is more useful in basic studies, where fluorescence enhancement corresponding to targets is measured.

In principle there could be two categories of useful probes. 1) The probes show high fluorescence enhancement upon matched hybridisation and low fluorescence enhancement or fluorescence decreases upon mismatched hybridisation. 2) The probes shows high fluorescence enhancement upon mismatched hybridisation and low enhancement or fluorescence decreases upon matched hybridisation.

The previous results have shown that (Figure 23) 70 % of the FIT-probes have more than 4 fold higher fluorescence in matched duplexes than on single strand. It would, hence facilitate the general applicability if the majority of FIT-probes were experiencing attenuation of fluorescence in mismatched duplexes. Indeed, of the 384 mismatched duplexes studied 80 % have lower fluorescence in mismatched duplexes than in matched duplexes. Only 20 % show the opposite behaviour. It can be concluded that FIT-probes belong to category 1 probes. 25 % of the probes discriminate against mismatches with ≥ 3 fold fluorescence selectivity. It is important to note that this discrimination is already achieved at 25°C where both matched and mismatched duplexes form. A striking observation is that the 14 best discriminating scenarios have a GC base pair as matched TO stacking partners. None of the probes contained a mismatched ‘g’ as intrastrand TO stacking partner.

2.4 Hybridization selectivity

Results and discussion

Table 2 shows the stability of matched and mismatched duplexes in which TO was paired against thymine in various stacking environment. Expectedly, higher T_M values were obtained for GC rich TO next neighbors. For example, duplexes featuring TO in between two guanines, two cytosines or between one guanine and cytosine exhibited $T_M = 77°C$. In contrast, AT rich stacking environments where TO was embedded between two thymines, two adenines or one adenine and thymine provided T_M value in the range of $T_M = 69\text{-}73°C$. This suggests that hybridisation obeys the "normal" Watson-Crick base pairing rules. Importantly, mismatched duplexes always showed lower stability than matched duplexes. The difference in T_M can be as high as $\Delta T_M = 16°C$ obtained for probe **17** and were lowest for the formation of g-T and t-T mismatches in the AT rich stacking environment of probe **5** and **9**. This study revealed that without any exception hybridisation of FIT-PNA is sequence selective. It is thus possible to perform hybridisation experiments at stringent conditions at temperatures over the T_M of mismatched probe-target duplexes.

The previous chapter has shown that the matched hybridisation can be distinguished from mismatched hybridisation by means of TO fluorescence emission. In addition to the matched base-pair specific signaling of TO the specificity of the hybridisation process itself can be exploited for match/mismatch discrimination.

Table 2: Thermal stabilities of PNA•DNA duplexes containing TO linked to Aeg.

^{AcHN}gccgt**xoy**tagccgGly^{CONH2} $^{3'}$CGGCA**MTN**ATCGGC$^{5'}$			o = Aeg (TO), x = t, a, g, c and y = t or a M and N = T, A, G and C		
PNA Probe ΔT_M°C[b]	duplex number	T_M[a]/ °C	PNA Probe ΔT_M°C[b]	duplex number	T_M[a]/ °C
	5•9' TTA	63		9•5'TTT	68
	5•10'ATA	**69**		**9•6'ATT**	**73**
	5•11'GTA	61		9•7'GTT	65
t-TO-t, **5**	5•12'CTA	61	t-TO-a, **9**	9•8'CTT	66
ΔT_M = 5-8	5•6' ATT	62	ΔT_M = 5-12	9•10'ATA	65
	5•14'ATG	64		9•14'ATG	64
	5•18'ATC	61		9•18'ATC	61
	6•9' TTA	**69**		**10•5'TTT**	**73**
	6•10'ATA	60		10•6'ATT	65
	6•11'GTA	60		10•7'GTT	65
a-TO-t, **6**	6•12'CTA	61	a-TO-a, **10**	10•8'CTT	64
ΔT_M = 8-10	6•5' TTT	59	ΔT_M = 8-13	10•9' TTA	62
	6•13'TTG	60		10•13'TTG	63
	6•17'TTC	59		10•17'TTC	60
	7•9' TTA	63		11•5'TTT	68
	7•10'ATA	59		11•6'ATT	63
	7•11'GTA	61		11•7'GTT	63
g-TO-t, **7**	**7•12'CTA**	**72**	g-TO-a, **11**	**11•8'CTT**	**77**
ΔT_M = 7-13	7•8'CTT	64	ΔT_M = 9-14	11•12'CTA	66
	7•16'CTG	65		11•16'CTG	67
	7•20'CTC	61		11•20'CTC	63
	8•9' TTA	60		12•5'TTT	65
	8•10'ATA	61		12•6'ATT	64
	8•11'GTA	**73**		**12•7'GTT**	**76**
c-TO-t, **8**	8•12'CTA	58	c-TO-a, **12**	12•8' CTT	66
ΔT_M = 8-15	8•7' GTT	65	ΔT_M = 9-12	12•11'GTA	65
	8•15'GTG	65		12•15'GTG	66
	8•19'GTC	62		12•19'GTC	67

^{AcHN}gccgt**xoy**tagccgGly^{CONH2} $^{3'}$CGGCA**MTN**ATCGGC$^{5'}$			o = Aeg (TO), x = t, a, g, c and y = g or c M and N = T, A, G and C		
PNA Probe ΔT_M°C[b]	duplex number	T_M[a]/ °C	PNA Probe ΔT_M°C[b]	duplex number	T_M[a]/ °C
	13•17'TTC	70		17•13'TTG	66
	13•18'ATC	**75**		**17•14'ATG**	**74**
	13•19'GTC	67		17•15'GTG	65
t-TO-g, **13**	13•20'CTC	69	t-TO-c, **17**	17•16'CTG	65
ΔT_M = 5-13	13•6' ATT	65	ΔT_M = 8-16	17•6' ATT	60
	13•10'ATA	62		17•10'ATA	60
	13•14'ATG	63		17•18'ATC	58
	14•17'TTC	**74**		**18•13'TTG**	**73**
	14•18'ATC	68		18•14'ATG	64
	14•19'GTC	68		18•15'GTG	65
a-TO-g, **14**	14•20'CTC	69	a-TO-c, **18**	18•16'CTG	64
ΔT_M = 5-11	14•5' TTT	65	ΔT_M = 8-13	18•5' TTT	61
	14•9' TTA	63		18•9' TTA	64
	14•13'TTG	64		18•17'TTC	60
	15•17'TTC	69		19•13'TTG	66
	15•18'ATC	65		19•14'ATG	62
	15•19'GTC	65		19•15'GTG	63
g-TO-g, **15**	**15•20'CTC**	**77**	g-TO-c, **19**	**19•16'CTG**	**77**
ΔT_M = 8-12	15•8' CTT	66	ΔT_M = 11-15	19•8' CTT	65
	15•12'CTA	64		19•12'CTA	66
	15•16'CTG	67		19•20'CTC	64
	16•17'TTC	69		20•13'TTG	64
	16•18'ATC	66		20•14'ATG	63
	16•19'GTC	**77**		**20•15'GTG**	**77**
c-TO-g, **16**	16•20'CTC	68	c-TO-c, **20**	20•16'CTG	63
ΔT_M = 8-11	16•7' GTT	67	ΔT_M = 11-14	20•7' GTT	65
	16•13'GTA	66		20•11'GTA	66
	16•15'GTG	67		20•19'GTC	63

[a] Measured as denaturation curves. Measurement conditions: see caption of Table 1. [b] the stability of matched duplex-average stability of corresponding mismatched duplexes.

2.5 Conclusions

Aeg-TO-PNA conjugates were synthesized in which thiazole orange replaces a nucleobase. The developed linear solid-phase synthesis protocol proved to provide rapid access to any type of sequences modified by thiazole orange. The replacement of a central nucleobase with thiazole orange afforded a PNA probe that fluoresced upon hybridisation.

The collected data suggests that the fluorescence of the thiazole orange base surrogate is most responsive to hybridisation when TO is flanked by adenine-adenine > adenine-thymine > thymine-thymine > cytosine-adenine > cytosine-guanine > guanine-adenine > guanine-cytosine > guanine-guanine > cytosine-cytosine > cytosine-thymine. The preferred pairing partner to achieve high fluorescence with matched DNA and high match/mismatch fluorescence discrimination is thymine > guanine > adenine > cytosine.

The sensitivity of thiazole orange fluorescence to a neighbouring base mismatch suggests that it is possible to distinguish a DNA target from its single base mutant by avoiding the usual need for stringent hybridisation conditions. The majority of FIT-probes show lower fluorescence in single-mismatched duplexes. This is an important result as hybridisation requires lower temperatures for the mismatched sequence than for the fully matched sequence. However, because the fluorescence enhancement of Aeg-FIT probes is lower for mismatched sequences, this strategy might allow mismatched duplexes to form but can still discriminate them from fully matched duplexes. It hence appears accomplishable to distinguish a target sequence from its single-base mutant even at temperatures below the T_M value of the mismatched probe target complexes. Studied mismatched duplexes always showed lower thermal stability than its corresponding matched duplexes. It hence revealed that without any exception hybridisation of FIT-PNA is sequence selective.

3. Solid-phase synthesis and evaluation of PNA containing thiazole orange as fluorescent base surrogate attached to ornithine.

The previous chapter dealt with the introduction of TO as base surrogate in peptide nucleic acid and its biophysical properties for mutational analysis. In this study TO was coupled to ornithine as backbone building block. There is literature precendence that binding properties of the PNA can be improved by backbone modifications.[71, 72] Hence, it was decided to study backbone modification of TO to reduce base stacking of TO in single stranded probes while still allowing base stacking in double strand.

Past work by Lars Röglin has shown that, in order to achieve a high fluorescence enhancement, replacement of the Aeg backbone of Aeg (TO) by ornithine is useful.[56] The idea behind, Orn residue has the requisite six covalent bonds in the monomeric backbone as in Aeg. The Orn monomers are linked via amide bonds between the carboxyl of thiazole orange and the δ-amino function of the Orn residue. High reactivity of primary amino group to link the thiazole orange rather than secondary amino group in Aeg is a synthetic advantage of Orn (TO) monomers over Aeg (TO).

Results in previous section proved that in Aeg-TO-PNA adjacent base of TO plays a vital role. Hence, it was decided to explore effect of stereogenic centre on fluorescence properties of FIT-PNA. Towards this end it was envisioned to explore TO-fluorescence ornithine-containing PNA in the contact of all possible adjacent and opposite nucleobases.

3.1 Synthesis of Orn-TO Labeled PNA

The synthesis of thiazole orange-Orn containing PNA was also performed by two approaches, the linear approach and the divergent. The linear solid phase synthesis was carried out for TO containing building blocks attached to D- and L-Orn. This strategy also requires a preformed thiazole orange-Orn building block. In the following the synthesis of such a building block is described. The second divergent strategy has been described by Lars Röglin (Diploma thesis 2002).[56] He synthesized two sub-monomers, Fmoc-D-Orn (Alloc)-OH and Fmoc-L-Orn (Alloc)-OH.

3.1.1 Design and synthesis of building blocks

The protected TO-Orn (Fmoc)-building blocks **24a** and **24b** were required for linear solid phase synthesis (Scheme 7). Scheme 7 shows the synthesis of PNA monomers containing thiazole orange as fluorescent base surrogate attached to L- or D-Orn. The reported Fmoc-L- or D-Orn[56] was allylated with allyl alcohol using thionyl chloride[60] to give Orn derivatives **22a** (84 %) and **22b** (88 %). Coupling of allylated **22a** or **22b** with thiazole orange derivative **1** is carried out using PyBOP,[62] NMM, PPTS[64] in DMF to yield **23a** and **23b** (Fmoc-L- or D-Orn (TO)-Oallyl). Finally the allyl ester in **23a** and **23b** was removed by Pd (0)-catalyzed allyl transfer using *N*-methyl aniline which afforded the TO–PNA monomer in 68 % and 65 % yield for **24a** and **24b** respectively.

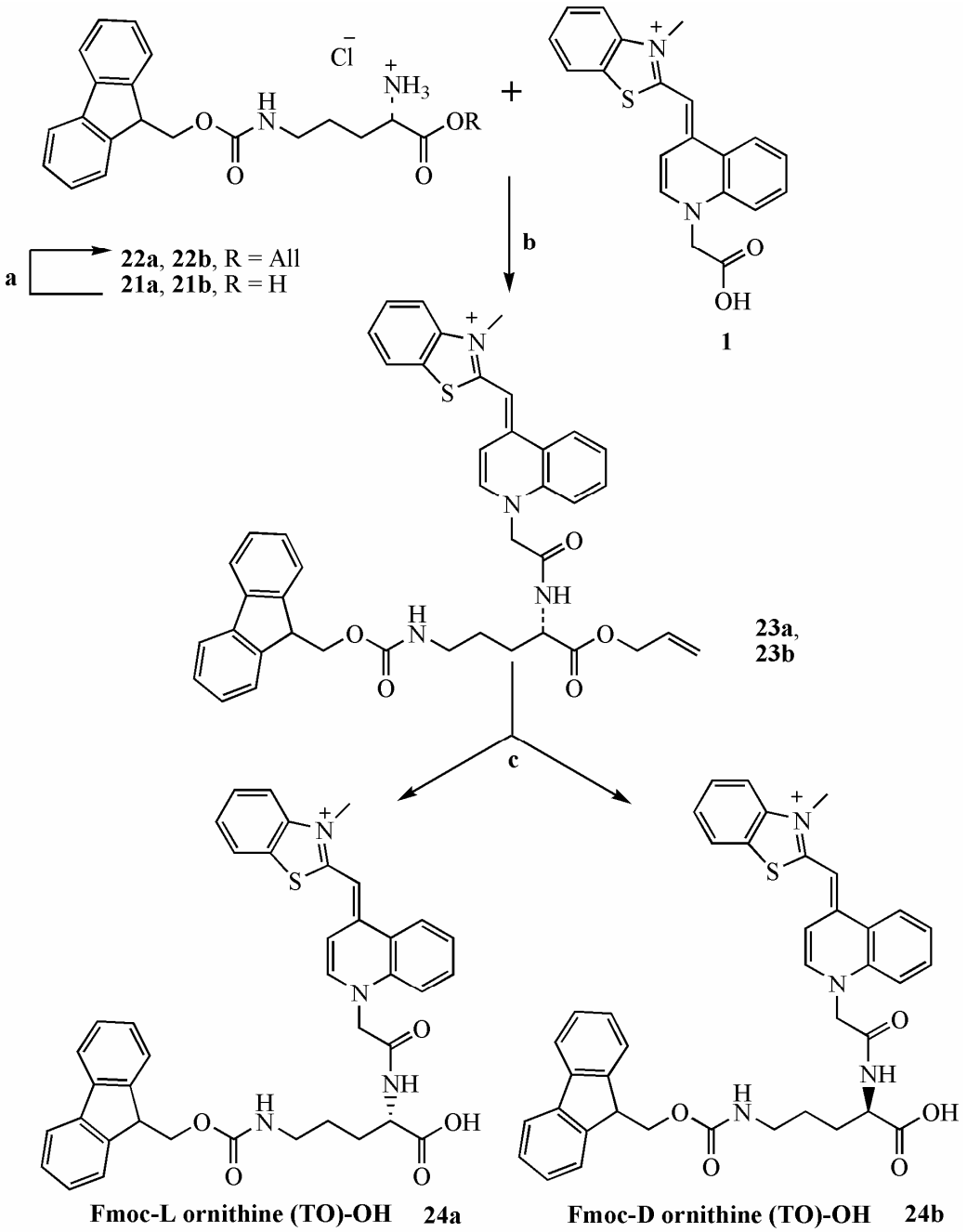

Scheme 7: a) Thionyl chloride, allyl alcohol, **22a** = 84 %, **22b** = 88 %; b) TO-CH_2-COOH (1), **22a** or **22b**, PyBOP, PPTS, NMM, DMF, **23a** = 63 %, **23b** = 55 %; c) [Pd (PPh_3)$_4$], $PhNHCH_3$, THF, **24a** = 68 %, **24b** = 65 %.

3.1.2 Linear Solid Phase Synthesis of D-Orn-TO Labeled PNA

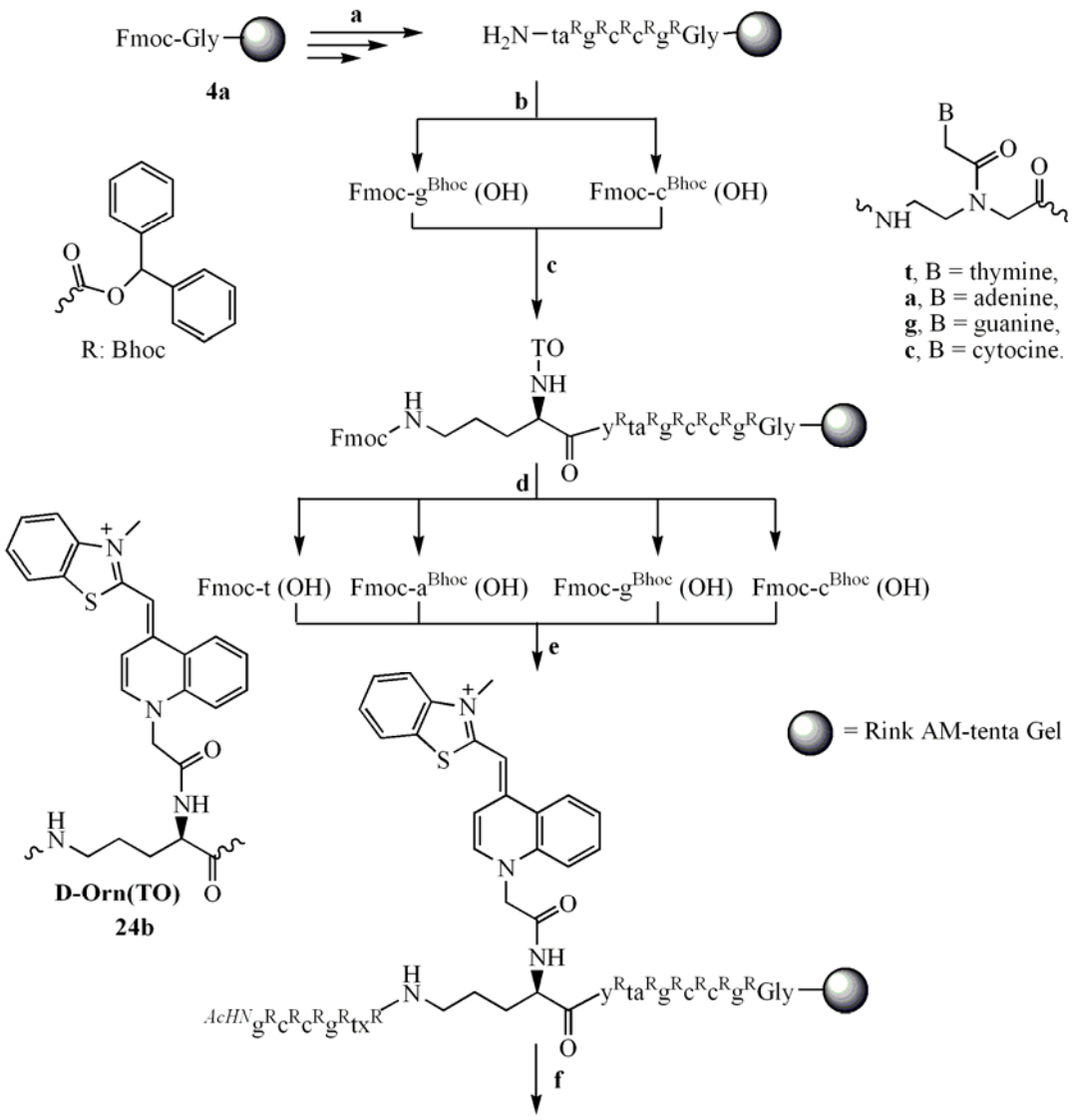

^{AcHN}gccgtt**D-Orn (TO)**gtagccgGly^{CONH2} 4.0 % **33,** ^{AcHN}gccgtt**D-Orn (TO)**ctagccgGly^{CONH2} 4.9 % **37**

^{AcHN}gccgta**D-Orn (TO)**gtagccgGly^{CONH2} 11.0 % **34,** ^{AcHN}gccgta**D-Orn (TO)**ctagccgGly^{CONH2} 7.1 % **38**

^{AcHN}gccgtg**D-Orn(TO)**gtagccgGly^{CONH2} 9.2 % **35,** ^{AcHN}gccgtg**D-Orn (TO)**ctagccgGly^{CONH2} 10.2 % **39**

^{AcHN}gccgtc**D-Orn (TO)**gtagccgGly^{CONH2} 6.2 % **36,** ^{AcHN}gccgtc**D-Orn (TO)**ctagccgGly^{CONH2} 9.6 % **40**

Scheme 8: a, b, d and e) Cycle of 1) piperidine/ DMF; 2) Fmoc–B (Bhoc)–OH, NMM, PyBop, DMF; 3) Ac_2O/ pyridine, DMF; c) Cycle of 1) piperidine/ DMF; 2) Fmoc-D-Orn (TO)-OH, NMM, PyBop, PPTS, DMF; 3) Ac_2O/ pyridine, DMF; f) TFA, m-cresol, H_2O, L-Cys-OMe.

The linear solid phase synthesis was performed using preformed monomer **24b** (TO-D-Orn (Fmoc)-OH). The synthesis was performed by using an automated synthesizer as described procedure in Section 2. The average overall yields achieved by linear solid-phase synthesis were comparable to the average yields reached in the

divergent synthesis (7.8 % in linear synthesis vs. 5.7 % in divergent synthesis). The D-Orn-TO-PNA probes **33-40** were synthesized by using linear solid phase synthesis.

3.1.3 Divergent Solid Phase Synthesis for D-Orn Labeled PNA

The divergent route was employed using Fmoc-D-Orn (Alloc)-COOH[56] monomer as preformed building block, in the synthesis of PNA-TO conjugates **25-32**. The synthesis was carried out using procedure reported in Section 2 (Scheme 2) for Aeg-TO-PNA.

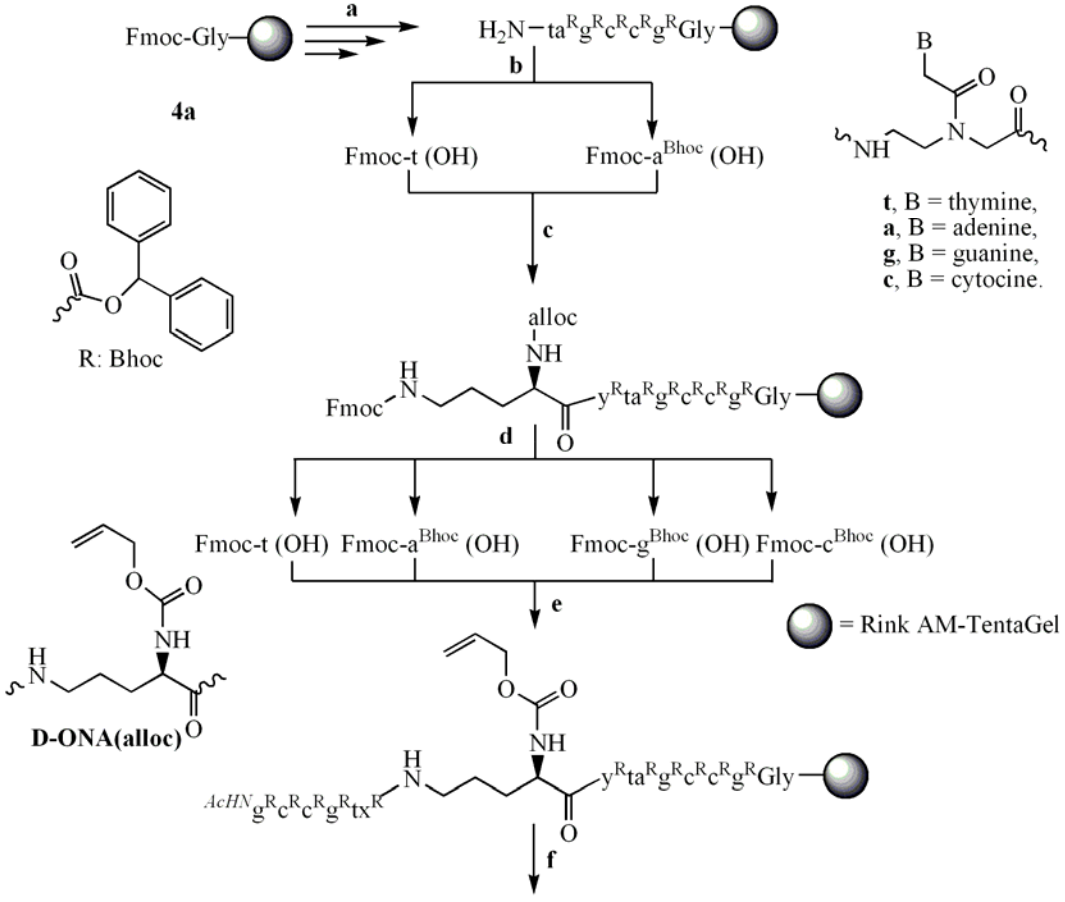

^{AcHN}gccgtt**D-ONA (TO)**ttagccgGly^{CONH2} 4.0 % **25,** ^{AcHN}gccgtt**D-ONA (TO)**atagccgGly^{CONH2} 5.0 % **29**

^{AcHN}gccgta**D-ONA (TO)**ttagccgGly^{CONH2} 2.6 % **26,** ^{AcHN}gccgta**D-ONA (TO)**atagccgGly^{CONH2} 4.8 % **30**

^{AcHN}gccgtg**D-ONA (TO)**ttagccgGly^{CONH2} 2.0 % **27,** ^{AcHN}gccgtg**D-ONA (TO)**atagccgGly^{CONH2} 10.4 % **31**

^{AcHN}gccgtc**D-ONA (TO)**ttagccgGly^{CONH2} 10.0 % **28,** ^{AcHN}gccgtc**D-ONA (TO)**atagccgGlyC^{CONH2} 7.1 % **32**

Scheme 9: a, b, d and e) Cycle of 1) piperidine/ DMF; 2) Fmoc–B (Bhoc)–OH, NMM, PyBop, DMF; 3) Ac_2O/ pyridine, DMF; c) Cycle of 1) piperidine/ DM; 2) Fmoc-D-Orn (Alloc)-OH, NMM, PyBop, DMF; 3) Ac_2O/ pyridine, DMF; f) 1) [Pd $(PPh_3)_4$], $Me_2NH{\cdot}BH_3$, CH_2Cl_2; 2) TO-CH_2-COOH, PyBOP, PPTS, NMM, DMF (double coupling); 3) TFA, m-cresol, H_2O, L-Cys-OMe.

Scheme 10: D-Orn-TO-PNA probes **25-40** and DNA's **5'-20'** (MZN) which were allowed to hybridise with differing by pairing partner, stacking partners to N-side and C-side of thiazole orange.

3.2 Sequence Dependent Fluorescence of D-Orn-TO-PNA (dye-nucleic acid conjugates)

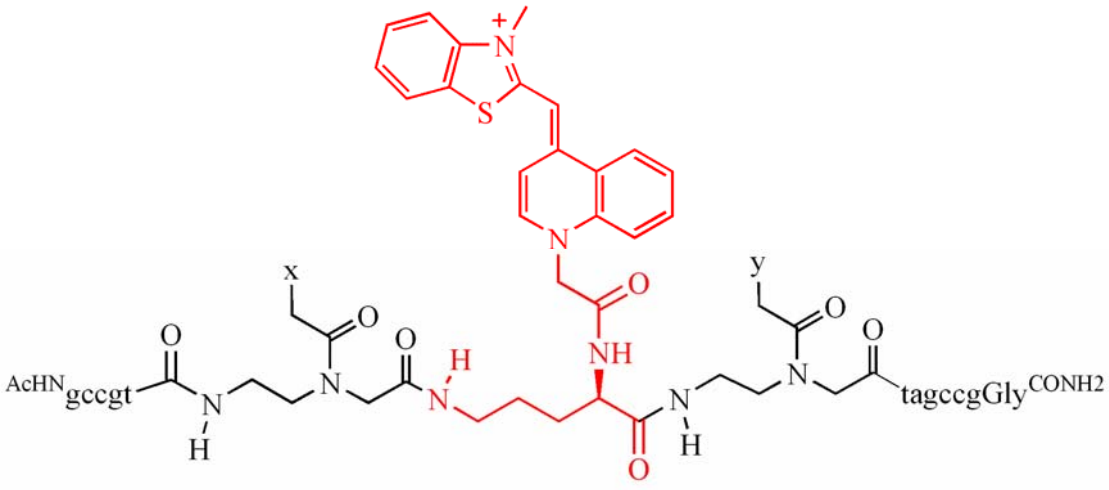

25;[x:y] = tt, 26;[x:y] at, 27;[x:y] = gt, 28;[x:y] ct,
29;[x:y] = ta, 30;[x:y] aa, 31;[x:y] = ga, 32;[x:y] ca,
33;[x:y] = tg, 34;[x:y] ag, 35;[x:y] = gg, 36;[x:y] cg,
37;[x:y] = tc, 38;[x:y] ac, 39;[x:y] = gc, 40;[x:y] cc.

Scheme 11: Structure of D-Orn (TO)-OH labeled peptide nucleic acids library.

D-Orn-TO-PNA oligomer (**25-40**) were hybridised with oligonucleotides (**5'-20'MZN**). The fluorescence properties were assessed as described for Aeg-TO-PNA (Section 2). The x and y were all variable DNA bases adjacent to D-Orn-TO.

3.2.1 Matched Hybridization

Figure 27 shows the fluorescence enhancement of TO-PNA conjugates after formation of matched duplexes with complementary oligonucleotides in which D-Orn (TO) was paired against and stack to each of the DNA bases (T, A, G and C).

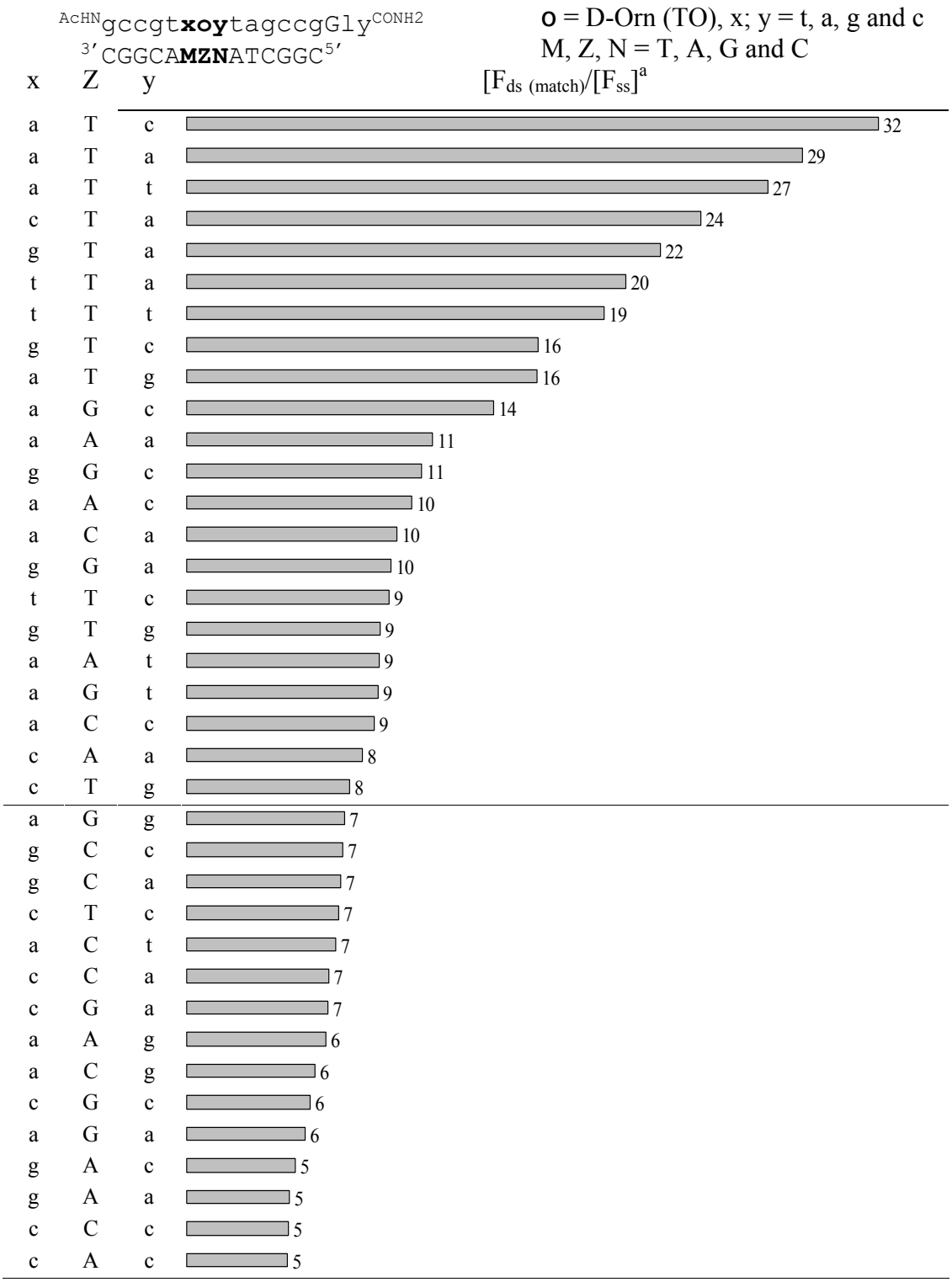

^{AcHN}gccgt**xoy**tagccgGly^{CONH2}
$^{3'}$CGGCA**MZN**ATCGGC$^{5'}$

o = D-Orn (TO), x; y = t, a, g and c
M, Z, N = T, A, G and C

x	Z	y	$[F_{ds\ (match)}/[F_{ss}]^a$
c	C	g	4
t	G	c	4
t	A	c	4
t	T	g	4
t	C	c	4
t	A	a	3
t	C	a	3
c	T	t	3
c	A	g	3
g	T	t	3
t	G	a	3
t	A	t	3
g	A	g	2
g	G	g	2
t	G	t	2
c	G	g	2
t	C	t	2
g	C	g	2
g	G	t	2
c	C	t	1
g	A	t	1
t	C	g	1
t	A	g	1
c	G	t	1
g	C	t	1
c	A	t	1
t	G	g	1

Figure 27: Fluorescence enhancement of PNA probes **25-32,** measured at 530 nm after formation of matched duplexes, when TO was paired against thymine, adenine, guanine and cytosine at 25°C in buffer. [$^a F_{ds}/ F_{ss}$ = Ratio between fluorescence intensities of FIT-PNA after and before addition of DNA at 530 nm. Measurement conditions: see Figure 23].

Discussion

Figure 27 shows relative fluorescence increase upon formation of matched duplex (top-bottom). The letters x and y are for adjacent nucleobases for TO in PNA probe from N'-side to C'-side respectively.

The fluorescence enhancement obtained upon hybridization of D-Orn-FIT-PNA probes with matched oligonucleotides are also classified into good probes ≥ 8 fold, mediocre probes ≥4 to <8 fold and modest probes < 4 fold. In the D-Orn-TO-PNA library there are 22 duplexes (34 %) producing more than 8 fold fluorescence

enhancement. In contrast only 14 of the Aeg-TO probes produced ≥8 fold fluorescence enhancement. Out of the 22 Orn-TO containing duplexes that show ≥8 fold intesification, 18 contain at least one a-T or t-A stacking base pair adjacent to TO. The D-Orn-TO-PNA library contains 6 duplexes which are producing ≥ 20 fold fluorescence enhancements. All of these probes contain at least one a-T as adjacent base pair for TO and feature thymine as TO pairing partner. D-Orn-TO-PNA probes provide 20 (32 %) duplexes showing 4-8 fold fluorescence enhancement (Figure 27). Lower than 4 fold fluorescence an enhancement was measured for 22 (34 %) duplexes. These duplexes have at least one thymine or guanine as TO adjacent base.

The hybridisation induced fluorescence enhancement provided by D-Orn-TO-PNA on average is higher than the fluorescence enhancement by Aeg-TO-PNA. Average fluorescence increase when at least one AT base pair acts as stacking partner for TO was measured 6.6 fold. It was recorded 6.7 fold if at least one GC base pair acts as TO stacking partner. The average fluorescence increase when TO is against T, A, G or C was measured 15.6, 5.0, 5.4 and 4.8 fold, respectively. Thymine is again the preferred pairing partner for TO. The adjacent base is also playing an important role in the fluorescence of single strand and matched double strand. Average fluorescence increase with one adenine as intrastrand TO stacking partner is 12 fold. Enhancement of 7.5 fold, 5.6 fold and 5.4 fold were obtained with c, g and t respectively, as stacking partner. To achieve high fluorescence labelled thiazole orange should place in between a bases a-c> a-a> a-g> a-t.

Comparing results obtained for Aeg-TO-PNA in section 2, D-Orn-TO labelled PNA was found to produce higher fluorescence enhancements upon matched hybridisation.

3.2.2 Fluorescence vs. Temperature study upon hybridization with matched oligonucleotides

Figure 28 shows the fluorescence enhancement against temperature profile of FIT-PNA **25** (t-TO-t), **30** (a-TO-a), **35** (g-TO-g) and **40** (c-TO-c) upon hybridization with corresponding matched oligonucleotides varying TO pairing partner.

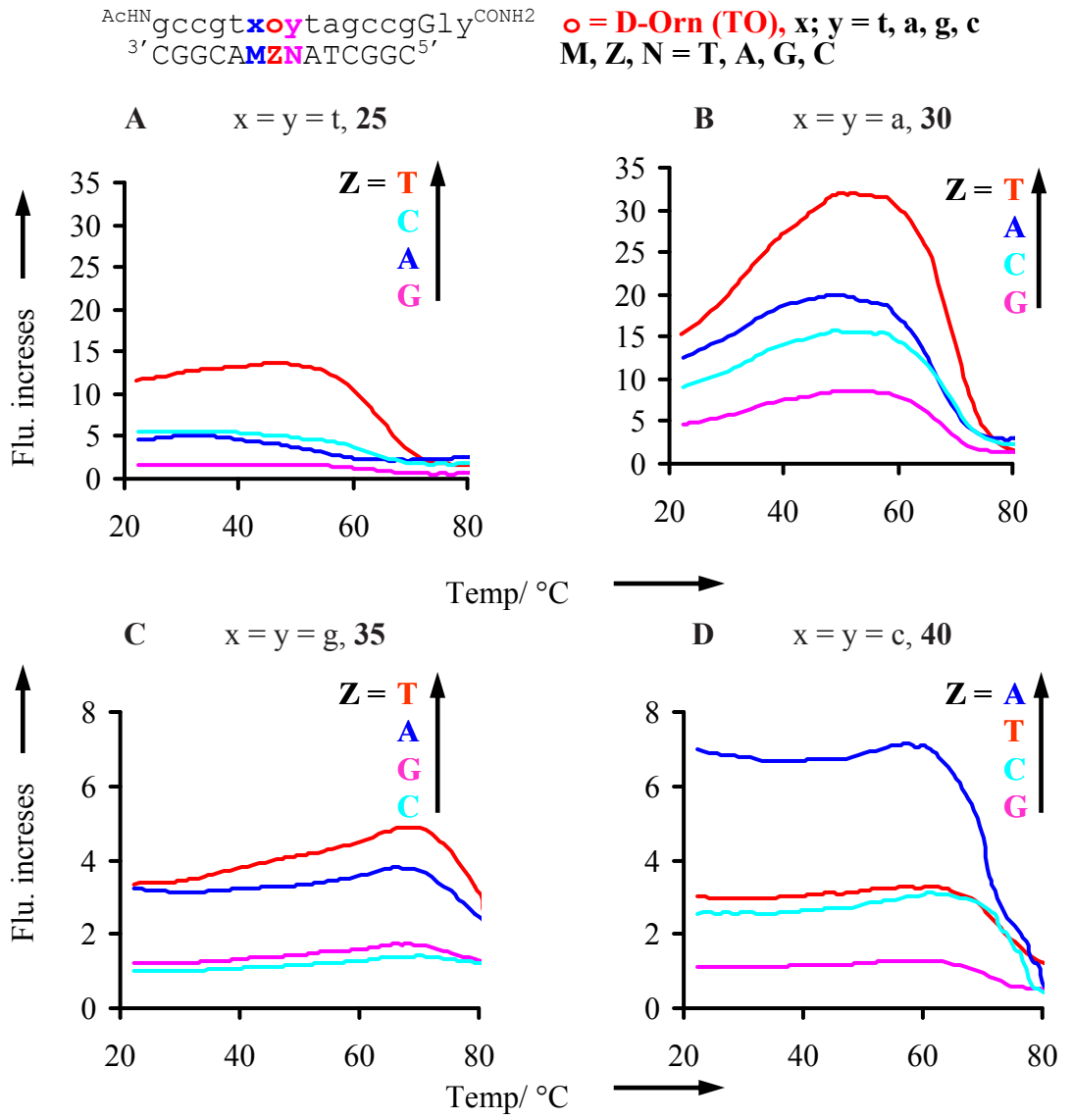

Figure 28: Fluorescence enhancement vs. temperature of D-Orn-FIT-PNA upon hybridization with matched DNA (TO vs T = red, TO vs A = blue, TO vs G = pink and TO vs C = turquoise). M and N are always complementary to x and y, A) **25** (t-TO-t), B) **30** (a-TO-a), C) **35** (g-TO-g) and D) **40** (c-TO-c). [Measurement conditions: see caption of Figure 24].

Discussion

Fluorescence enhancement is constant or even increased upon increases of temperatures. In the experimental setup, the PNA probe **30** (a-TO-a) gives 17 fold fluorescence enhancement at 25°C and it is 32 fold at 53°C upon hybridization with matched DNA **5'TTT** (Figure 28B). The matched duplexes where thiazole orange is in between two guanines shows lower fluorescence enhancement compared to in between two adenines, two thymines or two cytosines. Expectedly, on dissociation of TO-PNA•DNA duplex the fluorescence decreases rapidly.

The fluorescence enhancement versus temperature pattern is not similar in all above four probes. Guanine as pairing base for TO shows weaker fluorescence enhancement than other nucleobases in probes **25**, **30** and **35**. Probe **30** (a-TO-a) is best probe producing good fluorescence enhancement than all other three probes. The probe **25** (t-TO-t) is second best, but it is producing half of fluorescence enhancement than probe **30** after hybridization with corresponding matched oligonucleotides.

^{AcHN}gccgt**xoy**tagccgGly^{CONH2}
$^{3'}$CGGCA**MZN**ATCGGC$^{5'}$

o = D-Orn (TO), x; y = t, a, g and c
M, Z, N = T, A, G and C

x	Z	y	T°C[a]	$[F_{ds\ (match)}/F_{ss}]$[b]
a	**T**	a	52	32
t	**T**	a	57	25
a	**T**	t	52	22
a	**T**	c	58	20
a	**A**	a	47	20
a	**C**	a	52	16
a	**A**	c	55	14
t	**T**	t	45	14
a	**A**	t	30	10
t	**A**	a	45	10
a	**C**	c	54	10
a	**G**	c	52	9
g	**T**	a	52	9
a	**G**	a	52	9
c	**A**	a	36	8
c	**T**	a	40	8
a	**T**	g	60	7
c	**A**	c	56	7
t	**C**	a	56	7
g	**T**	c	30	7
a	**C**	t	25	7
a	**C**	g	52	7
a	**A**	g	54	6
t	**A**	c	25	6
a	**G**	t	25	6
t	**C**	t	30	6
t	**T**	c	60	5
t	**A**	t	35	5
g	**T**	g	66	5
g	**A**	c	25	5
g	**T**	t	58	5
g	**A**	a	37	5
t	**G**	a	54	4
g	**A**	t	58	4
t	**A**	g	25	4
g	**A**	g	65	4
t	**C**	c	56	4
g	**C**	c	25	4
g	**C**	a	62	4
c	**A**	g	25	4
c	**C**	a	35	3
t	**T**	g	53	3
c	**T**	c	52	3
c	**C**	c	60	3
g	**C**	t	52	3
t	**C**	g	62	3

^{AcHN}gccgt**xoy**tagccgGly^{CONH2}
$^{3'}$CGGCA**MZN**ATCGGC$^{5'}$

o = D-Orn (TO), x; y = t, a, g and c
M, Z, N = T, A, G and C

x	Z	y	T°C[a]	[$F_{ds\ (match)}$ /F_{ss}][b]
c	**T**	t	62	3
c	**T**	g	62	2
c	**C**	g	58	2
c	**A**	t	60	2
g	**G**	t	56	2
g	**G**	g	65	2
t	**G**	t	38	2
a	**G**	g	60	2
t	**G**	c	40	2
g	**G**	c	34	2
c	**G**	a	60	2
g	**C**	g	62	1
g	**G**	a	36	1
c	**G**	c	54	1
c	**C**	t	56	1
c	**G**	t	58	1
t	**G**	g	60	1
c	**G**	g	65	1

Figure 29: Fluorescence enhancement at optimal temperature of PNA probes **25-40,** measured at 530 nm after formation of matched duplexes, when TO was paired against thymine, adenine, guanine and cytosine. [[a] T = Temperature at which high fluorescence enhancement was recorded. [b] F_{ds}/ F_{ss} = Ratio between fluorescence intensities of FIT-PNA after and before addition of DNA at 530 nm. Measurement conditions: see caption of Figure 24].

Results and discussion

The fluorescence enhancement of FIT-PNA upon hybridization with matched DNA at optimal temperatures is also classified into good ≥ 8 fold, mediocre ≥4 to <8 fold and modest < 4 fold. Among 64 matched duplexes highest fluorescence (32 fold) was recorded at 52°C for probe **30** (a-TO-a) upon addition of matched DNA **5'TTT**. In the fluorescence vs. temperature experimental setup, it was found that high fluorescence enhancement was recorded at elevated temperature. Among 64 duplexes, 15 duplexes were found to fluoresce under the good category.Out of 16, 15 contain at least one adenine as adjacent base for TO. However, not a single duplex was able to produce good fluorescence when either two guanines or two cytosines or one guanine and cytosine were adjacent bases for TO.

The second mediocre category contains 24 (38 %) duplexes. The modest category contains 24 (38 %) duplexes. The fluorescence enhancement versus temperature study gives following hallmarks 1) thymine as first pairing base for TO, 2) adenine as first and thymine as second favored adjacent base for TO and 3) guanine as disfavored stacking or pairing base in the D-Orn-TO-PNA•DNA duplex.

3.2.3 Match/ mismatch discrimination

The experiment with hybridisation of D-Orn labelled PNA with matched DNAs showed that, D-Orn-TO labelled PNA can give higher fluorescence enhancement than Aeg-TO PNA. These encouraging results of D-Orn labelled PNA prompted to study fluorescence properties of D-Orn-TO labelled PNA upon hybridization with single base mismatched oligonucleotides. Studying the influence of neighbouring, stacking and pairing base for D-Orn-TO is important task for mutation analysis.

^{AcHN}gccgt**xoy**tagccgGly^{CONH2}
$^{3'}$CGGCA**MZN**ATCGGC$^{5'}$

o = D-Orn (TO), x; y = t, a, g and c
M, Z, N = T, A, G and C

x	Z	y	$[F_{ds\ (match)} - F_{ss}]/[F_{ds\ (mismatch)} - F_{ss}]^a$	$F_{ds\ (match)}/F_{ds\ (mismatch)}^b$
t•A	T	**t•G**	210.1	17.9
t•A	G	**c•C**	195.3	4.1
t•A	G	**c•T**	165.2	4.1
t•A	G	**c•A**	110.7	4.1
t•A	T	**a•A**	98.3	17.1
g•C	T	**t•T**	92.2	2.8
t•A	C	**t•C**	76.1	2.2
t•A	C	**t•G**	76.1	2.2
t•A	C	**t•T**	76.1	2.2
t•A	T	**t•C**	49.2	14.2
t•A	A	**a•A**	31.3	3.2
t•A	T	**a•C**	27.3	11.9
t•G	C	t•A	26.7	2.1
t•T	C	**t•A**	24.7	2.1
t•A	A	**t•G**	22.9	2.6
g•C	T	**t•C**	21.5	2.6
t•A	T	**a•G**	20.8	10.6
t•C	C	**t•A**	20.3	2.1
c•T	T	t•A	17.7	2.8
a•C	A	c•G	17.2	6.7
t•A	T	**t•T**	17.0	9.3
c•G	C	**t•T**	16.5	1.4
t•A	A	**a•G**	16.3	3.0
t•C	A	a•T	16.3	3.0
a•C	A	a•T	16.0	6.9
a•A	A	g•C	14.4	4.7
a•A	A	a•T	14.3	6.6
c•A	A	g•C	13.4	2.6
a•C	C	c•G	12.6	5.4
a•T	T	**c•A**	11.9	8.9
t•A	C	**a•C**	11.8	2.6
t•A	T	**c•A**	11.2	5.4
a•T	T	**t•G**	10.4	7.7

^{AcHN}gccgt**xoy**tagccgGly^{CONH2}
$^{3'}$CGGCA**MZN**ATCGGC$^{5'}$

o = D-Orn (TO), x; y = t, a, g and c
M, Z, N = T, A, G and C

x	Z	y	$[F_{ds\ (match)} - F_{ss}]/[F_{ds\ (mismatch)} - F_{ss}]^a$	$F_{ds\ (match)}/F_{ds\ (mismatch)}^b$
t•T	T	t•A	10.2	6.9
a•T	T	**a•A**	10.2	7.7
t•A	C	**a•A**	9.8	2.6
a•T	T	**c•T**	9.0	7.2
c•T	A	c•G	8.8	3.3
a•T	T	**c•C**	8.7	7.0
a•C	G	c•G	8.5	5.6
g•G	G	t•A	8.3	1.5
c•C	T	t•A	8.2	2.5
t•C	T	t•A	8.1	5.9
t•C	C	c•G	7.6	2.6
a•T	T	t•C	7.6	6.1
a•A	G	a•T	7.6	3.5
c•C	A	c•G	7.3	3.1
c•G	T	**a•A**	7.1	5.6
a•C	A	g•C	6.9	3.6
a•T	A	**a•C**	6.7	4.5
t•A	T	**g•T**	6.7	2.6
c•A	T	t•A	6.6	2.4
t•C	T	a•T	6.5	5.1
c•G	G	**t•C**	6.5	1.1
a•T	T	**t•T**	6.3	5.3
a•T	C	**a•C**	6.2	4.1
t•A	T	**c•C**	6.2	4.0
c•A	C	c•G	6.2	3.0
a•T	T	**a•C**	6.2	5.2
a•T	T	**a•G**	6.1	5.2
a•C	T	t•A	6.0	5.1
t•G	T	t•A	6.0	4.7
t•T	C	c•G	5.9	2.5
a•T	A	**a•A**	5.8	4.1
t•A	G	**t•C**	5.7	1.9
a•T	G	**c•T**	5.7	4.3
a•C	C	a•T	5.5	3.8
c•A	T	a•T	5.5	4.6
a•A	T	t•A	5.5	4.7
a•C	G	a•T	5.5	3.0
a•A	A	c•G	5.4	3.8
t•T	A	a•T	5.4	2.4
g•C	T	**g•G**	5.4	3.6
c•G	T	**g•T**	5.3	3.4
a•A	T	c•G	5.3	4.7
g•C	T	**g•T**	5.3	3.6
c•G	T	**a•G**	5.3	3.0
t•T	T	a•T	5.2	4.3
g•C	T	**c•A**	5.2	4.1

^{AcHN}gccgt**xoy**tagccgGly^{CONH2}
$^{3'}$CGGCA**MZN**ATCGGC$^{5'}$

o = D-Orn (TO), x; y = t, a, g and c
M, Z, N = T, A, G and C

x	Z	y	$[F_{ds\ (match)} - F_{ss}]/[F_{ds\ (mismatch)} - F_{ss}]^a$	$F_{ds\ (match)}/F_{ds\ (mismatch)}^b$
c•A	A	c•G	5.2	2.7
t•G	C	c•G	5.2	2.4
a•A	G	c•G	5.1	4.0
c•G	T	**a•C**	5.1	4.3
t•C	C	a•T	5.0	2.2
c•C	C	c•G	5.0	2.7
t•G	A	a•T	4.9	2.3
a•C	A	t•A	4.9	3.4
t•G	A	t•A	4.9	2.0
a•T	A	**t•G**	4.9	3.4
a•A	G	g•C	4.8	3.2
a•T	G	**c•C**	4.8	3.8
c•G	G	c•A	4.8	2.9
a•A	T	a•T	4.7	4.2
g•C	T	g•A	4.7	3.3
t•A	C	**c•C**	4.7	2.3
g•G	A	t•A	4.6	1.3
a•A	A	t•A	4.6	3.3
a•T	A	**a•G**	4.6	3.5
c•G	G	**c•C**	4.6	2.8
g•C	T	**a•A**	4.6	3.9
g•C	G	**c•C**	4.6	3.4
a•C	T	c•G	4.5	4.1
a•A	C	c•G	4.5	3.2
a•G	A	a•T	4.5	3.5
g•C	G	**c•A**	4.4	3.4
c•T	C	**c•G**	4.4	2.6
c•T	T	a•T	4.3	3.8
a•T	G	**t•G**	4.3	3.1
g•C	T	**c•T**	4.2	3.5
t•C	A	c•G	4.1	2.3
a•C	C	t•A	4.1	2.8
t•C	G	a•T	4.1	2.0
t•C	G	c•G	4.0	2.3
a•A	C	a•T	4.0	3.1
t•T	T	g•C	3.9	2.2
a•T	A	**c•C**	3.9	3.1
a•T	C	**a•A**	3.9	3.0
t•T	G	c•G	3.9	2.3
t•G	A	c•G	3.9	2.2
t•A	A	**c•C**	3.9	2.2
a•C	T	a•T	3.8	3.5
a•T	G	**c•A**	3.8	3.2
c•C	T	a•T	3.8	3.4
a•T	A	**c•A**	3.8	3.0
c•C	G	c•G	3.7	2.5

^{AcHN}gccgt**xoy**tagccgGly^{CONH2}
$^{3'}$CGGCA**MZN**ATCGGC$^{5'}$

o = D-Orn (TO), x; y = t, a, g and c
M, Z, N = T, A, G and C

x	Z	y	$[F_{ds\ (match)} - F_{ss}]/[F_{ds\ (mismatch)} - F_{ss}]^a$	$F_{ds\ (match)}/F_{ds\ (mismatch)}^b$
a•A	G	t•A	3.7	2.8
c•G	G	**c•T**	3.7	2.5
c•G	T	**c•A**	3.6	2.6
g•C	G	**c•T**	3.6	2.9
t•A	G	**a•A**	3.5	1.9
g•G	C	t•A	3.5	1.1
c•A	G	**c•G**	3.5	2.4
c•G	C	**c•C**	3.4	2.3
t•T	G	a•T	3.4	1.8
g•C	G	**a•C**	3.4	2.7
c•T	A	g•C	3.4	1.9
g•C	T	**a•G**	3.4	3.1
a•T	C	**c•C**	3.3	2.6
g•C	C	**c•T**	3.3	2.5
c•G	A	**a•C**	3.3	2.6
t•A	A	**t•C**	3.3	1.8
a•T	C	**a•G**	3.3	2.7
t•G	C	a•T	3.3	1.9
c•G	C	**c•T**	3.3	2.2
a•T	T	**g•T**	3.3	2.9
a•T	C	**t•G**	3.3	2.5
a•C	G	t•A	3.3	2.6
t•G	G	c•G	3.2	2.1
t•A	A	**c•A**	3.2	2.1
t•G	T	a•T	3.2	2.9
t•A	G	**a•G**	3.2	1.8
g•C	C	**c•C**	3.2	2.5
c•G	T	g•A	3.2	2.4
g•C	A	t•T	3.1	1.2
g•T	G	g•C	3.1	1.7
t•G	T	g•C	3.0	1.9
c•T	G	c•G	3.0	2.2
c•A	A	a•T	3.0	2.4
c•A	A	t•A	2.9	1.1
c•G	A	**c•C**	2.9	2.1
c•G	T	**g•G**	2.9	2.3
c•G	T	**c•T**	2.9	2.3
c•G	A	**c•A**	2.9	2.0
g•G	T	a•T	2.8	2.6
c•T	A	a•T	2.8	2.3
a•C	G	g•C	2.8	2.3
a•T	T	**g•G**	2.8	2.5
a•T	A	**c•T**	2.8	2.4
a•G	T	t•A	2.8	2.6
c•G	G	**a•C**	2.8	2.2
g•T	A	g•C	2.7	1.6

^{AcHN}gccgt**xoy**tagccgGly^{CONH2}
$^{3'}$CGGCA**MZN**ATCGGC$^{5'}$

o = D-Orn (TO), x; y = t, a, g and c
M, Z, N = T, A, G and C

x	Z	y	$[F_{ds\ (match)} - F_{ss}]/[F_{ds\ (mismatch)} - F_{ss}]^a$	$F_{ds\ (match)}/F_{ds\ (mismatch)}^b$
c•G	A	**c•T**	2.7	2.0
c•G	T	**c•C**	2.7	2.2
c•G	C	**a•C**	2.7	2.1
a•T	C	**t•C**	2.7	2.1
t•T	T	c•G	2.7	2.3
t•C	T	g•C	2.7	1.8
g•A	A	g•C	2.6	1.6
t•G	T	c•G	2.6	2.2
c•A	C	a•T	2.6	2.1
a•T	A	**t•C**	2.6	2.2
g•C	C	**a•C**	2.6	2.1
g•C	G	**a•A**	2.6	2.2
c•G	C	t•C	2.5	1.2
g•C	A	c•C	2.5	1.9
c•G	A	**a•A**	2.5	2.1
c•C	A	g•C	2.5	1.7
g•C	A	**g•T**	2.5	1.5
t•C	T	c•G	2.4	2.1
t•T	C	a•T	2.4	1.7
g•G	G	a•T	2.4	2.1
a•T	G	**a•A**	2.4	1.9
a•T	T	**g•A**	2.3	2.2
g•C	A	**g•G**	2.3	1.5
a•T	G	**a•C**	2.3	1.9
a•T	G	**t•C**	2.3	2.0
g•C	G	**a•G**	2.3	2.0
c•G	C	**g•G**	2.3	1.8
a•G	T	a•T	2.3	2.2
c•T	T	c•G	2.3	1.9
t•G	G	a•T	2.3	1.6
g•C	A	**c•A**	2.3	1.8
g•G	A	g•C	2.3	1.5
c•G	A	**g•T**	2.2	1.6
a•T	A	**t•T**	2.2	2.0
c•G	A	**g•G**	2.2	1.6
c•A	T	c•G	2.2	1.9
a•T	G	**t•T**	2.2	1.9
a•T	C	**t•T**	2.2	1.9
a•A	C	g•C	2.1	1.8
g•G	T	c•G	2.1	2.0
c•A	T	g•C	2.1	1.9
a•A	C	t•A	2.1	1.8
c•A	C	g•C	2.1	1.7
g•G	C	c•G	2.1	1.8
a•T	A	**g•G**	2.1	1.8
t•G	C	g•C	2.1	1.1

^{AcHN}gccgt**xoy**tagccgGly^{CONH2}
$^{3'}$CGGCA**MZN**ATCGGC$^{5'}$

o = D-Orn (TO), x; y = t, a, g and c
M, Z, N = T, A, G and C

x	Z	y	$[F_{ds\ (match)} - F_{ss}]/[F_{ds\ (mismatch)} - F_{ss}]^a$	$F_{ds\ (match)}/F_{ds\ (mismatch)}^b$
g•T	G	c•G	2.1	1.9
g•C	T	**a•C**	2.1	2.0
g•A	G	a•T	2.0	1.8
a•T	C	**c•A**	2.0	1.8
a•A	T	g•C	2.0	1.9
a•C	C	g•C	2.0	1.7
g•T	C	t•A	2.0	1.1
a•T	C	**c•T**	2.0	1.8
g•C	G	**g•G**	2.0	1.4
c•T	C	a•T	2.0	1.7
g•C	C	**a•A**	2.0	1.7
c•G	A	**a•G**	2.0	1.1
t•C	G	g•C	1.9	1.0
c•C	C	g•C	1.9	1.6
c•C	C	a•T	1.9	1.7
g•T	G	a•T	1.9	1.8
a•T	A	**g•T**	1.9	1.7
g•C	A	**a•C**	1.9	1.6
g•C	C	**c•A**	1.9	1.7
c•G	C	**a•G**	1.9	1.6
g•G	G	g•C	1.9	1.4
t•A	A	**c•T**	1.9	1.5
a•G	G	t•A	1.8	1.7
a•T	G	**g•T**	1.8	1.6
c•G	G	**a•A**	1.8	1.6
c•G	G	**t•T**	1.8	1.1
c•G	C	**a•A**	1.8	1.6
c•C	T	g•C	1.8	1.6
c•T	T	g•C	1.8	1.6
g•T	A	c•G	1.8	1.5
g•C	T	**c•C**	1.8	1.7
g•C	C	**a•G**	1.8	1.6
g•T	T	c•G	1.7	1.7
g•G	A	**c•G**	1.7	1.5
g•C	G	**g•T**	1.7	1.3
t•A	T	**c•T**	1.7	1.6
g•A	G	g•C	1.7	1.3
g•C	A	**c•T**	1.7	1.5
t•T	C	g•C	1.7	1.1
c•C	T	c•G	1.7	1.5
g•T	C	c•G	1.7	1.5
t•T	A	c•G	1.6	1.4
a•G	T	**c•G**	1.6	1.6
g•T	T	g•C	1.6	1.5
c•T	C	g•C	1.6	1.4
c•C	A	a•T	1.6	1.5

^{AcHN}gccgt**xoy**tagccgGly^{CONH2}
$^{3'}$CGGCA**MZN**ATCGGC$^{5'}$

o = D-Orn (TO), x; y = t, a, g and c
M, Z, N = T, A, G and C

x	Z	y	$[F_{ds\ (match)} - F_{ss}]/[F_{ds\ (mismatch)} - F_{ss}]^a$	$F_{ds\ (match)}/F_{ds\ (mismatch)}^b$
a•T	G	**g•G**	1.5	1.4
g•G	T	t•A	1.5	1.3
t•T	A	t•A	1.5	1.3
c•G	C	**g•T**	1.5	1.4
g•G	T	g•C	1.5	1.4
t•A	C	**a•G**	1.5	1.3
g•G	A	a•T	1.4	1.3
c•G	A	**t•C**	1.4	1.0
c•A	G	a•T	1.4	1.3
g•A	T	a•T	1.4	1.3
g•C	A	**a•A**	1.4	1.3
c•G	G	**a•G**	1.3	2.0
t•A	A	**t•T**	1.3	1.2
a•G	G	a•T	1.3	1.3
g•G	G	c•G	1.3	1.3
a•G	A	t•A	1.3	1.3
g•A	A	t•A	1.3	1.1
a•G	A	g•C	1.3	1.2
g•A	G	t•A	1.3	1.1
t•A	C	**c•T**	1.3	1.2
g•C	A	**g•A**	1.3	1.2
a•G	C	c•G	1.3	1.2
c•G	C	**g•A**	1.3	1.2
g•T	T	a•T	1.3	1.3
a•T	G	**a•G**	1.2	1.2
g•A	C	t•A	1.2	1.0
g•G	C	a•T	1.2	1.2
a•C	T	g•C	1.2	1.2
t•C	C	g•C	1.2	1.0
a•T	C	**g•G**	1.2	1.2
a•G	C	a•T	1.2	1.2
a•T	A	**g•A**	1.2	1.2
c•C	G	a•T	1.2	1.2
c•T	G	a•T	1.2	1.2
g•A	A	a•T	1.2	1.1
a•T	G	**g•A**	1.2	1.2
g•T	C	a•T	1.2	1.1
g•A	C	c•G	1.2	1.1
t•C	A	t•A	1.1	1.1
g•C	G	**g•A**	1.1	1.1
c•G	C	t•G	1.1	1.0
g•A	T	g•C	1.1	1.1
g•C	A	a•G	1.1	1.1
c•G	A	**t•T**	1.1	1.0
c•G	A	**g•A**	1.1	1.0
g•A	T	t•A	1.0	1.0

^{AcHN}gccgt**xoy**tagccgGly^{CONH2}
$^{3'}$CGGCA**MZN**ATCGGC$^{5'}$

o = D-Orn (TO), x; y = t, a, g and c
M, Z, N = T, A, G and C

x	Z	y	$[F_{ds\ (match)} - F_{ss}]/[F_{ds\ (mismatch)} - F_{ss}]$[a]	$F_{ds\ (match)}/F_{ds\ (mismatch)}$[b]
g•C	C	g•G	1.0	1.0
g•T	T	t•A	1.0	1.0
g•A	T	c•G	1.0	1.0
g•T	A	a•T	0.9	1.0
c•G	C	**c•A**	0.9	0.9
g•A	G	c•G	0.9	0.9
a•T	C	**g•T**	0.9	0.9
a•G	T	**g•C**	0.9	0.9
g•A	C	a•T	0.9	0.9
a•G	A	c•G	0.9	0.9
t•A	C	**c•A**	0.9	0.9
c•G	G	**g•G**	0.9	0.9
a•G	G	g•C	0.9	0.9
a•G	C	t•A	0.8	0.9
g•A	A	c•G	0.8	0.9
g•T	C	g•C	0.8	0.9
g•C	C	**g•T**	0.8	0.9
a•G	G	c•G	0.8	0.8
t•A	C	**g•G**	0.8	0.9
a•T	C	**g•A**	0.7	0.7
c•G	G	**g•A**	0.7	0.8
c•G	G	**g•T**	0.7	0.8
a•G	C	g•C	0.6	0.7
g•A	C	g•C	0.6	0.7
g•C	C	**g•A**	0.5	0.7
g•G	C	g•C	0.5	0.7
t•G	A	g•C	0.5	0.9
t•A	C	**g•T**	0.4	0.7
t•T	A	g•C	0.4	0.8
c•A	G	g•C	0.4	0.5
t•A	C	g•A	0.4	0.7
c•C	G	g•C	0.4	0.5
c•T	G	g•C	0.3	0.4
t•C	A	g•C	0.2	0.6
t•A	G	**g•A**	-0.2	1.7
t•A	G	**g•G**	-0.3	1.8
t•A	G	**g•T**	-0.3	1.7
t•T	G	g•C	-0.3	1.7
c•T	A	**t•A**	-0.3	2.2
c•C	A	t•A	-0.4	1.9
c•A	G	t•A	-0.5	2.1
c•T	G	t•A	-0.5	2.0
t•A	A	**g•G**	-0.5	1.9
g•C	C	**t•T**	-0.5	1.7
t•G	G	g•C	-0.6	1.3
c•C	G	t•A	-0.6	1.8

^{AcHN}gccgt**xoy**tagccgGly^{CONH2}
$^{3'}$CGGCA**MZN**ATCGGC$^{5'}$

o = D-Orn (TO), x; y = t, a, g and c
M, Z, N = T, A, G and C

x	Z	y	$[F_{ds\ (match)} - F_{ss}]/[F_{ds\ (mismatch)} - F_{ss}]^a$	$F_{ds\ (match)}/F_{ds\ (mismatch)}^b$
t•A	A	**g•T**	-0.9	1.5
g•C	C	**t•G**	-0.9	1.4
t•A	A	**g•A**	-0.9	1.5
g•C	A	**t•G**	-1.7	1.8
g•C	C	**t•C**	-2.0	1.3
c•A	C	t•A	-2.4	1.7
c•G	A	**t•G**	-2.7	1.2
c•G	G	**t•G**	-2.9	1.3
c•C	C	t•A	-2.9	1.7
g•C	G	**t•G**	-3.2	2.0
t•T	G	t•A	-4.5	3.5
g•T	G	t•A	-5.3	1.9
g•**C**	G	**t•T**	-7.3	1.8
t•G	G	t•A	-8.3	2.9
t•A	T	**g•G**	-9.1	5.1
t•C	G	t•A	-9.4	2.8
c•T	C	t•A	-10.5	1.5
g•C	G	**t•C**	-10.7	1.7
c•G	T	**t•G**	-10.8	3.8
t•A	T	**g•A**	-13.3	2.6
t•A	G	**a•C**	-14.0	3.3
g•C	T	**t•G**	-15.1	3.3
g•T	A	t•A	-15.9	1.4
c•G	T	**t•C**	-25.9	3.4
t•A	G	**t•T**	-38.8	2.5
c•G	T	**t•T**	-44.9	3.3
t•A	A	**a•C**	-55.7	3.6
g•C	A	**t•C**	-55.9	1.4
t•A	G	**t•G**	-75.6	2.4

Figure 30: Match/mismatch fluorescence discrimination of PNA probes **25-40,** measured at 530 nm, when TO was paired against thymine, adenine, guanine and cytosine at 25°C in buffer. $^a[F_{ds\ (match)} - F_{ss}]/[F_{ds\ (mismatch)} - F_{ss}]$ = Ratio between fluorescence intensities of FIT-PNA after formation matched duplex-sinlgle strand fluorescence/mismatched duplex-single strand fluorescence at 530 nm. $^b[F_{ds\ (match)}/F_{ds\ (mismatch)}]$ = Ratio between fluorescence intensities of FIT-PNA after formation matched duplex-mismatched duplex at 530 nm. Measurement conditions: 1μM probe and DNA in buffer (100 mM NaCl, 10 mM NaH_2PO_4, pH 7), excitation: 510 nm.

Discussion

Figure 30 shows match/mismatch fluorescence discrimination of probes **25-40** at 25°C. The fluorescence discrimination is described in similar fashion as reported in Section 2 for Aeg-TO-PNA.

Higher than 10 fold, match/mismatch fluorescence discrimination is measured in 35 duplexes. The probe **25** (t-TO-t) shows highest (210 fold) match/mismatch fluorescence discrimination upon hybridization with DNA **11'GTA**. Fluorescence of corresponding mismatched duplexes is higher than fluorescence of matched duplexes in 31 hybrids. Out of 384 mismatched duplexes negative discrimination is found in 41 duplexes. This type of discrimination is observed if mismatched duplexes are fluorescing less intensily than its corresponding single strand. 312 mismatched duplexes have higher fluorescence than corresponding single strand and less than match duplexes.

There are 353 (92 %) duplexes that have high fluorescence with match DNA and attenuated fluorescence with mismatched DNA. The thiazole orange as fluorescent base surrogate attached to D-Orn gives comparative good fluorescence properties. Fluorescence enhancements in response to matched hybridisation appear higher than those observed with Aeg-TO as the fluorescent base. There also is a better match/mismatch discrimination as evidenced by results in Figure 30.

3.3 Conclusions

D-Orn-TO-PNA conjugates, in which thiazole orange replaces a nucleobase as well as its backbone shows better fluorescence properties than Aeg-TO-PNA. TO attached to D-Orn is better distinguishing a DNA target from its single base mismatch than Aeg-TO.

The collected data from all measurements allow us to draw the conclusion that the fluorescence of the D-Orn-TO labelled PNA is most responsive to hybridisation when TO is flanked by cytosine-adenine > adenine-adenine > adenine-guanine > adenine-thymine > thymine-thymine > cytosine-guanine > guanine-thymine > guanine-guanine > guanine-cytosine > cytosine-cytosine > cytosine-thymine > thymine-guanine. The preferred pairing partner to achieve high fluorescence with matched DNA and match/mismatch discrimination is thymine > guanine > adenine > cytosine. D-Orn-TO labelled PNA gives similar responsiveness to its neighbouring base, stacking base and pairing base with added advantages of higher match duplex fluorescence and higher match/mismatch fluorescence discrimination.

4. Exploring base-pair specific optical properties of the DNA stain thiazole orange by forced intercalation

The advancements in bioscience would not have been possible without simple methods for detecting and visualization of biomolecules such as DNA and RNA. Staining of nucleic acids is usually achieved by the use of fluorescent or strongly absorbing chromophores.[57] Unsymmetrical cyanine dyes such as oxazole yellow (YO and its dimer YOYO), thiazole orange (TO and its dimer TOTO), SYBR Green or Pico Green are particularly interesting due to their extraordinary increase in fluorescence upon binding to nucleic acids.[67, 73, 74, 75] This property has lead to advancements in a range of applications such as DNA quantification in homogenous phase and in gels, real-time polymerase chain reaction and in DNA binding and DNA damage assays. Binding of cyanine dyes to nucleic acids has been widely investigated, and oxazole yellow and thiazole orange are probably amongst the most studied unsymmetrical cyanines.[1, 2, 4, 76, 77, 78, 79] It has been shown that the monomeric cyanines bind DNA in different ways; intercalation between base-pairs, association to the minor groove as monomers, dimers and higher aggregates and interaction of positively charged dyes with the negatively charged ribose phosphate backbone (Figure 31 B).[1, 2, 77] A great deal of research effort has been devoted to the base-pair specificity of DNA binding. While preferred binding motifs have been found for dimeric bisintercalators such as YOYO and TOTO,[80, 81, 82, 83, 84] there is yet no conclusive evidence for sequence specific binding of the monomeric forms YO and TO. In addition, measurements of non-covalently bound dye-nucleic acid complexes are measurements of an ensemble of chromophores located at various binding sites. Thus, it has not been possible to assign optical properties such as the observed fluorescence to base-specific binding modes of YO and TO or, vice versa, to obtain information about the local environment of cyanines in nucleic acids by using optical spectroscopy.

Sequence-specificity by design can be achieved by linking cyanine dyes to oligonucleotides or analogues thereof.[50, 59, 85, 86, 87, 88, 89, 90, 91, 92] Previous work has shown that the tether that connects the fluorochrome and the nucleic acid probe plays an important role.[88, 93] Long tethers provide sufficient flexibility to

allow multiple binding modes. In contrast, in the so-called FIT probes developed by Seitz, the flexibility has been constrained by linking thiazole orange as fluorescent base surrogate (Figure 31).[85]

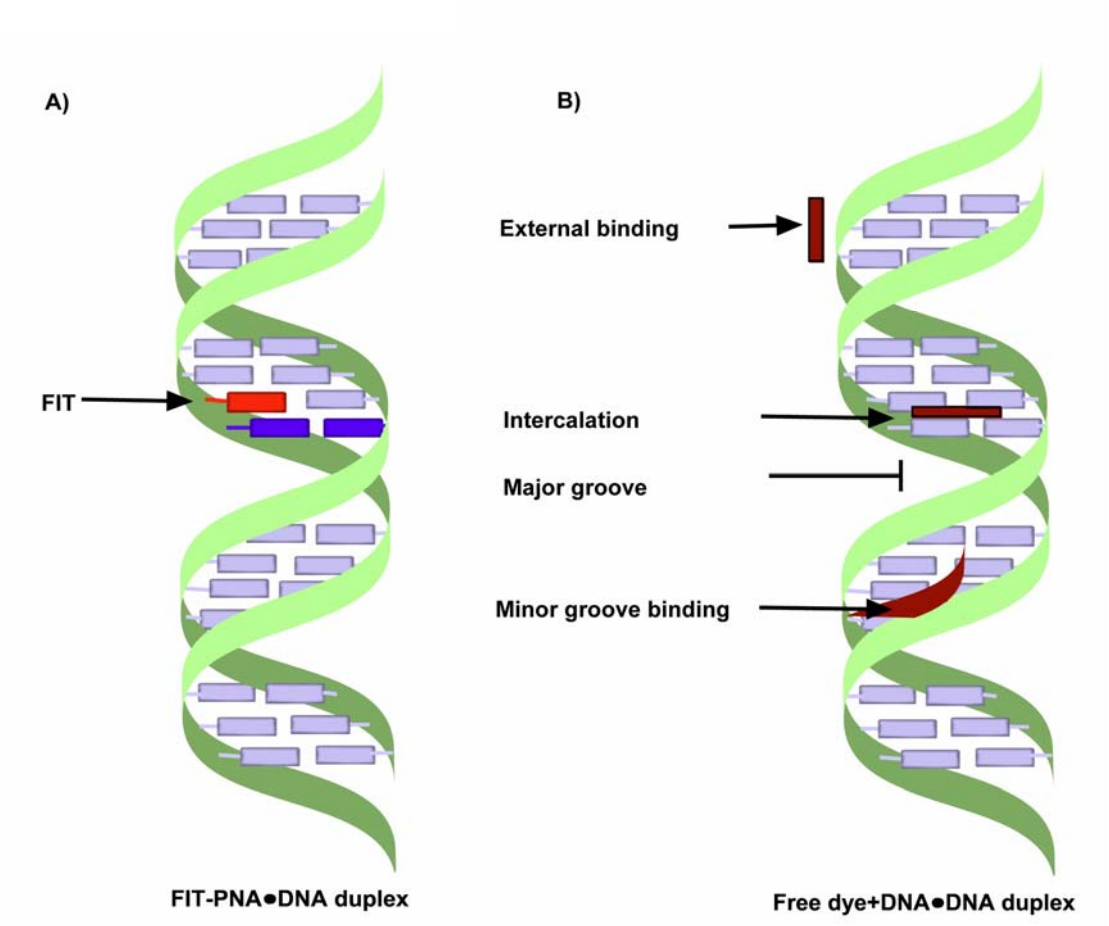

Figure 31: Schematic picture of A) specific binding mode (Intercalation) of Forced Intercalated Thiazole orange PNA complexed with DNA, and B) different binding modes of free dye to double stranded oligonucleotide.

One of the intriguing opportunities provided by such base replacement is to localize cyanine dyes to a specific site of the nucleic acid duplex and to assess the optical properties of this isolated binding mode without having to fear competition from other binding sites (Figure 31A). I herein provide a detailed analysis of the base-pair dependence of UV-VIS absorbance and steady state and time-resolved fluorescence emission properties and compare enforced binding of thiazole orange with "classical mode" binding of free TO-PRO1. It will be shown that forced intercalation, for the first time, reveals the influence of specific base-pairs on decay processes of the TO excited state. It will furthermore be demonstrated that interactions between TO and nucleobases result in both closing and opening of

different decay channels, and that the balance between these processes decides about the fluorescence output. It was also explored which decay processes are most responsive to local structure and perturbations introduced by the presence of mismatched base pairs.

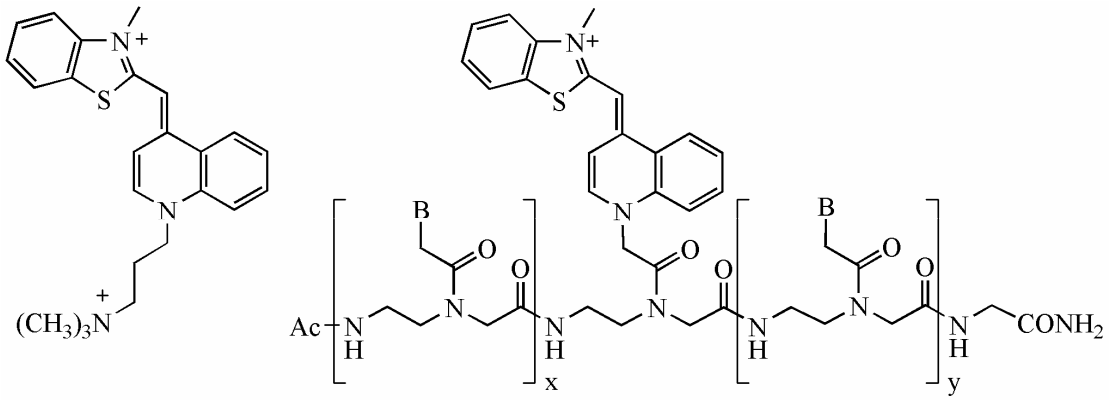

Scheme 12: Structure of TO-PRO1 and FIT-PNA.

```
  5'G-C-C-G-T-A-A-T-A-G-C-C-G3'                    4'AT, DNA
  3'C-G-G-C-A-T-T-A-T-C-G-G-C5'                    4'TA, DNA

ACHNg-c-c-c-t-a-a-t-a-g-c-c-g-GlyCONH2              4at, PNA
  3'C-G-G-C-A-T-T-A-T-C-G-G-C5'                    4'TA, DNA

ACHNg-c-c-c-t-x-Aeg(TO)-y-t-a-g-c-c-g-GlyCONH2      FIT-PNA
  3'C-G-G-C-A-M-   T   -N-A-T-C-G-G-C5'            DNA
```

	FIT-PNA	matched DNA	mismatched DNA
	-x-TO-*y*-	3'--*M*-T-*N*--5'	3'--*M*-T-*N*--5'
10,	-a-TO-a-	**5' TTT**, 3'--T-T-T--5'	**17'TTC**, 3'--T-T-C--5'
5,	-t-TO-t-	**10'ATA**, 3'--A-T-A--5'	**18'ATC**, 3'--A-T-C--5'
15,	-g-TO-g-	**20'CTC**, 3'--C-T-C--5'	**16'CTG**, 3'--C-T-G--5'
20,	-c-TO-c-	**15'GTG**, 3'--G-T-G--5'	**19'GTC**, 3'--G-T-C--5'
6,	-a-TO-t-	**9' TTA**, 3'--T-T-A--5'	**17'TTC**, 3'--T-T-C--5'
14,	-a-TO-g-	**17'TTC**, 3'--T-T-C--5'	**13'TTG**, 3'--T-T-G--5'
18,	-a-TO-c-	**13'TTG**, 3'--T-T-G--5'	**17'TTC**, 3'--T-T-C--5'
19,	-g-TO-c-	**16'CTG**, 3'--C-T-G--5'	**20'CTC**, 3'--C-T-C--5'

Scheme 13: Studied nucleic acids and nucleic acid dye conjugates.

4.1 Results and Discussion

In duplexes, containing TO-PNA conjugates such as FIT-PNA **5-20xy**, (Scheme 13) thiazole orange can be specifically embedded between two selected

base-pairs. Thus, it is possible to explore the responsiveness of the optical properties of thiazole orange to defined changes of the local environment. For comparison unconstrained binding of TO-PRO1 to both DNA•DNA and PNA•DNA duplexes was studied as well.

4.1.1 Absorbance

Previous spectroscopic studies of monomeric thiazole orange TO and TO-PRO1 have provided insight into the characteristics of thiazole orange binding to duplex DNA.[2, 4, 77] Figure 32A shows the absorption spectrum of free TO-PRO1 in aqueous buffer at 0.5 μM concentration. The dye exists as monomer under this condition as indicated by the broad band in the visible region with one peak at 508 nm and a small shoulder at λ≈485 nm. As duplex DNA **4'AT•4'TA** is added the absorption band undergoes a gradual shift. With increasing duplex concentration, the absorbance at 508 nm decreased while absorbance at 520 nm increased. The shoulder at 490 nm becomes more pronounced. Under saturation conditions the addition of DNA•DNA duplex **4'AT•4'TA** resulted in a 10 nm bathochromic shift and a decrease of absorbance at 508 nm by 27 % (Table 3). This data is in agreement with previous spectroscopic studies of TO-PRO1 DNA binding.[4] A similar reduction (34 %) of absorbance at 508 nm was observed upon addition of PNA•DNA duplex **4at•4'TA** (Figure 32B). However, in this case, the bathochromic shift was smaller (4 nm), the blue side shoulder at 490 nm was less pronounced, and the increase of absorbance at 520 nm was not observed.

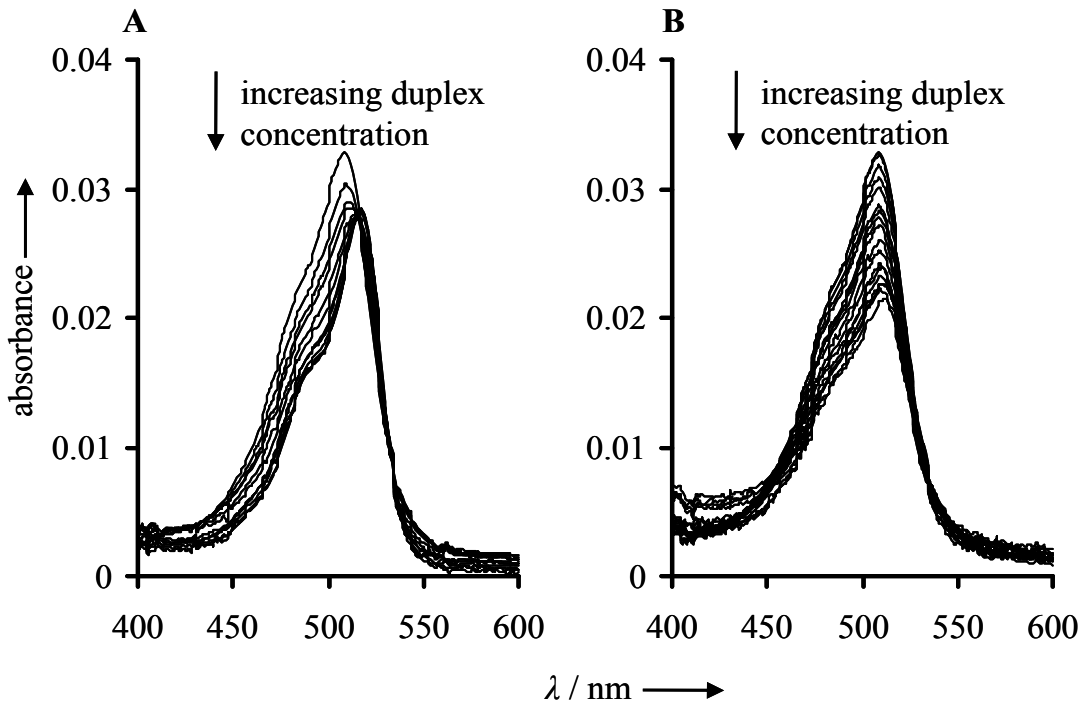

Figure 32: Absorbance of TO-PRO1 before and after addition of A) DNA•DNA duplex **4'AT•4'TA** (0.1, 0.2, 0.3, 0.5, 0.7, 1.0, 1.5, 2.0, 2.5, 3.0 and 4.0 µM) and B) PNA•DNA duplex **4at•4'TA** (0.1, 0.2, 0.3, 0.5, 0.7, 1.0, 1.5, 2.0, 2.5, 3.0, 4.0, 5.0, 6.0, 8.0, 10.0, 12.0 and 14.0 µM). Measurement conditions: 0.5 µM TO-PRO1 in degassed buffer (100 mM NaCl, 10 mM NaH_2PO_4 at pH 7.0).

Interestingly, the absorbance of TO in single stranded PNA conjugates **5tt, 6at, 20cc** and **10aa** was significantly lower than absorbance of TO-PRO1 in presence of duplex nucleic acids and the shoulder at $\lambda \approx 485$ nm became more pronounced (Figure 33). The absorption maximum of PNA conjugates **5-20xy** and their DNA complexes **5-20xy•5-20'MTN** are red-shifted by 6-11 nm when compared to the UV spectra of free TO-PRO1. Most remarkable was the observation that TO absorbance in FIT-PNA varied strongly as the nearest neighbor bases were changed. For example, TO absorbance was lowest in PNA **5tt** which featured TO flanked by two thymine residues. TO absorbance was double as high in PNAs **20cc** and **10aa** containing TO embedded between two cytosine or adenine bases, respectively. Very high absorbance (3-fold higher than TO absorbance of **5tt**) was measured for **19gc, 15gg** and **14ag** in which TO was next to one or two guanines. The pronounced nearest neighbor dependence of TO absorbance in FIT-PNAs **5-20xy** may indicate electronic coupling with the nucleobases.

Table 3: Spectroscopic parameters of TO-PRO1 before and after addition of DNA•DNA (**4'AT•4'TA**) and PNA•DNA (**4at•4'TA**) duplexes.

Substrate	$\lambda_{max\ (abs)}$[a]/ nm	ε_{508}[b]/ M^{-1} cm^{-1}	$\lambda_{max\ (em)}$[c]/ nm	Φ_{em}[d]	K_{app}[e]/ μM per base pair
TO-PRO1	508	63000	530	8×10^{-5}	-
TO-PRO1+ **4'AT•4'TA**	518	46000	530	0.21	134 ± 20
TO-PRO1+ **4at•4'TA**	512	42000	534	0.02	7.3 ± 0.4

[a] Wavelength of absorbance maximum, [b] extinction coefficient at 508 nm, [c] wavelength of fluorescence emission maximum, [d] fluorescence quantum yield, [e] affinity constant obtained from Scatchard analysis.

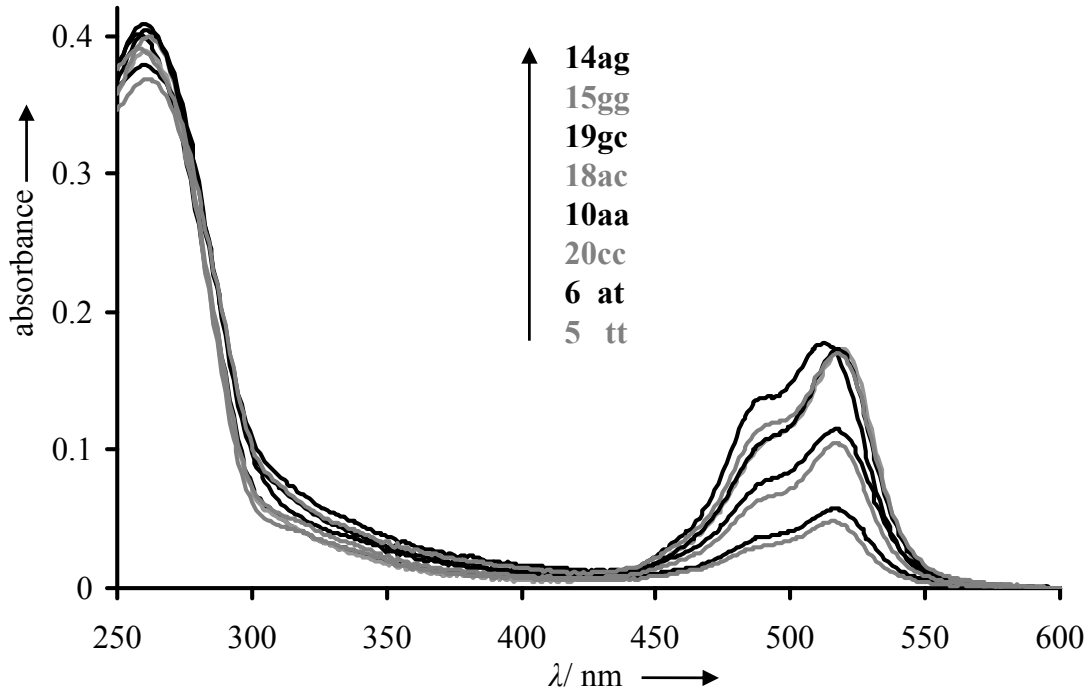

Figure 33: Absorbance spectra of single stranded PNA-TO conjugates (**5-20xy**). The absorbance at 600 nm was set to zero and the absorbance curves were calibrated to the calculated ε_{260}. Measurement conditions: 3 μM FIT-PNA in degassed buffer (100 mM NaCl, 10 mM NaH_2PO_4 at pH 7.0).

Surprisingly, the addition of complementary DNA **5'-20'MTN** to the FIT-PNA single strands **5-20xy** resulted in increases of TO absorbance at 515 nm by 18-53 % (Figure 34A-H). A blue shift by 3 nm and 2 nm was observed upon hybridization of FIT-PNA **6at**, **18ac** and **10aa** featuring an a-TO-t, a-TO-c and an a-TO-a motif, respectively. Overall, the band shapes of TO absorption in FIT-PNA•DNA duplexes **5-20xy•5'-20'MTN** resembled that of TO-PRO1 bound to DNA•DNA more closely

than that of TO-PRO1 bound to PNA•DNA. TO has been reported to exhibit environmentally sensitive absorption spectra. For example, ε_{max} of TO non-covalently bound to poly (dG-dC) duplexes was 16 % higher than that of TO bound to poly (dA-dT) duplexes.[94, 95] A similar, albeit markedly more pronounced trend was observed in single stranded FIT-PNA, in which ε_{max} of g-TO-c exceeded that of a-TO-t by 200 % (Table 4). The remarkably high responsiveness of TO absorbance in FIT-PNA may indicate tighter stacking interactions between TO and nucleobases in both single stranded and DNA-complexed FIT-PNA than of TO non-covalently associated with DNA•DNA and PNA•DNA duplexes.

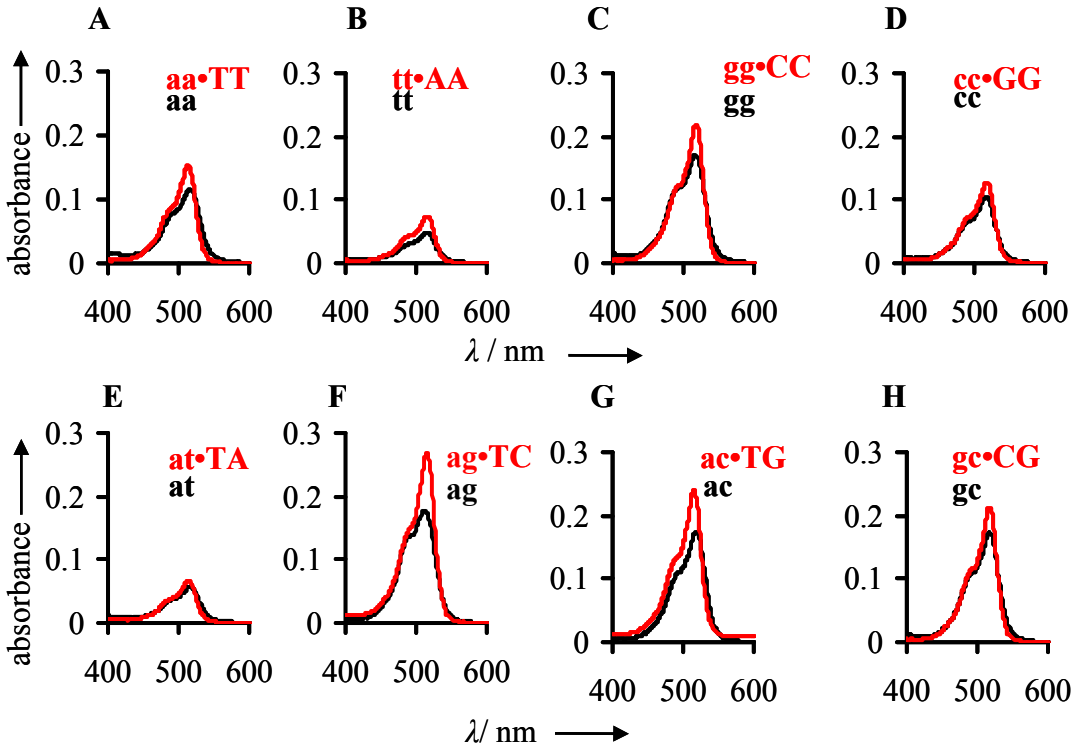

Figure 34: Absorbance spectra of FIT-PNA before (black) and after (red) addition of equimolar amount of complementary DNA. A) a-TO-a (**10aa, 10aa•5'TTT**), B) t-TO-t (**5tt, 5tt•·10'ATA**), C) g-TO-g (**15gg, 15gg•20'CTC**), D) c-TO-c (**20cc, 20cc•15'GTG**), E) a-TO-t (**6at, 6at•9'TTA**), F) a-TO-g (**14ag, 14ag•17'TTC**), G) a-TO-c (**18ac, 18ac•13'TTG**) and H) g-TO-c (**19gc, 19gc•16'CTG**). Measurement conditions: 3 µM FIT-PNA and 3 µM DNA (added after measurement of single strand PNA) in degassed buffer (100 mM NaCl, 10 mM NaH_2PO_4 at pH 7.0) at 25°C.

Table 4: Spectroscopic parameters of single stranded FIT-PNA **5-20xy** before and after addition of matched and single mismatched (**5'-20'MN**) DNA.

PNA		λ_{abs} [a] $_{(abs)}$/ nm		ε_{max} [b] / M^{-1} cm^{-1}		λ_{max} [c] $_{(em)}$/ nm		Φ_{em} [d]		F_{ds}/F_{ss} [e]
		single strand	double strand	single strand	double strand	single strand	double strand	single strand	double strand	matched
10aa	**a-TO-a**	516	514	38200	51300	543	531	0.03	0.27	28.2
5tt	**t-TO-t**	515	516	16100	24600	533	531	0.03	0.20	16.6
15gg	**g-TO-g**	517	518	56700	72900	540	536	0.04	0.16	4.8
20cc	**c-TO-c**	517	518	34800	42600	537	536	0.03	0.13	4.2
6at	**a-TO-t**	517	514	19000	22600	536	530	0.03	0.23	14.0
14ag	**a-TO-g**	513	515	59300	89800	548	535	0.05	0.25	18.0
18ac	**a-TO-c**	519	516	57500	80100	539	534	0.03	0.21	22.8
19gc	**g-TO-c**	517	518	57700	70900	536	537	0.02	0.14	6.8

[a] Wavelength of absorbance maximum, [b] extinction coefficient at wavelength of absorbance maximum, [c] wavelength of fluorescence emission maximum, [d] Φ_{em} = fluorescence quantum yield, [e] F_{ds}/F_{ss} = ratio between fluorescence intensities F_{ds} after and F_{ss} before addition of matched DNA at 525 nm.

4.1.2 Circular Dichroism

CD spectra were measured in order to obtain insight into possible modes of TO-nucleic acid interactions. Figure 35A and B show the induced CD spectra of TO-PRO1 due to binding to DNA•DNA and PNA•DNA duplexes, respectively. The induced CD is positive at low dye/base pair ratio. At high dye/ base pair ratios two bands of different sign appear. Such a structure can originate from a superimposed exciton CD induced by dye-dye interactions in the minor groove.[1]

In the PNA•DNA duplex the CD couplet is observed at lower dye/ base pair (d/BP) ratios (1:4) than in the DNA•DNA duplex (d/ BP = 1:2.5). This observation suggests that, for the studied sequence, association of TO-PRO1 in the PNA•DNA minor groove may occur at lower dye concentration than in the DNA•DNA minor groove. The TO chromophore in the FIT-PNA•DNA complex **19gc•16'CTG** shows a negative band with a maximum at 518 nm which coincide with the absorption bands (Figure 35C). Negative bands have been assigned to the intercalation mode.[1, 3, 4] It can be concluded that the TO chromophore in **19gc•16'CTG** predominantly accommodates an intercalated position in the interior of the duplex. In contrast, the mode of binding of TO-PRO1 to DNA•DNA and PNA•DNA appears less clearly defined.

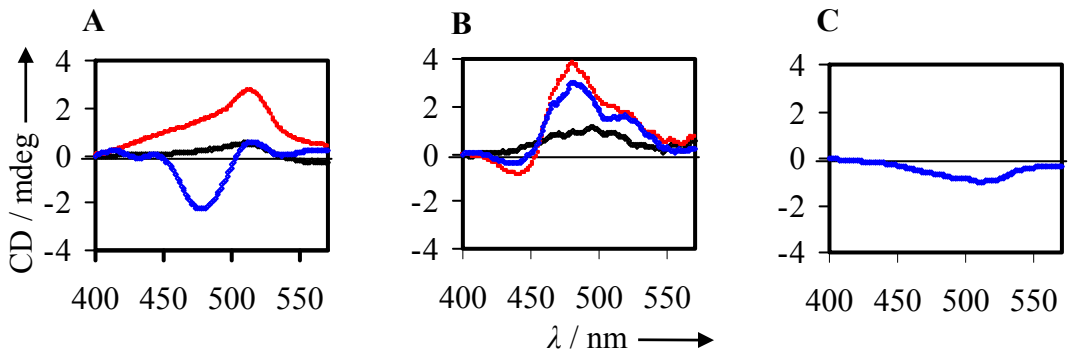

Figure 35: Induced CD spectra of TO-PRO1 in A) DNA•DNA duplex **4'AT•4'TA** and B) PNA•DNA duplex **4at•4'TA** at mixing ratios (dye: BP) 1:10 (black), 1:4 (red) and 1:2.5 (blue). C) CD Spectrum of FIT-PNA•DNA duplex **19gc•16'CTG** (blue). Spectra were set zero at 400 nm. Measurement conditions: 52 µM duplex 4'AT•4'TA or 4at•4'TA and varying amounts of dye, or 3 µM FIT-PNA 19gc and DNA 16'CG in buffer (100 mM NaCl, 10 mM NaH_2PO_4 at pH 7.0) at 15°C.

4.1.3 Fluorescence spectroscopy

The particular features of TO as base surrogate were further explored by comparing the fluorescence spectra of TO in response to "unconstrained"[96] and "enforced" binding. The fluorescence quantum yield of free TO-PRO1 had been determined to be extremely low ($\phi_{em} = 1.4 \times 10^{-4}$).[2] As expected, addition of duplex DNA **4'AT•4'TA** to free dye led to dramatic enhancements of fluorescence intensity (Figure 36A) and fluorescence quantum yield ($\phi_{em} = 0.21$, Table 3). It is interesting to note that TO-PRO1 also experienced increases of fluorescence ($\phi_{em} = 0.02$) when allowed to bind to PNA•DNA duplex **4at•4'TA** (Figure 36B, Table 3). This result is noteworthy in light of previous investigations in which typical intercalators such as ethidium bromide, 8-methoxypsoralen and $Ru(phen)_2dppz^{2+}$ have failed to exhibit fluorescence increases upon exposure to PNA•DNA duplexes.[97] However, the analysis of the fluorescence titration data (Figure 36C, D) revealed that TO-PRO1 binds PNA•DNA duplex **4at•4'TA** with lower affinity ($K_{app} = 7.3 \pm 0.4$ µM per base pair) than DNA•DNA duplex **4AT•4'TA** ($K_{app} = 134 \pm 20$ µM per base pair) (Table 6). Most remarkable were the results obtained with FIT-PNAs **5-20xy**. The TO dye in conjugates **5-20xy** had a higher fluorescence quantum yield ($\phi_{em} = 0.03$-0.05) than the free TO-PRO1 which indicates TO-base-stacking in the single-stranded form (Table 6). However, the formation of FIT-PNA•DNA duplexes **5-20xy•5'-20'MTN** was accompanied by significant increases of fluorescence intensity (Figure 37A) owing to the high fluorescence quantum yields ($\phi_{em} = 0.12$-0.27) in the double-stranded form. Optical measurements of PNA-TO conjugates **5-20xy** in which the TO stacking partner was varied exposed the nearest neighbor dependence of TO fluorescence quantum yields (Table 7). The lowest fluorescence quantum yield $\phi_{em} = 0.12$ within the studied sequence contexts was obtained when TO was embedded between two cytosines. The intercalation between two guanines or two thymines resulted in higher $\phi_{em} = 0.16$ and $\phi_{em} = 0.20$, respectively. High fluorescence quantum yield ($\phi_{em} \geq 0.27$) was obtained for duplex **10aa•5'TTT** which featured two adenines as intrastrand stacking partner. The high $\phi_{em} \geq 0.20$ obtained for duplexes **18ac•13'TTG** (a TO c) and $\phi_{em} \geq 0.25$ **14ag•17'TTC** (a TO g) and the comparatively low $\phi_{em} = 0{,}12$, $\phi_{em} = 0{,}14$ and $\phi_{em} = 0{,}16$ in duplexes **20cc•15'GTG** (c TO c), **19gc•16'CTG** (g TO c) and **15gg•20'CTC** (g TO g), respectively, suggested that one

guanine-cytosine pair was not sufficient to quench TO fluorescence. The high fluorescence quantum yield $\phi_{em} = 0.23$ of thiazole orange forced to intercalate between a-T and t-A base pair in **6at•9'TTA** is remarkable when considering that non-covalent association of TO-PRO1 to self-complementary $(dAdT)_{10}$ duplex has been reported to result in a lower quantum yield $\phi_{em} = 0.13$. TO-PRO 1 showed higher fluorescence quantum yields ($\phi_{em} = 0.23$) in self-complementary duplex $(dGdC)_6$.[2] In contrast, forced intercalation between c and g in **19gc•16'CTG** furnished low $\phi_{em} = 0.14$. It is evident that TO fluorescence not only responds to the base composition of the near environment but also to the TO-nucleic acid binding mode and perhaps also to more subtle changes such as local conformations. The latter feature is considered important for applications in single base mutation analysis (vide infra).

The responsiveness of TO to changes of the environment was most noticeable in measurements of fluorescence intensity, which is the monitored observable in applications. Table 4 also lists fluorescence enhancements F_{ds}/ F_{ss} upon hybridization to perfectly matched target DNA and single mismatched DNA. It became apparent that conjugated thiazole orange experienced increases of fluorescence intensity upon hybridization in any studied sequence context. Highest fluorescence enhancements (12-28 fold) were obtained upon formation of duplexes in which TO was allowed to stack to at least one adenine-thymine base pair.

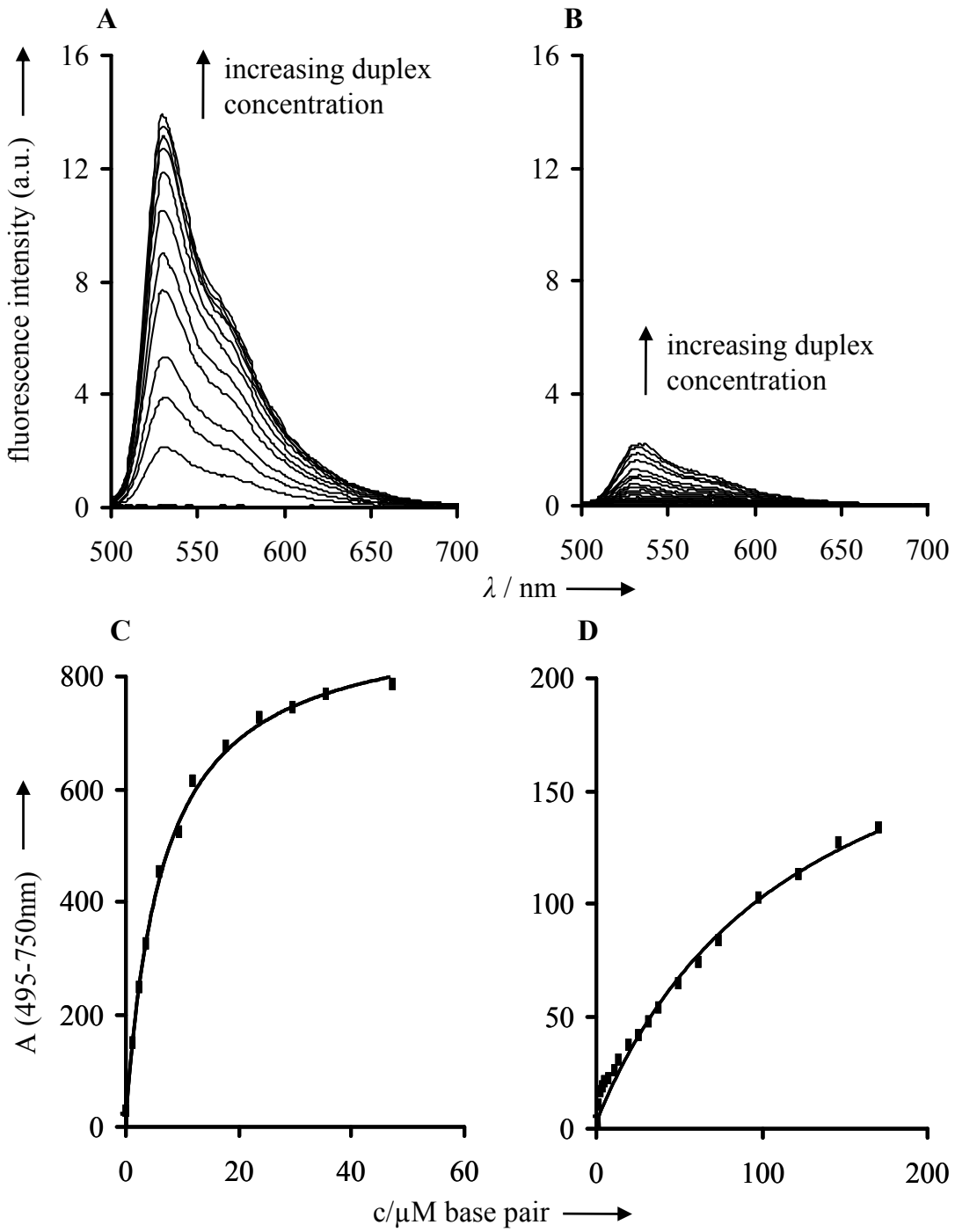

Figure 36: Fluorescence emission of TO-PRO1 before and after addition of A) DNA•DNA duplex **4'AT•4'TA** (0.1, 0.2, 0.3, 0.5, 0.7, 1.0, 1.5, 2.0, 2.5, 3.0 and 4.0 µM) and B) PNA•DNA duplex **4at•4'TA** (0.1, 0.2, 0.3, 0.5, 0.7, 1.0, 1.5, 2.0, 2.5, 3.0, 4.0, 5.0, 6.0, 8.0, 10.0, 12.0 and 14.0 µM). C) and D) Fluorescence titration data and binding curves obtained by Scatchard analysis of integrated fluorescence emission (495-750 nm) vs. concentration of base pairs (µM). Measurement conditions: see legend of Figure 32.

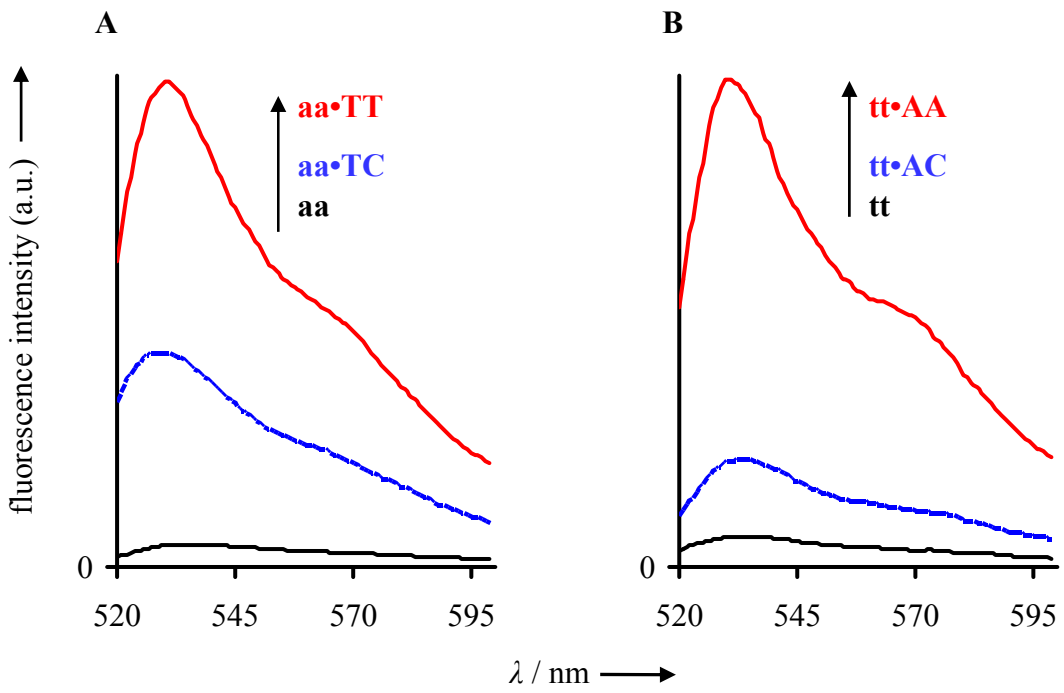

Figure 37: Fluorescence emission spectra of FIT-PNA before (black) and after addition of equimolar amount of complementary DNA (red) or mismatched DNA (blue). A) a-TO-a (**10aa, 10aa•5'TTT, 10aa•17'TTC**), B) t-TO-t (**5tt, 5tt•10'ATA, 5tt•18'ATC**). Measurement conditions: 1 µM FIT-PNA and 1 µM DNA (added after measurement of single strand PNA) in degassed buffer (100 mM NaCl, 10 mM NaH_2PO_4 at pH 7.0) at 25°C.

Interestingly, in six of the eight tested probes the presence of a single base mismatch resulted in attenuated intensities of TO fluorescence emission showing only 25-80 % of the fluorescence enhancements observed for matched hybridization. This property is of interest in DNA mutation analysis since it provides an additional level of sequence discrimination other than discrimination by hybridization alone. The two probes **15gg** and **14ag** in which single mismatched duplexes fluoresced with higher intensity than matched duplexes featured g-G mismatched base pairs as opposed to g-C matched base pairs. These results lend further support to the notion that TO responds to local changes of the π-stacking environment and it is conceivable that the congested π-stack provided by a g-G mismatch in **15gg** and 1**4ag** more efficiently closes non-radiative decay channels than a c-G match.

4.1.4 Time resolved fluorescence

Time resolved fluorescence study reported in this thesis have been carried out by Nils Krebs and Sebastian Tannert in the working group of Prof. Beate Röder (Institut für Physik, Humboldt-Universität zu Berlin. Newtonstr. 15, D-12489 Berlin, Germany).

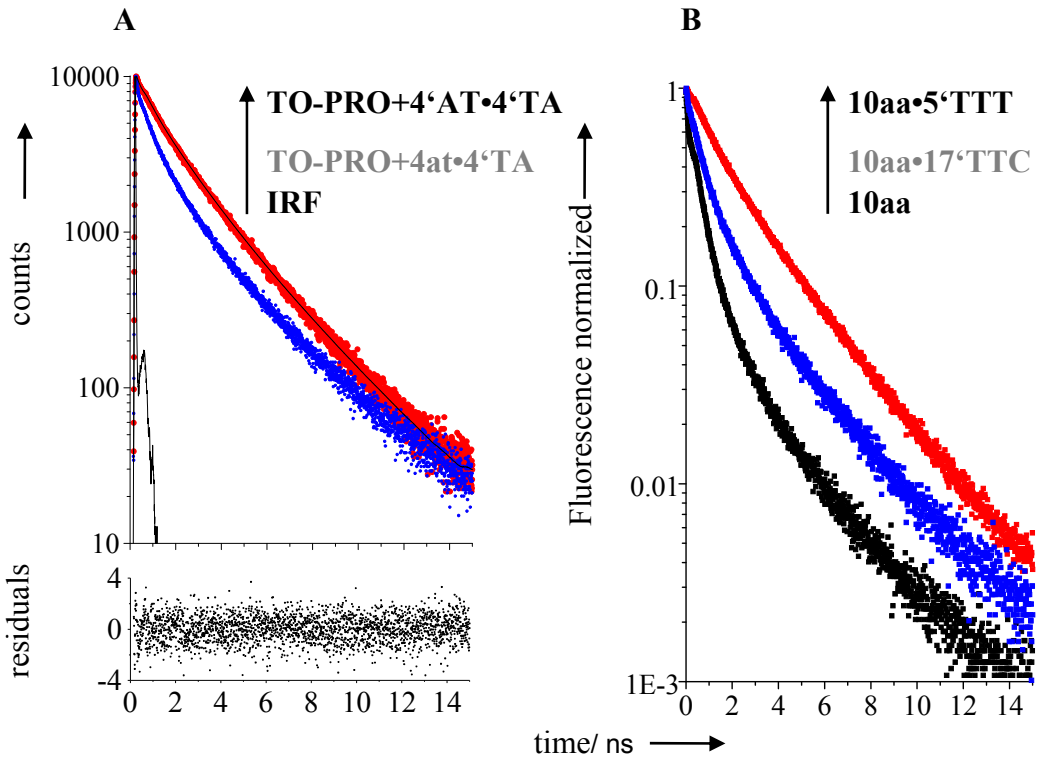

Figure 38: A) Fluorescence decay curves of TO-PRO1 after addition of DNA•DNA duplex **4'AT•4'TA** (red) and PNA•DNA duplex **4at•4'TA** (blue). Lower part: residuals of the fit of the red decay curve. B) Normalized fluorescence decay profiles of FIT-PNA **10aa** (a-TO-a) in single stranded form (black) and after mismatched (blue) and matched hybridisation (red). For life times and amplitudes see Table 8. (Conditions: $\lambda_{ex} = 532$ nm, $\lambda_{det} = 580$ nm)

To closer examine the fluorescent species fluorescence lifetimes were measured by time correlated single photon counting (TSPC). First, TO-PRO1 was immobilized in a polyvinyl alcohol film to explore its properties in a highly viscous medium. A biexponential fit with decay times 3.6 ns and 1.38 ns adequately described the fluorescence decay curve as demonstrated by a low $\chi^2 = 1.0$ obtained for the biexponential fit (Table 8). Three different decay times were observed for FIT-PNA

containing duplexes and for TO-PRO1 bound to DNA•DNA duplex **4'AT•4'TA**. In contrast a tetraexponential was necessary to fit the fluorescence decay of single stranded FIT-PNA and of TO-PRO1 complexed to PNA•DNA duplex **4at•4'TA** (Figure 38). Attempts to describe the decay curves with a triexponential resulted in unacceptably high $\chi^2 = 1.29$. The decay processes can be classified into very short decay processes within 0.04-0.07 ns, short decays within 0.22-0.48 ns and medium and long decays within 1.05-1.54 ns and 2.33-3.95 ns, respectively. As can be seen from Table 5, the two short decay times of single-stranded FIT-PNA have high amplitude (65 %-91 %). Remarkably, addition of complementary DNA to FIT-probes led to the complete disappearance of the very fast decay process. The very fast decay process was also absent in TO-PRO1 complexed to DNA•DNA duplex **4'AT•4'TA**. On the contrary, very fast decay still occurred in complexes of TO-PRO1 and PNA•DNA duplex **4at•4'TA**. A likely assignment to this decay process is contact of unconstrained TO with water and it seems that enforced intercalation in PNA•DNA effectively protected the TO dye from water while association of free TO-PRO1 with PNA•DNA furnished, amongst others, water-exposed fluorescent species.

The formation of matched FIT-PNA duplexes decreased the population of fast decaying species and increased the population of TO fluorophores emitting with the two longer decay times. The hybridization-induced change of the decay times was less clear since both increases and decreases of short and medium decay times were observed. However, a decrease of the long decay time was found in all studied cases of matched hybridization. Interestingly, the duration of the two long decay processes showed a correlation with the absorbance. For example, the two long decay times were shortest in duplexes containing FIT-PNA **14ag** (1.22 and 2.63 ns, $\varepsilon_{max} = 89800\ M^{-1}cm^{-1}$), **15gg** (1.28 ns and 2.55 ns, $\varepsilon_{max} = 80100\ M^{-1}cm^{-1}$) and **19gc** (1.26 and 2.33 ns, $\varepsilon_{max} = 70900\ M^{-1}cm^{-1}$). These PNAs had significantly higher absorbance than complexes **5tt** (1.39 ns and 3.03 ns, $\varepsilon_{max} = 24600\ M^{-1}cm^{-1}$) and **6at** (1.54 ns and 3.57 ns, $\varepsilon_{max} = 22600\ M^{-1}cm^{-1}$). The transition of FIT-single strands to single mismatched duplexes revealed a remarkable behavior. While the amplitude of the two long decaying processes still increased with single mismatched hybridization (albeit not to the extent observed in matched hybridization), the short decaying process experienced increases of amplitudes rather than decreases found in matched hybridization. For example, the population of the fluorescing species in single

stranded FIT-PNA **10aa** that decayed with a short decay time changed from 41 % to 53 % upon formation of the mismatched complex **10aa•5'TTT**. This population increase of fast decay species was even more dramatic (22 % to 53 %) with FIT-PNA **18ac**. Furthermore, the short decay times of TO in single mismatched duplexes were shorter (by 0.01-0.11 ns) than in matched duplexes and it can be concluded that the presence of mismatched base pairs apparently facilitated the fast decay process which often occurred even more rapidly than in the single-stranded form.

The comparison of the two longer decay processes in mismatched duplexes with the corresponding processes in matched duplexes revealed a complex interplay between increases and decreases of decay times and amplitudes sizes. For example, the FIT-PNA **14ag** containing TO between adenine and guanine featured higher fluorescence enhancements upon mismatched hybridization than upon matched hybridization, reflected by a marked increase of the medium decay time (by 0.22 ns rather than decreases) and an exceptional prolongation (by 0.27 ns vs. reduction by 0.54 ns in case of matched hybridization) of the long decay time. In all other studied mismatched duplexes, the medium decay process occurred faster (by 0.15-0.29 ns) but with similar amplitude than in matched duplexes. In contrast, the longer decay times were similar or longer (by 0.28-0.33 ns) in presence of single mismatches, albeit at the cost of amplitude. As a result, the averaged fluorescence lifetime of the TO excited state is reduced by $\Delta\tau$ = 0.31-0.88 ns in presence of single base mismatches in **10aa**, **6at**, **18ac** and **14gc**.

Table 5: Fluorescence decay analysis of TO-PRO1 and FIT-PNA before and after addition of matched and mismatched DNA. **τ** denotes the fluorescence decay life time and relative amplitudes **a.**

			τ / ns (a/ %)[a]				χ^2
			very fast	fast	medium	slow	
TO-PRO1		**+polymer**			1.38 (14.0)	3.60 (86.0)	1.00[c] [2.13][b]
		+4'AT•4'TA		0.33 (28.6)	1.36 (39.3)	2.74 (32.1)	1.09[d] [1.71][c]
		+4at•4'TA	0.04 (28.6)	0.35 (34.8)	1.37 (27.8)	3.47 (8.8)	1.06[e] [1.29][d]
10aa, (a-TO-a)	ss	**10aa**	0.05 (50.2)	0.48 (41.0)	1.49 (6.7)	3.64 (2.2)	1.11[e] [1.54][d]
	dsmt	**10aa•5'TTT**		0.39 (22.3)	1.39 (37.9)	3.03 (39.8)	1.05[d] [1.51][c]
	dsmm	**10aa•17'TTC**		0.28 (52.9)	1.10 (34.7)	3.31 (12.3)	1.05[d] [2.37][c]
6at, (a-TO-t)	ss	**6at**	0.05 (32.4)	0.26 (39.5)	1.24 (19.0)	3.95 (9.1)	1.08[e] [1.24][d]
	dsmt	**6at•9'TA**		0.35 (26.6)	1.54 (35.1)	3.57 (38.3)	1.04[d] [1.68][c]
	dsmm	**6at•17'TTC**		0.32 (43.7)	1.29 (38.4)	3.55 (17.8)	1.04[d] [2.67][c]
14ag, (a-TO-g)	ss	**14ag**	0.07 (41.2)	0.38 (32.2)	1.28 (21.2)	3.17 (5.4)	1.08[e] [1.55][d]
	dsmt	**14ag•17'TTC**		0.34 (17.0)	1.22 (46.5)	2.63 (36.5)	1.05[d] [1.31][c]
	dsmm	**14ag•13'TTG**		0.33 (29.0)	1.50 (40.4)	3.44 (30.6)	1.02[d] [1.95][c]
18ac, (a-TO-c)	ss	**18ac**	0.04 (42.9)	0.32 (22.1)	1.05 (31.9)	2.67 (3.1)	1.03[e] [1.45][d]
	dsmt	**18ac•13'TTG**		0.32 (19.8)	1.28 (51.5)	2.55 (28.7)	1.00[d] [1.44][c]
	dsmm	**18ac•17'TTC**		0.22 (52.5)	1.06 (36.1)	2.88 (11.5)	1.11[d] [4.46][c]
19gc, (g-TO-c)	ss	**19gc**	0.04 (33.2)	0.24 (45.3)	1.10 (15.5)	3.38 (5.7)	1.02[e] [1.33][d]
	dsmt	**19gc•16'CTG**		0.37 (26.0)	1.26 (53.5)	2.33 (20.5)	1.07[d] [1.74][c]
	dsmm	**19gc•20'CTC**		0.27 (55.8)	1.11 (25.2)	2.66 (19.0)	1.07[d] [3.28][c]

[a] Relative amplitudes a in the emission decay fits are given as decimal fractions in parenthesis, [b, c, d, e] χ^2 obtained by monoexponential, biexponential, triexponential and tetraexponential, respectively, fitting of fluorescence decay curves, ss = single strand, dsmt = matched duplex and dsmm = mismatched duplex.

4.2 Discussion

TO-PRO1

The binding of TO-PRO1 to double-stranded DNA has been shown to involve several binding modes, the most important being intercalation and minor-groove binding.[2, 4, 67, 77] The resulting enhancements of TO fluorescence emission are key to various DNA-detection assays. The presented data show that TO-PRO1 also binds to PNA•DNA duplexes as evidenced by decreases of TO absorbance and increases of fluorescent emission. This could open new opportunities for the detection of probe target complexes in PNA-based hybridization assays. However, data from fluorescence titration exposed that complexes of TO-PRO1 and PNA•DNA duplex **4at•4'TA** (K_{app} = 7.3 µM per base pair) are less stable than complexes with DNA•DNA duplex **4'AT•4'TA** (K_{app} = 134 µM per base pair). Previous investigations by Nordén showed that traditional intercalators such as ethidium, methoxypsoralen and ruthenium dipyridinophenazine complexes failed to bind to PNA•DNA duplexes, whereas minor groove binders such as DAPI and distamycin showed modest binding affinities.[97] Armitage demonstrated that the minor groove of PNA•DNA duplexes provides a high affinity template for the aggregation of the symmetrical cyanine dye $DiSC_2$.[98, 99] I have not attempted to resolve the stoichiometry of TO-PRO1•PNA•DNA complexes. However, it can be noted that in PNA•DNA the CD couplet, indicative for dye-dye interactions, appears at lower dye concentrations than in DNA•DNA complexes. Dye-dye interactions can only occur at non-intercalative binding sites at the duplex exterior. It is hence reasonable to assume that TO-PRO1 more readily accommodates extrahelical binding sites of PNA•DNA, presumably due to a lack of high affinity innerhelical binding sites (intercalation). Further support comes from fluorescence decay analysis, which revealed that TO-PRO1 in complex with PNA•DNA duplex **4at•4'TA** featured a very short decay time (0.04ns) attributed to contact with water.

TO-PNA (FIT-PNA)

Binding of TO-PRO1 to DNA duplexes has been reported to result in 8 % decrease of the extinction coefficient ε_{max}.[2] In single stranded FIT-PNAs, ε_{max} varied in

between 16100-59300 $M^{-1}cm^{-1}$. Double strand formation led to increases in ε_{max} by 22-53 %. The enhanced nearest-neighbor dependence of TO absorbance in single stranded and double stranded FIT-PNA is remarkable. At present I do not have an explanation but it is probably reasonable to assume ground state interactions between TO and nucleobases, which may be induced/ facilitated due to the use of TO as base surrogate. The steady-state fluorescence enhancements, the disappearance of the very short fluorescence decay process and the increased amplitude of long decay processes indicate that double-strand formation results in an efficient protection from water and a rigidification of the TO environment. The marked nearest neighbor dependence of TO absorbance and the negative band in the induced circular dichroism spectrum that coincides with the TO absorbance spectrum are most readily explained when assuming an innerhelical conformation of TO in FIT-PNA•DNA duplexes. It is, however, difficult to imagine that both the polycyclic TO and the opposing nucleobase can simultaneously intercalate without detriment to duplex stability. Indeed, the higher T_M (71°C) of duplexes in which TO is lacking an opposite base is in agreement with an innerhelical position of TO (see section 5). In contrast, TO-PRO1 seems to occupy extrahelical binding sites of PNA•DNA duplexes such as **4at•4'TA** (*vide supra*). The opposite binding modes nicely illustrate how a chromophore can be forced to intercalate at a specific position despite having alternative binding preferences.

Given the precisely located innerhelical position of TO in nucleic acid duplexes it is possible to explore the influence of individual adjacent nucleobases on TO photophysical properties. The fluorescence quantum yields were highest in duplexes that contained adenine-thymine base pairs as TO stacking partner and lowest with adjacent guanine-cytosine base pairs. This data stands in contrast to results of previous observations in which TO and TO-PRO1 showed higher fluorescence quantum yields when complexed to GC rich rather than AT rich duplexes. The previous observations led the authors to exclude TO excited state electron transfer quenching by guanine, even though estimations of the free energy revealed that this process may occur spontaneously.[2] In measurements of non-covalently associated dyes the identity of the fluorescence species (intercalated, minor-groove bound, backbone associated) is less clearly defined than in FIT-PNA. It is, hence, conceivable that in previous investigations TO also occupied binding sites, in which

electronic coupling to adjacent nucleobases was hampered. On the contrary, TO in FIT-PNA showed strong interactions with adjacent nucleobases demonstrated best by the pronounced nearest neighbor dependence of the absorbance spectra. Based on our data we cannot exclude the possibility of electron transfer from guanine to the excited state of intercalated TO. We speculate that forced intercalation allows TO interaction modes not accessible to non-covalent aggregates. However, it is noted that one guanine is not sufficient to quench fluorescence of the FIT-PNA duplex as indicated by high fluorescence quantum yields of complexes that featured at least one AT pair as stacking partner. Nevertheless, time-resolved fluorescence responded to the presence of even one GC base pair (*vide infra*).

Time Resolved Fluorescence

The TO-nucleic acid complexes studied in this work showed 3-4 decay times. The short decay time, which was assigned to a water-accessible fluorescent species, was detected only for single stranded FIT-PNA and the relatively weak complexes of TO-PRO1 and PNA•DNA duplex **4at•4'TA**. Only three decay times (0.22-0.48 ns, 1.05-1.54 ns, 2.33-3.95 ns) were found in FIT-PNA duplexes and in complexes of TO-PRO1 and dsDNA **4'AT•4'TA**. The decay times are in agreement with the decay times determined by Netzel et al. for complexes of TO-PRO1 and calf thymus DNA (0.23 ns, 1.57 ns, 2.76 ns).[2] Melvin and co-workers have studied DNA•DNA duplexes in which TO was appended via a flexible tether to the internucleotidic phosphate bridge.[86] They found 4 decay times, which are different from the ones reported before and by Netzel.[2] The differences were explained by the authors to arise from the use of different oligonucleotide sizes and sequences.

A comparison with the fluorescence decay times determined for polymer-immobilized TO-PRO1 (3.6 ns and 1.38 ns) suggests that the two slower decay processes found in nucleic acids (1.05-1.54 ns and 2.33-3.95 ns) are a characteristic of TO species in a highly viscous environment. These species presumably are in tight contact with a rigid scaffold that prevents twisting around the TO methine bridge. In FIT-PNA, it is most likely that the rigid scaffold is provided by the helical base stack. One could assume that the strong GC pairs confer a less flexible stacking environment than AT pairs. In the absence of electronic coupling between TO and the adjacent nucleobases one would expect longer decay times and thus higher fluorescence

enhancements for duplexes containing TO flanked by GC than by AT base pairs. However, the opposite was found since the presence of GC base pairs as stacking partner led to a reduction of the two longer decay times (eg. 3.03 ns and 3.57 ns in **10aa** (a TO a) and **6at** (a TO t) vs. 2.33 ns, 2.55 ns and 2.63 ns in **19gc** (g TO c), **18ac** (a TO c) and **14ag** (a TO g), respectively). These observations indicate that the decay processes that are characteristic for rigidified TO are also the ones that showed the highest responsiveness to the identity of the adjacent nucleobases. These processes may hence be suited to explore base-pair specific binding modes.

The fluorescence decay analysis of FIT-PNA before and after addition of complementary DNA showed that the transition from single stranded to double stranded FIT-PNA was dominated by the disappearance of the very fast decay process. However, the slow decay process also showed high hybridization-induced responses (shortening of decay time by 0.12-1.03 ns and increase of amplitude by factors of 4-18). While the fast decay process showed comparably little sensitivity to double strand formation, it was this decay along with the slow decay process that exhibited the highest responsiveness to the presence of single mismatched stacking partners.

One of the five FIT-PNA's studied in time-resolved fluorescence measurements had higher fluorescence in the mismatched duplex than in the matched duplex. In this case (FIT-PNA **14ag**), the slow decay process of TO in mismatched duplex showed only a minor decrease of amplitude that was overcompensated by a large increase of decay time when compared to matched duplexes. It is interesting to note that the fast decay process still responded as evidenced by 1.6-2.6 fold increase of amplitude.

The picture that emerges is that the decay processes are characterized by specific susceptibilities to changes of the environment. The very fast and the slow decay processes appear to be the ones that respond most to more global changes of the TO environment such as induced by double-strand formation. The local distortion of helix architecture and dynamics such as those induced by mismatched base pairs were sensed most reliably by the fast and, in some cases, the long decay process. It can be conclude that the disappearance of the very fast decay process and the increase of the amplitude factor of the long decay process are reliable hybridizations monitors. If, at the same time, an increase of the amplitude factor of the fast decay process is observed, it is likely that a distorted, mismatched duplex had formed.

4.3 Conclusions

It was the aim of this study to explore whether intercalated cyanine dyes such as the thiazole orange dye used in nucleic acid staining show optical properties that allow assignments of the DNA local environment. One requirement for this study was the ability to pinpoint the location of the affixed thiazole orange dye. The collected data from UV/ VIS absorbance, CD and fluorescence spectroscopy indicate that the use of thiazole orange as base surrogate in FIT-PNA enabled the site-specific intercalation in PNA•DNA duplexes. In fact, intercalation was an enforced binding mode since PNA•DNA duplexes appear not to provide high affinity intercalation sites to TO-PRO1 and other established intercalators.

Remarkable hallmarks of TO steady-state optical properties in FIT-PNA•DNA duplexes are 1) remarkable dependence of the extinction coefficient (± 60 % variation of the averaged $\varepsilon_{max} = 56800\ M^{-1}cm^{-1}$) on next neighbor base pairs, 2) attenuated steady-state fluorescence emission when positioned between two GC base pairs and 3) low emission quantum yields of TO adjacent to single mismatched base pairs. Such effects are not observed in classical "non-covalent" TO-nucleic acid complexes. We assume that the close analogy of TO in FIT-PNA to canonical nucleobases enforces base specific interaction modes, which normally would be unable to compete with alternative, probably more favored modes.

The studies of TO in FIT-PNA and in DNA-DNA and PNA•DNA complexes also highlighted four different fluorescence decay processes which responded differently to changes of the TO environment. This includes 4) a very fast fluorescence decay process in the range of 0.04-0.07 ns that disappears upon double-strand formation. 5) a fast decay between 0.22-0.48 ns, which showed the highest sensitivity to the presence of mismatched base-pairs, 6) a comparably unsusceptible medium decay process within 1.05-1.54 ns and 7) a long decay between 2.33-3.95 ns which is almost universally susceptible to changes conferred by hybridization and exchange of adjacent nucleobases.

The responsiveness of the optical properties to the stacking environment is a general feature of the forced intercalation mode and may therefore be applicable to other intercalator dyes. The observed sensitivity to changes of the nucleobase sequence should allow for the design of single-nucleotide specific probes that omit the need for stringent hybridization conditions in DNA mutation analysis.

5. Solid-phase synthesis and biophysical characterisation of FIT-TO PNA having abasic residue adjacent to thiazole orange

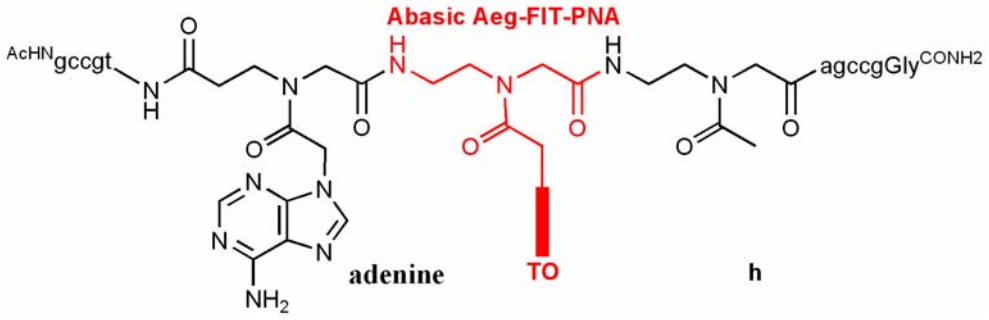

The studies shown in previous chapter suggested that TO as base surrogate responds to changes of its environment. It was observed that binding of TO-PNA conjugates to complementary DNA strands was accompanied by strong increases in fluorescent emission and that fluorescence was mostly attenuated in presence of next neighbour base mismatches. Base mismatches induce a significant perturbation of duplex structure. It has been shown that base mismatches increase the proclivity to accommodate an extrahelical position. As result, introduction of a base mismatch can remove a TO stacking partner. To study this effect, it was decided to explore duplexes containing an abasic site adjacent to the thiazole orange base.

5.1 Design and Synthesis of Abasic TO-PNA Probe

The residue was introduced by divergent solid phase synthesis. The solid-phase synthesis was commenced from rink amide resin **4a** loaded with Fmoc-glycine. In the subsequent assembly of PNA resin, Fmoc cleavage was achieved by treatment of the resin with piperidine in DMF. The coupling reactions were performed by using commercially available Fmoc/ Bhoc-protected building blocks as described. The abasic residue was introduced by coupling Fmoc-Aeg (Alloc)-OH building block (Scheme 14).

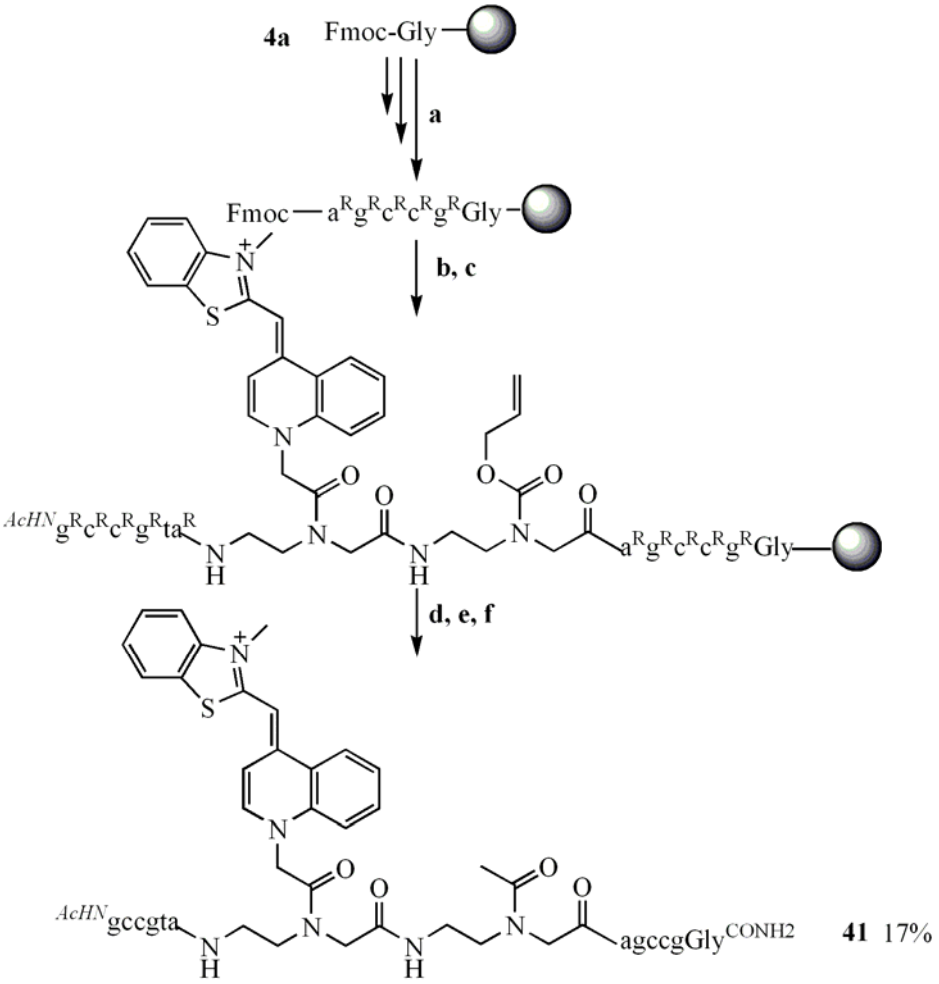

Scheme 14: a, c) Cycle of 1) piperidine/ DMF; 2) Fmoc–B (Bhoc)–OH, NMM, HCTU, NMP; 3) Ac_2O/ lutidine, DMF; b) Piperidine/ DMF; 2) Fmoc-Aeg (Alloc)-OH, HCTU, NMM, NMP (double coupling) or Fmoc-Aeg (TO)-OH, HCTU, NMM, PPTS, NMP (double coupling); d) [Pd $(PPh_3)_4$], $Me_2NH{\cdot}BH_3$, CH_2Cl_2 e) Ac_2O/ piperidine f) TFA, m-cresol, H_2O, L-Cys-OMe, 17 % overall yield .

The subsequent coupling of TO monomer proceeded as previously described. After completion of the iterative building block assembly, the removal of the Alloc group from fully protected PNA resin was performed using tetratriphenylphosphine palladium and dimethylamineborane complex as scavenger.[56] The abasic residue was constructed upon reaction with acetic anhydride/ pyridine (1/ 9). For the release of conjugate **41**, PNA resin was treated with TFA in the presence of *m*-cresol, water and cysteine methyl ester as cation scavengers. HPLC purification furnished **41** in 17 % overall yield based on the initial loading of **4a** with Fmoc groups. Analytical RP-HPLC, MALDI-TOF mass spectrometry and UV/ Vis and fluorescence spectroscopy confirmed the purity and molecular mass of **41** and the integrity of the abasic site adjacent to thiazole orange.

5.2 Results and Discussion

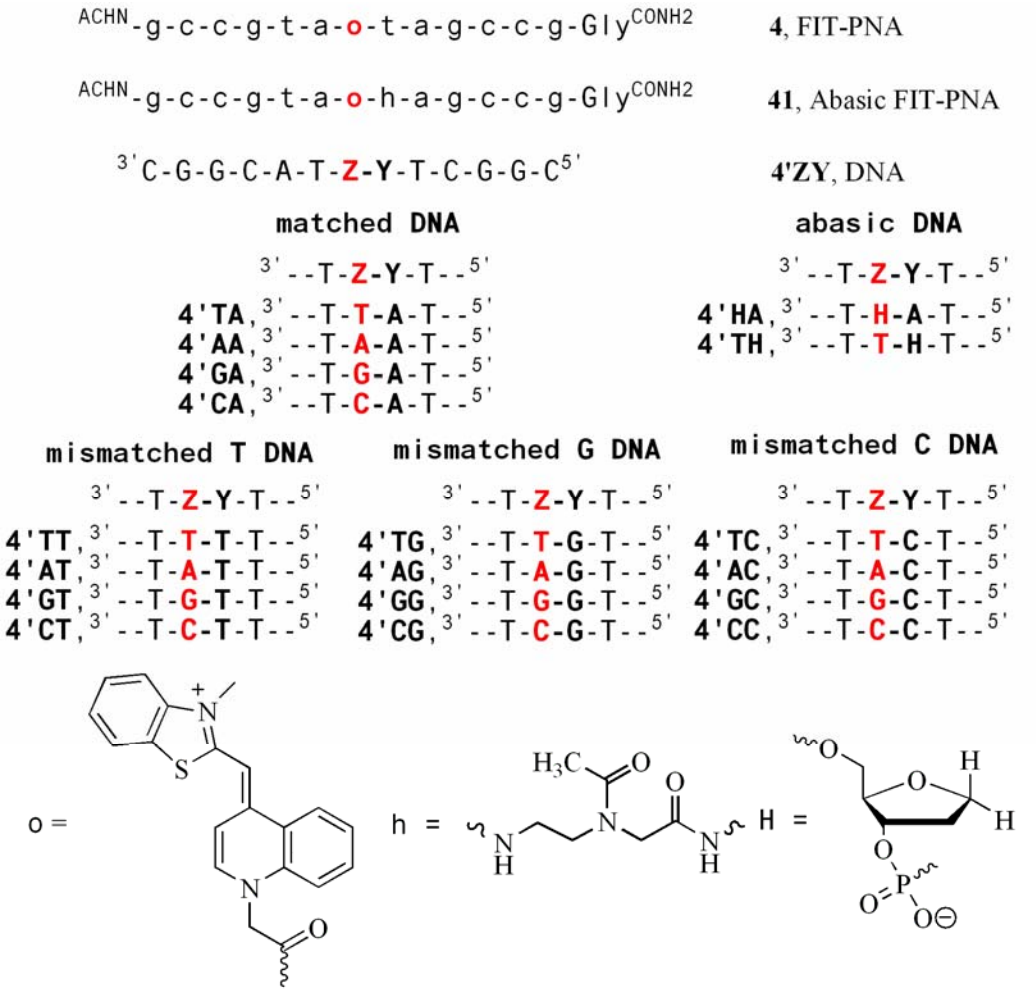

Scheme 15: Studied nucleic acids and nucleic acid dye conjugates.

The abasic-TO-PNA probe **41** lacks a C'-terminal TO intrastrand stacking partner (Scheme 15). The probe was first hybridised with DNA **4'TT** such that TO and adjacent hydrogen were paired against two thymine residues. The second hybridisation was carried out for probe **4** with DNA (**4'HA**) which lacked a pairing partner for thiazole orange. In duplexes comprised of **4** and DNA (**4'TH**) one interstrand stacking partner was removed. Stronger perturbation was introduced by hybridising abasic **TO** probe with both abasic DNA (**4'HA** and **4'TH**).

5.2.1 Fluorescence and Absorbance Study

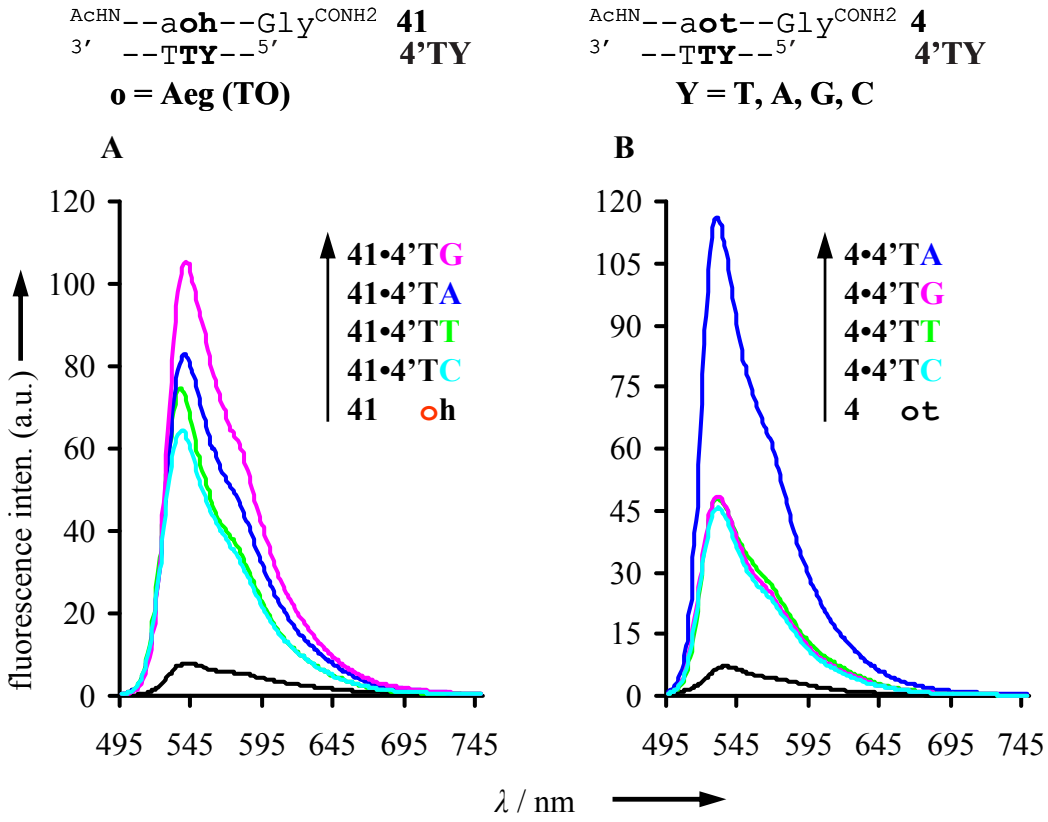

Figure 39: Fluorescence emission spectra of A) abasic FIT-PNA **41** and B) FIT-PNA **4** before (black), after addition of equimolar amount of DNA **4'TT** (green), **4'TA** (blue), **4'TG** (pink) and **4'TC** (turquoise). [Measurement conditions: 3 µM abasic FIT-PNA and 3 µM DNA (added after measurement of single strand PNA) in degassed buffer (100 mM NaCl, 10 mM NaH_2PO_4 at pH 7.0) at 25°C]. Ex. 485 nm. Em. 495-750 nm. Ex. Slit: 5 nm, Em. Slit: 2.5 nm.

Figure 39 shows Fluorescence spectra of TO-PNA **41** and **4** before and after hybridisation with oligonucleotide **4'TY** (Y = T, A, G and C). The thiazole orange was paired against thymine and the adjacent abasic site or thymine against all possible DNA bases. The binding event led to substantial increases in fluorescence intensity. Surprisingly, duplex **41•4'TA** gives 12.1 fold fluorescence enhancement at 530 nm. It is important to note that the duplex **4•4'TA** yields 18 fold fluorescence enhancement. The relative small loss of 6 fold suggest that the removal of only one interstrand stacking partner can be tolerated in presence of the good stacker adenine. Abasic FIT-TO-PNA gives 13.4 and 10.2 fold fluorescence with guanine and cytosine opposite to the abasic PNA residue in duplexes **41•4'TG** and **41•4'TC** respectively. The emission of the mismatched duplexes **4•4'TT, 4•4'TG** and **4•4'TC** was 3.1, 3.0

and 2.6 fold lower than emission of matched duplex (**4•4'TA**) when measured at 25°C. The fluorescence quantum yield ϕ_{em} = 0.02 for abasic FIT-PNA was half of the FIT-PNA (ϕ_{em} = 0.04).

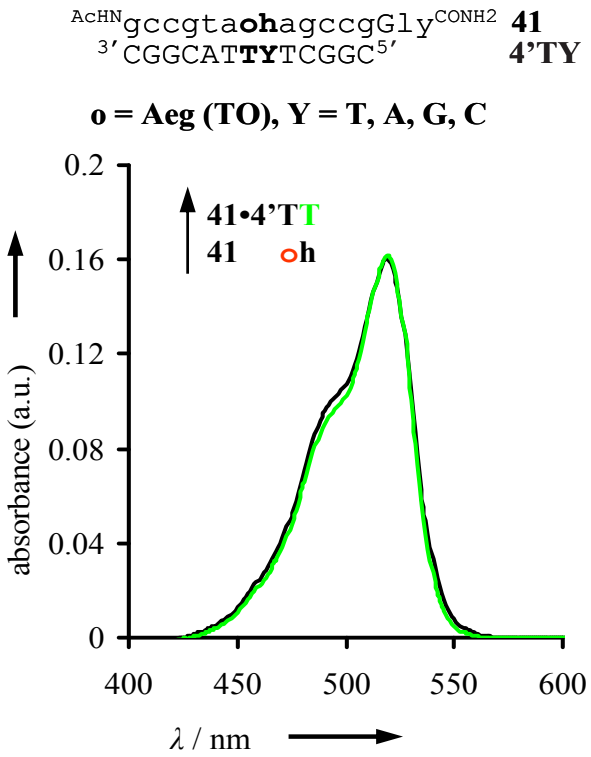

Figure 40: Absorbance spectra of abasic FIT-PNA **41** before (black) and after (green) addition of equimolar amount of **4'TT** DNA. The absorbance at 600 nm was set to zero and the absorbance curves for single strand were calibrated to the calculated ε_{260}. [Measurement conditions: 3 µM abasic FIT-PNA and 3 µM DNA (added after measurement of single strand PNA) in degassed buffer (100 mM NaCl, 10 mM NaH_2PO_4 at pH 7.0) at 25°C].

Figure 40 shows absorbance spectra of TO-PNA **41** before and after hybridisation with oligonucleotide **4'TT**. There is no spectral shift of absorbance maximum upon addition of **4'TT** and **4'TC** DNA. The addition of DNA **4'TG** gives 3 nm red shift at absorbance maximum. Addition of DNA **4'TA** gives a shift of 1 nm and 10 % increase in extinction coefficient (Table 6).

Table 6: Spectroscopic parameters of single stranded PNA **41**, before and after addition of DNA (**4'TY**).

^{ACHN}gccgta**oh**agccgGly^{CONH2} $^{3'}$CGGCAT**TY**TCGGC$^{5'}$			**o = Aeg (TO)** **Y = T, A, G and C**		
	$\lambda_{abs\ (nm)}$[a]	ε_{max}[b] (M^{-1} cm^{-1})	T_M[c] / °C	$\lambda_{em\ max}$[d] (nm)	F_{ds}/F_{ss}[e] (25°C)
41, (ss)	519	53482	-	540	-
41•4'TT	519	54058	62	538	10.3
41•4'TA	520	54032	59	540	12.1
41•4'TG	522	53821	60	541	13.4
41•4'TC	519	50836	59	539	10.1

[a] $_{abs}$ = Wavelength of absorbance maximum [b] ε_{max} = extinction coefficient at wavelength of absorbance maximum, [c] measured as denaturation curves, [d] λ_{em} = wavelength of emission maximum, [e] F_{ds}/F_{ss} = fluorescence enhancement at 530 nm of the double stranded PNA-TO comparable to single strand PNA-TO.

5.2.2 Melting Study

Previous work has shown that the introduction of TO as base surrogate does not affect the stability of PNA•DNA duplexes and that each of the four canonical nucleobases T, A, G and C was tolerated well opposite to TO.[54] Melting experiments with duplexes **41•4'TY, 41•4'AY, 41•4'GY** and **41•4'CY** (Y = T, A, G, C) were performed in order to evaluate the influence of abasic intrastrand residues adjacent to thiazole orange (Table 7 and 8). Duplex **4•4'TA** in which TO was opposite to thymine and embedded between a-T and t-A base pairs exhibited T_M = 68°C. The removal of a nucleobase adjacent to intercalated TO should lower the duplex stability due to a lack of stacking interactions. Indeed, the stability of abasic site conformation duplexes **41•4'TT, 41•4'TA, 41•4'TG** and **41•4'TC** were lower by ΔT_M = 6-9°C. Table 6 and 7 lists the thermal stability of duplexes featuring TO next to an intrastrand abasic residue and paired against A, G and C. All duplexes had lower T_M than the contiguously paired parent duplexes **4•4'AA, 4•4'GA** and **4•4'CA** (Table 8).

Table 7: Melting study and fluorescence data for abasic FIT-PNA **41** upon addition of DNA (**4'ZY**, Z = A, G, C; Y = T, A, G, C)

o-ZY	^{ACHN}gccgta**oh**agccgGly^{CONH2} $^{3'}$CGGCAT**ZY**TCGGC$^{5'}$		**41; o = Aeg (TO)** **4'ZY**; **Z, Y = T, A, G, C**	
o-AY	41•4'AT	41•4'AA	41•4'AG	41•4'AC
T_M/ °C[a]	59	57	62	57
F_{ds}/ F_{ss}[b]	7.7	5.4	10.7	5.2
o-GY	41•4'GT	41•4'GA	41•4'GG	41•4'GC
T_M/ °C[a]	58	58	61	57
F_{ds}/ F_{ss}[b]	7.7	4.5	6.1	6.0
o-CY	41•4'CT	41•4'CA	41•4'CG	41•4'CC
T_M/ °C[a]	60	58	60	59
F_{ds}/ F_{ss}[b]	9.7	9.9	10.7	10.6

[a] Measured as denaturation curves, [b] F_{ds}/ F_{ss} = fluorescence enhancement at 530 nm of the double stranded abasic PNA-TO comparable to single stranded PNA-TO.

Table 8: Melting study and fluorescence data for FIT-PNA **4** upon addition of DNA (**4'ZY**, Z = A, G, C; Y = T, A, G, C)

o-ZY	^{ACHN}gccgta**ot**agccgGly^{CONH2} $^{3'}$CGGCAT**ZY**TCGGC$^{5'}$		**4; o = Aeg (TO)** **4'ZY**; **Z, Y = T, A, G, C**	
o-AY	4•4'AT	**4•4'AA**	4•4'AG	4•4'AC
T_M/ °C[a]	59	**67**	59	58
F_{ds}/ F_{ss}[b]	7.0	**12.8**	5.0	8.7
o-GY	4•4'GT	**4•4'GA**	4•4'GG	4•4'GC
T_M/ °C[a]	57	**68**	58	57
F_{ds}/ F_{ss}[b]	5.5	**13.9**	4.9	7.0
o-CY	4•4'CT	**4•4'CA**	4•4'CG	4•4'CC
T_M/ °C[a]	56	**68**	58	56
F_{ds}/ F_{ss}[b]	6.0	**11.7**	6.1	4.7

[a] Measured as denaturation curves, [b] F_{ds}/ F_{ss} = fluorescence enhancement at 530 nm of the double stranded PNA-TO comparable to single stranded PNA-TO.

5.3 Hybridization of FIT-PNA and Abasic FIT-PNA with Abasic DNAs

In the previous section the effect of an abasic residue as intrastrand neighbor of TO was investigated. This section focuses on abasic site residues in the DNA target. It is difficult to imagine that TO and an opposing nucleobase adopt an innerhelical orientation without distortion of duplex geometry. It was, hence, considered to study the effect of an abasic site opposite to TO. Such an abasic site may provide more space to TO, which in response may adopt its preferred stacking orientation easier than in cases where TO is facing a nucleobase. I also explored the influence of an

abasic site as void interstrand stacking partner. These investigations are of interest not only for understanding the requirements for TO-based fluorescence signaling but also to evaluate scenarios in which the target features abasic residues as result of DNA damage.

5.3.1 Fluorescence study

Figure 41 shows the fluorescence spectra of abasic FIT-PNA **41** and FIT-PNA **4** in aqueous buffer at 3 µM concentration. High fluorescence quantum yield ($\phi_{em} \geq 0.36$) was obtained for duplex **4•4'TA** which featured adenines and thymine as intrastrand stacking partner. A high $\phi_{em} \geq 0.16$ was obtained for duplex **4•4'HT** and $\phi_{em} \geq 0.1$ for duplex **41•4'TH** and comparatively low $\phi_{em} = 0.09$ for both duplexes **4•4'TH** and **41•4'HT** respectively. It is evident that TO fluorescence not only responds to the adjacent base composition of the near environment but also to the bases in the partner strand.

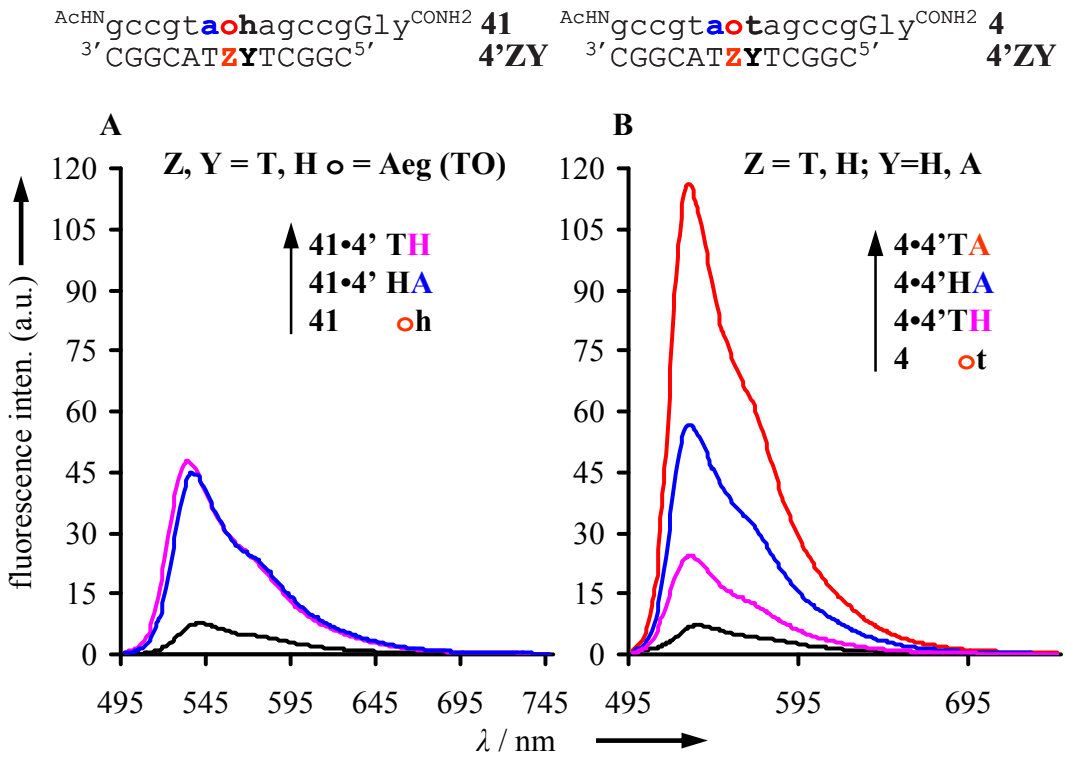

Figure 41: Fluorescence emission spectra of A) Abasic FIT-PNA **41** before (black), after addition of equimolar amount of DNA **4'TH** = (pink), **4'HA** = (blue) B) FIT-PNA **4** before (black), after addition of equimolar amount of DNA **4'TA** = (red), **4'TH** = (pink), **4'HA** = (blue). Measurement conditions: see caption of Figure 40.

5.3.2 Absorbance study

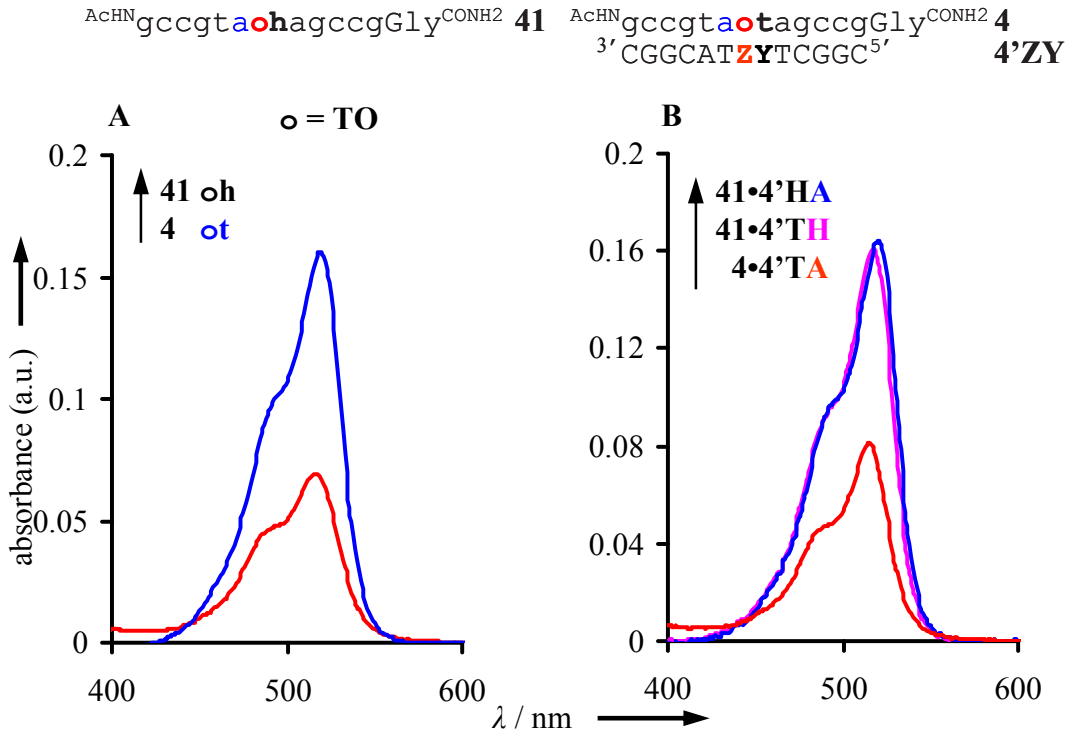

Figure 42: Absorbance spectra of A) Abasic FIT-PNA **41** (blue) and FIT-PNA **4** (red) and B) after formation of duplex of abasic FIT-PNA **41•4'HA** (blue), **41•4'TH** (pink) and FIT-PNA•DNA **4•4'TA** (red). The absorbance at 600 nm was set to zero and the absorbance curves for single strand were calibrated to the calculated ε_{260}. Measurement conditions: 3 µM PNA and 3 µM DNA, added after measurement of single strand PNA at 25°C.

Figure 42 and 43 shows the absorption spectra of abasic FIT-PNA **41** and FIT-PNA **4** before and after addition of corresponding matched and mismatched oligonucleotides. The FIT-PNA **4** shows a broad band in the visible region with one peak at 514 nm and a small shoulder at $\lambda \approx 485$ nm. Abasic FIT-PNA **41** shows broadband at 519 nm and shoulder at 490 nm. The extinction coefficient at absorbance maximum of single stranded abasic FIT-PNA **41** is increased by more than 200 % compared to FIT-PNA **4**. This effect is due to the absence of adjacent base of TO. At current the large difference between ε_{max} can not be explained. It is noted that the difference pertains in the duplex form as shown by Figure 42B.

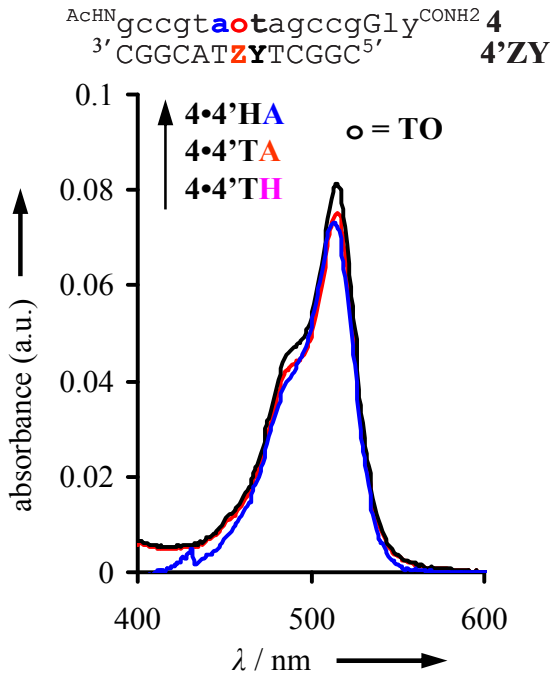

Figure 43: Absorbance spectra of FIT-PNA **4** after formation of duplex **4•4'HA** (blue), **4•4'TA** (red) and **4•4'TH** (pink). Measurement conditions: 3 µM FIT-PNA•DNA duplex at 25°C.

The UV spectra of TO paired against as abasic site in **4•4'HA** and with an abasic site as interstrand stacking partner in **4•4'TH** are not significantly different from spectra of TO "intact" duplex **4•4'TA** (Figure 43). These results show that, loss of TO intrastrand partner can result in dramatic enhancements of ε_{max}. In contrast, interstrand partner do not have a significant effect.

Table 9: Spectroscopic parameters of single stranded PNA **41** and **4**, before and after addition of DNA (**4'ZY**).

	$\lambda_{abs\ (nm)}$ [a]	ε_{max} [b] (M^{-1} cm^{-1})	$\lambda_{em\ max}$ [c] (nm)	Φ [d] (25°C)	F/ F_0 [e]
4, ss	516	23464	537	0.04	-
4•4'TA	515	25462	530	0.36	18.2
4•4'HA	515	27054	531	0.16	8.8
4•4'TH	514	24393	532	0.09	3.7
41, ss	519	53482	540	0.02	-
41•4'HA	517	54783	534	0.09	4.9
41•4'TH	521	53732	537	0.1	4.0

[a] Wavelength of absorbance maximum, [b] extinction coefficient at wavelength of absorbance maximum, [c] wavelength of emission maximum, [d] fluorescence quantum yield, [e] fluorescence enhancement at 530 nm of the double stranded PNA-TO comparable to single strand PNA-TO.

5.3.3 Circular Dichroism

CD spectra were measured in order to obtain insight into possible modes of TO-PNA•nucleic acid interactions. Figure 44A-B shows induced CD spectra of **4•4'TA** and **4•4'HA** respectively. The TO chromophore in the FIT-PNA•DNA complex **4•4'TA** shows a negative band with a maximum at 514 nm and in the FIT-PNA•abasic-DNA complex **4•4'HA** at 517 nm, which coincide with the absorption bands. Negative bands have been assigned to the intercalation mode.[1, 3, 4] It can be concluded that the TO chromophore in **4•4'TA** and **4•4'HA** predominantly accommodate intercalated position in the interior of the duplex.

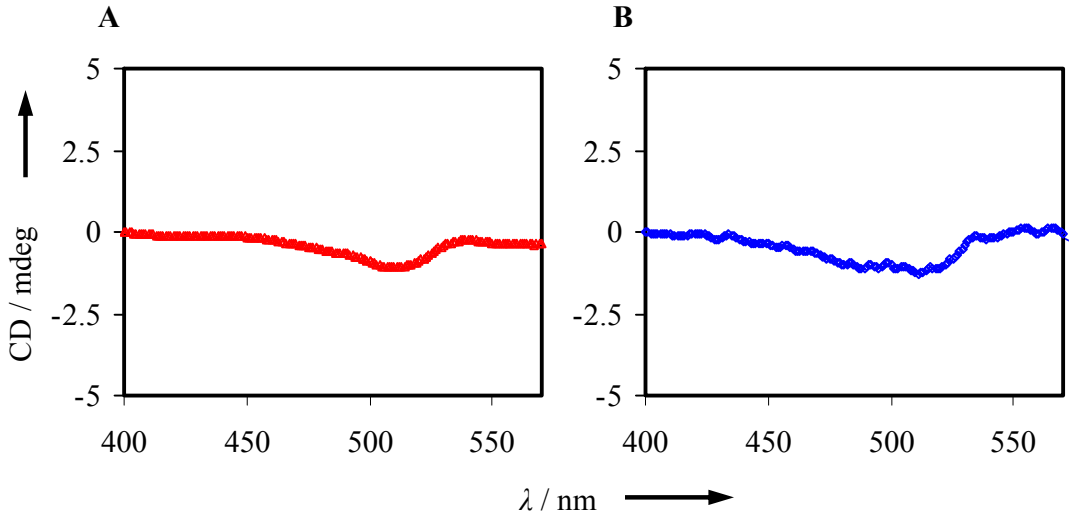

Figure 44: CD spectra of A) FIT-PNA•DNA duplex **4•4'TA** and B) FIT-PNA•Abasic-DNA duplex **4•4'HA**. Spectra were set zero at 400 nm. Measurement conditions: 3 µM FIT-PNA **4** and DNA **4'TA** or **4'HA** in buffer (100 mM NaCl, 10 mM NaH_2PO_4 at pH 7.0) at 15°C.

5.3.4 Time-resolved fluorescence

Time resolved fluorescence study have been carried out by Nils Krebs and Sebastian Tannert in the working group of Prof. Beate Röder (Institut für Physik, Humboldt-Universität zu Berlin. Newtonstr. 15, D-12489 Berlin, Germany). The TO-PNA and its complexes with DNA showed 3-4 decay times (Table 10). The short decay time, which was assigned to a water-accessible fluorescent species, was detected only for single stranded forms. Only three decay times (0.33-0.47 ns, 1.25-1.71 ns, 2.62-3.72 ns) were found in FIT-PNA and abasic FIT-PNA duplexes, with perfectly matched DNA, DNA containing abasic site. The results from section 4 have

led to the conclusion that the slow decay process is an indicator of hybridization that responds to adjacent base pairs. Typically, decay times are shortened and the amplitude factors are increased upon duplex formation. The increase of the amplitude factor and the decrease of decay times is significantly more pronounced when TO is allowed to pair against an abasic residue in **4•4'HA**. This would suggest higher stacking interactions. This is in agreement with the results from absorbance and T_M measurements. The obtained T_M for duplex **4•4'HA** was 71°C and 68°C for duplex **4•4'TA**. The presence of two abasic residues in duplex **41•4'HA** appears to introduce a significant perturbation to duplex structure.

Table 10: Fluorescence decay analysis of FIT-PNA **4** and abasic FIT-PNA **41**. **τ** denotes the fluorescence decay life time and relative amplitudes **a**.

	τ / ns (a/ %)[a]				χ^2
	very fast	fast	medium	slow	
4	0.06(47.3)	0.35 (27.8)	1.17 (19.8)	3.13 (5.1)	1.01[e] [1.04][d]
4•4'TA		0.43 (15.1)	1.71 (46.5)	3.56 (38.3)	1.04[d] [1.28][c]
4•4'HA		0.38 (13.1)	1.65 (37.6)	2.62 (49.3)	1.03[d] [1.17][c]
41	0.07(47.2)	0.35 (30.8)	1.25 (17.0)	3.53 (5.0)	1.05[e] [1.82][d]
41•4'TA		0.44 (21.3)	1.62 (47.0)	3.8 (31.7)	1.01[d] [1.42][c]
41•4'HA		0.47 (21.4)	1.35 (66.1)	2.87 (12.5)	1.02[d] [1.38][c]

[a] Relative amplitudes a in the emission decay fits are given as decimal fractions in parenthesis, [b, c, d, e] χ^2 obtained by monoexponential, biexponential, triexponential and tetraexponential, respectively, fitting of fluorescence decay curves.

5.4 Conclusions

1. Studied absorbance, circular dichroism and time resolved fluorescence results shows that thiazole orange is intercalated in PNA•DNA duplexes.
2. Absorbance and time resolved fluorescence results suggest that TO stacks well if opposing nucleobase is absent.
3. High interactions do not necessarily result in large fluorescence enhancements since tight stacking might open decay channels caused by interaction with nucleobases. For example: **4•4'TA** has higher fluorescence than **4•4'HA**.

6. Advantages of "FIT-Probes" over "Light-up" probes for homogeneous detection of single base mutation in DNA

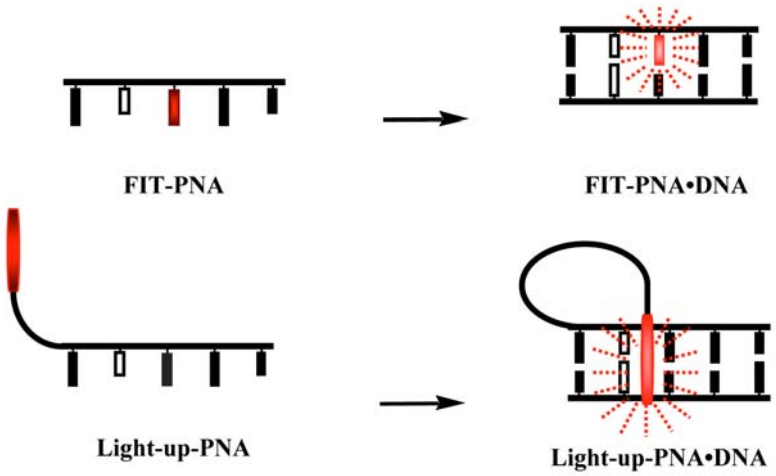

Figure 45: Schematic for FIT Probes and Light-up Probes

Thiazole orange has been introduced as a base surrogate in PNA by Seitz in 1999. Work from Ulysse Asseline,[100] Kubista and co-workers[48, 49, 50, 101, 102] reported the so-called Light-up probes which also employ TO as environmentally sensitive fluorphore and PNA for nucleic acid recognition. Light-up probes differ from FIT probes by the mode of attachment. TO in FIT probes is forced to intercalate at a specific position. TO in Light-up probes hangs by a flexible tether from the N'- or C'-terminal end. TO explore the influence of the different attachment modes, I decided to compare the optical properties.

6.1 Design and Synthesis

Svanvik et. al.[49] reported best results for conjugates in which TO was linked via a -NH-$(CH_2)_5$-CO- tether to the N'-terminus. The synthesis of TO_{Q5}-COOH and spacer was carried out using literature procedures.[103, 104] The dual thiazole orange labelled probe **43** which features TO as base surrogate and as end label was also studied for curiosity. Both probes were prepared by automated Fmoc-solid phase synthesis (Scheme 16). RP-HPLC, MALDI-TOF-MS, UV/ VIS confirmed the purity and molecular mass of **42** or **43** and the integrity of the chromophores.

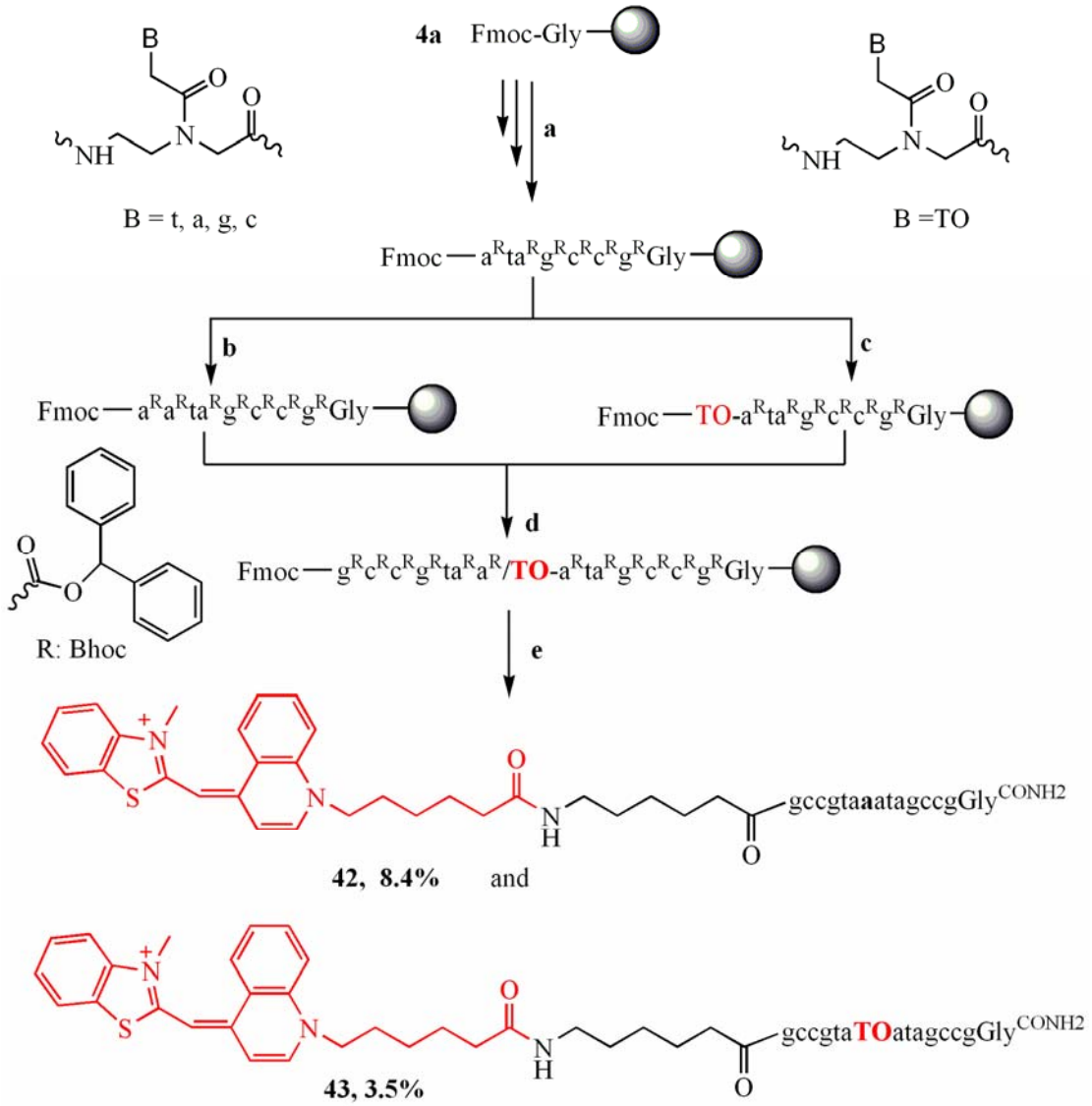

Scheme 16: a) Cycle of 1) piperidine/ DMF; 2) Fmoc–B (Bhoc)-OH, NMM, HCTU, NMP; 3) Ac_2O/ lutidine, DMF; b or c) 1) piperidine/ DMF; 2) Fmoc–a (Bhoc)-OH or Fmoc-Aeg (TO)-OH, HCTU, NMM, PPTS, NMP (double coupling); 3) Ac_2O/ lutidine, DMF; d) cycle of 1) piperidine/ DMF; 2) Fmoc–B (Bhoc)-OH, NMM, HCTU, NMP; 3) Ac_2O/ lutidine, DMF; e) 1) piperidine/ DMF; 2) Fmoc–NH-$(CH_2)_5$-COOH, NMM, PyBOP, DMF; 3) Ac_2O/ lutidine, DMF 4) TO_{Q5}-COOH, PyBOP, NMM, PPTS, DMF 5) TFA, m-cresol, H_2O, L-Cys-OMe.

6.2 Results and Discussion

The Light-up probe **42**, the FIT-Light-up probe **43** and FIT-probe **10** were hybridised with matched DNA **5'TTT** and single mismatched DNA **7'GTT**. The challenge is to distinguish between the a-T base pair in duplexes **42•5'TTT**, **43•5'TTT** and a-G mismatch duplexes **42•7'GTT**, **43•7'GTT** and **10•7'GTT**. The hybridisation was performed in buffer (100 mM NaCl and 10 mM NaH_2PO_4 adjusted

to pH 7.0, at 25°C) and the stability of the duplexes was evaluated by thermal denaturation experiments using UV spectroscopy. Most importantly, fluorescence was measured before and after addition of matched and mismatched oligonucleotides **5'TTT** and **7'GTT**.

42 TO-$(CH_2)_5$-CONH-$(CH_2)_5$-g-c-c-g-t-a-**a**-a-t-a-g-c-c-g-Gly^{CONH2}

43 TO-$(CH_2)_5$-CONH-$(CH_2)_5$-g-c-c-g-t-a-TO-a-t-a-g-c-c-g-Gly^{CONH2}

10 ^{ACHN}g-c-c-g-t-a-TO-a-t-a-g-c-c-g-Gly^{CONH2}

5'TTT $^{3'}$C-G-G-C-A-T-**T**-T-A-T-C-G-G-$C^{5'}$

7'GTT $^{3'}$C-G-G-C-A-**G-T**-T-A-T-C-G-G-$C^{5'}$

17'TTC $^{3'}$C-G-G-C-A-T-**T-C**-A-T-C-G-G-$C^{5'}$

Scheme 17: Sequences of DNA, PNA and position of TO linked in "Light-up", "FIT-Light-up" and "FIT" probe PNA.

6.2.1 Fluorescence Study

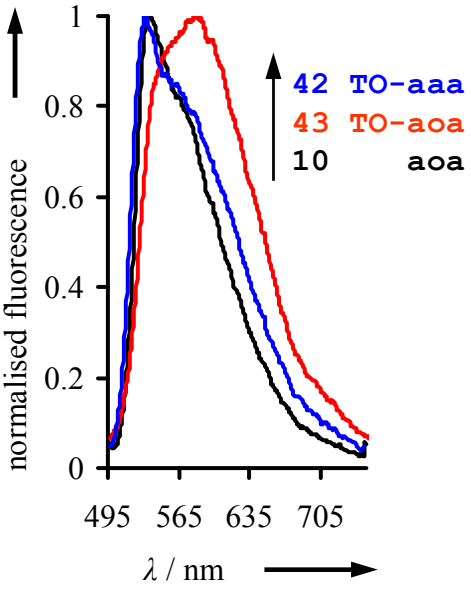

Figure 46: Normalized fluorescence emission spectra of single stranded "Light-up" probe **42**, "FIT-Light-up" probe **43** and "FIT" probe **10**. Measurement conditions: In degassed buffer [(100 mM NaCl, 10 mM NaH_2PO_4 at pH 7.0) Ex. 485 nm. Em. 495-750 nm. at 25°C].

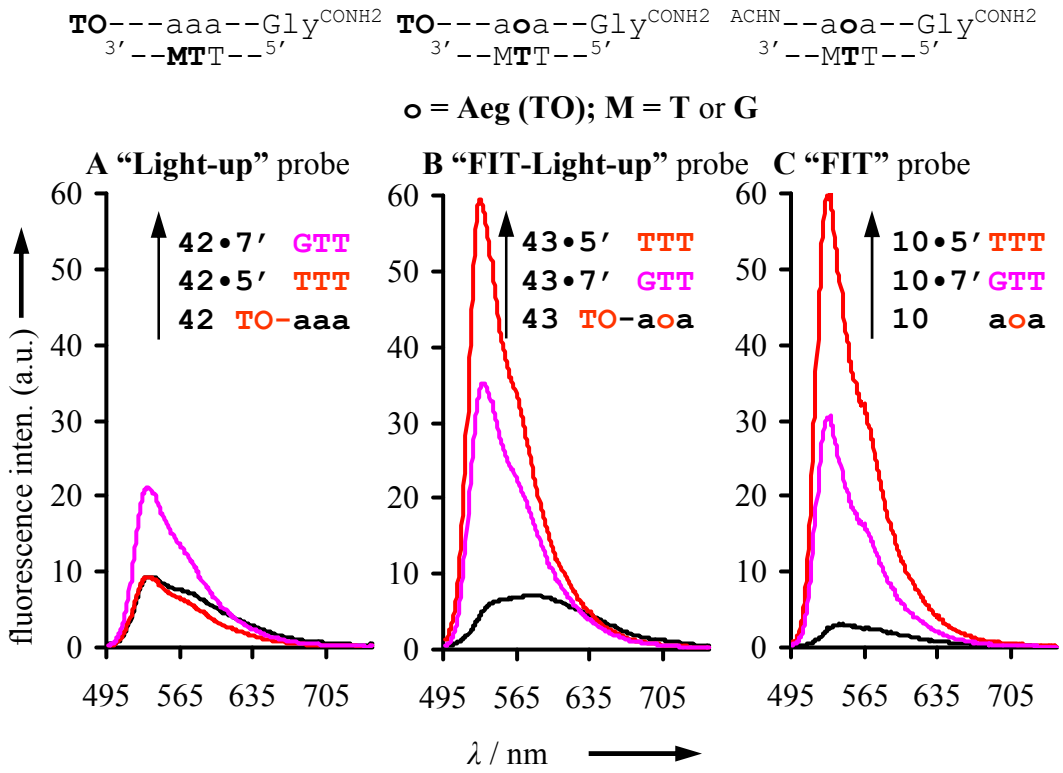

Figure 47: Fluorescence emission spectra before (black), after addition of equimolar amount of matched DNA **5'TT** = (red), and mismatched DNA **7'GTT** = (pink), for A) "Light-up" Probe **42**, B) "FIT-Light-up" Probe **43** and C) "FIT" Probe **10** at 25°C. Measurement conditions: 3 µM PNA and 3 µM DNA (added after measurement of single strand PNA) Ex. 485 nm. Em. 495-750 nm].

Figure 46 shows single stranded fluorescence emission of Light-up probe **42**, FIT-Light-up probe **43** and FIT probe **10**. Figure 47 shows the increase in fluorescence emission of A) "Light-up"**42**, B) "FIT-Light-up" **43** and C) "FIT" PNA conjugate **10** in response to addition of target DNAs **5'TTT** (matched) and DNA **7'GTT** (mismatched). The fluorescence of single stranded probe **42** gives broader emission at red side of the spectrum than single stranded FIT probe **10**. There was no fluorescence enhancement recorded upon formation of matched duplex **42•5'TTT**. In contrast to Light-up probe **42**, FIT-probe **10** and FIT-Light-up probe **43** give 23.8 and 13.8 fold fluorescence enhancement at 530 nm respectively, upon addition of DNA **5'TTT**. The lower fluorescence intensification in "FIT-Light-up" probe **43** is due to the high fluorescence of single stranded probe **43**. Interestingly, the Light-up probes **42** showed 2 fold fluorescence enhancement upon formation of single mismatched duplex **42•7'GTT**. This behaviour is in contrast to previous results from Kubista who reported unchanged fluorescence below the T_M of mismatched duplexes. As expected,

probe that contained TO as base surrogate exhibited significantly lower fluorescence increases upon in addition of mismatched DNA **7'GTT**.

Temperature exerts a major influence on probe fluorescence emission. Figure 48 shows fluorescence emission of probes **42, 43** and **10** before and after addition of DNA at 50°C. Upon increase of temperature in probe **42** fluorescence of single strand as well as matched duplex **42•5'TTT** decreases, while no fluorescence enhancement was observed for mismatched duplex **42•5'GTT**. The "FIT-Light-up" probe **43** and "FIT" **10** gives 10 and 17 fold fluorescence enhancement at 50°C.

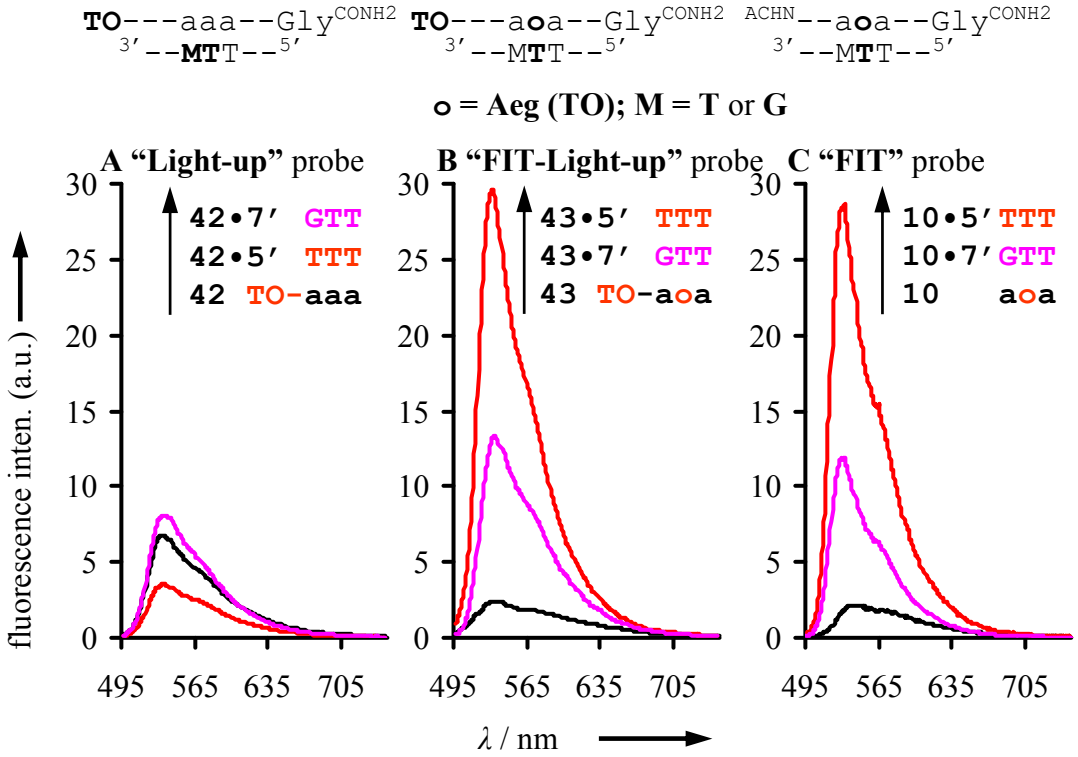

Figure 48: Fluorescence emission spectra before (black), after addition of equimolar amount of matched DNA **5'TT** = (red), and mismatched DNA **7'GTT** = (pink) for A) "Light-up" Probe **42**, B) "FIT-Light-up" Probe **43** and C) "FIT" Probe **10**, at 50°C. Measurement conditions: see caption of Figure 47.

Within these three studied probes highest quantum yield ($\Phi_F = 0.27$) was found for duplex **10•5'TTT** (FIT-Probe) and lowest ($\Phi_F = 0.027$) for duplex **42•5'TTT** (Light-up Probe). The significantly lower quantum yield for Light-up•DNA duplex is due to highest molar absorptivity (see Figure 49) and lowest fluorescence emission. The mixed or dual labeled probe **43** gives quantum yield $\Phi_F = 0.09$ with matched DNA **5'TTT** and ($\Phi_F = 0.06$) with mismatched DNA **7'GTT**. This observed variation

between "Light-up", "FIT-Light-up" and "FIT" probes shows superiority of FIT-probe over "Light-up" probe.

6.2.2 Absorbance Study

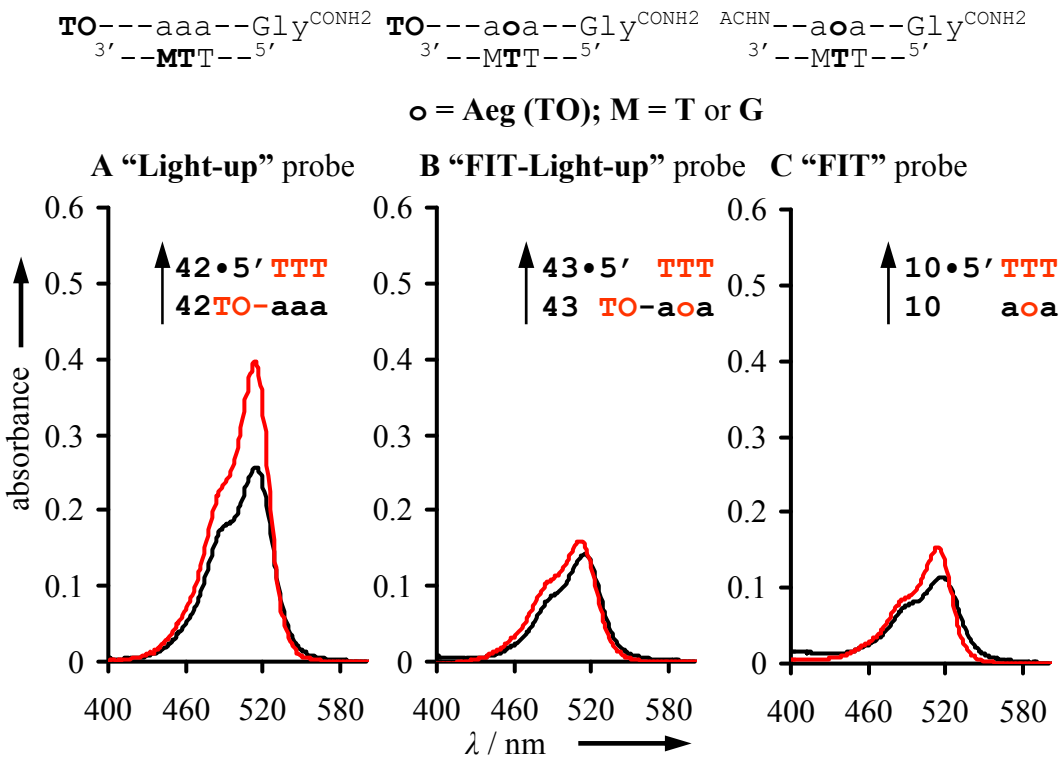

Figure 49: Absorbance spectra before (black), after addition of equimolar amount of matched DNA **5'TTT** for A) "Light-up" Probe **42,** B) "FIT-Light-up" Probe **43** and C) "FIT" Probe **10**. The absorbance at 600 nm was set to zero and the absorbance curves for single strand were calibrated to the calculated ε_{260}. Measurement conditions: 3 µM PNA and 3 µM DNA (added after measurement of single strand PNA) in degassed buffer (100 mM NaCl, 10 mM NaH_2PO_4 at pH 7.0, at 25°C).

Figure 49 shows absorption of 3 µM PNA-conjugates **42, 43** and **10** before and after addition of matched DNA **5'TTT** and single base mismatched DNA **7'GTT**. Single stranded Light up probe **42** experienced a dramatic increase in molar absorptivity from 85800 M^{-1} cm^{-1} to 109800 M^{-1} cm^{-1} at 514 nm upon addition of matched DNA **5'TTT**. This increase suggests that interactions between TO and the formed PNA•DNA duplexes **42•5'TTT** occur. However, the interaction fails to confer enhancements of fluorescence. Less pronounced increases of molar absorptivity were measured for duplexes **43•5'TTT** and **10•5'TTT** containing TO as base surrogate.

6.2.3 Melting Study

The melting curves measured for duplexes of PNA probes **42**, **43** and **10** revealed a sigmoidal behaviour. The thermal stabilities are summarised in Table 11. The Light-up probe **42** provided highest stability to a PNA•DNA duplex. The FIT probe containing duplex **10•5'TTT** and **43•5'TTT** have $T_M = 73°C$ and $T_M = 75°C$ respectively. The T_M of mismatched duplex **42•7'GTT**, is lower by $\Delta T_M = 6°C$ than the T_M of matched duplex **42•5'TTT**. Interestingly, the hybridisation specificity is higher for FIT-PNA **10**, as indicated by $\Delta T_M = 8°C$ between the stabilities of matched and mismatched duplexes.

Table 11: Spectroscopic parameters of "Light-up" **42**, "FIT-Light-up" **43**, and "FIT" **10** PNA probes.

PNA	λ_{abs} [a] (max)/ nm	ε_{max} [b] / M^{-1} cm^{-1}	λ_{max} [c] (em)/ nm	Φ_{em} [d]	F_{ds}/ F_{ss} [e]	T_M [f] / °C
42	514	85800	535	0.04	-	-
42•5'TTT	514	132000	536	0.02	1.0	76
42•7'GTT	514	109800	535	0.05	2.1	70
43	514	47400	581	0.03	-	-
43•5'TTT	511	53000	530	0.09	13.8	75
43•7'GTT	512	50000	534	0.06	9.5	64
10	516	38200	543	0.03	-	-
10•5'TTT	514	51300	531	0.27	23.8	73
10•7'GTT	515	43200	534	0.07	6.1	65

[a] Wavelength of absorbance maximum, [b] extinction coefficient at wavelength of absorbance maximum, [c] wavelength of fluorescence emission maximum, [d] Φ_{em} = fluorescence quantum yield, [e] F_{ds}/ F_{ss} = ratio between fluorescence intensities F_{ds} after and F_{ss} before addition of matched and single mismatched DNA at 530 nm. [f] measured as denaturation curves.

6.2.4 Circular Dichroism

CD spectra in visible region were measured in order to obtain information about binding modes. Figure 50 shows the CD in the region of TO absorption. There was no induced CD found in the duplex of "Light-up•DNA". By contrast, negative induced CD's became apparent in duplexes conforming FIT-PNA. For example, Figure 50B shows the induced CD spectrum of "FIT-PNA" **10** due to intercalation of TO. The observed a negative band has been assigned to the intercalation mode.[1, 3, 4] This

mode is also seen in FIT-Light-up **43** (Figure 50A). In contrast, CD-spectroscopy is not suited to assign the binding mode of end labelled TO in Light-up PNA **42**.

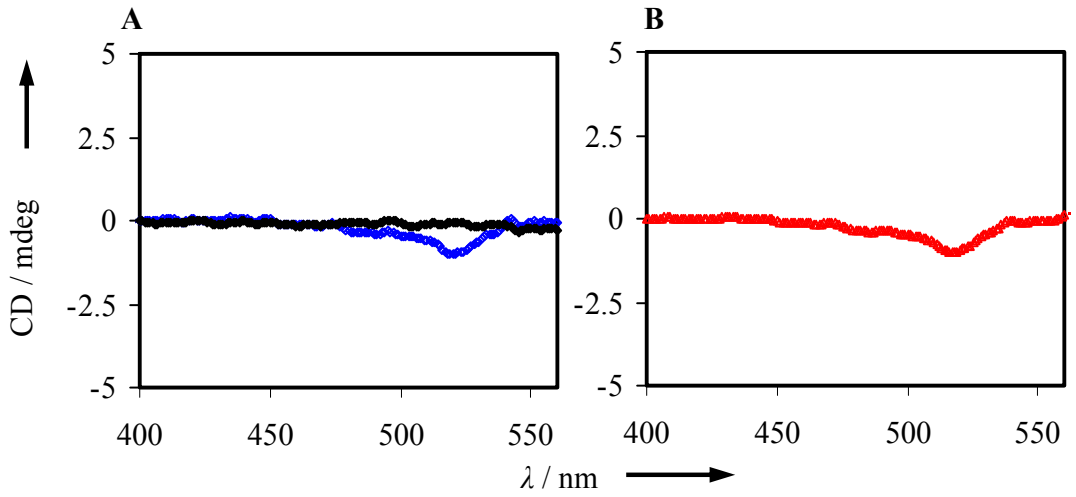

Figure 50: CD spectra of A) Light-up•DNA duplex **42•5'TTT** = (black), FIT-Light-up•DNA duplex **43•5'TTT** = (blue) and B) FIT-PNA•DNA duplex **10•5'TTT** = (red). Spectra were set zero at 400 nm. Measurement conditions: 3 µM PNA **42, 43** or **10** and DNA **5'TTT** in buffer (100 mM NaCl, 10 mM NaH_2PO_4 at pH 7.0) at 15°C.

6.2.5 Time-resolved Fluorescence

As described earlier (section 5), the PNA conjugates and their complexes with DNA showed 3-4 decay times. The TO-nucleic acid conjugates and their complexes with DNA studied in this work showed 3-4 decay times. The shortest decay time was assigned to a water-accessible fluorescent species which disappears upon hybridisation of FIT-PNA **10** to matched and mismatched DNA. Remarkably, the very fast decaying species remains during hybridization of Light-up PNA **42**. The previous results from section 4 have exposed the slow decay process as responsive to base stacking. For example, matched hybridisation of FIT-PNA **10** increased the population of the slowly decaying species from 2 % to 40 %. In contrast, Light-up PNA **42** showed reduction of slow decaying population. The results from section 4 suggested that the slow and the medium decay process are the hallmarks of TO in a rigid environment. The two processes have significantly lower amplitude factors in duplexes of Light-up PNA **42** than in duplexes of FIT-PNA **10**. It may be noteworthy that the decay times of the fast, medium and slow decay process are larger in Light-up duplexes than in FIT-PNA duplexes (Table 12). This observation, decrease of decay

times and a shift of population to slow decay processes, upon FIT-PNA hybridisation has been observed in section 4, and has been assigned to tight contact with nucleobases, which close and open decay channels.

Table 12: Fluorescence decay analysis of "Light-up" PNA **42** and "FIT-PNA" **10**. **τ** denotes the fluorescence decay life time and relative amplitudes **a**.

	τ / ns (a/ %)[a]				χ^2
	very fast	fast	medium	slow	
42	0.04 (48.3)	0.27 (20.8)	1.11 (20.7)	3.14 (10.2)	1.12[e] [1.17][d]
42•5'TTT	0.04 (58.1)	0.49 (16.9)	1.62 (17.0)	3.61 (7.9)	1.02[e] [1.39][d]
42•17'TTC	0.03 (72.8)	0.48 (11.9)	1.56 (10.7)	3.56 (4.6)	1.05[e] [1.37][d]
10	0.05 (50.2)	0.48 (41.0)	1.49 (6.7)	3.64 (2.2)	1.11[e] [1.54][d]
10•5'TTT		0.39 (22.3)	1.39 (37.9)	3.03 (39.8)	1.05[d] [1.51][c]
10•7'GTT		0.28 (52.9)	1.10 (34.7)	3.31 (12.3)	1.05[d] [2.37][c]

[a] Relative amplitudes a in the emission decay fits are given as decimal fractions in parenthesis, [c, d, e] χ^2 obtained by biexponential, triexponential and tetraexponential, respectively, fitting of fluorescence decay curves.

TO in FIT-PNA **10** is intercalated as has been shown in section 4. TO in Light-up PNA **42** interacts with the duplex formed upon hybridisation with target DNA as suggested by the increase of molar absorptivity. The lack of an induced CD, the occurrence of a water exposed species seen in times resolved fluorescence measurements, may indicate that TO in duplexes of Light-up PNA **42** associates to the backbone. Minor groove binding is less likely to prevail since this binding mode should give rise to enhancement of fluorescent emission.[97]

6.3 Evaluation of "FIT-PNA vs. Light-up-PNA" probes detection of the G12V mutation in the Ras Gene

Analysis of above three sequences suggested the superiority of FIT-probes. However, the harvesting of fluorescence from Light-up-PNA has been said to depend upon back bonding of TO to the PNA bases in single strands. This mainly depends upon the sequence of selected PNA. Hence, it was decided to study another independent sequence context (Scheme 18).

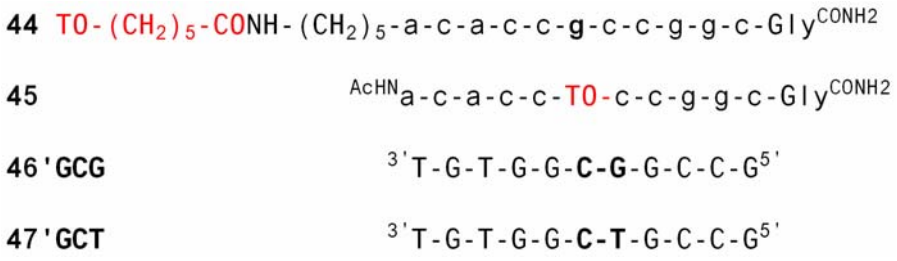

Scheme 18: Sequences of DNA, PNA in "Light-up" and "FIT" probe PNA.

Point mutations in codons 12 of the K-*ras* gene occur early in the development of colorectal cancer. These mutations can serve as biomarkers for shed or circulating tumour cells and may be useful for diagnosis of early, curable tumours and for staging of advanced cancers. Here two probes (FIT and Light-UP) have been synthesised for detection of such G12V mutation of ras gene.

6.3.1 Synthesis, Fluorescence and Melting Study

The modified Fmoc-solid phase synthesis procedure was applied for synthesis of "Light-up" probe **44** and "FIT" probe **45** (Scheme 18). RP-HPLC, MALDI-TOF-MS, UV/ VIS confirmed the purity and molecular mass of **44** and **45** and the integrity of the chromophore. The probe **44** or **45** were hybridised with DNA **46'GCG** and **47'GCT**. Both probe **44** and probe **45** will form a perfect duplex with DNA **46'GCG** and a-G mismatched base pair containing duplex with DNA **47'GCT**. The FIT-PNA **45** upon hybridisation with matched DNA will feature TO embedded by c-G base pairs and paired against cytosine. The mismatched duplexes **44•47'GCT** and **45•47'GCT** have c-T as mismatched base pair. Hybridisation of the **44** or **45** conjugates was performed in buffer (100 mM NaCl and 10 mM NaH_2PO_4 adjusted to

pH 7.0) and the stability of these formed complexes was evaluated by thermal denaturation experiments using UV spectroscopy. Figure 51 shows fluorescence intensity measured before and after addition of matched and mismatched oligonucleotides **46'GCG** and **47'GCT** respectively.

The single strand fluorescence of Light-up probe **44** gives broader emission spectra than FIT-probe **45**. Addition of matched DNA **46'GCG** furnished 2 fold fluorescence enhancements. Probe **45** gives 15.7 fold fluorescence enhancements at 530 nm upon addition of matched DNA **46'GCG**. Only 2.2 fold fluorescence enhancement was recorded for formation of duplex **44•47'GCT**, where thymine acts as mismatched base. The duplexes **44•46'GCG** and **45•46'GCG** have similar stabilities (T_M = 71°C and T_M = 70°C, respectively). Again, FIT-PNA seems to bind target DNA more specifically than Light-up PNA. The melting temperature of matched duplex **45•46'GCG** (T_M = 70°C) is higher by ΔT_M = 18°C than the T_M of mismatched FIT-PNA•DNA duplex **45•47'GCT**. With Light-up PNA **44** the difference in stability amounted to ΔT_M = 6°C.

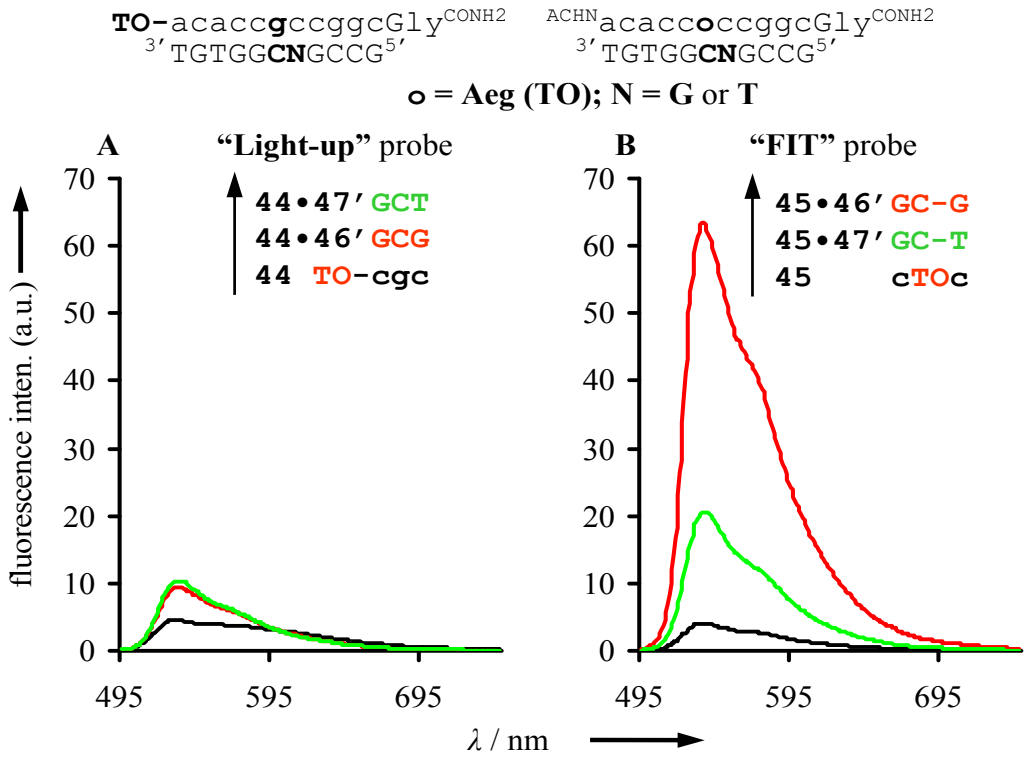

Figure 51: Fluorescence emission spectra before (black), after addition of equimolar amount of matched DNA **46'GCG** = (red) and mismatched DNA **47'GCT** = (green) for A) "Light-up" Probe **44**, B) "FIT" Probe **45** at 25°C. Measurement conditions: see caption of Figure 47.

6.4 Conclusions

The hybridisation experiment performed with 'FIT-PNA' and 'Light-up PNA' in two sequence contexts suggest that, FIT-PNA is superior to Light-up PNA as far as hybridisation specificity, fluorescence enhancement and match/mismatch discrimination is concerned. The collected data from UV/ VIS absorbance, circular dichroism, and fluorescence spectroscopy indicate that the use of thiazole orange as base surrogate in FIT-PNA enabled the site-specific intercalation in PNA•DNA duplexes. In contrast TO in Light-up PNA does not show such sign for intercalation.

Steady state Fluorescence: In the studied two different sequences, FIT-PNA yields higher fluorescence enhancements (16-24 folds) upon binding with matched DNA and attenuated fluorescence with single base mismatched DNA. The Light-up probes were failed to discriminate matched from single base mismatched DNA. Moreover, TO in FIT-PNA gives far better fluorescence enhancements.

Time resolved fluorescence: The studies of FIT-PNA and Light-up PNA also highlighted four different fluorescence decay processes which responded differently to changes of the TO environment. This includes a very fast and sensitive fluorescence decay process, which disappears upon double-strand formation in FIT-PNA. Such decay remains unchanged in hybridisation of Light-up-PNA.

Absorbance: Remarkable changes in absorbance spectra were recorded. 1) FIT-PNA gives extinction coefficient of $\varepsilon_{max} = 38200$ $M^{-1}cm^{-1}$ and Light-up PNA of $\varepsilon_{max} = 85800$ $M^{-1}cm^{-1}$. The ε_{max} of Light-up PNA **42** increased to 132000 upon double strand formation. The duplex of FIT-PNA **10** has 2.6 fold lower $\varepsilon_{max} = 51300$. These differences indicate different interactions between TO and nucleobases in PNA•DNA duplexes. Circular diachroism: Negative band in FIT-PNA•DNA confirms its predominant intercalation. No intercalation of thiazole orange was seen in 'Light-up•DNA' duplex.

The results suggest that TO in FIT-PNA is always intercalated upon addition of target DNA. The Light-up probes are less sensitive and intercalation may mainly depend upon sequence of probe.

7. Dual labeled "FIT-PNA" for homogeneous detection of single base mutation in DNA

TO in FIT-PNA is responsive to changes of the base stack. While adjacent matched base pairs resulted in high fluorescence intensity, low fluorescence was detected in case adjacent base mismatches formed. One of the questions that arouse was whether fluorescence signalling could be improved if two dyes were placed adjacent to the base mismatches. The idea was to sandwich the base mismatch between two ''TO-bases''. It was anticipated that the two TO chromophores could be in contact in the single strand and that hybridisation would separate the chromophores. As a result fluorescence spectra of double strands were expected to be significantly different from fluorescence spectra of the single strands. The latter were anticipated to have some similarity to fluorescence spectra of the thiazole orange dimer TOTO.[67, 73, 74, 75, 105] Furthermore, base mismatches perturb and destabilise duplex structure. Thus it was deemed possible that the two TO-chromophores could come into contact when separated by a base mismatch, resulting in changes of fluorescence.

7.1 Design and Synthesis

In dual-FIT PNA **48** intercalating thiazole orange is linked to the aminoethyglycine backbone by replacing two nucleobases from position six and eight such that there was a nucleobase in between these two dyes. The mismatched DNA base position was opposite to the sandwiched adenine. Linear Fmoc-solid phase synthesis was used to prepare "Dual-FIT-PNA" probe **48** (Scheme 19). RP-HPLC, MALDI-TOF-MS, UV/ VIS confirmed the purity and molecular mass of **48** and the integrity of the chromophores.

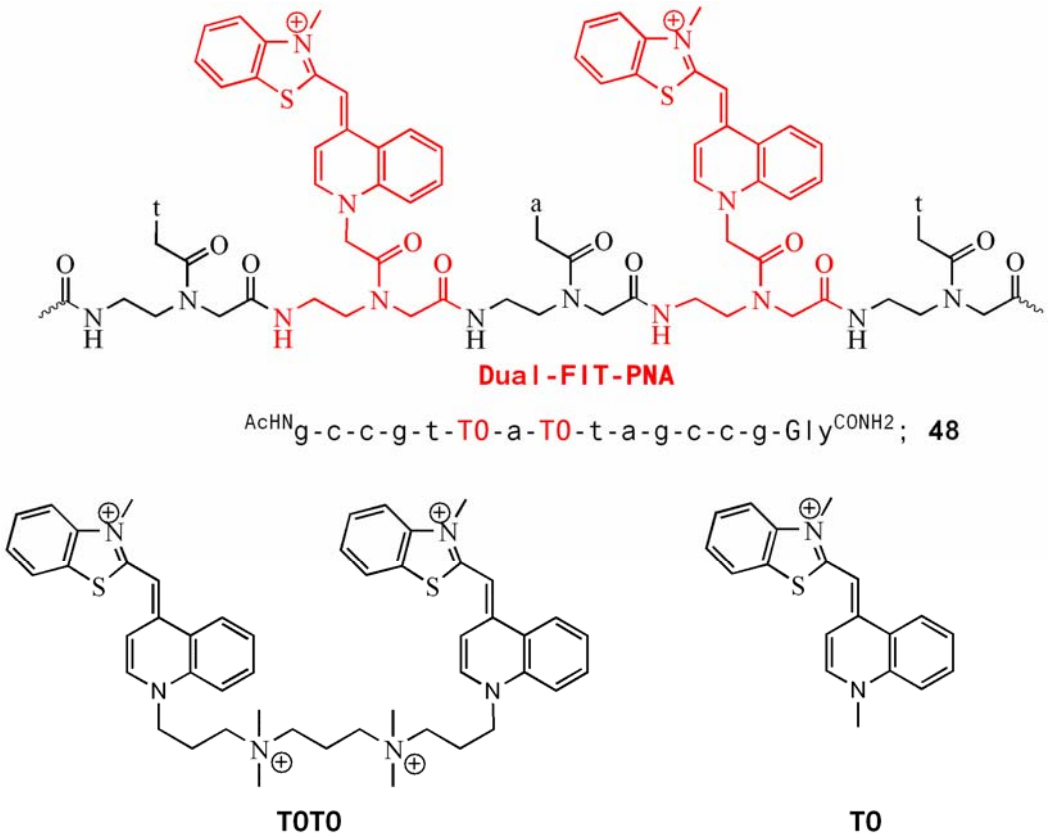

Scheme 19: Structure of dual-labeled FIT-PNA, TOTO and TO.

Probe **48** was hybridised with DNA **5'TYT, 10'AYA, 17'GYG, 20'CYC** (Y = T, A, G, C) such that both TO-dyes were paired against T, A, G and C respectively. The adenine residue flanked by two TO dyes was paired against all DNA nucleobases. The hybridisation experiments gave rise to four matched duplexes and twelve mismatched duplexes. The stability of each $(TO)_2$-PNA•DNA complex was evaluated by thermal denaturation experiments using absorbance spectroscopy. The fluorescence spectra at two different temperatures (25°C and 60°C) were measured before and after addition of matched and mismatched DNA. The UV-absorbance spectra for **48** before and after addition of DNA **5'TYT** (Y = T, A, G, C) were recorded at 3 µM concentration.

7.2 Absorbance Study

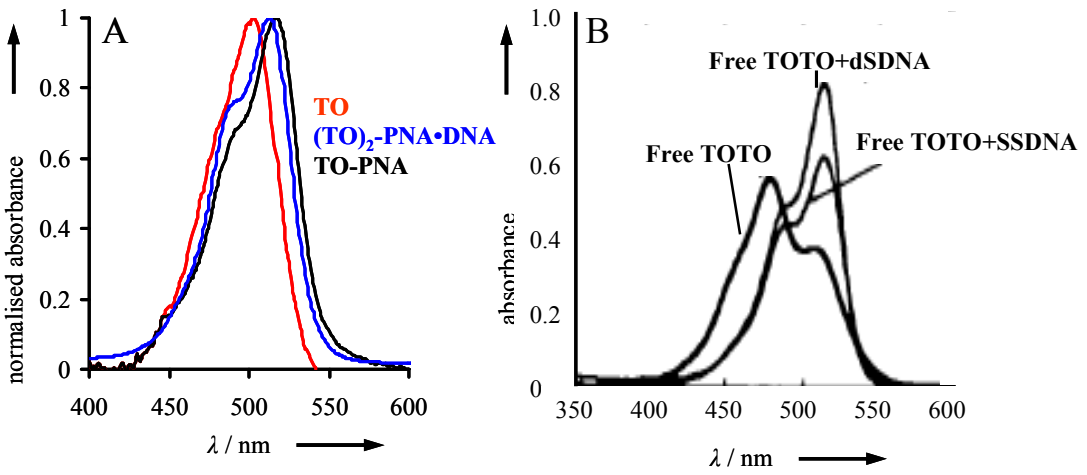

Figure 52: A) Normalised absorbance spectra of free TO, single stranded TO-PNA **10** (a-TO-a) and $(TO)_2$-PNA•DNA complex **48**. B) Absorbance spectra of free TOTO, TOTO•ssDNA and TOTO•dsDNA. (Spectra taken)[106]

Figure 52A shows normalised absorbance spectra of free TO, single stranded TO-PNA and $(TO)_2$-PNA. Single stranded dual labeled FIT-PNA **48** shows an absorption maximum at 512 nm and molar absorptivity of 132600 M^{-1} cm^{-1}. An additional pronounced band at 481 nm is observed. The absorbance maximum for free TOTO is at wavelength (480 nm).[73] The blue side band (485 nm) is less pronounced in TO-PNA compared to $(TO)_2$-PNA. There is no such band recorded for free TO. Free TO shows absorbance maximum (501 nm) at shorter wavelength than TO-PNA and $(TO)_2$-PNA. Interestingly, the band shape of single stranded $(TO)_2$-PNA coincides with reported absorption band of TOTO complexed to DNA (compare Figure 52B).[106]

Figure 53 shows absorbance spectra of $(TO)_2$-PNA before and after hybridisation of matched and single base mismatched DNA. Dual labeled PNA-conjugate **48** experienced an increase in molar absorptivity at 512 nm by 24 % (164700 M^{-1} cm^{-1}) upon addition of matched DNA **5'TTT** but no spectral shift. The pronounced band at 481 nm was red shifted by 6 nm in matched duplex **48•5'TTT**. Dual-FIT-PNA **48**, upon addition of mismatched DNA **5'TAT, 5'TGT** and **5'TCT** gives 143600 M^{-1} cm^{-1}, 144600 M^{-1} cm^{-1} and 146900 M^{-1} cm^{-1} molar absorptivity at 512 nm, respectively.

The complexes 'TOTO•dsDNA' and '$(TO)_2$-PNA•DNA' have same absorbance spectral shape (compare Figure 52B with Figure 52A). This resemblance could be due to a similar bisintercalation hybridising mode. It has to be noted, however that the two TO dyes in DNA complexes of TOTO are separated by two base pairs while only one base pair is expected to lay between the TO units in DNA duplexes of $(TO)_2$-PNA **48**. Both the complex of TOTO with ssDNA and dual FIT-PNA **48** experience increases of absorptivity upon formation of double strand complexes.

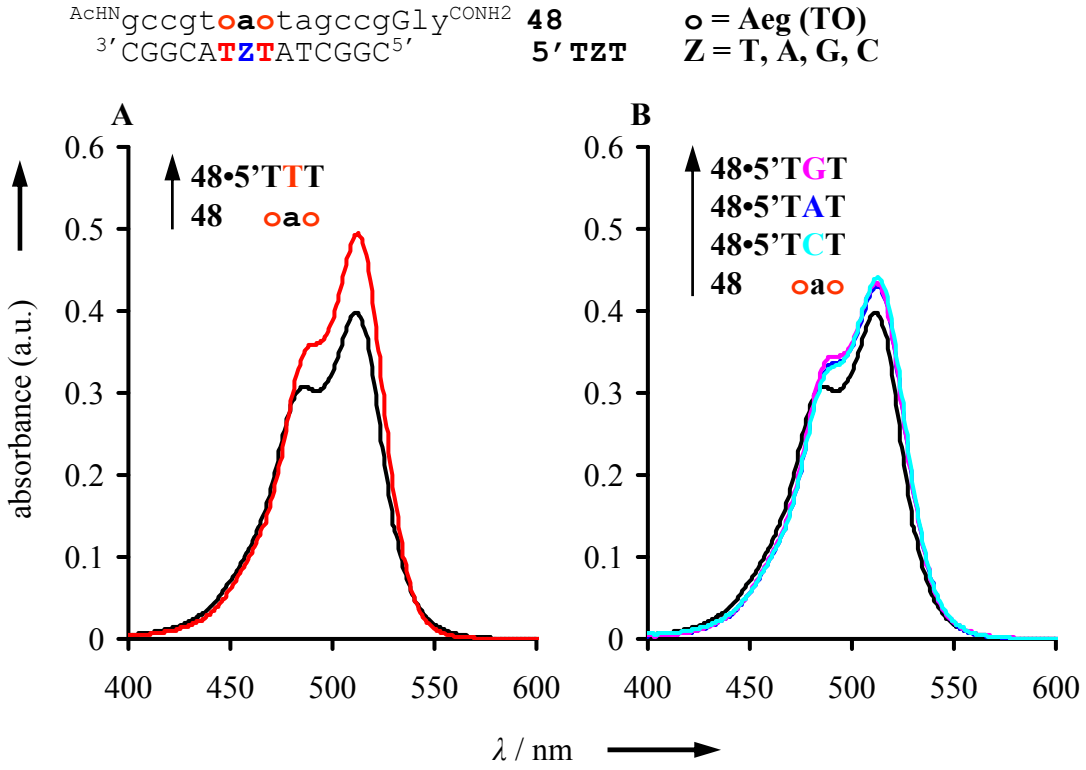

Figure 53: Absorbance spectra of PNA probe **48** before (black), after addition of equimolar amount of A) matched DNA **5'TTT** = (red), B) mismatched DNA **5'TAT** = (blue), DNA **5'TGT** = (pink) and **5'TCT** = (turquoise), at 25°C. The absorbance at 600 nm was set to zero and the absorbance curves for single strand were calibrated to the calculated ε_{260}. Measurement conditions: see caption of Figure 49.

7.3 Fluorescence Study

Figure 54 shows fluorescence emission maximum of free TO, single strand TO-PNA and $(TO)_2$-PNA. Fluorescence emission of TO-PNA **10** gives emission maximum at 546 nm and TO at 640 nm.[73] The broader and red shifted emission maximum for TO is due to dimerisation. The fluorescence spectrum of $(TO)_2$-PNA **48** shows a broader TO emission than in TO. The emission maximum is red shifted. It can be imagined that the two TO-chromophores in **48** are at least partially in contrast.

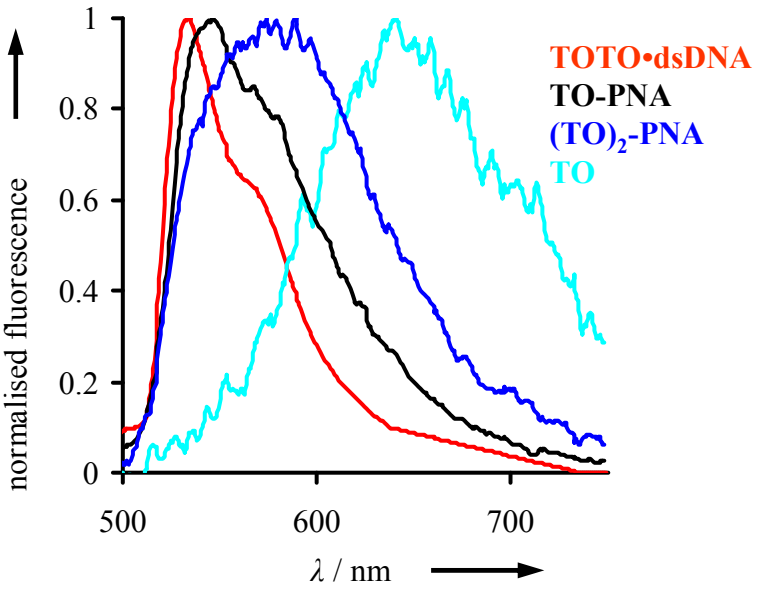

Figure 54: Normalised fluorescence emission spectra of free TO, single strand TO-PNA **10** (a-TO-a) and $(TO)_2$-PNA **48**.

Figure 55 shows the fluorescence emission of single stranded labeled PNA **48** before and after addition of DNA **5'TYT** and **20'CYC**. The single strand fluorescence emission maximum of $(TO)_2$-PNA appears at wavelength 574 nm. It became apparent that the formation of matched duplex was accompanied by a shift of the emission maximum from 574 nm to 535 nm and 533 nm for duplex **48•5'TTT** and **48•20'CTC** respectively. Formation of duplex with mismatched DNA also leads to a hypsochromic shift (Table 13), however the fluorescence maximum appears at longer wavelength than for matched duplexes. Interestingly, TOTO upon binding with dsDNA also shows hypsochromic shift (98 nm).[73] The probe **48** gives 39.4 fold fluorescence enhancement at 530 nm upon addition of DNA **5'TTT** featuring thymine as pairing partner for TO.

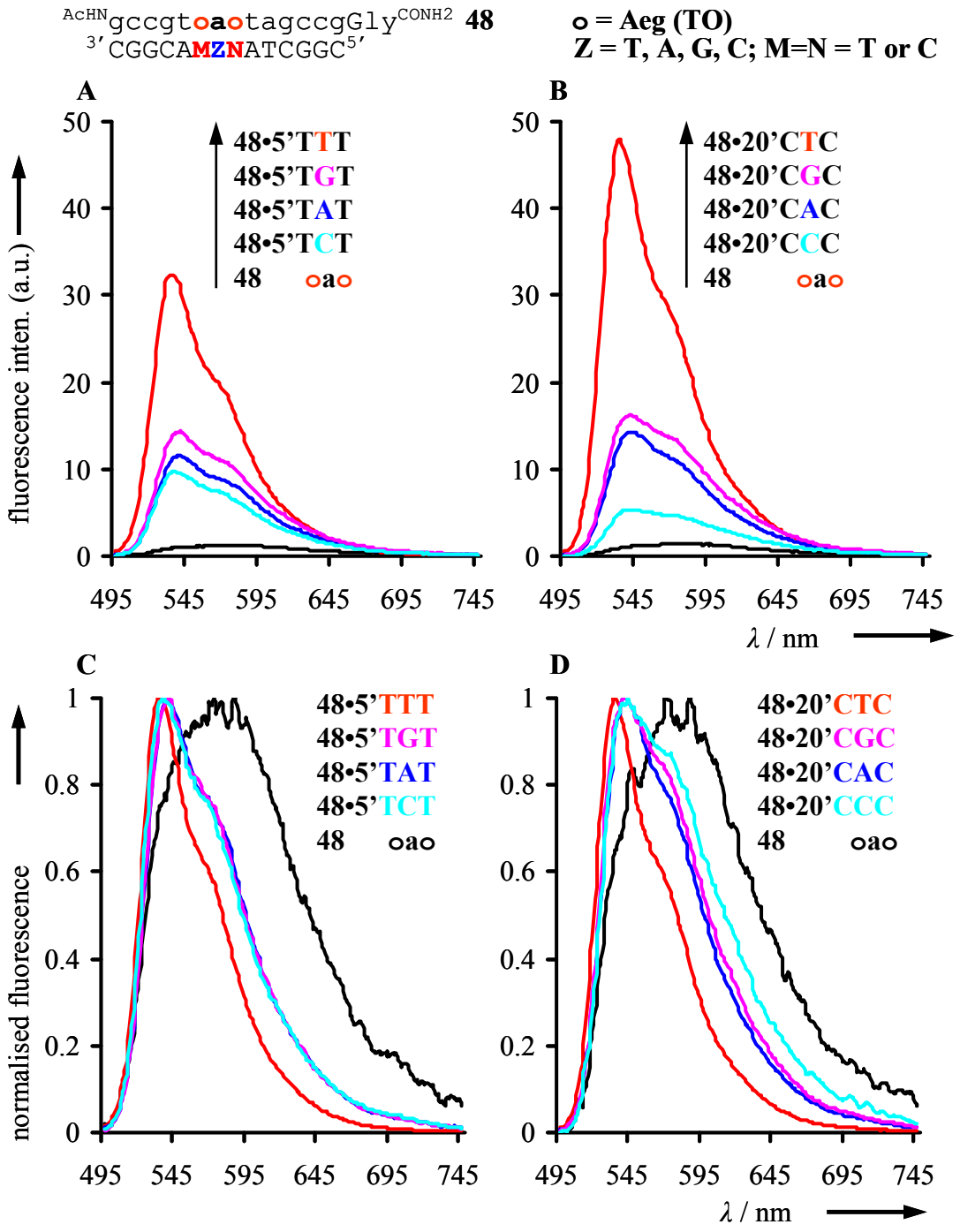

Figure 55: Fluorescence emission spectra of PNA probe **48** before (black), after addition of equimolar amount of A) matched DNA **5'TTT** = (red), mismatched DNA **5'TAT** = (blue), DNA **5'TGT** = (pink) and **5'TCT** = (turquoise) B) matched DNA **20'CTC** = (red), mismatched DNA **20'CAC** = (blue), DNA **20'CGC** = (pink) and **20'CCC** = (turquoise) C) Normalised fluorescence spectra from Figure 55A and D) Normalised fluorescence spectra from Figure 55B. Measurement conditions: 1 µM PNA and 1 µM DNA (added after measurement of single strand PNA) in degassed buffer (100 mM NaCl, 10 mM NaH_2PO_4 at pH 7.0) Ex. 485 nm. Em. 495-750 nm at 25°C.

The fluorescence quantum yields were significantly lower than those obtained for FIT-PNA. Due to the exceptionally high absorbance of dual labeled PNA probe [10 fold higher than that of PNA **10**, see data in **6.2.2**] **48** was brighter than **10** (a-TO-a). The single stranded PNA **48** gives $\Phi_{em} = 0.007$ and $\Phi_{em} = 0.08$ upon addition of matched DNA **5'TTT**. The mismatched duplexes gives quantum yield ($\Phi_{em} = 0.03$) which is almost equal to single labeled FIT-PNA. The lowest fluorescence enhancement was observed with guanine as TO pairing partner.

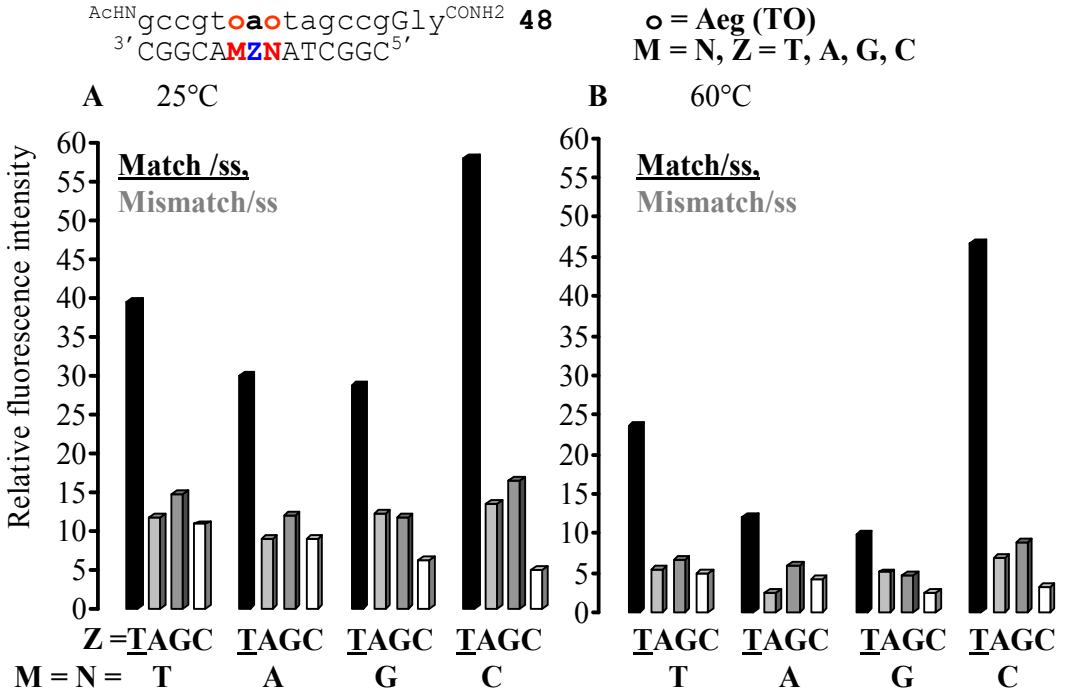

Figure 56: Fluorescence enhancement of PNA probe **48**, varying pairing base (M =N = T, A, G and C) and common stacking base for both TO as a-Z (Z = T, A, G ad C), measured at 530 nm after formation of match duplexes and mismatch duplexes at A) 25°C and B) 60°C. [Measurement conditions: 1 µM probes and DNA (Ex.: 485 nm)].

The highest fluorescence enhancement was found (57.9 fold) on addition of DNA **20'CTC**, in which cytosine was paired against TO. The characteristic of FIT-PNA to show attenuated fluorescence with mismatched DNA was also apparent with 'Dual-FIT-PNA'. The duplexes **48•5'TAT, 48•5'TGT** and **48•5'TCT** containing a-A, a-G and a-C mismatches, respectively give only 9.0, 12.0 and 9.0 fold fluorescence enhancement. Remarkably, the shoulder at 577nm is more pronounced in mismatched duplexes. (Figure 55C and Figure 55D) This shoulder may indicate that the two TO chromophores can contact each other, required that they are spaced by a mismatched

pair. Figure 56 shows graphical presentation of $(TO)_2$-FIT-PNA fluorescence enhancement obtained upon addition of matched and single base mismatched DNA at 25°C and 60°C. Results show that in $(TO)_2$-FIT-PNA highest fluorescence enhancement was found if cytosine is pairing against TO.

7.4 Melting Study

The thermal stabilities measured for duplexes that contained two TO dyes as base surrogates are summarised in Table 13 and 14. The $(TO)_2$-FIT-PNA probe **48** had highest affinity to perfectly matched DNA. Highest stabilities were measured for matched complexes that contained T (T_M = 73°C) or C (T_M = 73°C) as TO pairing partner. The lower T_M = 67°C and T_M = 64°C determined for A and G containing duplexes suggests that accommodation of TO in the duplex is more facile when TO is paired against pyrimidines rather than purines. Hybridisation of **48** was sequence specific. The T_M values of mismatched duplexes were lower by ΔT_M = 4-9°C. However, pairing TO against G in duplexes **48•15'AGZGA** resulted in low match/mismatch discrimination ΔT_M = 1-3°C. The comparison of the sequence specificity of the hybridisation of FIT-PNA **10** with that of Dual-FIT-PNA **48** suggests that two TO dyes can compensate losses of duplex stability imposed by base mismatches.

Table 13: Spectroscopic parameters of dual-labeled-FIT-TO conjugate **48**.

o = Aeg (TO)
Z = T, A, G, C

PNA	λ_{abs}[a] (max)/ nm	ε_{max}[b]/ M^{-1} cm^{-1}	λ_{max}[c] (em)/ nm	Φ_{em}[d]	F_{ds}/F_{ss}[e] 25°C	F_{ds}/F_{ss}[e] 60°C	T_M[f]/ °C
48	512	132600	574	0.007	-	-	-
48•5'TTT	512	164700	535	0.08	39.4	23.5	73
48•5'TAT	512	143600	542	0.03	11.8	5.4	68
48•5'TGT	512	144600	542	0.03	14.7	6.8	69
48•5'TCT	512	146900	538	0.03	10.9	5.0	68

[a] Wavelength of absorbance maximum, [b] extinction coefficient at wavelength of absorbance maximum, [c] wavelength of fluorescence emission maximum, [d] Φ_{em} = fluorescence quantum yield, [e] F_{ds}/F_{ss} = ratio between fluorescence intensities F_{ds} after and F_{ss} before addition of matched and single mismatched DNA at 530 nm. [f] measured as denaturation curves.

Table 14: Spectroscopic parameters of dual-labeled-FIT-TO conjugate **48**.

AdN gccgtoaotagccgGly CONH2 3' CGGCAMZNATCGGC 5'	**48** **5'MZN**	**o = Aeg (TO)** **M=N = A, G, C ; Z = T, A, G, C**		
PNA probe	duplex number	λ_{max} [a] $_{(em)}$/ nm	F_{ds}/F_{ss} [b] 25°C	60°C	T_M [c]/ °C
	48•10'ATA	**538**	**30.0**	**12.0**	**67**
	48•10'AAA	545	9.1	2.6	58
	48•10'AGA	543	12.0	5.9	65
	48•10'ACA	540	9.0	4.3	62
	48•15'GTG	**537**	**28.8**	**9.8**	**64**
48, o-a-**o**,	48•15'GAG	542	12.4	5.1	62
	48•15'GGG	542	11.8	4.6	63
	48•15'GCG	541	6.4	2.6	61
	48•20'CTC	**533**	**57.9**	**46.7**	**73**
	48•20'CAC	543	13.6	6.9	66
	48•20'CGC	542	16.6	9.0	66
	48•20'CCC	545	5.0	3.2	65

[a] Wavelength of fluorescence emission maximum, [b] ratio between fluorescence intensities F_{ds} after and F_{ss} before addition of matched and single mismatched DNA at 530 nm. [c] measured as denaturation curves.

7.5 Conclusions

The fluorescence enhancement obtained upon hybridisation of Dual-FIT-PNA is higher than that of FIT-PNA. Highest fluorescence increases were obtained upon pairing of TO against pyrimidines. The shape of UV absorbance spectrum of ss $(TO)_2$-PNA complex is similar to the shape of absorbance spectrum of TOTO complexed to ssDNA. The T_M measurements showed that two TO chromophores reduce the specificity of hybridisation.

8. Forced intercalation of pyridine benzothiazole for homogeneous detection of single base mutation in DNA

The previous sections have revealed that TO as base surrogate in PNA can signal hybridisation. The collected data indicated that TO responds to changes of its environment within the formed duplex. For example the fluorescence of mismatched probe-target complexes was lower than the fluorescence of matched ones. This property is of interest in mutational analysis. Better typing of single nucleotide polymorphisms should be achievable when using an additional colour, one that is specific for the wild type sequence and one that calls for the mutant.

The TOTO-family of dyes is comprised of benzo- or pyridino-annulated oxazoles and thiazoles linked via methine bridges to pyridinium or quinolium groups.[94, 95, 107, 108] I chose to explore the utility of the BO dye in which the quinolium ring of TO is replaced by a pyridinium ring.

8.1 Synthesis

The pyridine benzothiazole (BO) was synthesized by using literature procedure.[109, 110, 111] The incorporation of BO as base surrogate into PNA was performed by means of divergent solid phase synthesis (Scheme 20). Pyridine benzothiazole (BO) was linked to the PNA backbone *via* a carboxymethylene spacer in order to mimic the linker length of FIT-PNA **10** (Scheme 20). The coupling of BO-CH_2-COOH was carried out using PyBOP and NMM in DMF. The BO derivative is clearly soluble in DMF, hence, no additional PPTS was required. RP-HPLC, MALDI-TOF-MS, UV/ VIS confirmed the purity and molecular mass of **49** and the integrity of the chromophore.

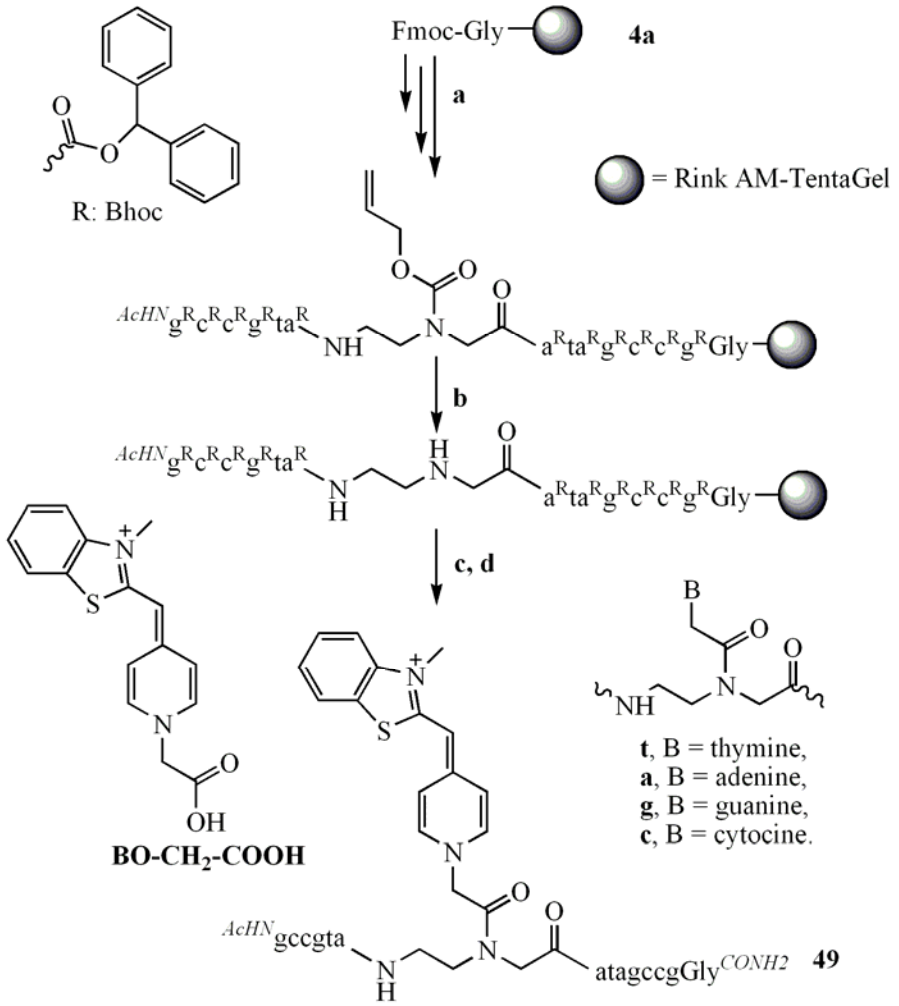

Scheme 20: a) Cycle of 1) piperidine/ DMF; 2) Fmoc–B (Bhoc)–OH or Fmoc-Aeg (Alloc)-OH, NMM, PyBop, NMP; 3) Ac_2O/ lutidine, DMF; b) [Pd $(PPh_3)_4$], $Me_2NH{\cdot}BH_3$, CH_2Cl_2; c) BO-CH_2-COOH, PyBOP, NMM, DMF (double coupling); d) TFA, m-cresol, H_2O, L-Cys-OMe, 11.4 % overall yield.

8.2 Results and Discussion

The BO probe **49** was hybridised with oligonucleotides **5'-8'** (**MZT**), where **Z** is the pairing partner for BO and M is the pairing partner for the TO neighbour adenine. Z and M was varied by all possible DNA nucleobases giving rise to 4 matched and 12 mismatched duplexes. Hybridisation of the PNA-BO conjugate **49** was performed in buffer (100 mM NaCl and 10 mM NaH_2PO_4 adjusted to pH 7.0) and the stability of each of these BO-PNA•DNA complexes was evaluated by thermal denaturation experiments using absorbance spectroscopy. The fluorescence at three different temperatures (25°C, 50°C and 60°C) was measured before and after addition of matched and mismatched oligonucleotides (**5'-8' MZT**).

8.2.1 Fluorescence Study

Figure 57 shows the increase in BO emission of probe **49** in response to addition of oligonucleotides **5'-8' MTT,** (M = T, A, G and C) at different temperatures (25°C, 50°C and 60°C). It became apparent that the formation of matched duplexes was accompanied by a shift of the emission maximum from 488 nm to 486-487 nm. The mismatched duplex formation gives either smaller hypsochromic shift or 1-2 nm bathochromic shift (Table 15). The probe **49** gives 6.3 fold fluorescence enhancement at 480 nm upon addition of DNA **5'TTT**, where thymine act as pairing partner for BO and two a-T base pairs as stacking partners. This is significantly lower than the 23.8 fold fluorescence enhancement observed upon hybridization of TO-PNA **10**.

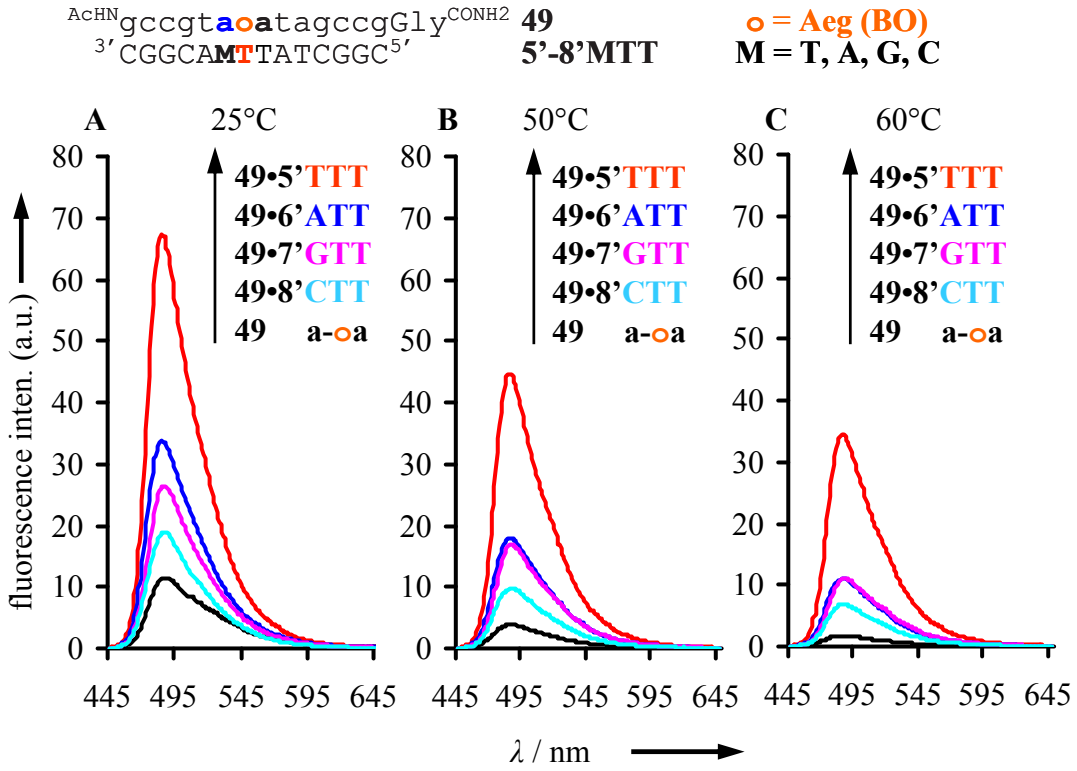

Figure 57: Fluorescence emission spectra of BO-PNA conjugates **49** before (black) and after addition of equimolar amount of DNA **5'TTT** = (red), **6'ATT** = (blue), **7'GTT** = (pink) and **8'CTT** = (turquoise) A) 25°C B) 50°C and C) 60°C. [Measurement conditions: 1 µM FIT-PNA and 1 µM DNA (added after measurement of single strand PNA) in degassed buffer (100 mM NaCl, 10 mM NaH_2PO_4 at pH 7.0, at 25°C). Ex. 435 nm. Em. 445-650 nm. Ex. Slit: 5 nm, Em. Slit: 2.5 nm.

Fluorescence enhancements improved when hybridisation was performed at elevated temperature. At 50°C fluorescence of BO-PNA **49** complexed to **5'TTT** was

11.3 fold more intense than fluorescence of single strand **49**. The fluorescence enhancement was even higher (18.8 fold) at 60°C (Figure 57C). The results from section 2 and 3 suggested that the temperature dependence of fluorescence of single stranded probes is higher than the temperature dependence of duplexes. The behaviour is also seen with BO-PNA **49**. For example, probe **49** gives 9.4 (a.u.) at 25°C, 3.4 (a.u.) at 50°C and 1.6 (a.u.) at 60°C. The fluorescence of single strand probe **49** decreases by 6 fold where as fluorescence of double strand **49•5'TTT** decreases only 3 fold. Different observations were made for mismatched duplexes. Here fluorescence decreased as rapidly with increasing temperature as single strands. The higher hybridisation-induced fluorescence enhancement and the better match/mismatch discrimination at elevated temperature is an advantage for mutational analysis by real time PCR. Figure 58 is a bar presentation of fluorescence enhancement of probe **49**, upon addition of varying pairing partner and N'-side mismatched stacking bases.

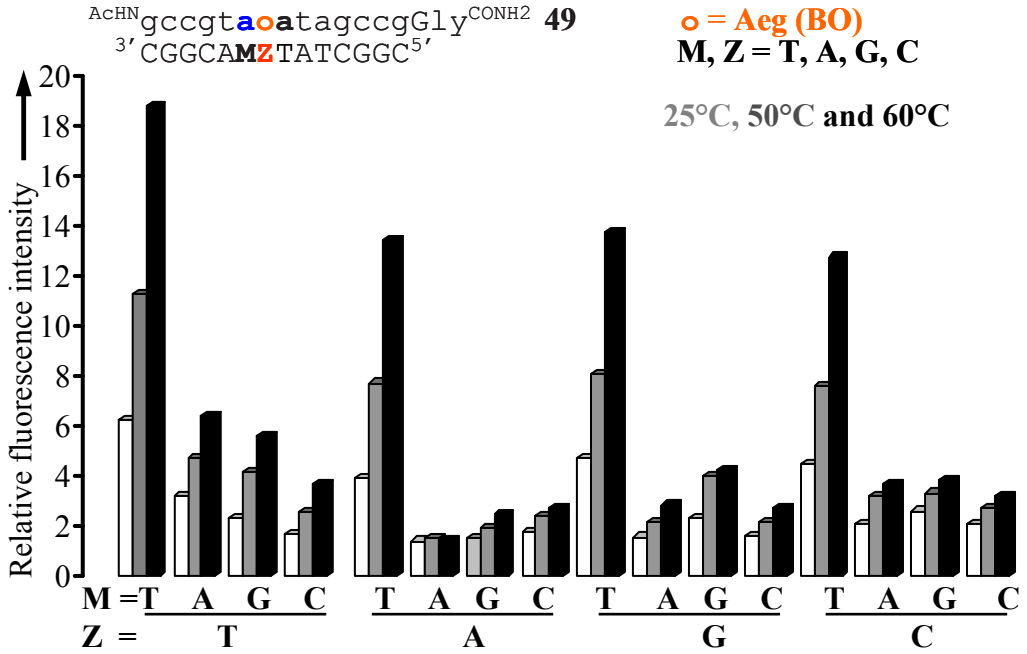

Figure 58: Fluorescence enhancement of PNA probe **49**, varying pairing base (Z = T, A, G and C) and N'-side adjacent stacking bases (M = T, A, G ad C), measured at 480 nm at 25°C (white columns), 50°C (grey columns), and 60°C (black columns). Measurement conditions: see caption of Figure 57.

The left, middle and right columns shows florescence enhancement at 25°C, 50°C and 60°C respectively. The BO-PNA conjugates gives 13.4, 13.8 and 12.8 fold fluorescence enhancement upon addition of matched DNA **5'TAT, 5'TGT** and

5'TCT (A, G and C as pairing partner for BO) respectively. The mismatched fluorescence for adenine as mismatched base at 60°C gives 1.5, 2.8 and 3.6 fold fluorescence when A, G and C was pairing bases for BO respectively. The attenuation of fluorescence in response to mismatched hybridisation suggests that the pyridine based BO derivative may also be useful in the mutational analysis of DNA.

8.2.2 Absorbance Study

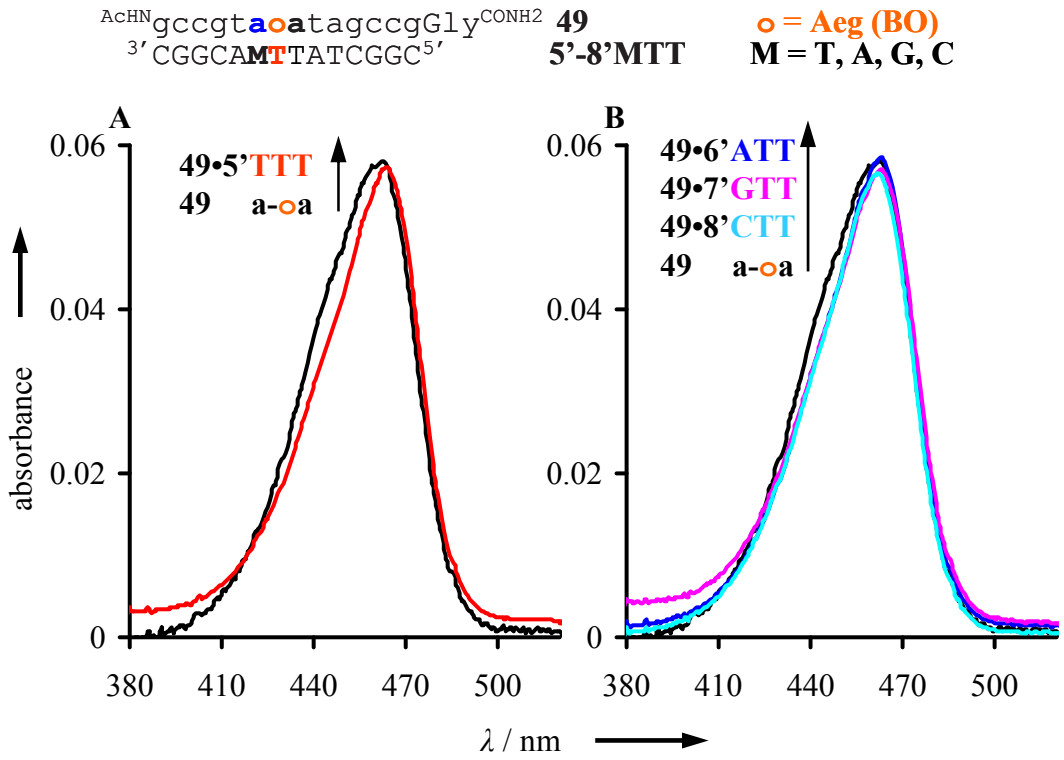

Figure 59: Absorbance spectra of BO-conjugate **49** before (black) and after addition of equimolar amount of DNA, A) matched DNA **5'TTT** (red), B) mismatched DNA **6'TTT** (blue), **7'GTT** (pink) and **8'CTT** (turquoise). [Measurement conditions: 1 µM BO-PNA and 1 µM DNA (added after measurement of single strand PNA) in degassed buffer (100 mM NaCl, 10 mM NaH_2PO_4 at pH 7.0)] at 25°C.

Figure 59 shows the absorption spectra of BO-PNA conjugate **49** in aqueous buffer at 1.0 µM concentration before and after addition of equimolar amount of corresponding matched (**5'TTT**) and single base mismatched (**6'ATT, 7'GTT** and **8'CTT**) DNA. The single stranded BO-PNA shows a broad band in the visible region with a peak at 462 nm. As matched DNA **5'TTT** is added the absorption band at 462 nm gives 1 nm bathochromic shift. Due to interaction with pairing and stacking

base, the absorbance at blue side decreased while absorbance at red side of visible spectrum is increased. The addition of mismatched DNA **6'ATT, 7'GTT** and **8'CTT** also gives smaller spectral shift towards longer wavelength. The absorbance at 462 nm decreases. The absorbance at blue side decreased while no considerable change found at red side of spectra. However, in this case, the bathochromic shift was smaller (1 nm), the absorbance maximum at 462 nm was more pronounced.

8.2.3 Melting Study

Table 15: Spectroscopic parameters of BO-PNA conjugate **49** after addition of DNA (**5'-8'MZT**).

o = Aeg (BO)
Z, M = T, A, G, C

PNA probe	duplex number	λ_{max}[a] $_{(em)}$/ nm	F_{ds}/F_{ss}[b] 25°C	50°C	60°C	T_M[c]/ °C	ΔT_M[d]/°C
	49•5'TTT	**486**	**6.3**	**11.3**	**18.3**	**73**	
	49•6'ATT	485	3.2	4.7	6.4	68	
	49•7'GTT	488	2.3	4.1	5.6	67	ΔT_M = 5-6
	49•8'CTT	488	1.7	2.6	3.6	67	
	49•5'TAT	**487**	**3.9**	**7.7**	**13.4**	**71**	
	49•6'AAT	488	1.4	1.5	1.5	66	
49,	49•7'GAT	488	1.5	1.9	2.5	65	ΔT_M = 5-6
a-BO-a	49•8'CAT	488	1.8	2.4	2.7	65	
	49•5'TGT	**487**	**4.7**	**8.1**	**13.8**	**70**	
	49•6'AGT	487	1.6	2.2	2.8	64	
	49•7'GGT	488	2.3	4.0	4.2	64	ΔT_M = 6-7
	49•8'CGT	488	1.6	2.2	2.7	63	
	49•5'TCT	**487**	**4.4**	**7.6**	**12.8**	**74**	
	49•6'ACT	490	2.1	3.2	3.6	65	
	49•7'GCT	489	2.6	3.3	3.8	63	ΔT_M = 9-11
	49•8'CCT	490	2.1	2.7	3.2	63	

[a] Wavelength of fluorescence emission maximum, [b] F_{ds}/F_{ss} = ratio between fluorescence intensities of BO-PNA after and before addition of matched and single base mismatched DNA at 580 nm. [c] measured as denaturation curves. [d] melting temperature difference between matched and mismatched duplex. (Measurement conditions: see caption of Table 2 and Figure 57).

The BO-PNA probe **49** containing pyridine-linked at an internal position was hybridised to oligodeoxynucleotides **5'-8'MZT** (Table 15). The melting curves showed sigmoidal behaviour in all cases which indicates co-operative base pairing. In BO-PNA•DNA duplexes **49•5'TZT**, BO was paired against each of the four natural DNA bases. Melting analysis suggested that each of the four nucleobases was tolerated by BO (Table 15). The T_M values were within a range of 4°C and amounted

to 72°C on average. Most interestingly, a comparison with the T_M = 73°C provided by duplex **49•5'TTT** and T_M = 74°C by duplex **49•5'TCT** revealed that the BO binding to pyrimidine provides higher stability than pairing of BO with purine bases duplexes **49•5'TAT** and **49•5'TGT**. The average decreased T_M values (ΔT_M = 6, 7 and 7°C, respectively) observed with duplexes **49•6'AZT**, **49•7'GZT** and **49•6'CZT** containing adenine, guanine and cytosine as mismatched stacking base adjacent to BO revealed that probe hybridisation was sequence selective.

8.3 Conclusions

The above study reveals that hybridisation-induced enhancements of BO fluorescence are not as high as that of TO. However, useful 13-18 fold fluorescence enhancements were obtained at temperature in the range of PCR applications. Additionally, the melting study showed that matched duplexes melt at higher temperature than corresponding single base mismatched duplexes. The responsiveness of BO fluorescence to a neighbouring base mismatch at high temperature is as high as or even slightly higher than that of the TO derivative. This suggests that it might be possible to distinguish a DNA target from its single base mutant by using BO-labeled FIT-PNA.

9. Comparison of "FIT-PNA" containing TO attached over aminoethylglycine, L-ornithine, and D-ornithine in homogeneous detection of DNA corresponding to roX RNA.

The non coding RNA roX 1 and roX 2 from Drosophila participate in the modification of histone structure required in males to up-regulate transcription of the male X chromosome. Probes directed against roX RNA could give information about cellular localisation of roX RNA and its timing of expression. In this chapter FIT-PNA was evaluated for its ability to detect roX sequences, however, with DNA as first target. The previous section (3) suggested that contained TO attached to ornithine provides for strong fluorescence enhancement than PNA featuring TO attached to aminoethyglycine. In this section Aeg, D-Orn and L-Orn containing FIT-PNA is compared.

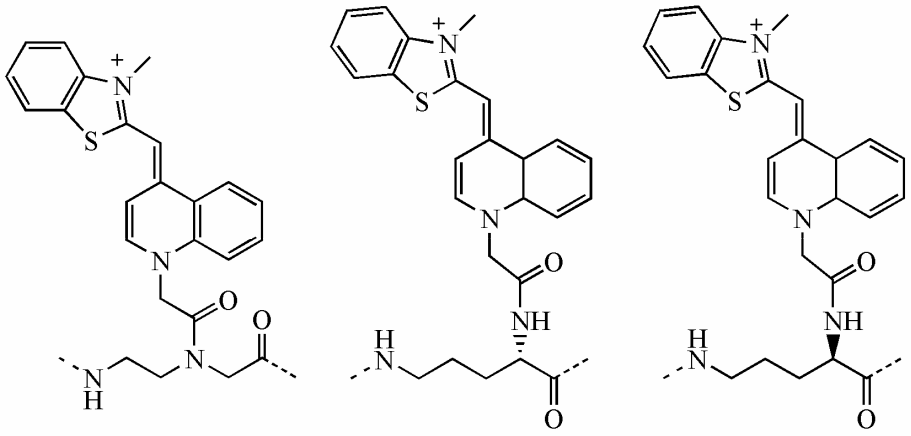

Scheme 21: Chemical structure of TO derivatives with three different backbones.

9.1 Results and Discussion

Probes **50-52** were hybridised with DNA **56'-57'** and probes **53-55** were hybridised with DNA **58'-59'**. The former probe set will form duplexes with DNA **56'** in which TO will be embedded between a-T and t-A base pairs and paired against

T. Probes **53-55** will form duplexes with DNA **58'** featuring TO in between c-G and a-T and again, paired against thymine (Scheme 22).

o = Aeg (TO), **50**; L-Orn (TO), **51**; D-Orn (TO), **52**.	
FIT-PNA	**50-52**, ^{ACHN}ttcgtatoacatttcLys^{CONH2}
matched DNA	**56'**, $^{3'}$TCAAAGCAA**T**TGTAAAGTGA$^{5'}$
mismatched DNA	**57'**, $^{3'}$AAGCATA**TC**GTAAAG$^{5'}$
o = Aeg (TO), **53**; L-Orn (TO), **54**; D-Orn (TO), **55**.	
FIT-PNA	**53-55**, ^{ACHN}aacaccoatttacLys^{CONH2}
matched DNA	**58'**, $^{3'}$ACATTGTGG**T**TAAATGGGA$^{5'}$
mismatched DNA	**59'**, $^{3'}$TTGTGG**TC**AAATG$^{5'}$

Scheme 22: Studied nucleic acids and FIT-PNA conjugates.

9.1.1 Fluorescence study

Figure 60 shows the fluorescence emission of single stranded labeled PNA **50-52** before and after addition of matched DNA **56'TT** and single base mismatched DNA **57'TC**. Probe **50** gives 9.8 fold fluorescence enhancement at 530 nm upon addition of DNA **56'TT**. Higher fluorescence enhancement was found (12.3 fold) on addition of DNA **56'TT** to L-Orn-TO probe **51**, while probe **52** gives only 8.2 fold fluorescence enhancement with matched DNA. The characteristics of FIT-PNA to show attenuated fluorescence with mismatched DNA **57'TC** was again observed. The duplex **50•57'TC, 51•57'TC** and **52•57'TC** give 2.6, 1.4 and 1.3 fold fluorescence enhancement, respectively. The experiments reveal that, L-Orn provided the highest fluorescence emission as well as the best match/mismatch discrimination. These results confirm data discussed in previous sections 2 and 3 in that TO attached to D-ornithine provides for stronger fluorescence enhancement than PNA featuring TO attached to aminoethyglycine. Interestingly, in this section TO attached to L-Ornithine shows even better fluorescence properties than D-ornithine.

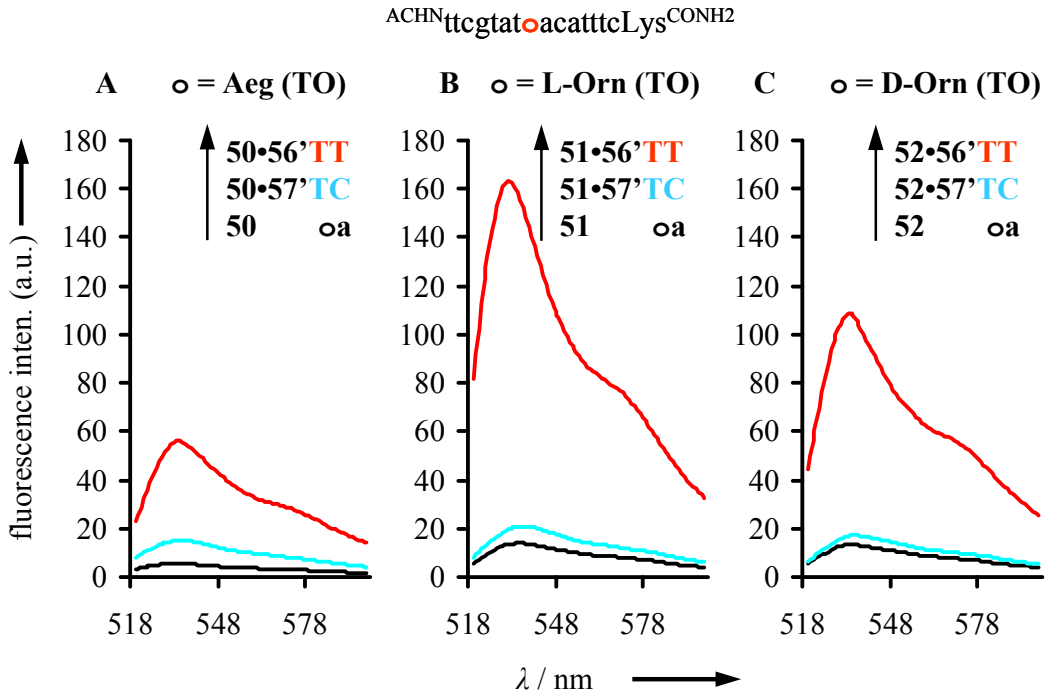

Figure 60: Fluorescence emission spectra of FIT-PNA before (black), after addition of equimolar amount of matched DNA (red) and mismatched DNA (turquoise). A) Aeg (TO) (**50oa, 50oa•56'TT, 50oa•57'TC**), B) L-Orn (TO) (**51oa, 51oa•56'TT, 51oa•57'TC**) and, C) D-Orn (TO) (**52oa, 52oa•56'TT, 52oa•57'TC**), at 25°C. Measurement conditions: see caption of Figure 47.

Figure 61 shows the fluorescence emission of FIT-PNA **53-55** before and after addition of matched DNA **58'TT** and single base mismatched DNA **59'TC**. The probe **53** gives 8.7 fold fluorescence enhancement at 530 nm upon addition of DNA **58'TT**. The probe **54** (L-Orn-TO), gives only 2.7 fold fluorescence enhancement and only 2 fold was recorded for probe **55** (D-Orn-TO) with matched DNA **58'TT**. In terms of high fluorescence with matched DNA, probe **53** gives advantages when compared to L- and D-Orn-TO-PNA probes. Interestingly, fluorescence of L-Orn and D-Orn FIT-PNA is decreased upon addition of mismatched DNA **57'**, while fluorescence of Aeg•FIT-PNA **53** experienced 2 fold fluorescence enhancement of PNA. Hence, highest 7.2 fold match/mismatch discrimination was again found for L-Orn•FIT-PNA

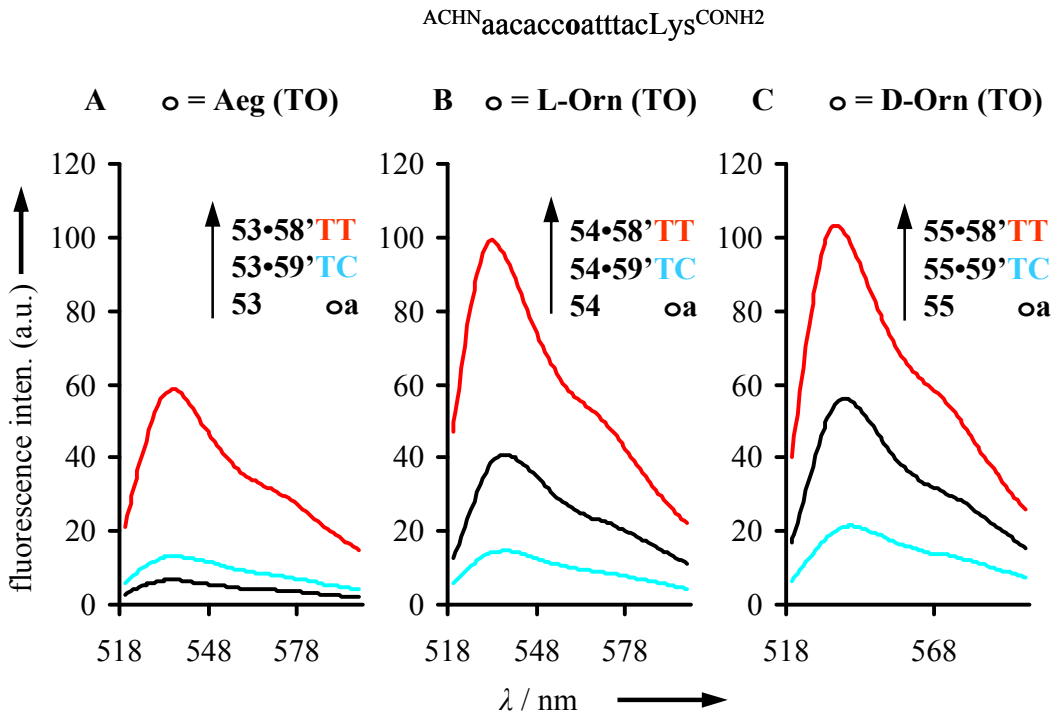

Figure 61: Fluorescence emission spectra of FIT-PNA before (black), after addition of equimolar amount of matched DNA (red) and mismatched DNA (turquoise). A) Aeg (TO) (**53oa, 53oa•58'TT, 53oa•59'TC**), B) L-Orn (TO) (**54oa, 54oa•58'TT, 54oa•59'TC**), C) D-Orn (TO) (**55oa, 55oa•58'TT, 55oa•59'TC**), Measurement conditions: at 25°C. Measurement conditions: see caption of Figure 47.

9.1.2 Fluorescence versus temperature study

The previous FIT-PNA studies revealed that the fluorescence emission and match/mismatch discrimination is dependent on temperature. Figure 62A-C shows the fluorescence emission of single stranded PNA **50-52** before and after addition of matched DNA **56'TT** and single base mismatched DNA **57'TC**. Figure 62E-G shows the fluorescence enhancement of single stranded PNA **50-52** before and after addition of matched DNA **56'TT**, single base mismatched DNA **57'TC** and match/mismatch discrimination obtained from Figure 62A-C respectively over the range of 25-85°C.

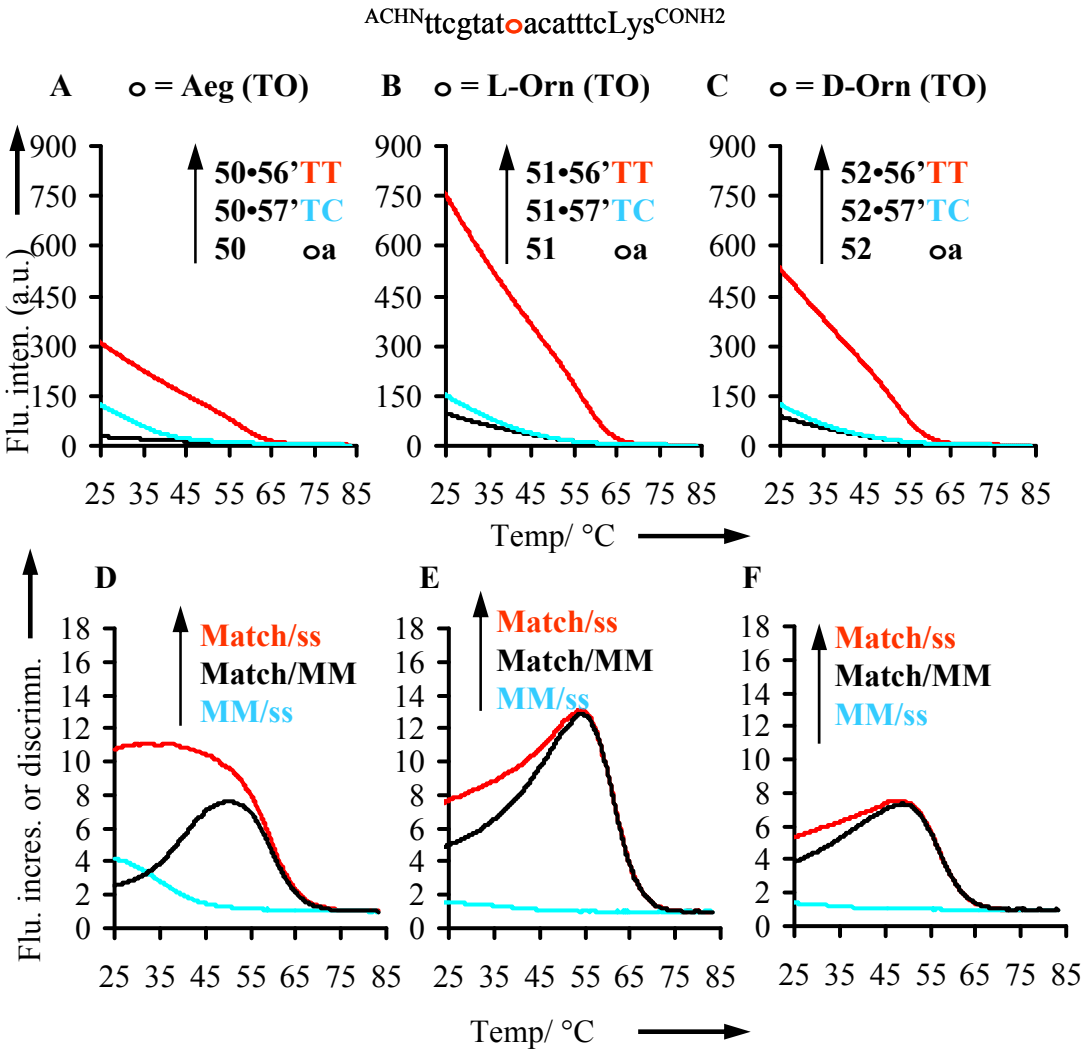

Figure 62: Fluorescence emission of FIT-PNA plotted against temperature before (black), after addition of equimolar amount of matched DNA (red) and mismatched DNA (turquoise). A) Aeg (TO) (**50oa, 50oa•56'TT, 53oa•58'TC**), B) L-Orn (TO) **(51oa, 51oa•56'TT, 51oa•57'TC**) C) D-Orn (TO) (**52oa, 52oa•56'TT, 52oa•57'TC**), and fluorescence increase after addition of equimolar amount of matched DNA (red) and mismatched DNA (turquoise) and fluorescence match/mismatch discrimination (black). D) Aeg (TO), E) L-Orn (TO) F) D-Orn (TO). [Measurement conditions: 1 µM FIT-PNA or 1 µM FIT-PNA•DNA duplex in degassed buffer (100 mM NaCl, 10 mM NaH_2PO_4 at pH 7.0, Ex. 510 nm, Em. 530 nm, rate of heating 1°C/min.)].

The fluorescence emission of FIT-PNA, its matched and mismatched duplexes decreases upon increase in temperature. This is not surprising, as this is the characteristic of thiazole orange itself. It is however, important to note that fluorescence of matched duplexes is always higher than fluorescence of mismatched duplexes. Match/mismatch discrimination is increasing upon increase in temperature. For example, probe **50** gives 10.9 fold fluorescence enhancement at 25°C upon

addition of matched DNA **56'TT** and 4 fold for mismatched DNA **57'TC**. Increases of temperature from 25°C to 52°C improve the match/mismatch discrimination from 2.7 fold to 7.8 fold (Figure 62D). It is important to note that highest fluorescence match/mismatch discrimination (12.5 fold) was found at 55°C for probe **51** (L-Orn (TO)-PNA). For D-Orn (TO) (**52**) 7 fold match/mismatch fluorescence discrimination was recorded at 51°C.

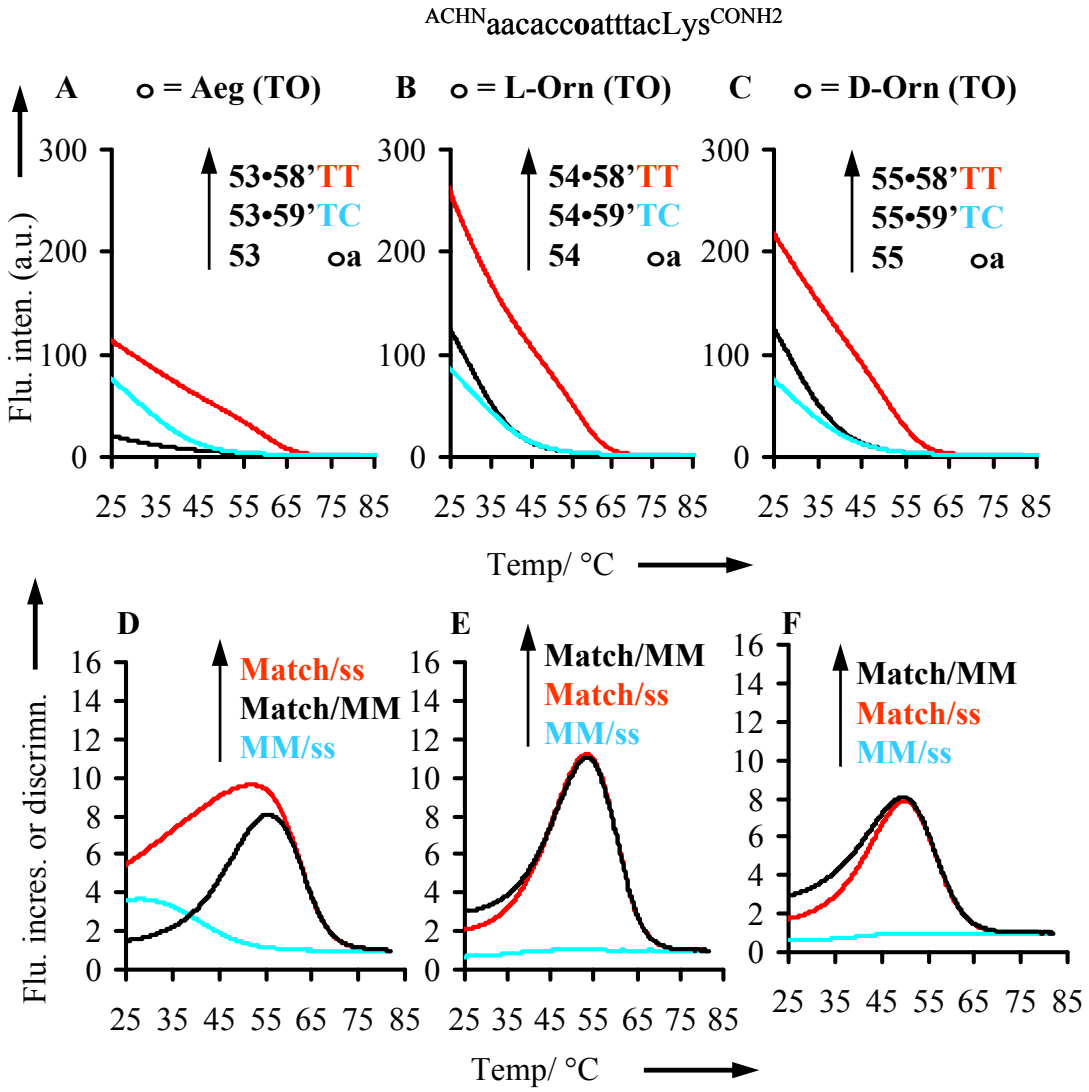

Figure 63: Fluorescence emission of FIT-PNA plotted against temperature before (black), after addition of equimolar amount of matched DNA (red) and mismatched DNA (turquoise). A) Aeg (TO) (**53oa**, **53oa•58'TT, 53oa•59'TC**), B) L-Orn (TO) (**54oa, 54oa•58'TT, 54oa•59'TC**) C) D-Orn (TO) (**55oa, 55oa•58'TT, 55oa•59'TC**), and fluorescence increase after addition of equimolar amount of matched DNA (red), and mismatched DNA (turquoise) and fluorescence match/mismatch discrimination (black). D) Aeg (TO), E) L-Orn (TO) F) D-Orn (TO). [Measurement conditions: see caption of Figure 62].

Figure 63A-C shows the fluorescence emission of single stranded PNA **53-55** before and after addition of matched DNA **58'TT** and single base mismatched DNA **59'TC**. Figure 63E-G shows the corresponding fluorescence enhancements obtained upon hybridisation with matched DNA **58'TT** and single base mismatched DNA **59'TC** as well as match/mismatch discrimination over the range of 25-85°C. Probe **53** gives 4 fold fluorescence enhancement at 25°C upon addition of matched DNA **58'TT** and 1.8 fold for mismatched DNA **59'TC**. Upon increasing in temperature the discrimination increases, at 25°C the probe **53** gives 1.5 fold match/mismatch discrimination and at 56°C it is 8.1 fold (Figure 63D). High fluorescence match/mismatch discrimination (10.9 fold) was found at 55°C for probe **54** L-Orn (TO). This temperature study also revealed that matched hybridisation of L-Orn-FIT-PNA **55** is accompanied by significantly higher fluorescence enhancement, when performed at 55°C (10.7 fold) rather than 25°C (2.1 fold). Apparently, temperature dependence of single strand fluorescence is higher than that of the double strand.

9.1.3 Duplex stability

Table 16: T_M data of thiazole orange containing PNA•DNA duplexes.

^{ACHN}ttcgtat**o**acatttcLys^{CONH2}			
T_M/ °C[a]	o = Aeg (TO) **50**	o = L-Orn (TO) **51**	o = D-Orn (TO) **52**
Match duplex	59	59	55
Mismatch duplex	36	37	35
ΔT_M	23	22	20
^{ACHN}aacacc**o**atttacLys^{CONH2}			
T_M/ °C[a]	o = Aeg (TO) **53**	o = L-Orn (TO) **54**	o = D-Orn (TO) **55**
Match duplex	61	57	54
Mismatch duplex	38	36	36
ΔT_M	23	21	18

[a] Measured as denaturation curves at 1 µM concentration in a buffered solution (100 mM NaCl, 10 mM NaH_2PO_4, pH = 7).

The FIT-PNA probes **50-55** containing TO linked to varying backbones was hybridised to corresponding oligodeoxynucleotides **56'-59'** (Table 16). The melting curves showed sigmoidal behaviour in all cases which indicates co-operative base

pairing. The introduction of D-Orn into PNA resulted in destabilisation of duplexes by ΔT_M = 4-7°C when compared to Aeg (TO)-PNA. Aeg-PNA provided an average the highest stability of matched duplexes which can be explained by its resemblance of the ‘’natural’’ backbone. Interestingly, aminoethylglycine also provided the highest hybridisation selectivity as evidenced by large ΔT_M upon mismatched hybridisation.

9.2 Conclusions

The study of three TO-backbones revealed that L-Orn gives highest fluorescence emission as well as best match/mismatch discrimination compared to Aeg (TO) and D-Orn (TO) when performed at elevated temperature. The melting analysis showed that duplexes containing Aeg (TO) have higher duplex stability than L or D-Orn.

10. Summary of the work

Intercalator dyes such as thiazole orange have been linked into PNA by replacing an internal nucleobase. In these conjugates (Figure 64) the DNA stain thiazole orange (TO) was forced to intercalate next to mismatched base pairs in a PNA•DNA duplex. These conjugates were named as FIT (*F*orced *I*ntercalation of *T*hiazole orange) probes.

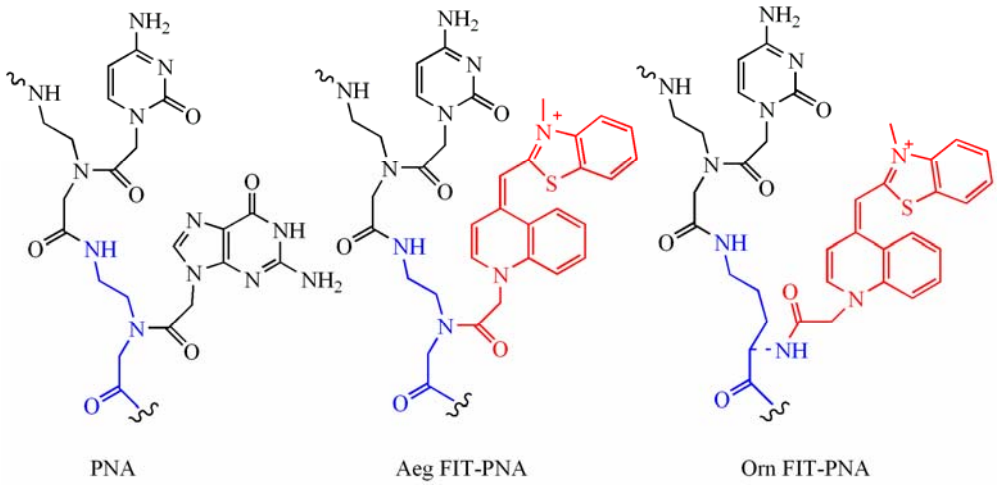

Figure 64: Single strand of PNA (left), Aeg-FIT-PNA (middle), and Orn-FIT-PNA (right).

10.1 Synthesis

This work was first concerned with the development of a linear strategy for the solid-phase synthesis of FIT-PNA. Towards this end a new thiazole orange containing monomer building block had to be prepared. The new building blocks Fmoc-Aeg (TO)-OH and the backbone-modified Fmoc-L- or D-Orn (TO)-OH building blocks were synthesised by coupling thiazole orange carboxylic acid to the Fmoc/Allyl-protected building blocks **2b** and **22b**. Subsequent Pd (0)-catalysed cleavage of the allyl group furnished the desired TO-building blocks **3b** and **24b** in 73 and 65 % yield. (Scheme 23). The new monomers were used in the linear solid-phase synthesis of FIT-PNA oligomers. For example, the synthesis of TO-containing probes such as **13-20** or **33-40**. A fully protected PNA resin was assembled (Scheme 24). Building blocks **3b** and **24b** were used in the subsequent coupling. The challenging coupling was achieved by using PPTS as additive, which enhances the solubility of TO-containing monomers. After the incorporation of the critical building block linear assembly of the PNA-oligomer was completed.

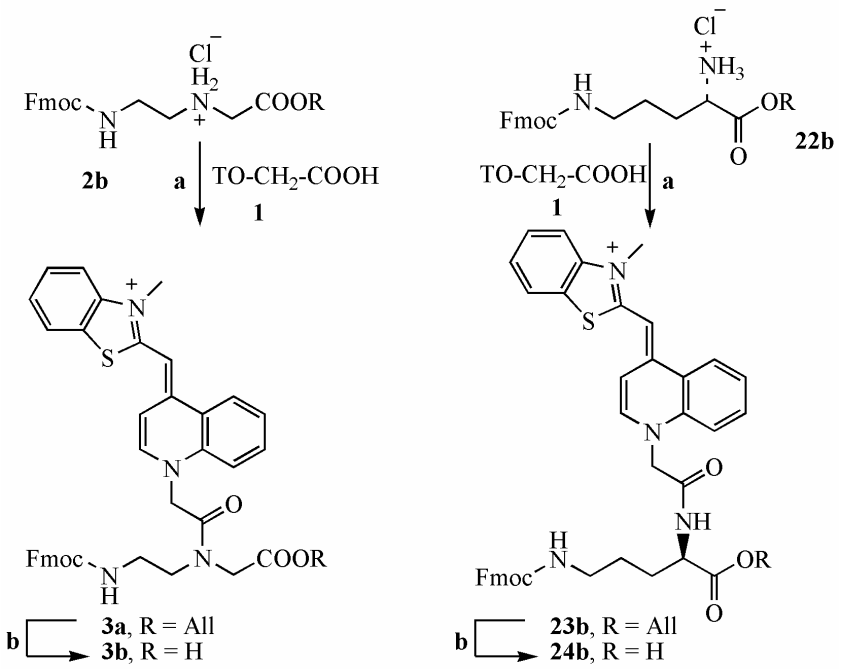

Scheme 23: a) TO-CH_2-COOH (**1**), **2b** or **22b**, PyBOP, PPTS, NMM, DMF; b) [Pd (PPh_3)$_4$], $PhNHCH_3$, THF.

The desired TO-PNA conjugates were detached from the soild phase by treatment with TFA. The purity of the crude products was higher than the purity of crude products obtained by divergent solid phase synthesis. By using this protocol **13-20** and **33-40** different TO-containing PNA-oligomers have been synthesized in 9.4-7.8 % overall yield.

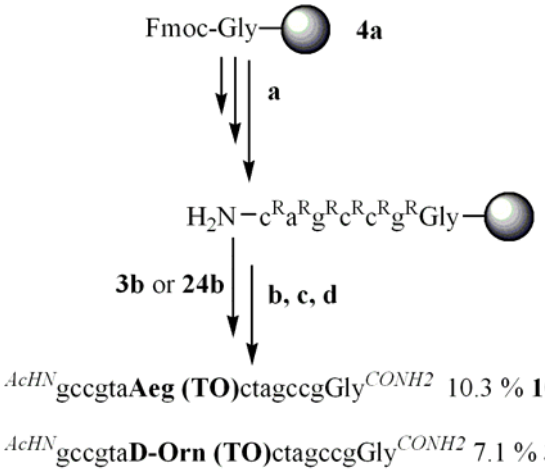

Scheme 24: Linear route for PNA synthesis: a) and c) Cycle of 1) piperidine/ DMF; 2) Fmoc-B (Bhoc)-OH, NMM, PyBop, DMF; 3) Ac_2O/ pyridine, DMF; b) Cycle of 1) piperidine/ DMF; 2) Fmoc-Aeg (TO)-OH, **3b** or Fmoc-D-Orn (TO)-OH, **24b** NMM, PyBop, PPTS, DMF; 3) Ac_2O/ pyridine, DMF; d) TFA, m-cresol, H_2O, L-Cys-OMe.

10.2 Next neighbour influence

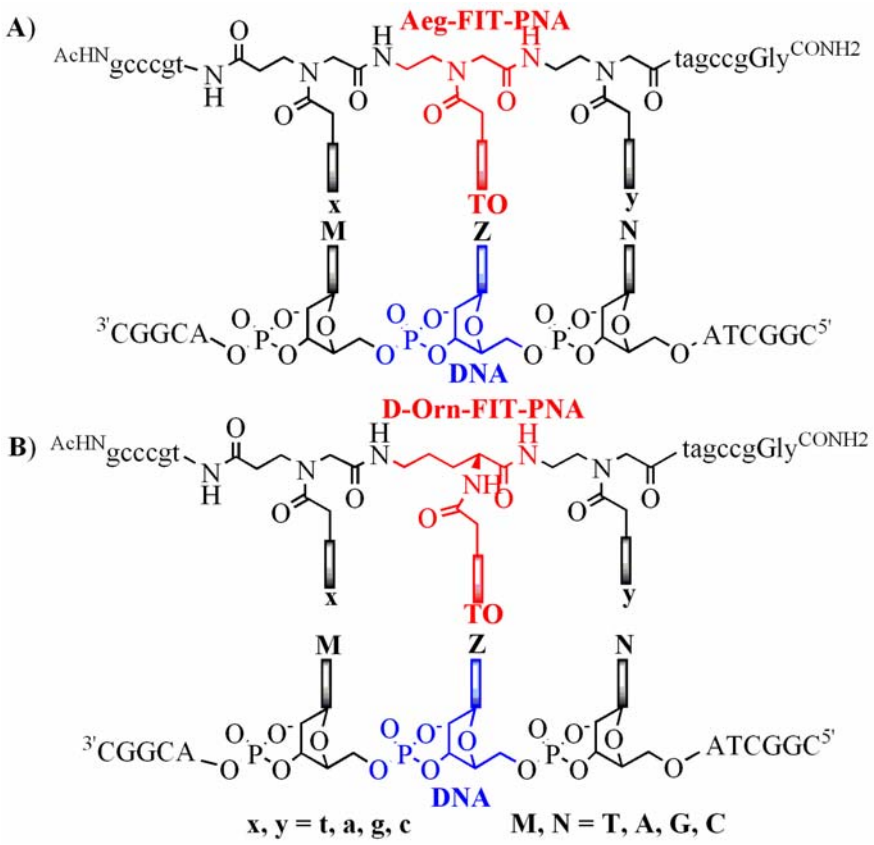

Figure 65: Studied libraries of A) Aeg-FIT-PNA and B) D-Orn-FIT-PNA, with matched and single base mismatched target DNA.

To explore the influence of thiazole orange stacking and pairing partners on stability and optical properties of duplexes the N'-terminal (x) and C'-terminal (y) bases of thiazole orange environment were varied (Figure 65) for both Aeg-TO and D-Orn-TO containing oligomers. Sixteen different probes were hybridised to oligonucleotides **5'-20'MZN** such that TO was paired against base Z of the target strand and flanked by each possible base pair.

Thermal stability

Melting curves analysis showed that GC rich TO next neighbors (T_M = 77°C) provided for higher duplex stability than AT rich stacking environments where TO was embedded between two thymines, two adenines or one adenine and thymine (T_M = 69-73°C). Importantly, mismatched duplexes always showed lower stability than matched duplexes. The data from independent section **2.4** revealed that hybridisation of FIT-PNA is without any exception sequence selective. Melting

analysis also showed that each of the four canonical nucleobases A, C, G and T was tolerated well opposite to TO. An interesting observation was made when TO was paired against an abasic site. The thermal stability was higher by $\Delta T_M = 3°C$ when compared to a duplex that contained TO paired against T. This suggests that intercalation of the TO chromophore is even more facile when the steric demand exerted by an opposing base is reduced. The removal of a nucleobase adjacent to intercalated TO lowered the duplex stability by 9°C due to a lack of stacking interactions.

Absorbance study

In single stranded FIT-PNAs, ε_{max} varied in between 16100-59300 $M^{-1}cm^{-1}$ (Figure 66). Double strand formation led to increases in ε_{max} by 22-53 %. The marked nearest-neighbor dependence of TO absorbance in single stranded and double stranded FIT-PNA is without precedence. For comparison binding of the free dye TO-PRO 1 to DNA•DNA and PNA•DNA was studied. Association to double strands resulted in 23 and 33 % of decrease of $\varepsilon_{max,}$ respectively.

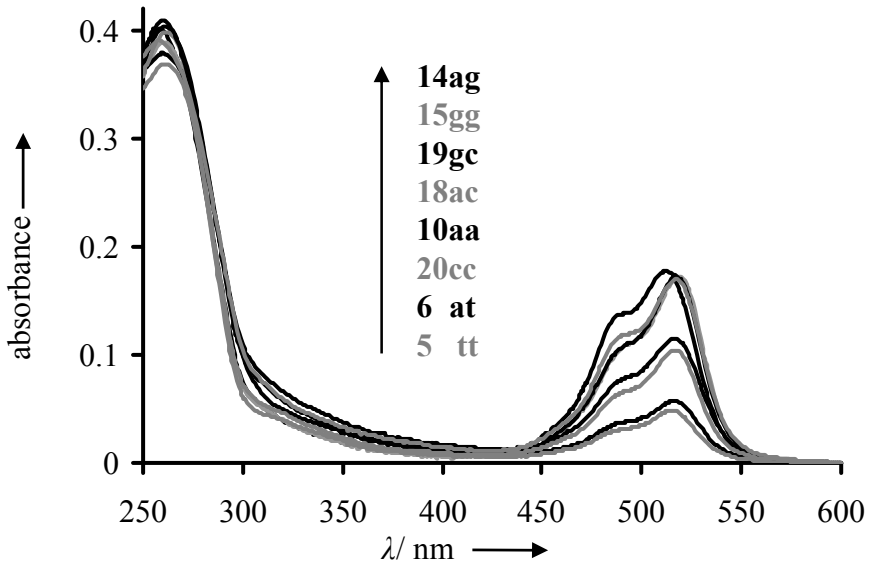

Figure 66: Absorbance spectra of single stranded PNA-TO conjugates (**5-20xy**). The absorbance at 600 nm was set to zero and the absorbance curves were calibrated to the calculated ε_{260}.

Fluorescence study

Figure 67 shows the fluorescence enhancement of Aeg-TO-PNA (gray bar) and D-Orn-TO-PNA (black bar) conjugates after formation of matched duplexes with complementary oligonucleotides in which TO was paired against all DNA bases. The results are summarized in table format.

o = Aeg/D-Orn (TO), x; y = t, a, g and c
M, Z, N = T, A, G and C

x	Z	y	$(F_{ds\ (match)}/\ F_{ss})^a$
a	**T**	a	29 / 24
a	**T**	c	32 / 20
t	**T**	a	20 / 19
t	**T**	t	19 / 16
a	**T**	g	16 / 16
a	**T**	t	27 / 14
g	**T**	a	22 / 13
a	**G**	a	6 / 11
c	**G**	g	2 / 10
a	**A**	a	11 / 9
t	**G**	a	3 / 9
a	**G**	c	14 / 8
a	**A**	c	10 / 8
a	**A**	g	6 / 8
c	**T**	g	7 / 7
a	**C**	a	10 / 7
t	**A**	a	3 / 7
t	**T**	g	4 / 6
t	**T**	c	9 / 6
t	**C**	t	2 / 6
t	**C**	a	3 / 6
g	**A**	a	5 / 6
g	**T**	c	16 / 6
g	**T**	t	3 / 5
a	**G**	t	9 / 5
t	**A**	t	3 / 5
c	**A**	g	3 / 5
g	**T**	g	9 / 5
a	**C**	c	9 / 5
c	**T**	c	10 / 4
g	**G**	a	7 / 4
g	**C**	a	7 / 4
c	**T**	a	24 / 4
g	**G**	c	11 / 4
a	**A**	t	9 / 4
a	**C**	g	4 / 4
c	**G**	a	7 / 4

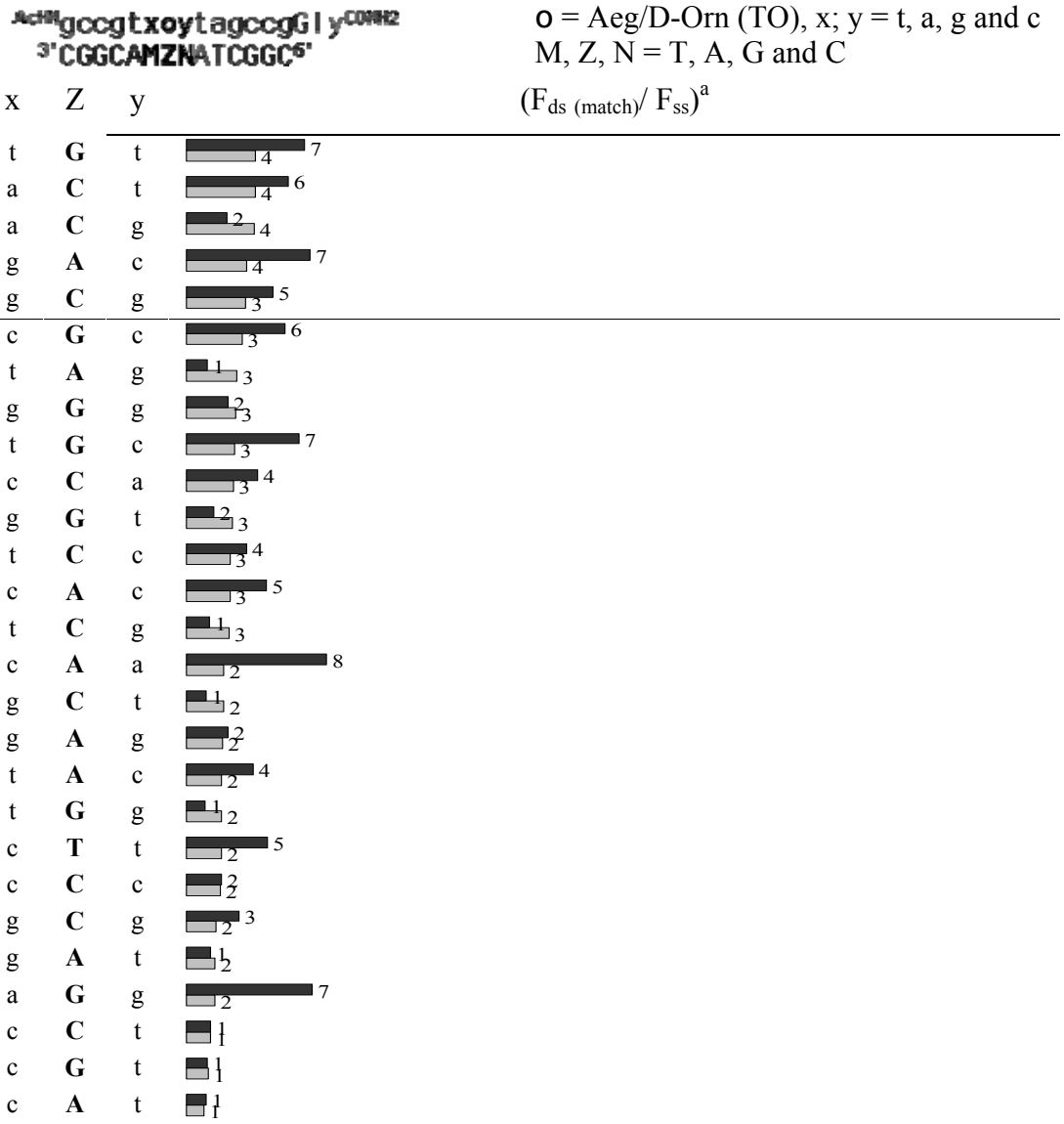

Figure 67: Fluorescence enhancement of PNA probes **5-20** (gray) and **25-40** (black), measured at 530 nm after formation of matched duplexes, when TO was paired against thymine, adenine, guanine and cytosine at 25°C in buffer. [$^{a}F_{ds}/F_{ss}$ = Ratio between fluorescence intensities of FIT-PNA after and before addition of DNA at 530 nm.]

Aeg-TO-PNA

1) ≥8 fold fluorescence enhancement is found in 14 duplexes (22 %).

2) ≥4 fold fluorescence enhancement found in 42 (66 %) hybrids.

3) <4 fold fluorescence enhancements is found in 22 (34 %) hybrids.

D-Orn-PNA

1) ≥8 fold fluorescence enhancement is found in 22 duplexes (34 %).

2) ≥4 fold fluorescence enhancement found in 42 (66 %) hybrids.

3) <4 fold fluorescence enhancements is found in 22 (34 %) hybrids.

4) Average fluorescence increase when at least one AT base pair acts as stacking partner for TO was measured 6.9 fold and 4.9 fold with at least one GC as stacking partner.

5) The average fluorescence increase when TO is against T, A, G or C was measured 10.4, 4.3, 4.7 and 3.7 fold, respectively.

6) Average fluorescence increase with one adenine as intrastrand TO stacking partner is 8.8 fold. Enhancement of 4.4 fold, 4.6 fold and 5.5 fold were obtained with c, g and t respectively, as stacking partner.

7) Fluorescence enhancement is constant or even increased upon increases of temperatures and at temperature around the T_M fluorescence of the duplex strand rapidly decreases

8) Among studied 384 mismatched duplexes 80 % have lower fluorescence than in matched duplexes.

9) 25 % of the probes discriminate against mismatches with ≥ 3 fold selectivity at 25°C.

10) Average fluorescence enhancement of Aeg-TO labelled oligomers against all bases in matched duplexes at 25°C is 5.8 fold.

4) Average fluorescence increase when at least one AT base pair acts as stacking partner for TO was measured 6.6 fold and 6.7 fold with at least one GC as stacking partner.

5) The average fluorescence increase when TO is against T, A, G or C was measured 15.6, 5.0, 5.4 and 4.8 fold, respectively.

6) Average fluorescence increase with one adenine as intrastrand TO stacking partner is 12 fold. Enhancement of 7.5 fold, 5.6 fold and 5.4 fold were obtained with c, g and t respectively, as stacking partner.

7) Fluorescence enhancement is constant or even increased upon increases of temperatures and at temperature around the T_M fluorescence of the duplex strand rapidly decreases

8) Among studied 384 mismatched duplexes 92 % have lower fluorescence than in matched duplexes.

9) 41 % of the probes discriminate against mismatches with ≥ 3 fold selectivity at 25°C.

10) Average fluorescence enhancement of D-Orn-TO labelled oligomers against all bases in matched duplexes at 25°C is 7.8 fold.

10.3 Binding mode of thiazole orange

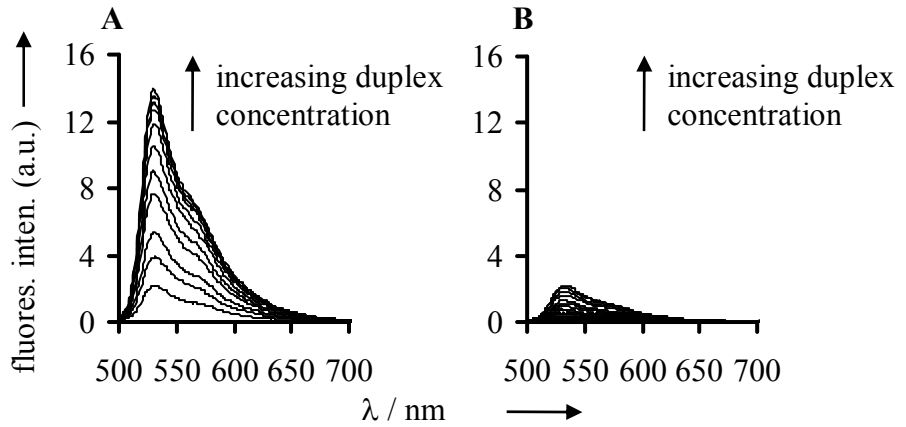

Figure 68: Fluorescence emission of TO-PRO1 before and after addition of A) DNA•DNA duplex **4'AT•4'TA** (0.1, 0.2, 0.3, 0.5, 0.7, 1.0, 1.5, 2.0, 2.5, 3.0 and 4.0 μM) and B) PNA•DNA duplex **4at•4'TA** (0.1, 0.2, 0.3, 0.5, 0.7, 1.0, 1.5, 2.0, 2.5, 3.0, 4.0, 5.0, 6.0, 8.0, 10.0, 12.0 and 14.0 μM).

In this work it was found that the thiazole orange dye TO-PRO1 experienced increases of fluorescence ($\phi_{em} = 0.02$) and ($\phi_{em} = 0.21$) when allowed to bind to PNA•DNA **(4at•4'TA)** and DNA•DNA (**4AT•4'TA)** duplexes, respectively. The analysis of the fluorescence titration data revealed that TO-PRO1 binds PNA•DNA with lower affinity ($K_{app} = 7.3 \pm 0.4$ μM per base pair) than DNA•DNA duplex **4AT•4'TA** ($K_{app} = 134 \pm 20$ μM per base pair).

Measurements of time resolved fluorescence [performed by by Nils Krebs and Sebastian Tannert in the working group of Prof. Beate Röder (Institut für Physik, Humboldt-Universität zu Berlin. Newtonstr. 15, D-12489 Berlin, Germany)] of TO-PRO 1 in DNA•DNA and PNA•DNA and in FIT-PNA complexes highlighted four different fluorescence decay processes which responded differently to changes of the TO environment. This includes 1) a very fast fluorescence decay process in the range of 0.04-0.07 ns that disappears upon binding of FIT-PNA to DNA and upon binding of TO-PRO 1 to dsDNA but not upon binding of TO-PRO 1 to PNA•DNA. 2) a fast decay between 0.22-0.48 ns, which showed the highest sensitivity to the presence of mismatched base pairs. 3) a comparably unsusceptible medium decay process within 1.05-1.54 ns and 4) a long decay between 2.33-3.95 ns which is almost universally susceptible to changes conferred by hybridization and exchange of adjacent nucleobases in FIT-PNA•DNA duplexes. The very fast decay process has been assigned to a water accesible species. Accordingly, TO-PRO 1 in complex with

PNA•DNA duplex **4at•4TA** has water accessible binding mode as opposed to TO-PRO 1 complexed to dsDNA and TO in FIT-PNA•DNA duplexes.

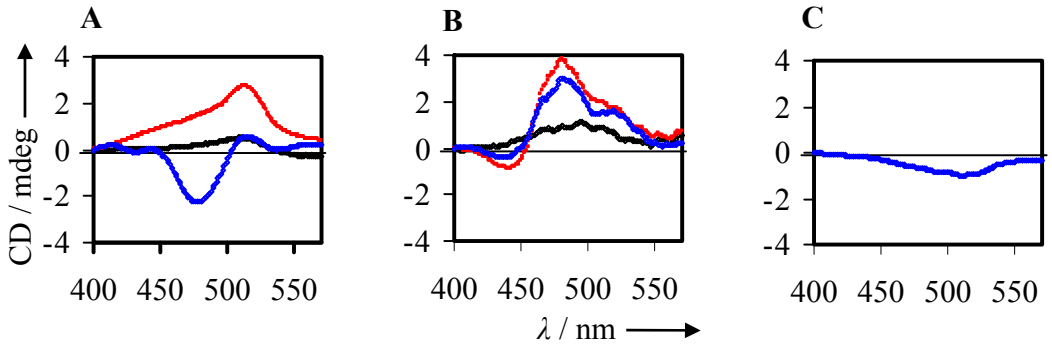

Figure 69: Induced CD spectra of TO-PRO1 A) DNA•DNA duplex **4'AT•4'TA** and B) PNA•DNA duplex **4at•4'TA** at mixing ratios (dye: BP) 1:10 (black), 1:4 (red) and 1:2.5 (blue). C) CD Spectrum of FIT-PNA•DNA duplex **19gc•16'CTG** (blue). Spectra were set zero at 400 nm.

The induced CD spectra of TO-PRO1 obtained upon binding to DNA•DNA and PNA•DNA duplexes are positive at low dye/base pair ratio (Figure 69). At high dye/ base pair ratios two bands of different sign appear. Such a structure can originate from a superimposed exciton CD induced by dye-dye interactions in the minor groove. In the PNA•DNA duplex the CD couplet is observed at lower dye/ base pair (d/BP) ratios (1:4) than in the DNA•DNA duplex (d/ BP = 1:2.5). This observation suggests that, for the studied sequence, association of TO-PRO1 in the PNA•DNA minor groove may occur at lower dye concentration than in the DNA•DNA minor groove.

The TO chromophore in the FIT-PNA•DNA complex **19gc•16'CTG** shows a negative band with a maximum at 518 nm which coincides with the absorption bands. Negative bands have been assigned to the intercalation mode.[1, 2, 3, 4] It can be concluded that the TO chromophore in FIT-PNA•DNA duplex **19•16'** predominantly accommodates an intercalated position in the interior of the duplex. In contrast, the mode of binding of TO-PRO1 to DNA•DNA and PNA•DNA appears less clearly defined.

The comparibly low affinity of TO-PRO 1 for PNA•DNA, the existence of water accessible bound TO species and the CD-spectra suggest that TO-PRO 1 occupies extrahelical binding site in PNA•DNA duplexes. It can be concluded that intercalation of TO in FIT-PNA•DNA duplexes is an enforced binding mode as PNA•DNA duplexes appear not to provide high-affinity intercalation site for TO-PRO 1. The

defined intercalative binding mode of TO in FIT-PNA renders the fluorescence properties particularly responsive to changes of the environment. The fluorescence quantum yield were highest in duplexes that contained adenine-thymine base pairs as TO stacking partner and lowest with adjacent guanine-cytosine pairs. This data is in contrast to results of previous observations in which TO and TO-PRO 1 showed higher fluorescence quantum yield when compared to GC rich rather than AT rich duplexes. This data as well as the remarkable responsiveness of ε_{260} suggest that TO in FIT-PNA•DNA duplexes accomodates binding modes, which may facilitate electronic coupling with adjacent nucleobases.

The above studies showed that the fluorescence of the thiazole orange base surrogate is most responsive to hybridisation when TO is flanked by adenine-adenine. The preferred pairing partner to achieve high fluorescence with matched DNA and high match/mismatch fluorescence discrimination is thymine. The majority, of FIT-probes show lower fluorescence in single-mismatched duplexes than in matched duplexes. It is, hence, possible to discriminate matched against mismatched targets even at temperature below the T_M of the mismatched probe-target complex. In addition, one can take advantage of the hybridisation selectivity of FIT-probes. The studied mismatched duplexes always showed lower thermal stability, than the corresponding matched duplexes. At temperature below the T_M of matched duplex and above the T_M of mismatched duplex, it is possible to distinguish all single mutated DNA targets from its matched one by using FIT-PNA oligomers.

The D-Orn-TO labelled PNA gives similar responsiveness to its neighbouring base, stacking base and pairing base with added advantages of higher match duplex fluorescence and higher match/mismatch fluorescence discrimination.

10.4 ‘FIT-PNA’ vs. ‘Light-up PNA’

Light-up probes differ from FIT probes (Figure 70) by the mode of attachment. TO in Light-up probes hangs by a flexible tether from the N’- or C’-terminal end. The influence of the different attachment modes was explored by the hybridisation experiments.

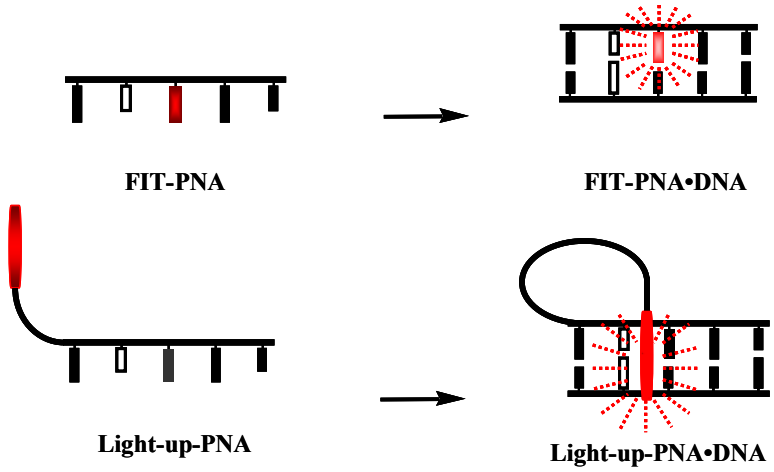

Figure 70: Schematic of FIT-PNA and Light-up PNA.

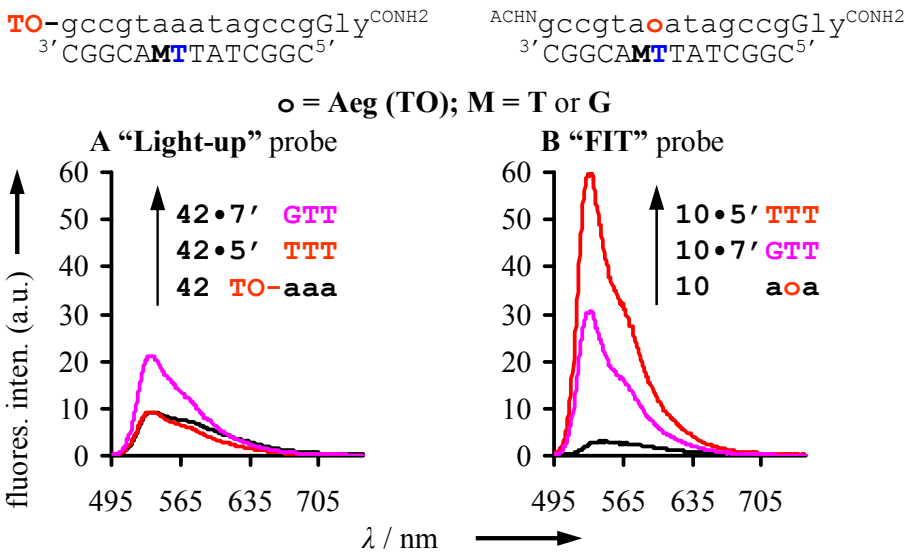

Figure 71: Fluorescence emission spectra before (black), after addition of equimolar amount of matched DNA **5'TTT** = (red), and mismatched DNA **7'GTT** = (pink), for A) Light-up probe **42**, B) FIT probe **10** at 25°C.

The collected data from UV/ VIS absorbance, circular dichroism, and fluorescence spectroscopy (Figure 71 and 72) indicate that the use of thiazole orange as base surrogate in FIT-PNA enabled the site-specific intercalation in PNA•DNA duplexes. In contrast TO in Light-up PNA does not show any sign for intercalation. FIT-PNA yielded high fluorescence enhancements (16-24 fold) upon binding with matched DNA. In contrast, fluorescence of Light-up-PNA **42** and **45** experienced little changes upon addition of matched DNA. Single base mismatch duplexes of FIT-PNA **10** and **46** resulted in attenuation of fluorescence. The opposite behaviour, fluorescence enhancement upon mismatched hybridization was observed for Light-up PNA **42**.

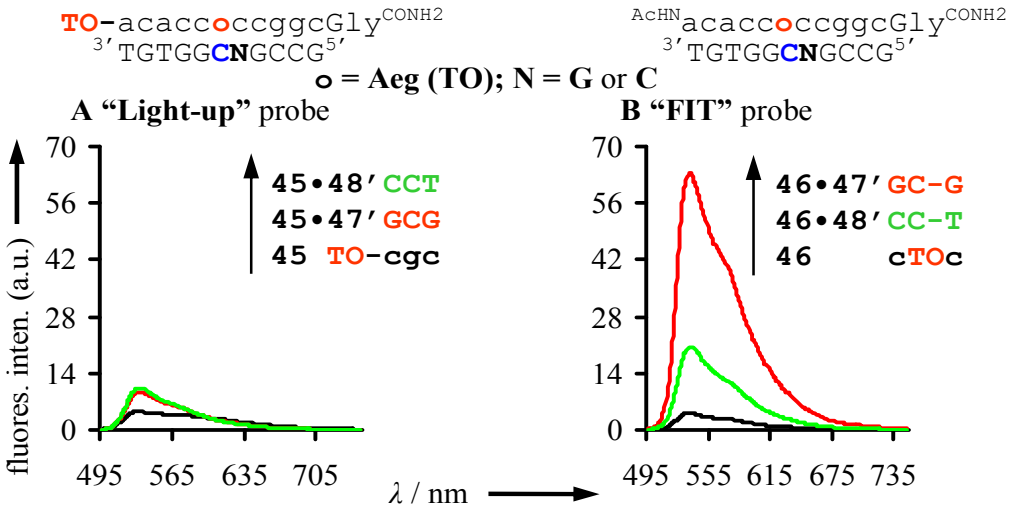

Figure 72: Fluorescence emission spectra before (black), after addition of equimolar amount of matched DNA **47'CGC** = (red), and mismatched DNA **48'GCT** = (green), for A) Light-up probe **45**, B) FIT probe **46** at 25°C.

Time resolved measurements showed a very fast fluorescence decay process, which disappears upon double-strand formation in FIT-PNA. This decay remained unchanged upon hybridisation of Light-up-PNA. Remarkable changes in absorbance spectra were recorded. FIT-PNA gives extinction coefficient of $\varepsilon_{max} = 38200\ M^{-1}cm^{-1}$ and Light-up PNA of $\varepsilon_{max} = 85800\ M^{-1}cm^{-1}$. These differences indicate different interactions between TO and nucleobases. It can be concluded that for the two studied sequences, FIT-PNA provides for higher hybridisation specificity, fluorescence enhancement and match/mismatch dicrimination.

10.5 Dual labeled FIT-PNA

Dual labeled FIT-PNA features two cyanine dyes that flanked the SNP site. It was considered possible that two TO-chromophores could come into contact when separated by a base mismatch, resulting in changes of fluorescence (Figure 73).

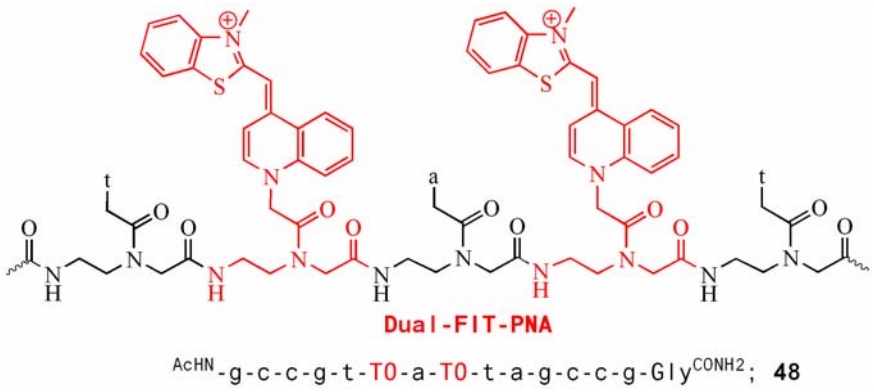

Figure 73: Structure of dual labeled FIT-PNA.

The fluorescence enhancement obtained upon hybridisation of $(TO)_2$-PNA is higher than that of FIT-PNA. Interestingly, the shoulder at longer wavelength (577 nm) is more pronounced in mismatched duplexes. This shoulder may indicate that the two TO chromophores spaced by a mismatched base pair can contact each other.

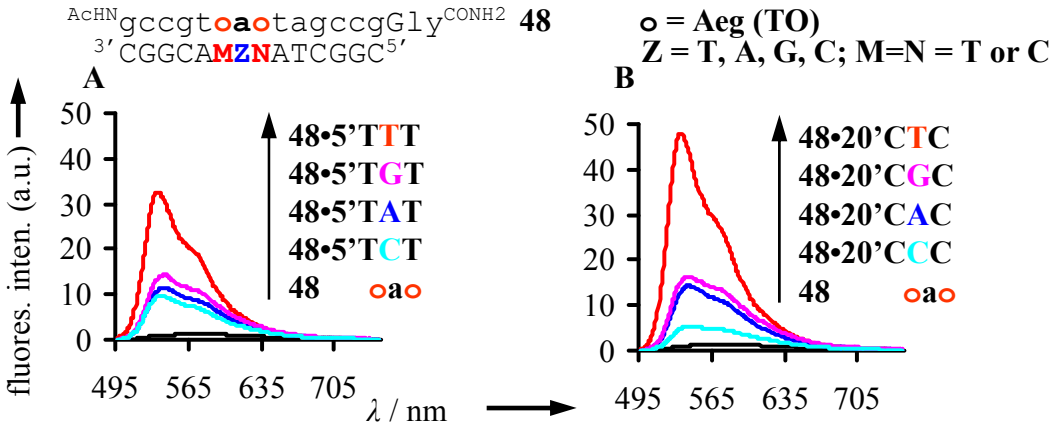

Figure 74: Fluorescence emission spectra of PNA probe **48** before (black), after addition of equimolar amount of A) matched DNA **5'TTT** = (red), mismatched DNA **5'TAT** = (blue), DNA **5'TGT** = (pink) and **5'TCT** = (turquoise) B) matched DNA **20'CTC** = (red), mismatched DNA **20'CAC** = (blue), DNA **20'CGC** = (pink) and **20'CCC** = (turquoise).

Highest fluorescence increases were obtained upon pairing of TO against pyrimidines. The T_M measurements showed that two TO chromophores reduce the specificity of hybridisation. Due to the reduction of hybridisation specificity the dual labelled probes may not be better than FIT-PNA for PCR applications. However they may be superior to FIT-PNA at room temperature.

10.6 Pyridine benzothiazole as base surrogate

To facilitate typing of single nucleotide polymorphisms an additional colour is required one that is specific for the wild type sequence and one that calls for mutant. It was chose to explore the utility of the BO dye in which the quinolium ring of TO is replaced by a pyridinium ring.

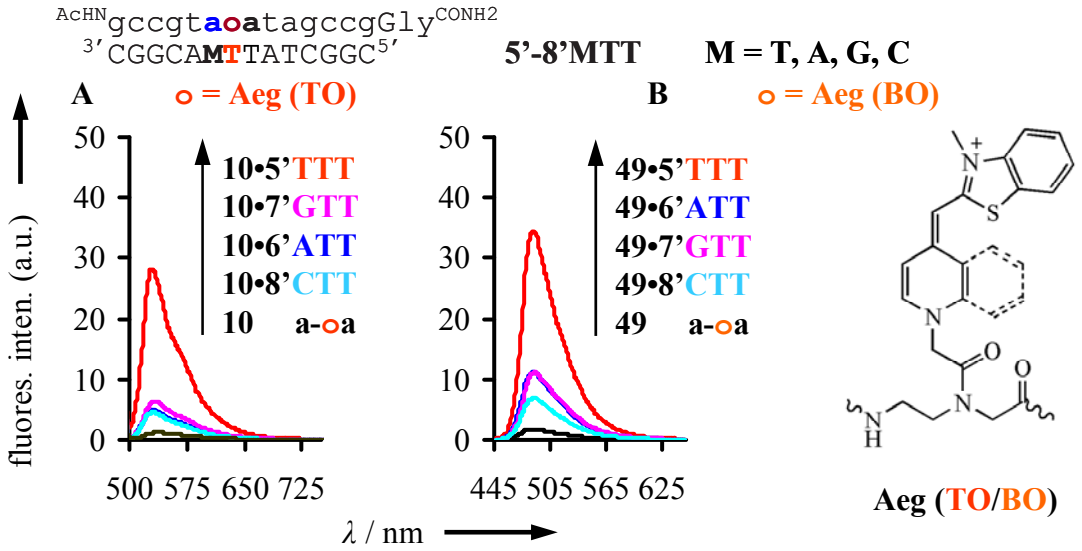

Figure 75: Fluorescence emission spectra of A) TO-PNA conjugate **10** and B) BO-PNA conjugates **48** before (black) and after addition of equimolar amount of DNA **5'TTT** = (red), **6'ATT** = (blue), **7'GTT** = (pink) and **8'CTT** = (turquoise) at 60°C.

This study revealed that hybridisation-induced enhancements of BO fluorescence are not as high as that of TO. However, useful 18 fold fluorescence enhancements (Figure 75) were obtained at elevated temperature (60°C) which is in the range of PCR applications. The melting study showed that matched duplexes melt at higher temperature than corresponding single base mismatched duplexes. The responsiveness of BO fluorescence to a neighbouring base mismatch at high temperature is as high as or even slightly higher than that of the TO derivative. This suggests that it might be possible to distinguish a DNA target from its single base mutant by using BO-labeled FIT-PNA.

11. EXPERIMENTAL

11.1 General Protocol

Chemicals: DNA were purchased from MWG-Biotech in HPSF quality. Fmoc/Bhoc-protected PNA-monomers were purchased from Applied Biosystems. Other chemicals were purchased from Novabiochem, Acros, Aldrich, Lancaster or Merk.

Water purification: Water was purified with a Milli-Q® Ultrapure Water Purification System (Millipore Corp.).

PNA synthesiser: Automated solid phase synthesis was performed on an Intavis ResPep parallel synthesizer equipped with 1 ml reactors.

Fluorescence spectroscopy: Fluorescence spectroscopy was performed with a Varian Cary Eclipse fluorescence spectrophotometer.

UV-VIS-spectroscopy: A Varian Cary 100 Bio-UV visible spectrophotometer was used for optical and melting analysis.

CD spectroscopy: CD measurements were performed on a JASCO J-710 spectropolarimeter equipped with a Julabo F 25 as cooling device to control temperature.

HPLC: HPLC was performed with a Gilson 321 instrument using RP-C18 columns CC-250/ 4 NUCLEOSIL (100-5) C18-HD for analytical runs and SP125/ 10 NUCLEODUR C18-gravity for semipreparative runs. Columns were heated to 50°C. Eluent A (0.1 % TFA in water + 1 % MeCN) and B (0.1 % TFA in MeCN + 1 % water) were used in a linear gradient with flow rate of 1 mL/ min for analytical and 6 mL/ min for preparative HPLC. [HPLC conditions: flow: 6 mL/ min or 1 mL/ min; gradient: 0–1 min: 3 % eluent A; 1–25 min: 3–30 % eluent B].
Gradient A: 3 %→20% B in 20 min, 80 % B for 10 min, 3 % B for 5 min
Gradient B: 3 %→30% B in 30 min, 80 % B for 10 min, 3 % B for 5 min

Determination of yields (PNA oligomers): PNA probes were diluted with 500 µl of milipore water and vortexed for 2 minutes. Then 5 µl of the probe solution was taken and diluted by adding 995 µl of milipore water. Optical density was measured at 260 nm using quartz cuvette with 10 mm path length. By considering TO = T (thymine, the base having nearest absorption coefficient value with TO at 260 nm) probe concentration was calculated using oligo calculation at www.Gensetoligos.com

Mass Spectrometer: Mass spectra were measured on a Finnigan LTQFT spectrometer for FAB-MS and ESI-MS. MALDI-TOF mass spectra were recorded on a Voyager-DE^{TM} Pro Biospectrometry Workstation of PerSeptive Biosystems. Matrix for DNA's: 3-Hydroxy Picolinic acid (50 mg/ mL in 50:50 water: acetonitrile and 50 mg diammonium citrate in water), Matrix for PNA's: Sinapinic acid (saturated solution of 3, 5-dimethoxy, 4-hydroxy cinamic acid in 300 µL acetonitril, 600 µL milipore water and 1.8 µL trifluoro acetic acid).

Chromatography: Column chromatography was performed on SDS 60 ACC silica gel and TLC (thin layer chromatography) on E. Merck Silica Gel 60 F_{254} plates.

Nuclear Magnetic Resonance Spectroscopy: The NMR spectra were recorded on Bruker AC 250, DPX 300, AM 300 or AM 400 spectrometers. The signals of the residual protonoted solvent ($CDCl_3$ or d_6-DMSO) were used as reference signals. Coupling constants are given in Hz. Signal multiplication is presented as s = singlet, d = doublet, t = triplet and m = multiplet.

Loading of Novagen TGR resin (4a or 4a''):

The resin (500 mg, 0.29 mmol/ g) was washed (3x DCM (2 mL), 3x DMF (2 mL), 3x DCM and 3x DMF). The resin was allowed to swell in DMF (10 mL) for 30 minutes. For preactivation PyBOP (301.2 mg, 0.58 mmol) and NMM (87.7 mg, 0.87 mmol) were added to a solution of Fmoc-protected glycine or Fmoc-protected lysine (0.58 mmol) in DMF (5.8 mL). After 3 minutes the mixture was added to the resin. After 4 h the resin was washed (3x DMF, 3x DCM, 3x DMF). For capping the resin was treated with a solution of Ac_2O/ py (1:4; 5 mL). After 5 minutes the procedure was repeated once. The resin was washed (3x DMF, 3x DCM, 3x DMF and 5x DCM) and finally dried in vacuo.

Linear solid-phase synthesis:

Linear solid-phase synthesis was performed by using an Intavis ResPep parallel synthesizer equipped with 1-mL reactors. Resin **4a** (ca. 2 μmol) was allowed to swell in DMF (2 mL). After 30 min, the resin was transferred to the synthesizer reactor. The resin was washed (2 × 180 μL DMF). Fmoc Cleavage: DMF/piperidine (4:1, 100 μL) was added to the resin. After 2 min, the procedure was repeated once. The resin was washed with DMF (1 × 180 μL, 3 × 100 μL and 1 × 180 μL). Coupling of Standard PNA Building Blocks: A preactivation vessel was charged with a 0.6 M HCTU solution in NMP (12 μL), a 4 M NMM solution in DMF (4 μL), and a 0.6 M PNA monomer solution in NMP (27 μL). After 8 min, 40 μL of preactivation solution was transferred to the resin. After 30 min, the resin was washed (2 × 180 μL DMF). Coupling of Fmoc–Aeg/D-Orn (TO)–COOH (**3b**/**24b**): A preactivation vessel was charged with a 0.6 M HCTU solution in NMP (12 μL), a 4 M NMM solution in DMF (4 μL), and a solution of **3b**/**24b** in NMP (0.6 m PPTS, 27 μL). After 8 min, 40 μL of preactivation solution was transferred to the resin. After 30 min, the resin was washed (2 × 180 μL DMF). Capping: Ac_2O/2,6-lutidine (9:11, 100 μL), 3 min. The resin was washed (3 × 200 μL DMF, 3 × 100 μL DMF).

Divergent solid phase synthesis:

Resin **4a** was allowed to swell in DMF (2 mL). After 30 minutes the resin was washed (3x 2 mL DMF, 3x 2 mL DCM, 3x 2 mL DMF). Fmoc-cleavage: DMF/ piperidine (4:1, 2 mL) was added to the resin. After 3 minutes the resin was washed with DMF. This procedure was repeated twice. Finally the resin was washed with DMF (3x 2 mL DMF), DCM (3x 2 mL) and DMF (3x 2 mL). Coupling: The resin was suspended in a solution of 4 eq. Fmoc-protected building block in 0.125 mM NMM in DMF (0.1 M final building block concentration) which was preactivated for 2 minutes by addition of 4 eq. PyBop. After 2 h, the resin was washed (3x 2 mL DMF, 3x 2 mL DCM, 3x 2 mL DMF). Capping: Ac_2O/ pyr. (1:10, 2 mL) 2x 5 minutes. Resin was washed (3x 2 mL DMF, 3x 2 mL DCM, 3x 2 mL DMF). Alloc removal: Above resin was aliquoted correspond to 1 μmol based on the initial Fmoc-loading of resin **4a**. A degassed solution of [Pd $(PPh_3)_4$] and 8 eq. dimethyl amine borane complex in dry DCM (2 mL) was added to resin. After 20 minutes the solvent was removed by filtration. The procedure was repeated once and the resin was washed with DMF (3x 2 mL), DCM (3x 2 mL) and DMF (3x 2 mL). Thiazole orange

coupling: To 6 µmol of the thiazole orange derivative (TO-COOH) in DMF (60 µL) was added PPTS (1.5 mg, 6 µmol) and PyBop (3.1 mg, 6 µmol). After vortexing NMM (0.65 µL, 8 µmol) was added to the resulting solution. After vortexing this mixture was added to the resin. After 12 h of shaking the solvent was removed by filtration. The thiazole orange coupling was repeated once (coupling time: 2 h). Finally, the resin was washed with DMF (3x 2 mL), DCM (3x 2 mL) and again DMF (3x 2 mL) and DCM (5x 2 mL).

Cleavage

The dried resin was suspended in a solution of cystine methyl ester hydrochloride (5 mg, 29.1 µmol) in TFA/ m-cresol/ H_2O (37:2:1, 1 mL) and was shaken for 3 h. The resin was washed with TFA (200 µL). The combined filtrates were concentrated in vacuo. Purification: To the concentrated cleavage solution was added cold diethyl ether. The precipitate was collected by centrifugation and disposal of the supernatant. The residue was dissolved in water and precleaned by using a water equilibrated Sep-pak® C18 cartridge. Coloured eluates obtained upon gradient elution (1x 20:80 AcN: H_2O: 0.1 % TFA; 1x 40:60 AcN: H_2O: 0.1 % TFA; 1x 80:20 AcN: H_2O: 0.1 % TFA; 1x 80:20 AcN: H_2O: 0.1 % TFA; 2 mL each) were analyzed by HPLC and MALDI-TOF/ MS and purified by semipreparative HPLC.

11.2 Experimental

11.2.1 Experimental part for Section 2

***N*-[2-(Fluorenylmethoxycarbonyl-amino) ethyl]-*N*-[2-(1-Carboxy-methyl-1H-quinoline-4-ylidenmethyl)-3-methyl-benzothiazol-3-ium Bromide] allyl ester, Fmoc-Aeg (TO)-OAll (3a):** To TO-COOH (100 mg, 0.23 mmol) in dry DMF (2.3 mL) was added PyBop (145 mg, 0.279 mmol), pyridinium *p*-toluene sulfonate (58 mg, 0.232 mmol) and N-methyl morpholine (23 mg, 0.23 mmol). The suspension was stirred under argon until a clear solution was obtained. This solution was added to a solution of amine hydrochloride **2b** (96 mg, 0.23 mmol) and N-methyl morpholine (23 mg, 0.23 mmol) in DMF (2.3 mL). The reaction mixture was stirred for 12 h under argon. The volatiles were removed under reduced pressure. Methanol (2 mL) was added to the residue. After stirring for 1 h the precipitate was collected by

filtration and washed with methanol (5 mL). The crude product was purified by column chromatography ($CHCl_3$:MeOH 97:3, 1 % formic acid) to yield an orange coloured solid (114 mg, 62 %).

Molecular formula:	$C_{42}H_{39}O_5N_4{}^{32}S^+$
R_f-value:	0.64 ($CHCl_3$/ MeOH 80:20, 1 % HCOOH)
^{1}H-NMR:	(300 MHz, [D_6]DMSO:TFA, 10:1.5): δ = 8.73 (d, J = 8.4, 1H, Ar-H^{q5}), 8.51 (d, J = 7.3, 1H, Ar-H^{q2}), 8.01 (d, J = 7.7, 1H, Ar-H^{b1}), 7.91-7.86 (m, 2H, Fmoc-$H^{4,5}$), 7.80-7.72 (m, 2H, Ar-$H^{q7,8}$), 7.68 (m, 1H, Ar-H^{b4}), 7.66-7.63 (m, 2H, Fmoc-$H^{1,8}$), 7.58-7.56 (m, 1H, Ar-H^{b3}), 7.53-7.48 (m, 1H, Ar-H^{b2}), 7.47-7.44 (m, 1H, Ar-H^{q6}), 7.40-7.37 (m, 2H, Fmoc-$H^{3,6}$), 7.37-7.33 (m, 2H, Fmoc-$H^{2,7}$), 7.31-7.28 (m, 1H, Ar-H^{q3}), 6.87 (s, 1H, Cyanin-H), 5.98-5.85 (m, 1H, All-H^1), 5.46 (s, 2H, methylene-H), 5.33 (d, J = 17.1, 1H, All-H^{3trans}), 5.24 (d, J = 10.5, 1H, All-H^{3cis}), 4.68 (d, J = 5.3, 2H, All-H^1), 4.31 (d, J = 6.6 , 2H, Fmoc-CH_2), 4.22-4.18 (m, 1H, Fmoc-H^9), 4.05 (s, 2H, Aeg-H^1, 3.98 (s, 3H, Me-H), 3.33 (t, 2H, Aeg-H^3), 3.04 (m, 2H), Aeg-H^2).
^{13}C-NMR:	(300 MHz, [D_6] DMSO:TFA, 10:1.5): δ = 168.7, 166.4, 156.4, 148.5, 144.8, 143.8, 140.8, 140.3, 137.8, 137.7, 133.3, 131.8, 128.3, 128.2, 127.7, 127.1, 126.7, 125.6, 125.2, 124.8, 124.2, 123.7, 122.9, 120.2, 118.6, 117.6, 113.3, 107.5, 88.9, 65.9, 65.7, 54.6, 46.7, 46.6, 34.0
HR-MS:	(ESI$^+$, MeOH): m/ z: 711.2636 $[M]^+$, calc.: 711.2636.

***N*-[2-(Fluorenylmethoxycarbonyl-amino)ethyl]-*N*-[2-(1-Carboxy-methyl-1H-quinoline-4-ylidenmethyl)-3-methyl-benzothiazol-3-ium Bromide] OH, Fmoc-Aeg(TO)-OH (3b):** To a solution of **3a** (90 mg, 0.1 mmol) in THF (5 mL) was added N-Methylaniline (11.3 mg, 0.1 mmol). The solution was degassed by freeze-thaw-pump cycles. After addition of [Pd (PPh_3)$_4$] (12 mg, 0.01 mmol) the mixture was stirred for 14 h under exclusion of light. The solvent was removed in vacuo. To the residue was added methanol (2 mL). The resulting precipitate was collected by

filtration. The crude product was purified by column chromatography ($CHCl_3$:MeOH 97:3, 1 % formic acid) to yield an orange coloured solid (62 mg, 73 %).

Molecular formula:	$C_{39}H_{35}O_5N_4{}^{32}S^+$
R_f-value:	0.28 ($CHCl_3$/ MeOH 80:20, 1 % HCOOH)
^{1}H-NMR:	(300 MHz, [D_6]DMSO:TFA, 10:1.5): δ = 8.74 (d, J = 8.4, 1H, Ar-H^{q5}), 8.50 (d, J = 7.3, 1H, Ar-H^{q2}), 8.02 (d, 1H, J = 7.8, Ar-H^{b1}), 7.90-7.87 (m, 2H, Fmoc-H^{4,5}), 7.86-7.8 (m, 2H, Ar-H^{q7,8}), 7.69 (m, 1H, Ar-H^{b4}), 7.67-7.65 (m, 2H, Fmoc-H^{1,8}), 7.63-7.58 (m, 1H, Ar-H^{q6}), 7.55-7.52 (m, 1H, Ar-H^{b3}), 7.47-7.44 (m, 1H, Ar-H^{b2}), 7.42-7.38 (m, 2H, Fmoc-H^{3,6}), 7.39-7.34 (m, 2H, Fmoc-H^{2,7}), 7.32 (m, 1H, Ar-H^{q3}), 6.89 (s, 1H, Cyanin-H), 5.50 (s, 2H, methylene-H), 4.33 (d, J = 6.7, 2H, Fmoc-CH_2), 4.21 (m, 1H, Fmoc-H^9), 3.99 (s, 3H, Me-H), 3.89 (s, 2H, Aeg-H^1), 3.29 (t, 1H, Aeg-H^3), 3.00 (m, 2H, Aeg-H^2)**.**
^{13}C-NMR:	(300 MHz, [D_6] DMSO:TFA, 10:1.5): δ = 168.7, 165.8, 158.7, 158.2, 156.4, 148.6, 143.8, 140.8, 137.7, 133.2, 128.2, 128.1, 127.7, 127.1, 126.6, 125.1, 124.8, 124.1, 123.7, 122.9, 120.2, 117.6, 113.8, 113.3, 107.4, 88.8, 65.6, 54.6, 47.4, 46.7, 46.5, 34.0.
HR-MS:	(ESI$^+$, MeOH): m/ z: 671.2323 [M]$^+$, calc.: 671.2328.

FIT-PNAs

^{AcHN}gccgta-Aeg (TO)-tagccgGly^{CONH2}, 4

7 mg (≈ 2 µmol) of resin **4a** was used. The PNA was synthesised by linear solid phase synthesis using automated solid phase PNA synthesis.

Yield: OD_{260} = 5.54, 176 nmol, 8.8 %

ε_{260}	124.000 L•mol^{-1}•cm^{-1}
MALDI-TOF/MS; m/z	3799 [M+H]$^+$, calc.: 3798
HPLC	t_R = 11.3 min (Gradient B)
$C_{156}H_{189}N_{76}O_{40}S^+$	3798.5

^{AcHN}gccgtaatagccgGly^{CONH2}, 4at

7 mg (≈ 2 µmol) of resin **4a** was used. The PNA was synthesised by linear solid phase synthesis using automated solid phase PNA synthesis

Yield: OD_{260} = 10.82, 344 nmol, 17.2 %

ε_{260}	126.000 L•mol^{-1}•cm^{-1}
MALDI-TOF/MS; *m/z*	3644 $[M+H]^+$, calc.: 3642
HPLC	t_R = 12.3 min (Gradient B)
$C_{156}H_{189}N_{76}O_{40}S^+$	3642.4

^{AcHN}gccgtt-Aeg (TO)-ttagccgGly^{CONH2}, 5

13 mg (≈ 4 µmol) of resin **4a** was used. The PNA was manually synthesised by divergent solid phase synthesis.

Yield: OD_{260} = 18.56, 140 nmol, 3.5 %

ε_{260}	133.000 L•mol^{-1}•cm^{-1}
MALDI-TOF/MS; *m/z*	4059 $[M+H]^+$, calc.: 4056
HPLC	t_R = 14.5 min (Gradient B)
$C_{156}H_{189}N_{76}O_{40}S^+$	4055.6

^{AcHN}gccgta-Aeg (TO)-ttagccgGly^{CONH2}, 6

13 mg (≈ 4 µmol) of resin **4a** was used. The PNA was manually synthesised by divergent solid phase synthesis.

Yield: OD_{260} = 14.8, 110 nmol, 2.8 %

ε_{260}	134.000 L•mol^{-1}•cm^{-1}
MALDI-TOF/MS; *m/z*	4069 $[M+H]^+$, calc.: 4065
HPLC	t_R = 13.9 min (Gradient B)
$C_{156}H_{189}N_{76}O_{40}S^+$	4064.6

^{AcHN}gccgtg-Aeg (TO)-ttagccgGly^{CONH2}, 7

13 mg (≈ 4 µmol) of resin **4a** was used. The PNA was manually synthesised by divergent solid phase synthesis.

Yield: OD_{260} = 14.9, 114 nmol, 2.9 %

ε_{260}	131.000 L•mol^{-1}•cm^{-1}
MALDI-TOF/MS; *m/z*	4083 $[M+H]^+$, calc.: 4081

HPLC	t_R = 14.0 min (Gradient B)
$C_{156}H_{189}N_{76}O_{40}S^+$	4080.6

^{AcHN}gccgtc-Aeg (TO)-ttagccgGly^{CONH2}, 8

13 mg (≈ 4 µmol) of resin **4a** was used. The PNA was manually synthesised by divergent solid phase synthesis.

Yield: OD_{260} = 82.3, 645 nmol, 16.1 %

ε_{260}	128.000 L•mol^{-1}•cm^{-1}
MALDI-TOF/MS; *m/z*	4042 $[M+H]^+$, calc.: 4041
HPLC	t_R = 14.7 min (Gradient B)
$C_{156}H_{189}N_{76}O_{40}S^+$	4040.6

^{AcHN}gccgtt-Aeg (TO)-atagccgGly^{CONH2}, 9

13 mg (≈ 4 µmol) of resin **4a** was used. The PNA was manually synthesised by divergent solid phase synthesis.

Yield: OD_{260} = 25.54, 200 nmol, 5.0 %

ε_{260}	134.000 L•mol^{-1}•cm^{-1}
MALDI-TOF/MS; *m/z*	4066 $[M+H]^+$, calc.: 4065
HPLC	t_R = 14.8 min (Gradient B)
$C_{156}H_{189}N_{76}O_{40}S^+$	4064.6

^{AcHN}gccgta-Aeg (TO)-atagccgGly^{CONH2}, 10

13 mg (≈ 4 µmol) of resin **4a** was used. The PNA was manually synthesised by divergent solid phase synthesis.

Yield: OD_{260} = 20.58, 151 nmol, 3.7 %

ε_{260}	136.000 L•mol^{-1}•cm^{-1}
MALDI-TOF/MS; *m/z*	4074 $[M+H]^+$, calc.: 4074
HPLC	t_R = 13.9 min (Gradient B)
$C_{156}H_{189}N_{76}O_{40}S^+$	4073.6

^{AcHN}gccgtg-Aeg (TO)-atagccgGly^{CONH2}, 11

13 mg (≈ 4 µmol) of resin **4a** was used. The PNA was manually synthesised by divergent solid phase synthesis.

Yield: OD_{260} = 13.31, 100 nmol, 2.5 %

ε_{260}	133.000 L•mol^{-1}•cm^{-1}
MALDI-TOF/MS; *m/z*	4094 $[M+H]^+$, calc.: 4090
HPLC	t_R = 13.2 min (Gradient B)
$C_{156}H_{189}N_{76}O_{40}S^+$	4089.6

^{AcHN}gccgtc-Aeg (TO)-atagccgGly^{CONH2}, 12

13 mg (≈ 4 µmol) of resin **4a** was used. The PNA was manually synthesised by divergent solid phase synthesis.

Yield: OD_{260} = 19.81, 153 nmol, 3.8 %

ε_{260}	130.000 L•mol^{-1}•cm^{-1}
MALDI-TOF/MS; *m/z*	4053 $[M+H]^+$, calc.: 4050
HPLC	t_R = 13.7 min (Gradient B)
$C_{156}H_{189}N_{76}O_{40}S^+$	4049.6

^{AcHN}gccgtt-Aeg (TO)-gtagccgGly^{CONH2}, 13

7 mg (≈ 2 µmol) of resin **4a** was used. The PNA was synthesised by linear solid phase synthesis using automated solid phase PNA synthesis.

Yield: OD_{260} = 22.5, 172 nmol, 8.8 %

ε_{260}	131.000 L•mol^{-1}•cm^{-1}
MALDI-TOF/MS; *m/z*	4082 $[M+H]^+$, calc.: 4081
HPLC	t_R = 14.5 min (Gradient B)
$C_{156}H_{189}N_{76}O_{40}S^+$	4080.6

^{AcHN}gccgta-Aeg (TO)-gtagccgGly^{CONH2}, 14

7 mg (≈ 2 µmol) of resin **4a** was used. The PNA was synthesised by linear solid phase synthesis using automated solid phase PNA synthesis.

Yield: OD_{260} = 28.3, 212 nmol, 10.6 %

ε_{260}	133.000 L•mol^{-1}•cm^{-1}
MALDI-TOF/MS; *m/z*	4092 $[M+H]^+$, calc.: 4090
HPLC	t_R = 13.1 min (Gradient B)
$C_{156}H_{189}N_{76}O_{40}S^+$	4089.6

^{AcHN}gccgtg-Aeg (TO)-gtagccgGly^{CONH2}, 15

7 mg (≈ 2 μmol) of resin **4a** was used. The PNA was synthesised by linear solid phase synthesis using automated solid phase PNA synthesis.

Yield: OD_{260} = 25.7, 198 nmol, 9.9 %

ε_{260}	130.000 L•mol^{-1}•cm^{-1}
MALDI-TOF/MS; *m/z*	4108 $[M+H]^+$, calc.: 4106
HPLC	t_R = 13.9 min (Gradient B)
$C_{156}H_{189}N_{76}O_{40}S^+$	4105.6

^{AcHN}gccgtc-Aeg (TO)-gtagccgGly^{CONH2}, 16

7 mg (≈ 2 μmol) of resin **4a** was used. The PNA was synthesised by linear solid phase synthesis using automated solid phase PNA synthesis.

Yield: OD_{260} = 43.07, 341 nmol, 17.06 %

ε_{260}	126.000 L•mol^{-1}•cm^{-1}
MALDI-TOF/MS; *m/z*	4068 $[M+H]^+$, calc.: 4066
HPLC	t_R = 13.2 min (Gradient B)
$C_{156}H_{189}N_{76}O_{40}S^+$	4065.6

^{AcHN}gccgtt-Aeg (TO)-ctagccgGly^{CONH2}, 17

7 mg (≈ 2 μmol) of resin **4a** was used. The PNA was synthesised by linear solid phase synthesis using automated solid phase PNA synthesis.

Yield: OD_{260} = 16.96, 132 nmol, 6.65 %

ε_{260}	128.000 L•mol^{-1}•cm^{-1}
MALDI-TOF/MS; *m/z*	4045 $[M+H]^+$, calc.: 4041
HPLC	t_R = 12.7 min (Gradient B)
$C_{156}H_{189}N_{76}O_{40}S^+$	4040.6

^{AcHN}gccgta-Aeg (TO)-ctagccgGly^{CONH2}, 18

7 mg (≈ 2 μmol) of resin **4a** was used. The PNA was synthesised by linear solid phase synthesis using automated solid phase PNA synthesis.

Yield: OD_{260} = 26.7, 206.4 nmol, 10.3 %

ε_{260}	130.000 L•mol^{-1}•cm^{-1}
MALDI-TOF/MS; *m/z*	4053 $[M+H]^+$, calc.: 4050

HPLC	t_R = 12.5 min (Gradient B)
$C_{156}H_{189}N_{76}O_{40}S^+$	4049.6

^{AcHN}gccgtg-Aeg (TO)-ctagccgGly^{CONH2}, 19

7 mg (≈ 2 μmol) of resin **4a** was used. The PNA was synthesised by linear solid phase synthesis using automated solid phase PNA synthesis.

Yield: OD_{260} = 26.74, 211 nmol, 10.5 %

ε_{260}	126.000 L•mol^{-1}•cm^{-1}
MALDI-TOF/MS; *m/z*	4068 $[M+H]^+$, calc.: 4066
HPLC	t_R = 14.5 min (Gradient B)
$C_{156}H_{189}N_{76}O_{40}S^+$	4065.6

^{AcHN}gccgtc-Aeg (TO)-ctagccgGly^{CONH2}, 20

7 mg (≈ 2 μmol) of resin **4a** was used. The PNA was synthesised by linear solid phase synthesis using automated solid phase PNA synthesis.

Yield: OD_{260} = 20.3, 166 nmol, 8.3 %

ε_{260}	123.000 L•mol^{-1}•cm^{-1}
MALDI-TOF/MS; *m/z*	4030 $[M+H]^+$, calc.: 4026
HPLC	t_R = 13.9 min (Gradient B)
$C_{156}H_{189}N_{76}O_{40}S^+$	4025.6

Fluorescence measurements: FIT-PNA (dissolved in water) was added into a quartz cuvette (4 x 10 mm) and diluted with aq. degassed buffer (100 mM NaCl, 10 mM NaH_2PO_4 at pH 7.0) to a final duplex concentration of 1 μM. The fluorescence spectra were recorded at specified temperature. An equimolar amount of DNA target was added to give a total volume of 1 mL fluorescence spectra were recorded after 20 min at specified temperature. (Ex. 510 nm. Em. 518-600 nm. Ex. slit width: 5 nm, Em. slit width: 2.5 nm).

Temperature vs. fluorescence measurements: The FIT-PNA or FIT-PNA•DNA duplex (dissolved in water) was added into a quartz cuvette (4 x 10 mm) and diluted with aq. degassed buffer (100 mM NaCl, 10 mM NaH_2PO_4 at pH 7.0) to a final duplex concentration of 1 μM. Prior to fluorescence measurement, the samples were

heated to 85°C and cooled within 1 h to the starting temperature of 20°C. The samples were heated to 85°C with a rate of 1°C/ min. The fluorescence spectra were recorded against temperature. (Ex. 510 nm. Em. 530 nm. Ex. slit width: 5 nm, Em. slit width: 2.5 nm).

Melting analysis: UV melting curves were measured at 260 nm. A degassed aqueous solution of 100 mM NaCl, 10 mM NaH_2PO_4 at pH 7.0 was used as buffer. The DNA and FIT-PNA oligomers were mixed to 1:1 stochiometry and the solutions adjusted to a final duplex concentration of 1 μM. Prior to analysis, the samples were heated to 85°C and cooled within 1 h to the starting temperature of 20°C. The samples were heated to 85°C with a rate of 1°C/ min. T_M values were defined as the maximum of the first derivative of the melting curve. The experiments were performed for twice.

Fluorescence of TO-PNA before and after hybridisation with matched DNA:

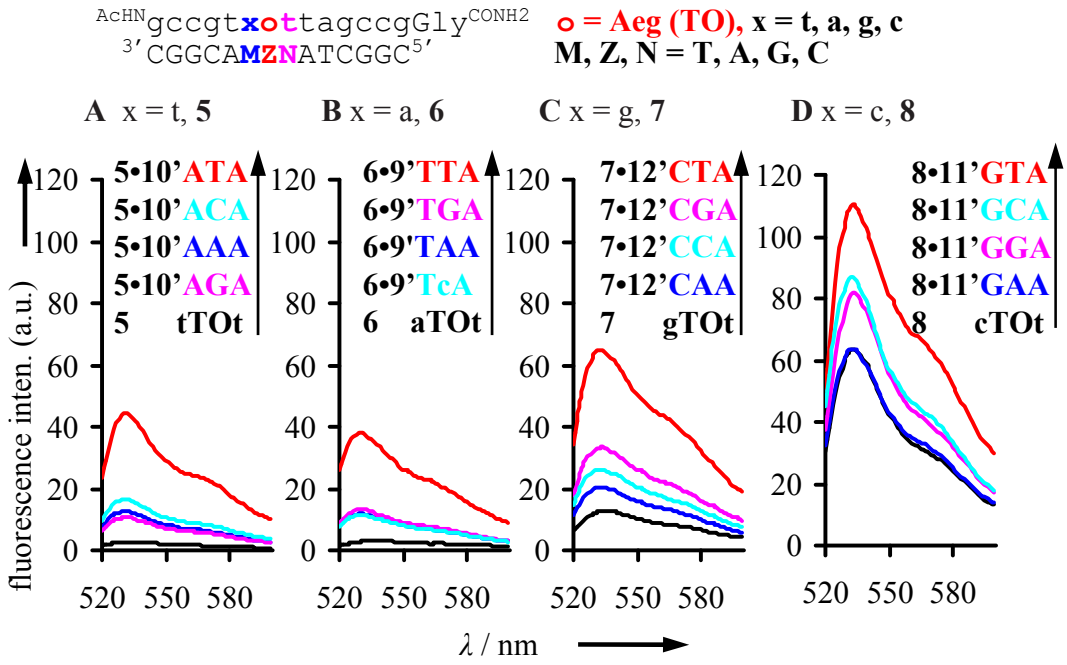

Figure 76: Fluorescence spectra of Aeg-PNA before (black) and after addition of matched DNA [Z = T (red), Z = A (blue), Z = G (pink) and Z = C (turquoise)] A) t-TO-t **5, 10' (ATA, AAA, AGA** and **ACA),** B) a-TO-t **6, 9' (TTA, TAA, TGA** and **TCA)**, C) g-TO-t **7, 12' (CTA, CAA, CGA** and **CCA)**, D) c-TO-t **8, 11' (GTA, GAA, GGA** and **GCA)** at 25°C. Measurement conditions: Ex. 510 nm, Em. 518-600 nm. Ex. Slit: 5 nm and Em. Slit: 2.5 nm.

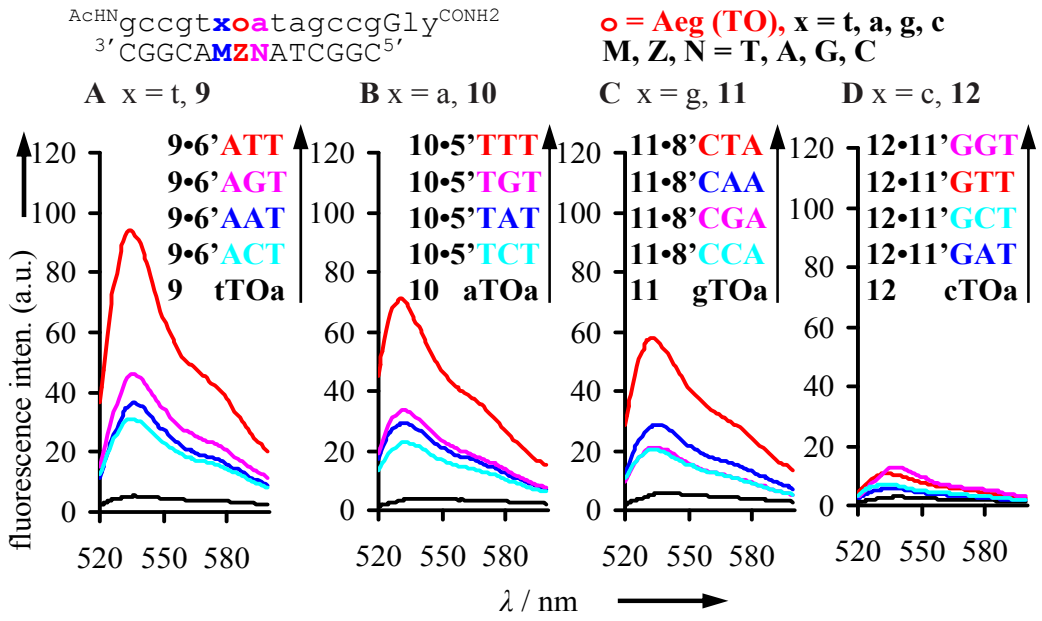

Figure 77: Fluorescence spectra of Aeg-PNA before (black) and after addition of matched DNA [Z = T (red), Z = A (blue), Z = G (pink) and Z = C (turquoise) A) t-TO-a **9, 6' (ATT, AAT, AGT** and **ACT),** B) a-TO-a **10, 5' (ATT, AAT, AGT** and **ACT)**, C) g-TO-t **11, 8' (CTA, CAA, CGA** and **CCA)**, D) c-TO-t **12, 7' (GTA, GAA, GGA** and **GCA)** at 25°C. Measurement conditions: Ex. 510 nm, Em. 518-600 nm. Ex. Slit: 5 nm and Em. Slit: 2.5 nm.

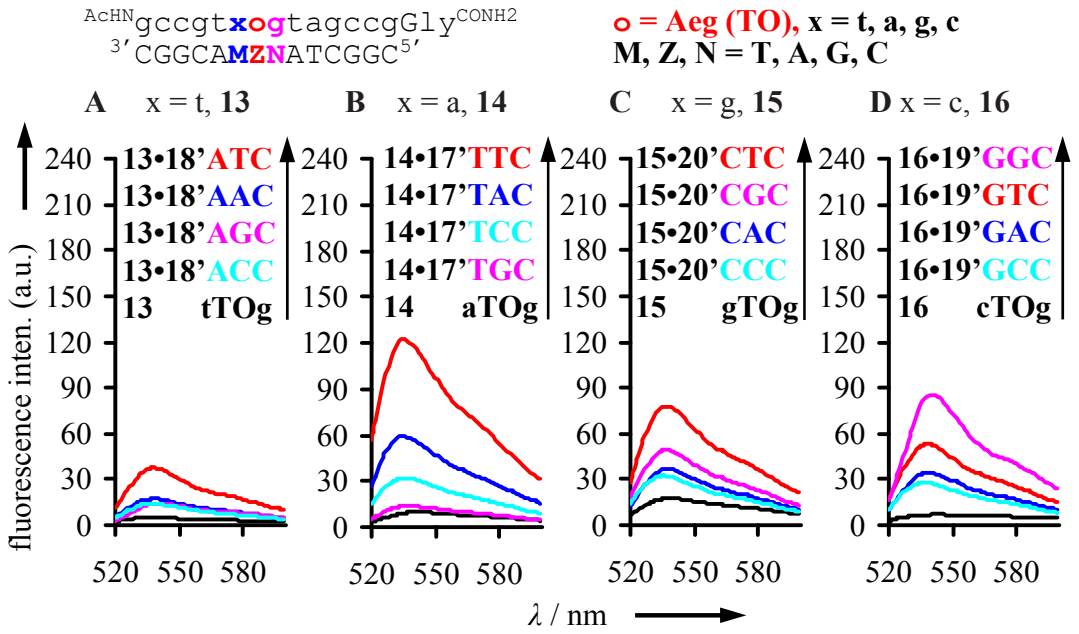

Figure 78: Fluorescence spectra of Aeg-PNA before (black) and after addition of matched DNA [Z = T (red), Z = A (blue), Z = G (pink) and Z = C (turquoise) A) t-TO-g **13, 18' (ATC, AAC, AGC** and **ACC),** B) a-TO-g **14, 17' (TTC, TAC, TGC** and **TCC)**, C) g-TO-g **15, 20' (CTC, CAC, CGC** and **CCC)**, D) c-TO-g **16, 19' (GTC, GAC, GGC** and **GCC)** at 25°C. Measurement conditions: Ex. 510 nm, Em. 518-600 nm. Ex. Slit: 5 nm and Em. Slit: 2.5 nm.

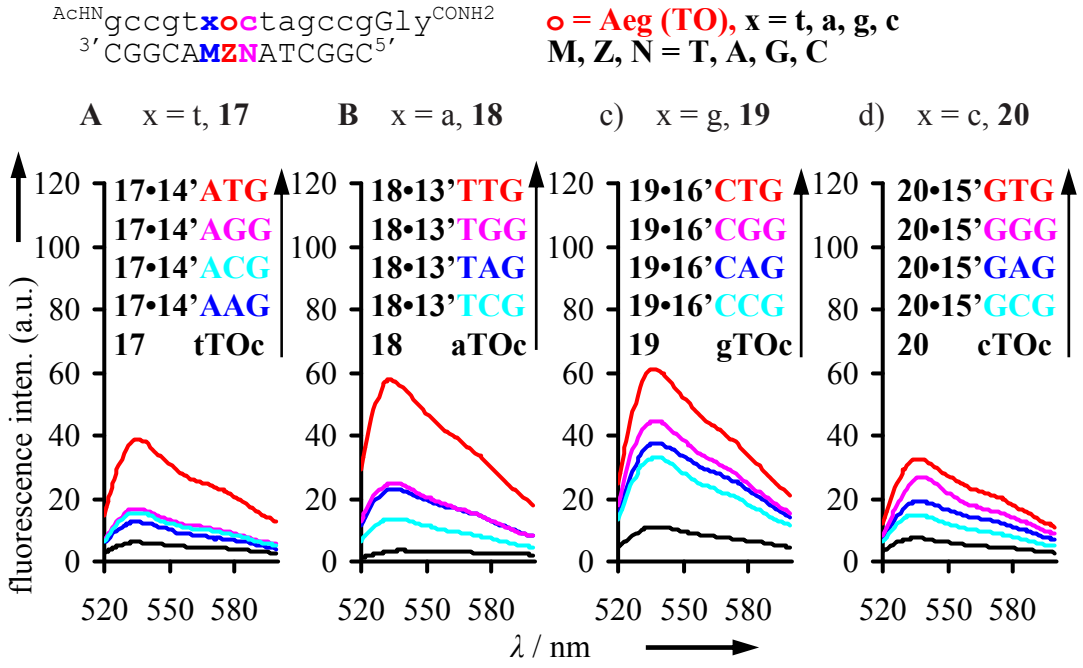

Figure 79: Fluorescence spectra of Aeg-PNA before (black) and after addition of matched DNA [Z = T (red), Z = A (blue), Z = G (pink) and Z = C (turquoise). A) t-TO-c **17, 14' (ATG, AAG, AGG** and **ACG),** B) a-TO-c **18, 13' (TTG, TAG, TGG** and **TCG)**, C) g-TO-c **19, 16' (CTG, CAG, CGG** and **CCG)**, D) c-TO-c **20, 15' (GTG, GAG, GGG** and **GCG)** at 25°C. Measurement conditions: Ex. 510 nm, Em. 518-600 nm. Ex. Slit: 5 nm and Em. Slit: 2.5 nm.

Fluorescence of TO-PNA before and after hybridisation with match and single base mismatch DNA when thymine is opposite to TO:

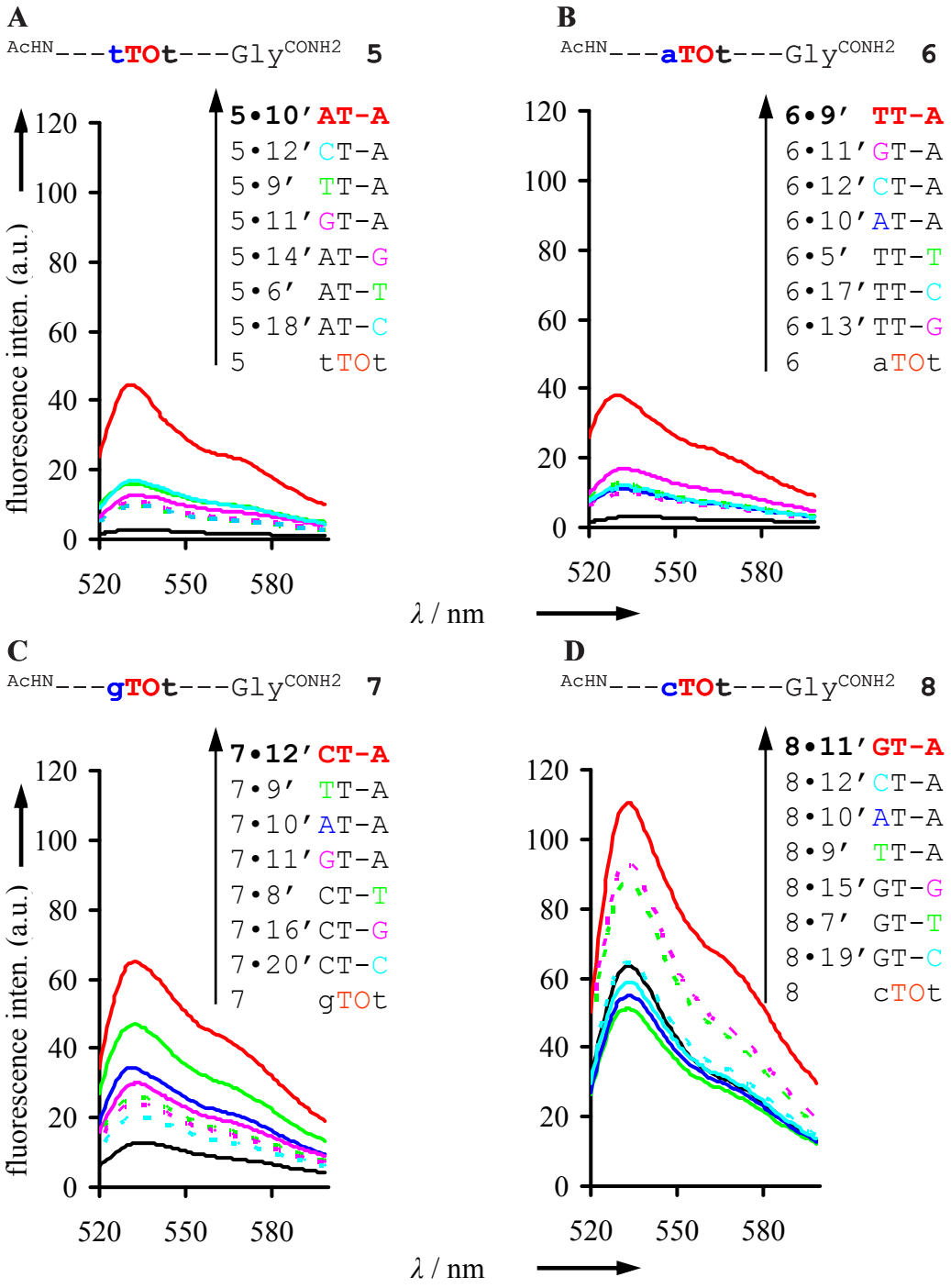

Figure 80: Fluorescence spectra of Aeg-PNA probes **5-8** A) t-TO-t, B) a-TO-t, C) g-TO-t and D) c-TO-t, before (black) and after addition of matched and mismatched DNA [red = matched, smoothed lines = mismatched towards N-side, dotted lines = mismatched towards C-side. (M or N = T green, A blue, G pink and C turquoise) when thymine act as pairing partner for Aeg-TO] at 25°C. Measurement conditions: Ex. 510 nm, Em. 518-600 nm. Ex. Slit: 5 nm and Em. Slit: 2.5 nm.

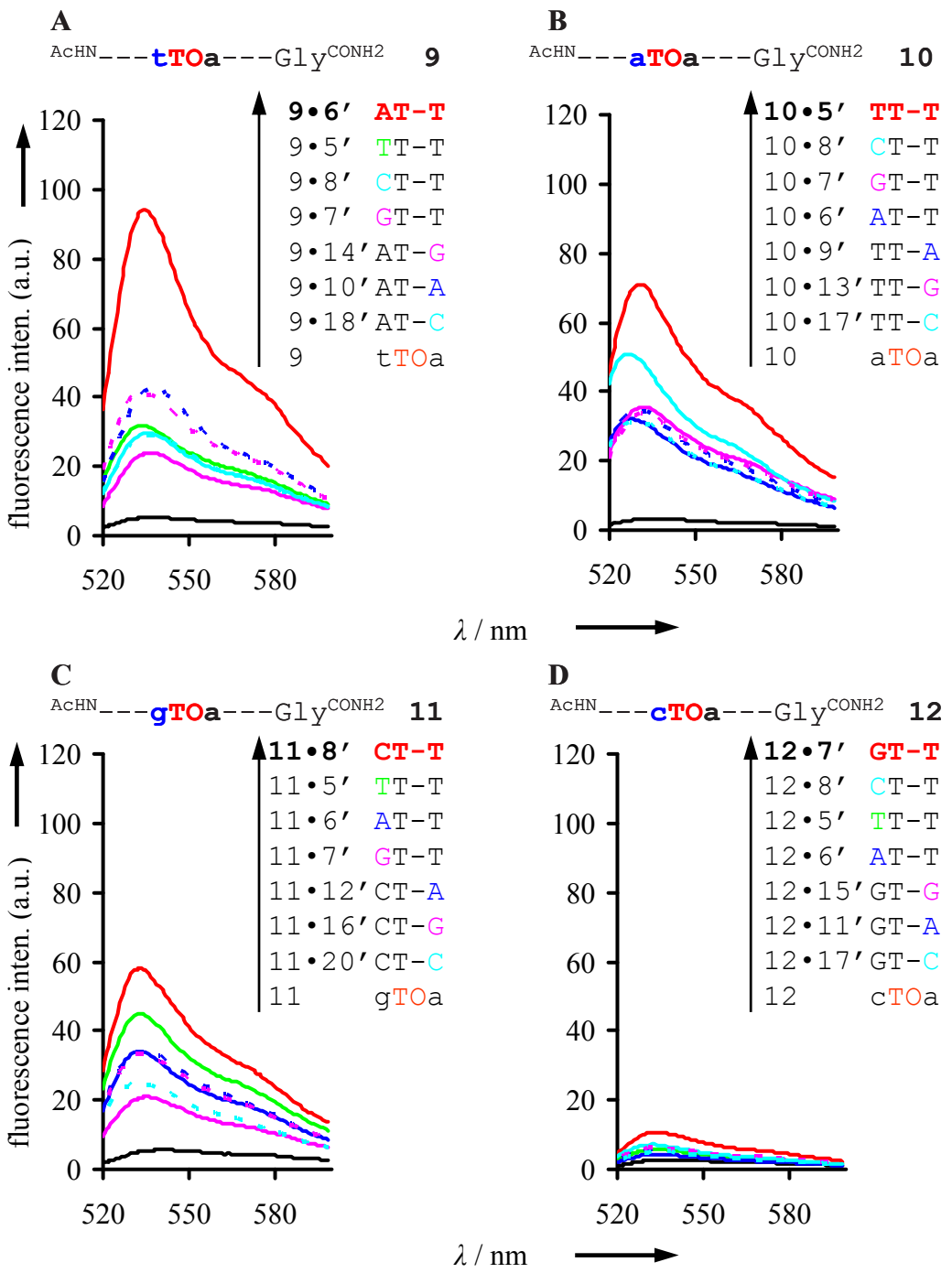

Figure 81: Fluorescence spectra of Aeg-PNA probes **9-12** A) t-TO-a, B) a-TO-a, C) g-TO-a and D) c-TO-a, before (black) and after addition of matched and mismatched DNA [red = matched, smoothed lines = mismatched towards N-side, dotted lines = mismatched towards C-side. (M or N = T green, A blue, G pink and C turquoise) when thymine act as pairing partner for Aeg-TO] at 25°C. Measurement conditions: Ex. 510 nm, Em. 518-600 nm. Ex. Slit: 5 nm and Em. Slit: 2.5 nm.

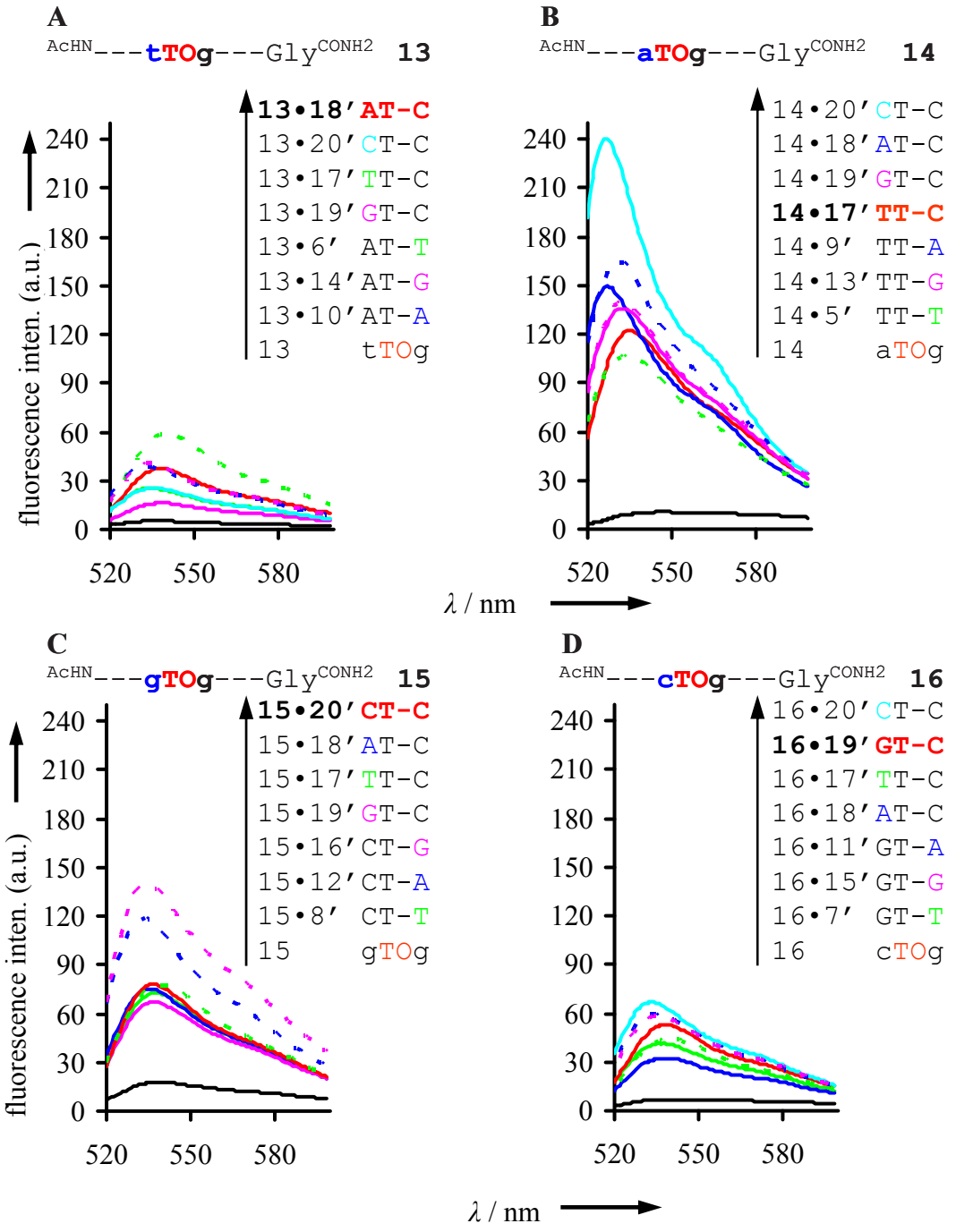

Figure 82: Fluorescence spectra of Aeg-PNA probes **13-16,** A) t-TO-g, B) a-TO-g, C) g-TO-g and D) c-TO-g, before (black) and after addition of matched and mismatched DNA [red = matched, smoothed lines = mismatched towards N-side, dotted lines = mismatched towards C-side. (M or N = T green, A blue, G pink and C turquoise) when thymine act as pairing partner for Aeg-TO] at 25°C. Measurement conditions: Ex. 510 nm, Em. 518-600 nm. Ex. Slit: 5 nm and Em. Slit: 2.5 nm.

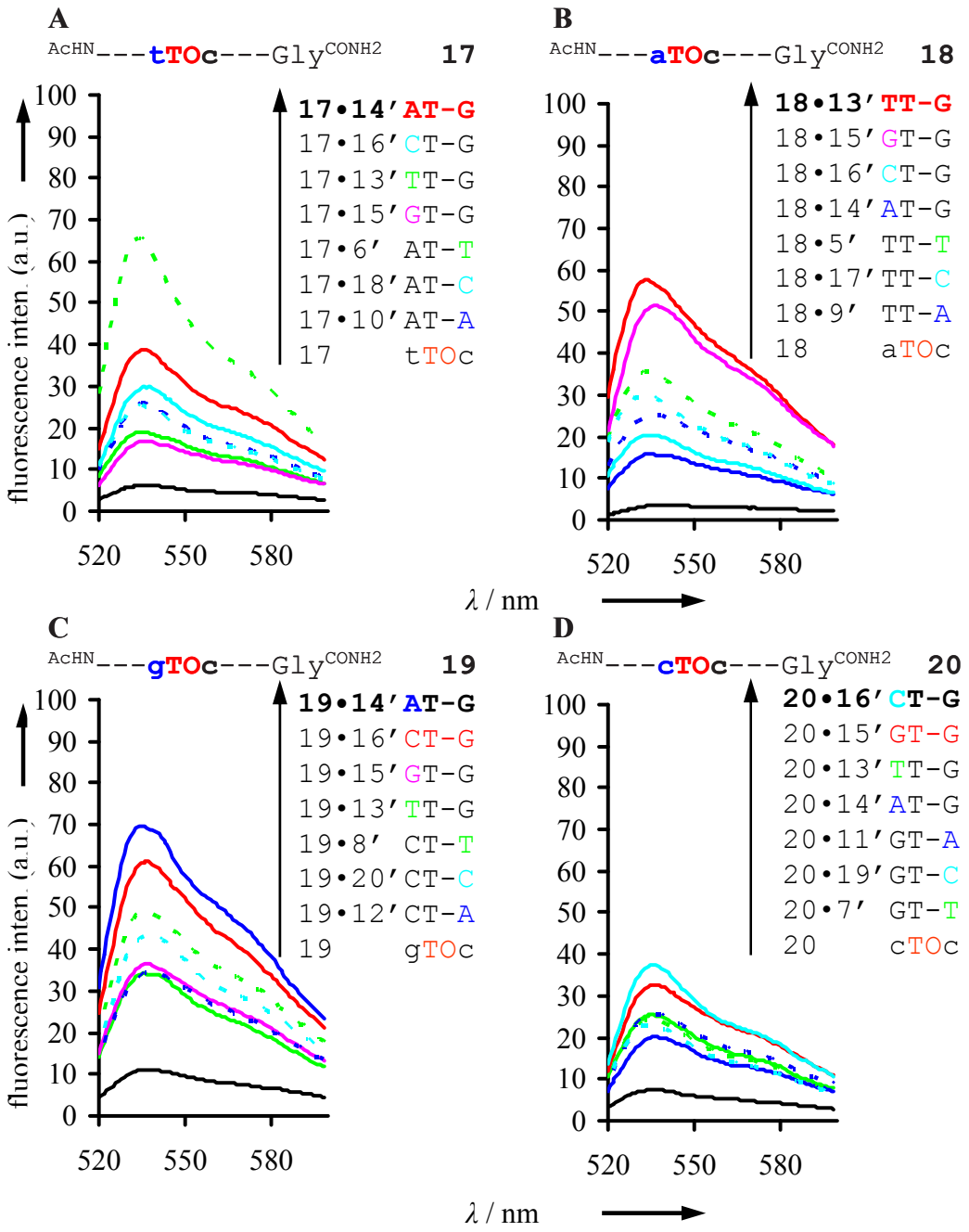

Figure 83: Fluorescence spectra of Aeg-PNA probes **17-20** A) t-TO-c, B) a-TO-c, C) g-TO-c and D) c-TO-c, before (black) and after addition of matched and mismatched DNA [red = matched, smoothed lines = mismatched towards N-side, dotted lines = mismatched towards C-side. (M or N = T green, A blue, G pink and C turquoise) when thymine act as pairing partner for Aeg-TO] at 25°C. Measurement conditions: Ex. 510 nm, Em. 518-600 nm. Ex. Slit: 5 nm and Em. Slit: 2.5 nm.

Fluorescence vs. temperature for TO-PNA before and after hybridisation with match DNA:

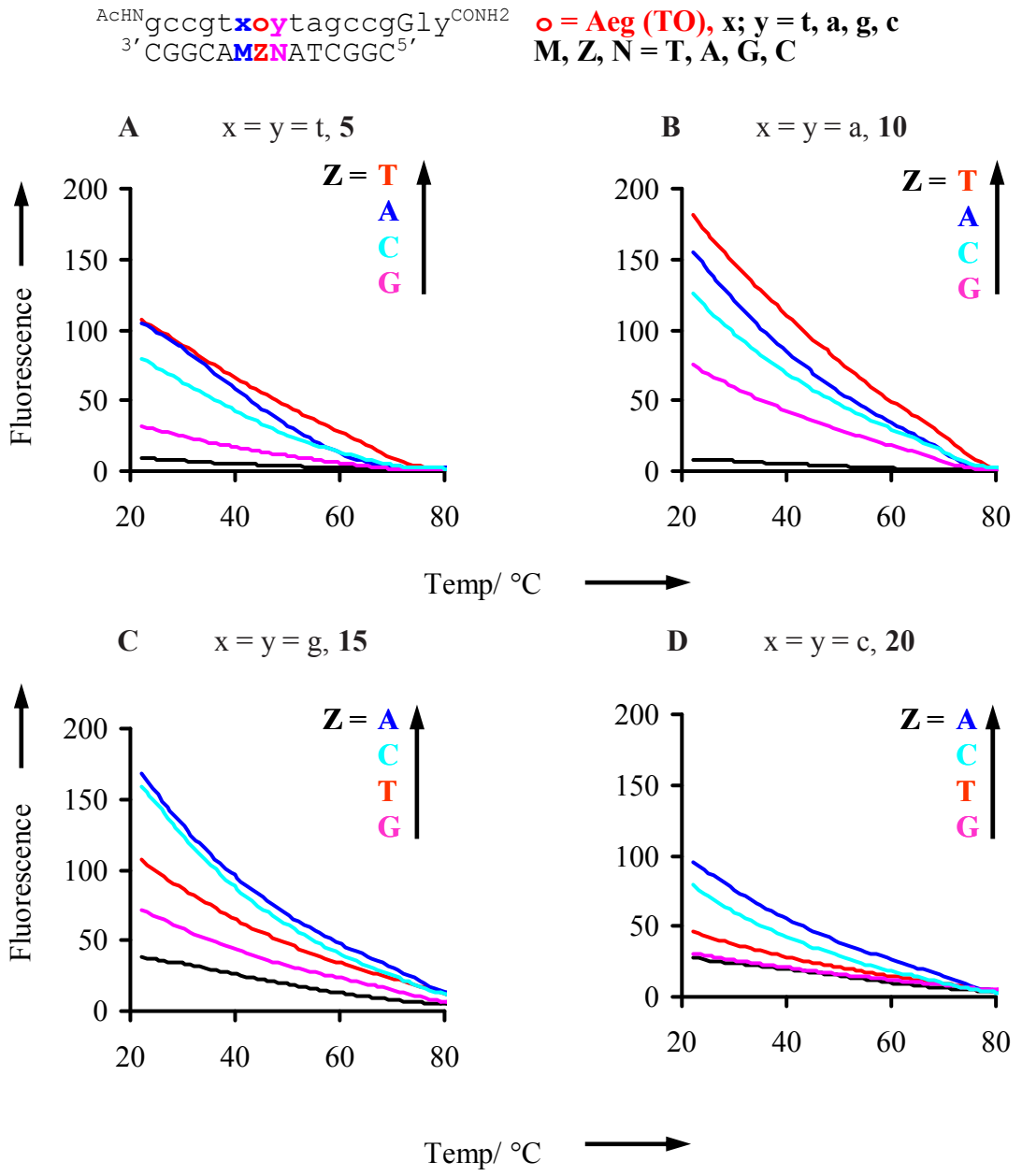

Figure 84: Fluorescence emission of Aeg-PNA plotted against temperature before (black), after addition of equimolar amount of matched DNA (TO vs T = red, TO vs A = blue, TO vs G = pink and TO vs C = turquoise). M and N are always complementry to x and y, A) **5** (t-TO-t), B) **10** (a-TO-a), C) **15** (g-TO-g) and D) **20** (c-TO-c). [Measurement conditions: 1 µM FIT-PNA or 1 µM FIT-PNA•DNA duplex in degassed buffer (100 mM NaCl, 10 mM NaH_2PO_4 at pH 7.0, Ex. 510 nm, Em. 530 nm, rate of heating 1°C/ min.)].

11.2.2 Experimental part for Section 3

***N_δ*-[9-(Fluorenylmethoxycarbonyl)-L-Ornithin]-*N_α*-[H_2]allyl ester•hydrochloride, Fmoc-L-Orn-OAll•HCl (22a):** To Fmoc-L-Orn-COOH (150 mg, 0.42 mmol) was supended in allyl alcohol (2 mL). At 0°C thionylchloride (0.2 mL) was added dropwise in 10 minutes. The mixture was stirred at 100°C for 1.5 h. After cooling to room temperature diethylether (10 mL) was added. The precipitate was collected by filtration. Repeated washings with diethyl ether yielded a colourless powder (152 mg, 84 %). The material was used without further purification.

Molecular formula:	$C_{23}H_{27}O_4N_2Cl$
R_f-value:	0.68 ($CHCl_3$/ MeOH 95:5, 1 % HCOOH)
^{1}H-NMR:	(300 MHz, [D_6] DMSO): 7.89-7.87 (m, 2H, Fmoc-$H^{4,5}$), 7.69-7.67 (m, 2H, Fmoc-$H^{1,8}$), 7.44-7.38 (m, 2H, Fmoc-$H^{3,6}$), 7.34-7.29 (m, 2H, Fmoc-$H^{2,7}$), 5.94-5.85 (m, 1H, All-H^1), 5.39 (d, J = 17.2, 1H, All-H^{3trans}), 5.20 (d, J = 10.5, 1H, All-H^{3cis}), 4.66 (d, *J* = 5.3, 2H, All-H^1), 4.28 (d, *J* = 6.6 , 2H, Fmoc-CH_2), 4.2-4.01 (m, 1H, Fmoc-H^9), 3.4-3.39 (m, 1H, α-CH), 3.02 (m, 2H, *δ*-CH_2), 1.86-1.72 (m, 2H, γ-CH_2), 1.63-1.38 (m, 2H, β-CH_2).
^{13}C-NMR:	(300 MHz, [D_6] DMSO): *δ* = 170.77, 169.06, 156.09, 143.8, 140.6, 131.6, 127.5, 127.02, 125.1, 120.0, 118.5, 65.7, 65.2, 50.5, 46.6, 27.3, 24.8.
HR-MS:	(ESI$^+$, MeOH): m/ *z*: 430.18 $[M]^+$, calc.: 430.17

***N_δ*-[9-(Fluorenylmethoxycarbonyl)-L-Orn]-*N_α*-[2-(1-Carboxy-methyl-1H-quinoline-4-ylidenmethyl)-3-methyl-benzothiazol-3-ium Bromide] allyl ester, Fmoc-L-Orn (TO)-OAll (23a):**To TO-COOH (100 mg, 0.23 mmol) in dry DMF (2.3 mL) was added PyBop (145 mg, 0.279 mmol), pyridinium *p*-toluene sulfonate (58 mg, 0.232 mmol) and N-methyl morpholine (23 mg, 0.23 mmol). The suspension was stirred under argon until a clear solution was obtained. This solution was added to a solution of amine hydrochloride **22a** (100 mg, 0.23 mmol) and N-methyl morpholine (23 mg, 0.23 mmol) in DMF (2.3 mL). The reaction mixture was stirred

for 12 h under argon. The volatiles were removed under reduced pressure. To the residue methanol (2 mL) was added. After stirring for 1 h the precipitate was collected by filtration and washed with methanol (5 mL). The crude product was purified by column chromatography ($CHCl_3$:MeOH 97:3, 1 % formic acid) to yield an orange coloured solid (118 mg, 63 %).

Molecular formula:	$C_{43}H_{41}O_5N_4{}^{32}S^+$
R_f-value:	0.56 ($CHCl_3$/ MeOH 80:20, 1 % HCOOH)
^{1}H-NMR:	(300 MHz, [D_6] DMSO:TFA, 10:1.5): δ = 8.73 (d, J = 8.4, 1H, Ar-H^{q5}), 8.51 (d, J = 7.3, 1H, Ar-H^{q2}), 8.01 (d, J = 7.7, 1H, Ar-H^{b1}), 7.91-7.86 (m, 2H, Fmoc-$H^{4,5}$), 7.80-7.72 (m, 2H, Ar-$H^{q7,8}$), 7.68 (m, 1H, Ar-H^{b4}), 7.66-7.63 (m, 2H, Fmoc-$H^{1,8}$), 7.58-7.56 (m, 1H, Ar-H^{b3}), 7.53-7.48 (m, 1H, Ar-H^{b2}), 7.47-7.44 (m, 1H, Ar-H^{q6}), 7.40-7.37 (m, 2H, Fmoc-$H^{3,6}$), 7.37-7.33 (m, 2H, Fmoc-$H^{2,7}$), 7.31-7.28 (m, 1H, Ar-H^{q3}), 6.87 (s, 1H, Cyanin-H), 5.96-5.83 (m, 1H, All-H^1), 5.45 (s, 2H, methylene-H), 5.32 (d, J = 17.2, 1H, All-H^{3trans}), 5.24 (d, J = 10.5, 1H, All-H^{3cis}), 4.67 (d, J = 5.3, 2H, All-H^1), 4.29 (d, J = 6.6, 2H, FmoC-CH_2), 4.21-4.16 (m, 1H, Fmoc-H^9), 4.08-4.06 (m, 1H, α-CH), 3.99 (s, 3H, Me-H), 2.99 (m, 2H, δ-CH_2), 1.81-1.71 (m, 2H, γ-CH_2), 1.58-1.43 (m, 2H, β-CH_2).
^{13}C-NMR:	(300 MHz, [D_6] DMSO:TFA, 10:1.5): δ = 169.7, 169.2, 161.3, 159.2, 158.7, 156.7, 149.1, 145.5, 141.2, 140.8, 137.8, 139.04, 138.2, 133.6, 132.1, 128.6, 128.0, 127.9, 127.5, 126.1, 126.0, 125.6, 125.4, 124.6, 124.2, 123.3, 122.9, 121.2, 120.5, 120.4, 119.1, 118.1, 117.5, 113.7, 107.9, 89.3, 65.4, 65.8, 55.1, 52.2, 47.2, 34.4.
HR-MS:	(ESI$^+$, MeOH): m/ z: 725.20 [M]$^+$, calc.: 725.28

***N_δ*-[9-(Fluorenylmethoxycarbonyl)-L-Orn]-*N_α*-[2-(1-Carboxy-methyl-1H-quinoline-4-ylidenmethyl)-3-methyl-benzothiazol-3-ium Bromide] OH, Fmoc-L-Orn (TO)-OH (24a):** To a solution of **23a** (81 mg, 0.1 mmol) in THF (5 mL) was added N-Methylaniline (11.3 mg, 0.1 mmol). The solution was degassed by

freeze-thaw-pump cycles. After addition of [Pd $(PPh_3)_4$] (12 mg, 0.01 mmol) the mixture was stirred for 14 h under exclusion of light. The solvent was removed in vacuo. To the residue was added methanol (4 mL). The resulting precipitate was collected by filtration. The crude product was purified by column chromatography ($CHCl_3$: MeOH 97:3, 1 % formic acid) to yield an orange coloured solid (53 mg, 68 %).

Molecular formula:	$C_{40}H_{37}O_5N_4{}^{32}S^+$
R_f-value:	0.22 ($CHCl_3$/ MeOH 80:20, 1 % HCOOH)
^{1}H-NMR:	(300 MHz, [D_6] DMSO:TFA, 10:1.5): δ = 8.74 (d, J = 8.4, 1H, Ar-H^{q5}), 8.50 (d, J = 7.3, 1H, Ar-H^{q2}), 8.02 (d, 1H, J = 7.8, Ar-H^{b1}), 7.90-7.87 (m, 2H, Fmoc-$H^{4,5}$), 7.86-7.8 (m, 2H, Ar-$H^{q7,8}$), 7.69 (m, 1H, Ar-H^{b4}), 7.67-7.65 (m, 2H, Fmoc-$H^{1,8}$), 7.63-7.58 (m, 1H, Ar-H^{q6}), 7.55-7.52 (m, 1H, Ar-H^{b3}), 7.47-7.44 (m, 1H, Ar-H^{b2}), 7.42-7.38 (m, 2H, Fmoc-$H^{3,6}$), 7.39-7.34 (m, 2H, Fmoc-$H^{2,7}$), 7.32 (m, 1H, Ar-H^{q3}), 6.89 (s, 1H, Cyanin-H), 5.45 (s, 2H, methylene-H), 4.29-4.27 (d, J = 6.8, 2H, Fmoc-CH_2), 4.18 (m, 1H, Fmoc-H^9), 3.98 (s, 3H, Me-H), 3.90 (m, 1H, -α-CH), 3.01-2.94 (m, 2H, δ-CH_2), 1.80-1.70 (m, 2H, γ-CH_2), 1.57-1.49(m, 2H, β-CH_2).
^{13}C-NMR:	(300 MHz, [D_6] DMSO:TFA, 10:1.5): δ = 171.1, 168.4, 160.9, 159.3, 158.8, 158.3, 148.6, 144.0, 140.8, 137.8, 133.2, 128.3, 128.3, 127.7, 127.1, 126.6, 125.1, 124.8, 124.1, 123.7, 122.9, 120.2, 117.1, 113.8, 113.3, 109.5, 107.5, 88.9, 65.4, 51.9, 46.8, 34.0.
HR-MS:	(ESI$^+$, MeOH): m/ z: 685.24 [M]$^+$, calc.: 685.24

N_δ-[9-(Fluorenylmethoxycarbonyl)-D-Ornithin]-N_α-[H_2]allyl ester•hydrochlorid, Fmoc-D-Orn-OAll•HCl (22b): Fmoc-D-Orn-OAll•HCl was synthesised starting from Fmoc-D-Orn-COOH using procedure described for **22a** (160 mg, 88 %).

Molecular formula:	$C_{23}H_{27}O_4N_2Cl$
R_f-value:	0.68 ($CHCl_3$/ MeOH 95:5, 1 % HCOOH)
^{1}H-NMR:	(300 MHz, [D_6] DMSO): 7.89-7.87 (m, 2H, Fmoc-$H^{4,5}$), 7.69-

	7.67 (m, 2H, Fmoc-$H^{1,8}$), 7.44-7.38 (m, 2H, Fmoc-$H^{3,6}$), 7.34-7.29 (m, 2H, Fmoc-$H^{2,7}$), 5.94-5.85 (m, 1H, All-H^{1}), 5.39 (d, J = 17.2, 1H, All-H^{3trans}), 5.20 (d, J = 10.5, 1H, All-H^{3cis}), 4.66 (d, *J* = 5.3, 2H, All-H^{1}), 4.28 (d, *J* = 6.6 , 2H, FmoC-CH_2), 4.2-4.01 (m, 1H, Fmoc-H^{9}), 3.4-3.39 (m, 1H, α-CH), 3.02 (m, 2H, *δ*-CH_2), 1.86-1.72 (m, 2H, γ-CH_2), 1.63-1.38 (m, 2H, β-CH_2).
^{13}C-NMR:	(300 MHz, [D_6] DMSO): *δ* = 187.17, 169.0, 156.09, 143.8, 140.6, 131.6, 127.5, 127.02, 125.1, 120.0, 118.5, 65.7, 65.2, 55.5, 46.6, 27.3, 24.8.
HR-MS:	(ESI$^+$, MeOH): m/ *z*: 430.17 $[M]^+$, calc.: 430.17

***N*$_\delta$-[9-(Fluorenylmethoxycarbonyl)-D-Ornithin]-*N*$_\alpha$-[2-(1-Carboxy-methyl-1H-quinoline-4-ylidenmethyl)-3-methyl-benzothiazol-3-ium Bromide] allyl ester, Fmoc-D-Orn (TO)-OAll (23b):** Fmoc-D-Orn (TO)-OAll•HCl was synthesised starting from Fmoc-D-Orn-OAll•HCl using procedure described for **23a** (103 mg, 55 %).

Molecular formula:	$C_{43}H_{41}O_5N_4{}^{32}S^+$
R_f-value:	0.56 ($CHCl_3$/ MeOH 80:20, 1 % HCOOH)
^{1}H-NMR:	(300 MHz, [D_6] DMSO:TFA, 10:1.5): *δ* = 8.73 (d, *J* = 8.4, 1H, Ar-H^{q5}), 8.51 (d, *J* = 7.3, 1H, Ar-H^{q2}), 8.01 (d, *J* = 7.7, 1H, Ar-H^{b1}), 7.91-7.86 (m, 2H, Fmoc-$H^{4,5}$), 7.80-7.72 (m, 2H, Ar-$H^{q7,8}$), 7.68 (m, 1H, Ar-H^{b4}), 7.66-7.63 (m, 2H, Fmoc-$H^{1,8}$), 7.58-7.56 (m, 1H, Ar-H^{b3}), 7.53-7.48 (m, 1H, Ar-H^{b2}), 7.47-7.44 (m, 1H, Ar-H^{q6}), 7.40-7.37 (m, 2H, Fmoc-$H^{3,6}$), 7.37-7.33 (m, 2H, Fmoc-$H^{2,7}$), 7.31-7.28 (m, 1H, Ar-H^{q3}), 6.87 (s, 1H, Cyanin-H), 5.96-5.83 (m, 1H, All-H^{1}), 5.45 (s, 2H, methylene-H), 5.32 (d, J = 17.2, 1H, All-H^{3trans}), 5.24 (d, J = 10.5, 1H, All-H^{3cis}), 4.67 (d, *J* = 5.3, 2H, All-H^{1}), 4.29 (d, *J* = 6.6 , 2H, FmoC-CH_2), 4.21-4.16 (m, 1H, Fmoc-H^{9}), 4.08-4.06 (m, 1H, α-CH), 3.99 (s, 3H, Me-H), 2.99 (m, 2H, *δ*-CH_2), 1.81-1.71 (m, 2H, γ-CH_2), 1.58-1.43 (m, 2H, β-CH_2).
^{13}C-NMR:	(300 MHz, [D_6] DMSO:TFA, 10:1.5): *δ* = 169.7, 169.2,

	161.3, 159.2, 158.7, 156.7, 149.1, 145.5, 141.2, 140.8, 137.8, 139.04, 138.2, 133.6, 132.1, 128.6, 128.0, 127.9, 127.5, 126.1, 126.0, 125.6, 125.4, 124.6, 124.2, 123.3, 122.9, 121.2, 120.5, 120.4, 119.1, 118.1, 117.5, 113.7, 107.9, 89.3, 65.4, 65.8, 55.1, 52.2, 47.2, 34.4.
HR-MS:	(ESI$^+$, MeOH): m/ z: 430.17 $[M]^+$, calc.: 430.17

***N*$_\delta$-[9-(Fluorenylmethoxycarbonyl)-D-Ornithin]-*N*$_\alpha$-[2-(1-Carboxy-methyl-1H-quinoline-4-ylidenmethyl)-3-methyl-benzothiazol-3-ium Bromide] OH, Fmoc-D-Orn (TO)-OH (24b):** Fmoc-D-Orn (TO)-OH was synthesised starting from Fmoc-D-Orn (TO)-OAll•HCl using procedure described for **24a** (52 mg, 65 %).

Molecular formula:	$C_{40}H_{37}O_5N_4{}^{32}S^+$
R_f-value:	0.22 ($CHCl_3$/ MeOH 80:20, 1 % HCOOH)
^{1}H-NMR:	(300 MHz, [D_6]DMSO:TFA, 10:1.5): δ = 8.74 (d, J = 8.4, 1H, Ar-H^{q5}), 8.50 (d, J = 7.3, 1H, Ar-H^{q2}), 8.02 (d, 1H, J = 7.8, Ar-H^{b1}), 7.90-7.87 (m, 2H, Fmoc-H^{4,5}), 7.86-7.8 (m, 2H, Ar-H^{q7,8}), 7.69 (m, 1H, Ar-H^{b4}), 7.67-7.65 (m, 2H, Fmoc-H^{1,8}), 7.63-7.58 (m, 1H, Ar-H^{q6}), 7.55-7.52 (m, 1H, Ar-H^{b3}), 7.47-7.44 (m, 1H, Ar-H^{b2}), 7.42-7.38 (m, 2H, Fmoc-H^{3,6}), 7.39-7.34 (m, 2H, Fmoc-H^{2,7}), 7.32 (m, 1H, Ar-H^{q3}), 6.89 (s, 1H, Cyanin-H), 5.45 (s, 2H, methylene-H), 4.29-4.27 (d, J = 6.8, 2H, Fmoc-CH_2), 4.18 (m, 1H, Fmoc-H^9), 3.98 (s, 3H, Me-H), 3.90 (m, 1H, -α-CH), 3.01-2.94 (m, 2H, δ-CH_2), 1.80-1.70 (m, 2H, γ-CH_2), 1.57-1.49(m, 2H, β-CH_2).
^{13}C-NMR:	(300 MHz, [D_6] DMSO:TFA, 10:1.5): δ = 171.1, 168.4, 160.9, 159.3, 158.8, 158.3, 148.6, 144.0, 140.8, 137.8, 133.2, 128.3, 128.3, 127.7, 127.1, 126.6, 125.1, 124.8, 124.1, 123.7, 122.9, 120.2, 117.1, 113.8, 113.3, 109.5, 107.5, 88.9, 65.4, 51.9, 46.8, 34.0.
HR-MS:	(ESI$^+$, MeOH): m/ z: 685.24 $[M]^+$, calc.: 685.24

^{AcHN}gccgtt-D-Orn (TO)-ttagccgGly^{CONH2}, 25

13 mg (≈ 4 µmol) of resin **4a** was used. The PNA was manually synthesised by divergent solid phase synthesis.

Yield: OD_{260} = 19.8, 150 nmol, 4.0 %

ε_{260}	133.000 L•mol^{-1}•cm^{-1}
MALDI-TOF/MS; *m/z*	4070 $[M+H]^+$, calc.: 4070
HPLC	t_R = 14.5 min (Gradient B)
$C_{156}H_{189}N_{76}O_{40}S^+$	4069.6

^{AcHN}gccgta-D-Orn (TO)-ttagccgGly^{CONH2}, 26

13 mg (≈ 4 µmol) of resin **4a** was used. The PNA was manually synthesised by divergent solid phase synthesis.

Yield: OD_{260} = 13.5, 101 nmol, 2.6 %

ε_{260}	134.000 L•mol^{-1}•cm^{-1}
MALDI-TOF/MS; *m/z*	4083 $[M+H]^+$, calc.: 4079
HPLC	t_R = 13.9 min (Gradient B)
$C_{156}H_{189}N_{76}O_{40}S^+$	4078.6

^{AcHN}gccgtg-D-Orn (TO)-ttagccgGly^{CONH2}, 27

13 mg (≈ 4 µmol) of resin **4a** was used. The PNA was manually synthesised by divergent solid phase synthesis.

Yield: OD_{260} = 10.4, 80 nmol, 2.0 %

ε_{260}	131.000 L•mol^{-1}•cm^{-1}
MALDI-TOF/MS; *m/z*	4096 $[M+H]^+$, calc.: 4095
HPLC	t_R = 14.0 min (Gradient B)
$C_{156}H_{189}N_{76}O_{40}S^+$	4094.6

^{AcHN}gccgtc-D-Orn (TO) -ttagccgGly^{CONH2}, 28

13 mg (≈ 4 µmol) of resin **4a** was used. The PNA was manually synthesised by divergent solid phase synthesis.

Yield: OD_{260} = 51.0, 400 nmol, 10.0 %

ε_{260}	128.000 L•mol^{-1}•cm^{-1}
MALDI-TOF/MS; *m/z*	4058 $[M+H]^+$, calc.: 4055

HPLC	t_R = 14.7 min (Gradient B)
$C_{156}H_{189}N_{76}O_{40}S^+$	4054.6

^{AcHN}gccgtt-D-Orn (TO)-atagccgGly^{CONH2}, 29

13 mg (≈ 4 μmol) of resin **4a** was used. The PNA was manually synthesised by divergent solid phase synthesis.

Yield: OD_{260} = 26.88, 200 nmol, 5.0 %

ε_{260}	134.000 L•mol^{-1}•cm^{-1}
MALDI-TOF/MS; *m/z*	4080 $[M+H]^+$, calc.: 4079
HPLC	t_R = 14.8 min (Gradient B)
$C_{156}H_{189}N_{76}O_{40}S^+$	4078.6

^{AcHN}gccgta-D-Orn (TO)-atagccgGly^{CONH2}, 30

13 mg (≈ 4 μmol) of resin **4a** was used. The PNA was manually synthesised by divergent solid phase synthesis.

Yield: OD_{260} = 24.5, 180 nmol, 4.8 %

ε_{260}	136.000 L•mol^{-1}•cm^{-1}
MALDI-TOF/MS; *m/z*	4091 $[M+H]^+$, calc.: 4088
HPLC	t_R = 13.9 min (Gradient B)
$C_{156}H_{189}N_{76}O_{40}S^+$	4087.6

^{AcHN}gccgtg-D-Orn (TO)-atagccgGly^{CONH2}, 31

13 mg (≈ 4 μmol) of resin **4a** was used. The PNA was manually synthesised by divergent solid phase synthesis.

Yield: OD_{260} = 55.34, 416 nmol, 10.4 %

ε_{260}	133.000 L•mol^{-1}•cm^{-1}
MALDI-TOF/MS; *m/z*	4106 $[M+H]^+$, calc.: 4104
HPLC	t_R = 13.2 min (Gradient B)
$C_{156}H_{189}N_{76}O_{40}S^+$	4103.6

^{AcHN}gccgtc-D-Orn (TO)-atagccgGly^{CONH2}, 32

13 mg (≈ 4 μmol) of resin **4a** was used. The PNA was manually synthesised by divergent solid phase synthesis.

Yield: OD_{260} = 36.91, 285 nmol, 7.14 %

ε_{260}	130.000 L•mol^{-1}•cm^{-1}
MALDI-TOF/MS; *m/z*	4065 $[M+H]^+$, calc.: 4064
HPLC	t_R = 13.7 min (Gradient B)
$C_{156}H_{189}N_{76}O_{40}S^+$	4063.6

^{AcHN}gccgtt-D-Orn (TO)-gtagccgGly^{CONH2}, 33

7 mg (≈ 2 μmol) of resin **4a** was used. The PNA was synthesised by linear solid phase synthesis using automated solid phase PNA synthesis.

Yield: OD_{260} = 10.48, 80 nmol, 4.0 %

ε_{260}	131.000 L•mol^{-1}•cm^{-1}
MALDI-TOF/MS; *m/z*	4095 $[M+H]^+$, calc.: 4095
HPLC	t_R = 14.5 min (Gradient B)
$C_{156}H_{189}N_{76}O_{40}S^+$	4094.6

^{AcHN}gccgta-D-Orn (TO)-gtagccgGly^{CONH2}, 34

7 mg (≈ 2 μmol) of resin **4a** was used. The PNA was synthesised by linear solid phase synthesis using automated solid phase PNA synthesis.

Yield: OD_{260} = 29.26, 220 nmol, 11.0 %

ε_{260}	133.000 L•mol^{-1}•cm^{-1}
MALDI-TOF/MS; *m/z*	4107 $[M+H]^+$, calc.: 4104
HPLC	t_R = 14.7 min (Gradient B)
$C_{156}H_{189}N_{76}O_{40}S^+$	4103.6

^{AcHN}gccgtg-D-Orn (TO)-gtagccgGly^{CONH2}, 35

7 mg (≈ 2 μmol) of resin **4a** was used. The PNA was synthesised by linear solid phase synthesis using automated solid phase PNA synthesis.

Yield: OD_{260} = 24.18, 185 nmol, 9.25 %

ε_{260}	130.000 L•mol^{-1}•cm^{-1}
MALDI-TOF/MS; *m/z*	4121 $[M+H]^+$, calc.: 4120

HPLC	t_R = 13.9 min (Gradient B)
$C_{156}H_{189}N_{76}O_{40}S^+$	4119.6

^{AcHN}gccgtc-D-Orn (TO)-gtagccgGly^{CONH2}, 36

7 mg (≈ 2 μmol) of resin **4a** was used. The PNA was synthesised by linear solid phase synthesis using automated solid phase PNA synthesis.

Yield: OD_{260} = 15.8, 125 nmol, 6.25 %

ε_{260}	126.000 L•mol^{-1}•cm^{-1}
MALDI-TOF/MS; *m/z*	4082 $[M+H]^+$, calc.: 4080
HPLC	t_R = 13.2 min (Gradient B)
$C_{156}H_{189}N_{76}O_{40}S^+$	4079.6

^{AcHN}gccgtt-D-Orn (TO)-ctagccgGly^{CONH2}, 37

7 mg (≈ 2 μmol) of resin **4a** was used. The PNA was synthesised by linear solid phase synthesis using automated soild phase PNA synthesiser.

Yield: OD_{260} = 12.14, 99 nmol, 4.95 %

ε_{260}	128.000 L•mol^{-1}•cm^{-1}
MALDI-TOF/MS; *m/z*	4058 $[M+H]^+$, calc.: 4055
HPLC	t_R = 12.7 min (Gradient B)
$C_{156}H_{189}N_{76}O_{40}S^+$	4054.6

^{AcHN}gccgta-D-Orn (TO)-ctagccgGly^{CONH2}, 38

7 mg (≈ 2 μmol) of resin **4a** was used. The PNA was synthesised by linear solid phase synthesis using automated solid phase PNA synthesis.

Yield: OD_{260} = 18.11, 142 nmol, 7.1 %

ε_{260}	130.000 L•mol^{-1}•cm^{-1}
MALDI-TOF/MS; *m/z*	4065 $[M+H]^+$, calc.: 4064
HPLC	t_R = 12.4 min (Gradient B)
$C_{156}H_{189}N_{76}O_{40}S^+$	4063.6

^{AcHN}gccgtg-D-Orn (TO)-ctagccgGly^{CONH2}, 39

7 mg (≈ 2 μmol) of resin **4a** was used. The PNA was synthesised by linear solid phase synthesis using automated solid phase PNA synthesis.

Yield: OD_{260} = 25.93, 205 nmol, 10.25 %

ε_{260}	126.000 L•mol^{-1}•cm^{-1}
MALDI-TOF/MS; *m/z*	4081 $[M+H]^+$, calc.: 4080
HPLC	t_R = 14.5 min (Gradient B)
$C_{156}H_{189}N_{76}O_{40}S^+$	4079.6

^{AcHN}gccgtc-D-Orn (TO)-ctagccgGly^{CONH2}, 40

7 mg (≈ 2 μmol) of resin **4a** was used. The PNA was synthesised by linear solid phase synthesis using automated solid phase PNA synthesis.

Yield: OD_{260} = 23.61, 192 nmol, 9.6 %

ε_{260}	123.000 L•mol^{-1}•cm^{-1}
MALDI-TOF/MS; *m/z*	4041 $[M+H]^+$, calc.: 4040
HPLC	t_R = 13.9 min (Gradient B)
$C_{156}H_{189}N_{76}O_{40}S^+$	4039.6

Fluorescence measurements: Fluorescence emission measurements were performed by applying procedures described in section **11.2.1**.

Fluorescence of TO-PNA before and after hybridisation with matched DNA:

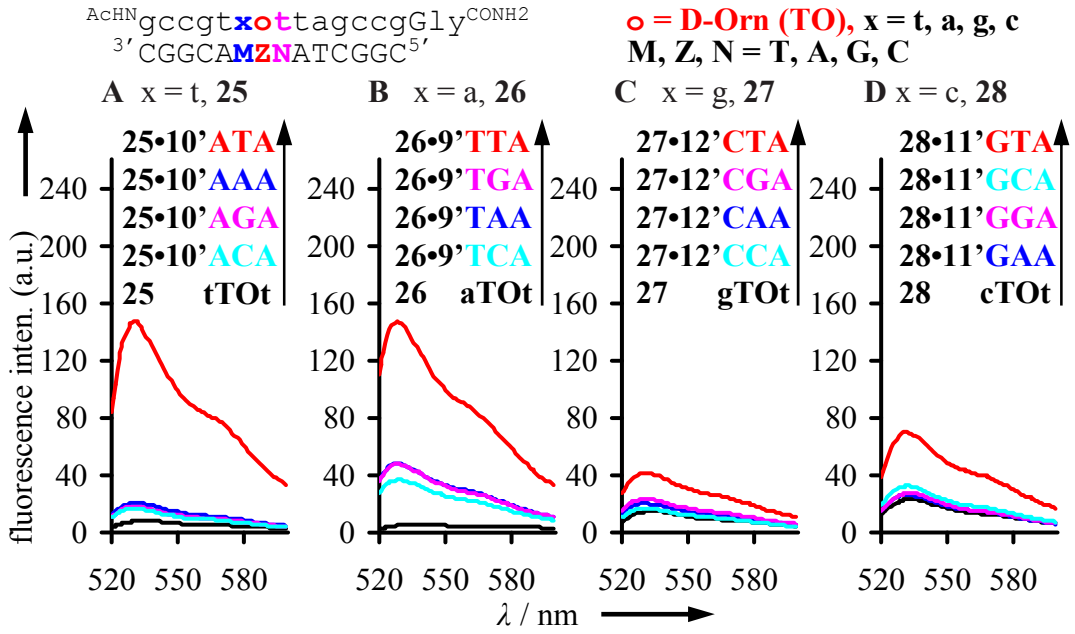

Figure 85: Fluorescence spectra of D-Orn-PNA before (black) and after addition of matched DNA [Z = T (red), Z = A (blue), Z = G (pink) and Z = C (turquoise), A) t-TO-t **25, 10'** (ATA, AAA, AGA and ACA), B) a-TO-t **26, 9'** (TTA, TAA, TGA and TCA), C) g-TO-t **27, 12'** (CTA, CAA, CGA and CCA), D) c-TO-t **28, 11'** (GTA, GAA, GGA and GCA) at 25°C. Measurement conditions: Ex. 510 nm, Em. 518-600 nm. Ex. Slit: 5 nm and Em. Slit: 2.5 nm.

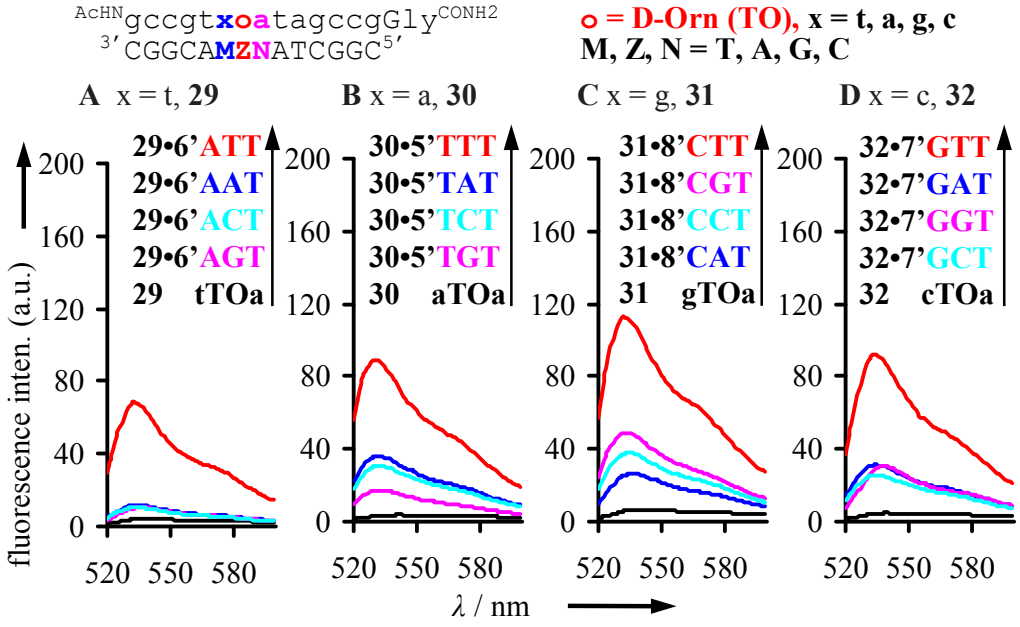

Figure 86: Fluorescence spectra of D-Orn-PNA before (black) and after addition of matched DNA [Z = T (red), Z = A (blue), Z = G (pink) and Z = C (turquoise), A) t-TO-a **29, 6'** (ATT, AAT, AGT and ACT), B) a-TO-a **30, 5'** (TTT, TAT, TGT and TCT), C) g-TO-a **31, 8'** (CTT, CAT, CGT and CCT), D) c-TO-a **32, 7'** (GTT, GAT, GGT and GCT) at 25°C. Measurement conditions: Ex. 510 nm, Em. 518-600 nm. Ex. Slit: 5 nm and Em. Slit: 2.5 nm.

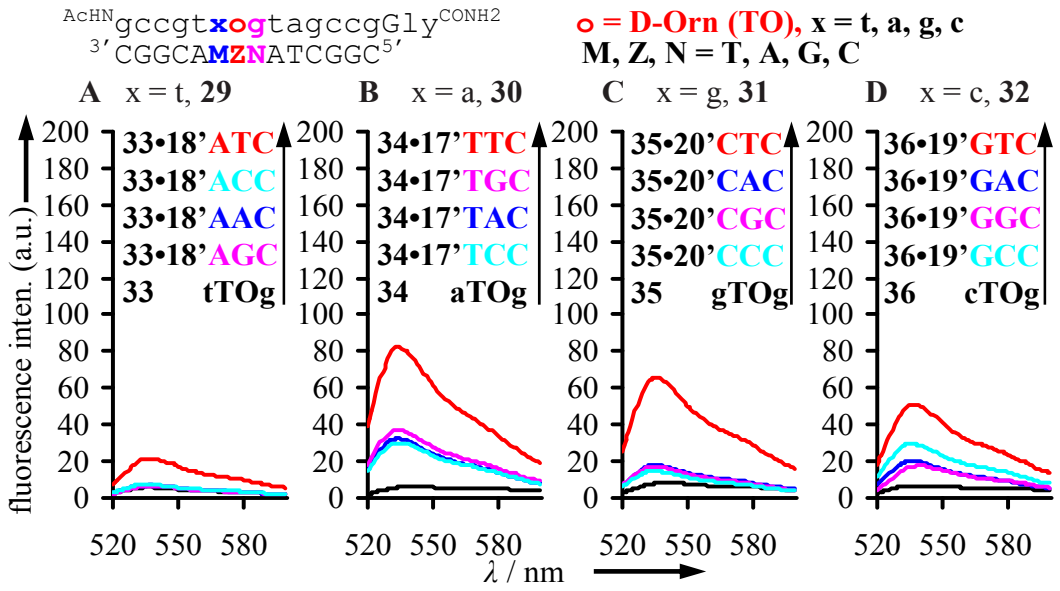

Figure 87: Fluorescence spectra of D-Orn-PNA before (black) and after addition of matched DNA [Z = T (red), Z = A (blue), Z = G (pink) and Z = C (turquoise), A) t-TO-g **33, 18'** (ATC, AAC, AGC and ACC), B) a-TO-g **34, 17'** (TTC, TAC, TGC and TCC), C) g-TO-g **35, 20'** (CTC, CAC, CGC and CCC), D) c-TO-g **36, 19'** (GTC, GAC, GGC and GCC)] at 25°C. Measurement conditions: Ex. 510 nm, Em. 518-600 nm. Ex. Slit: 5 nm and Em. Slit: 2.5 nm.

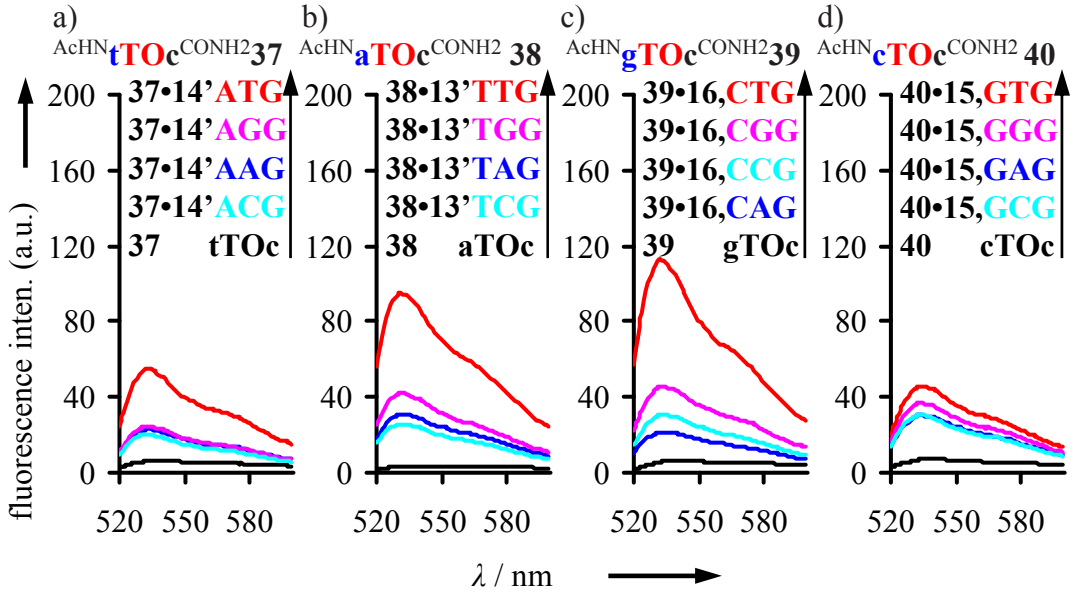

Figure 88: Fluorescence spectra of D-Orn-PNA before (black) and after addition of matched DNA [Z = T (red), Z = A (blue), Z = G (pink) and Z = C (turquoise), A) t-TO-c **37, 14'** (ATG, AAG, AGG and ACG), B) a-TO-c **38, 13'** (TTG, TAG, TGG and TCG), C) g-TO-c **39, 16'** (CTG, CAG, CGG and CCG), D) c-TO-c **40, 15'** (GTG, GAG, GGG and GCG)] at 25°C. Measurement conditions: Ex. 510 nm, Em. 518-600 nm. Ex. Slit: 5 nm and Em. Slit: 2.5 nm.

Fluorescence of TO-PNA before and after hybridisation with match and single base mismatch DNA when thymine is opposite to TO:

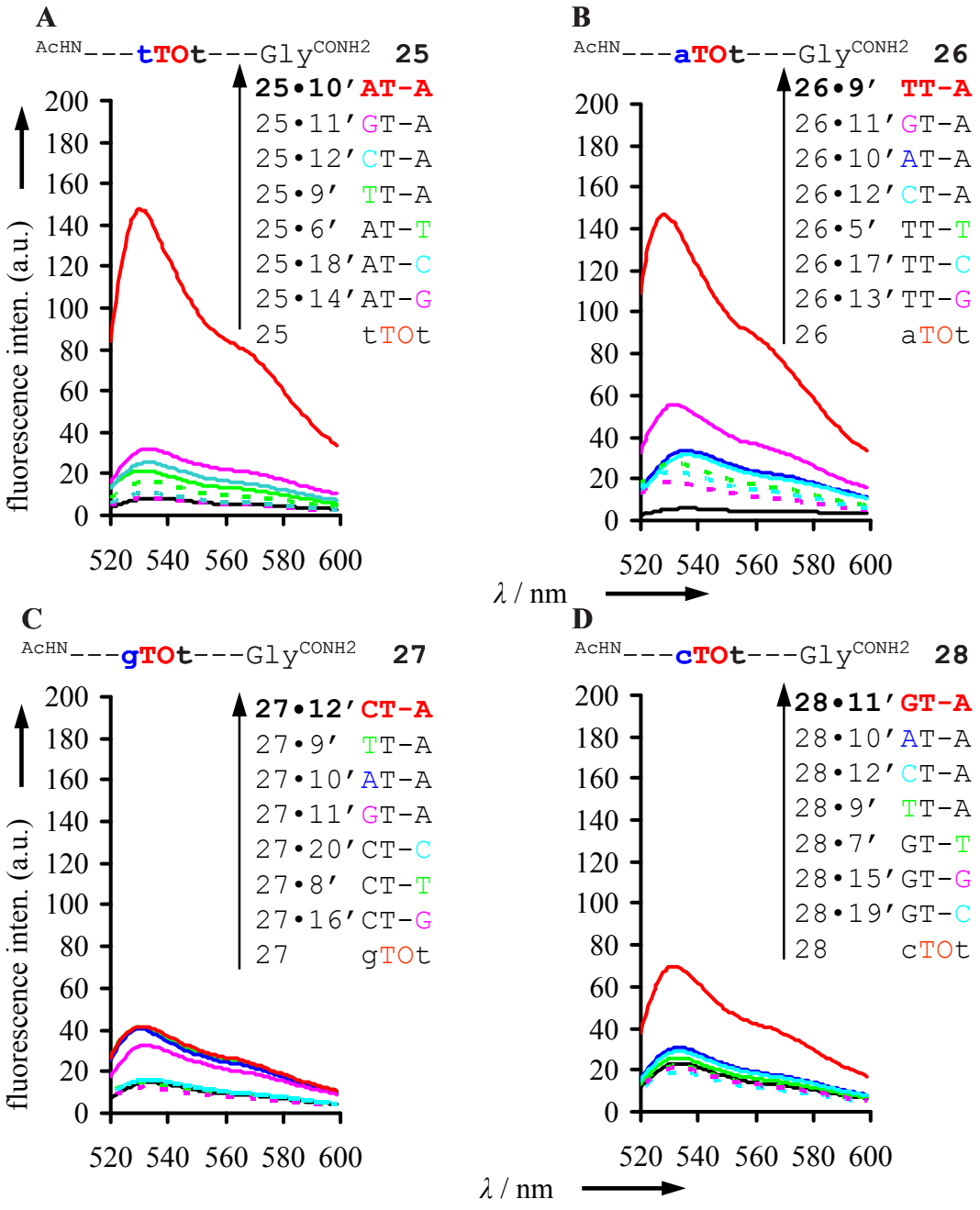

Figure 89: Fluorescence spectra of D-Orn-PNA probes **25-28** A) t-TO-t, B) a-TO-t, C) g-TO-t and D) c-TO-t, before (black) and after addition of matched and mismatched DNA [red = matched, smoothed lines = mismatched towards N-side, dotted lines = mismatched towards C-side. (M or N = T green, A blue, G pink and C turquoise) when thymine act as pairing partner for ONA-TO] at 25°C. Measurement conditions: Ex. 510 nm, Em. 518-600 nm. Ex. Slit: 5 nm and Em. Slit: 2.5 nm.

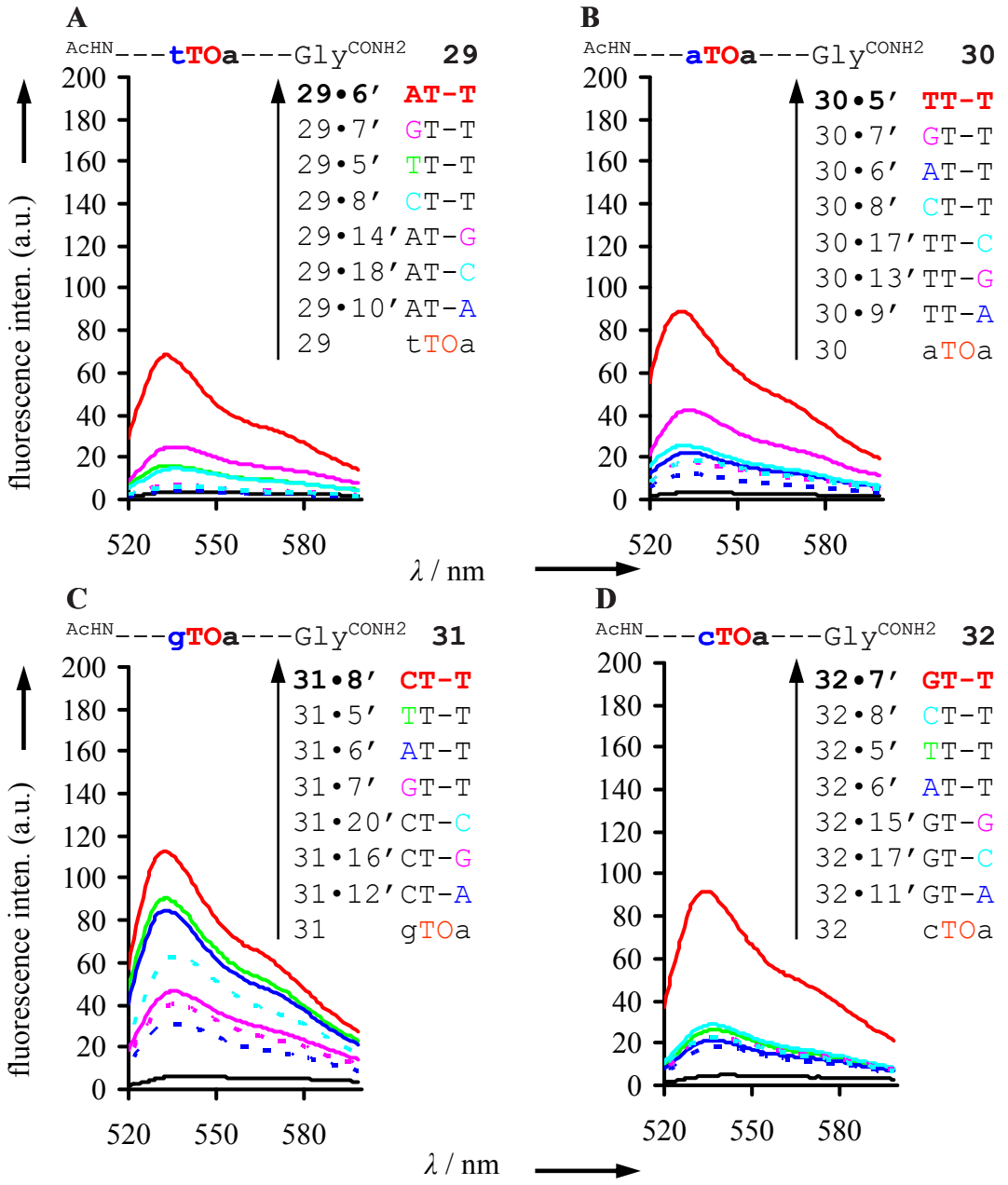

Figure 90: Fluorescence spectra of D-Orn-PNA probes **29-32** A) t-TO-a, B) a-TO-a, C) g-TO-a and D) c-TO-a, before (black) and after addition of matched and mismatched DNA [red = matched, smoothed lines = mismatched towards N-side, dotted lines = mismatched towards C-side. (M or N = T green, A blue, G pink and C turquoise) when thymine act as pairing partner for D-ONA-TO] at 25°C. Measurement condition: Ex. 510 nm, Em. 518-600 nm. Ex. Slit: 5 nm and Em. Slit: 2.5 nm.

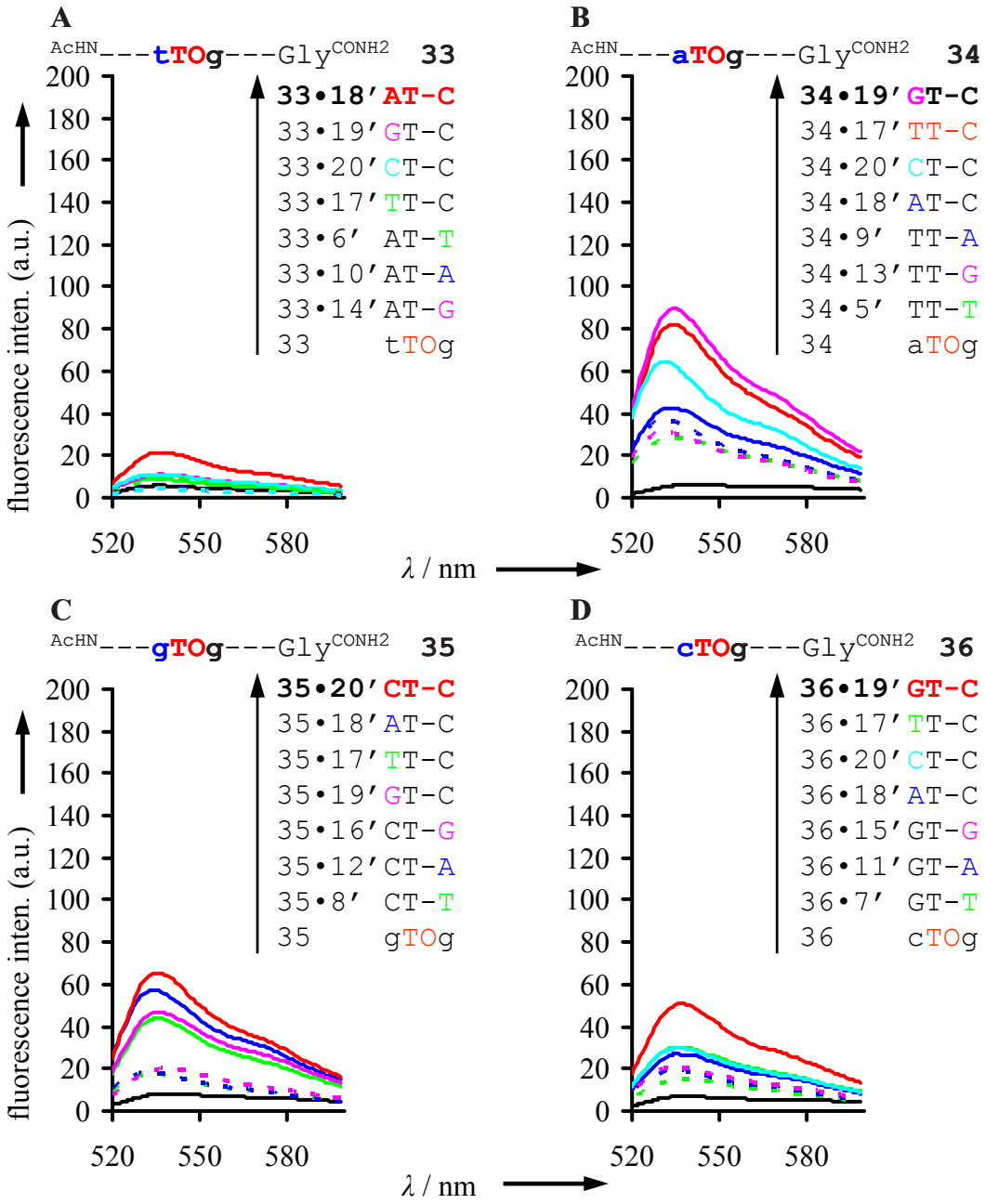

Figure 91: Fluorescence spectra of D-Orn-PNA probes **33-36** A) t-TO-g, B) a-TO-g, C) g-TO-g and D) c-TO-g, before (black) and after addition of matched and mismatched DNA [red = matched, smoothed lines = mismatched towards N-side, dotted lines = mismatched towards C-side. (M or N = T green, A blue, G pink and C turquoise) when thymine act as pairing partner for ONA-TO] at 25°C. Measurement conditions: Ex. 510 nm, Em. 518-600 nm. Ex. Slit: 5 nm and Em. Slit: 2.5 nm.

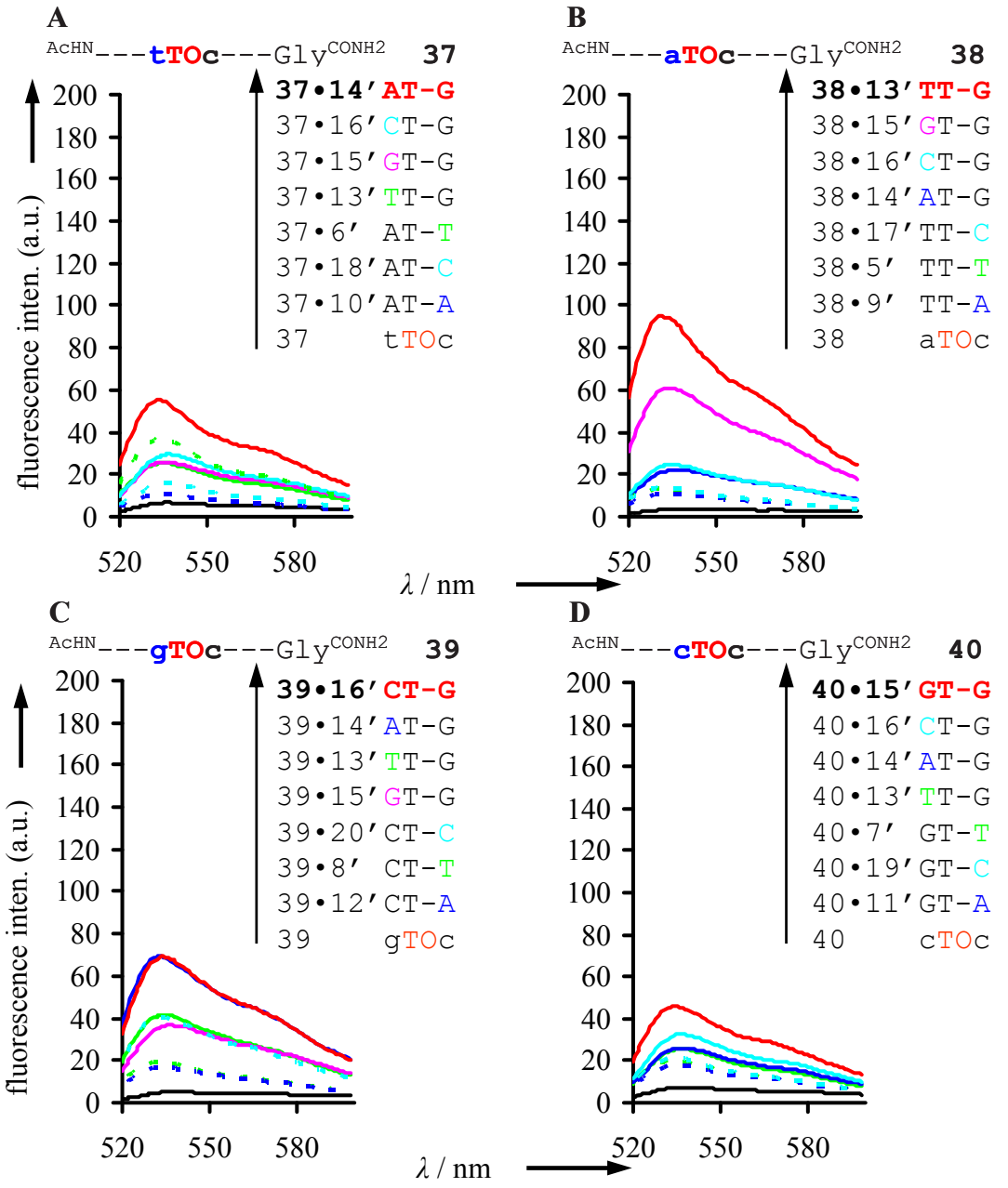

Figure 92: Fluorescence spectra of D-Orn-PNA probes **37-40** A) t-TO-c, B) a-TO-c, C) g-TO-c and D) c-TO-c, before (black) and after addition of matched and mismatched DNA [red = matched, smoothed lines = mismatched towards N-side, dotted lines = mismatched towards C-side. (M or N = T green, A blue, G pink and C turquoise) when thymine act as pairing partner for D-ONA-TO] at 25°C. Measurement conditions: Ex. 510 nm, Em. 518-600 nm. Ex. Slit: 5 nm and Em. Slit: 2.5 nm.

Fluorescence vs. temperature for TO-PNA before and after hybridisation with match DNA:

^{AcHN}gccgtxoytagccgGly^{CONH2}
$^{3'}$CGGCAMZNATCGGC$^{5'}$

o = D-Orn (TO), x; y = t, a, g, c
M, Z, N = T, A, G, C

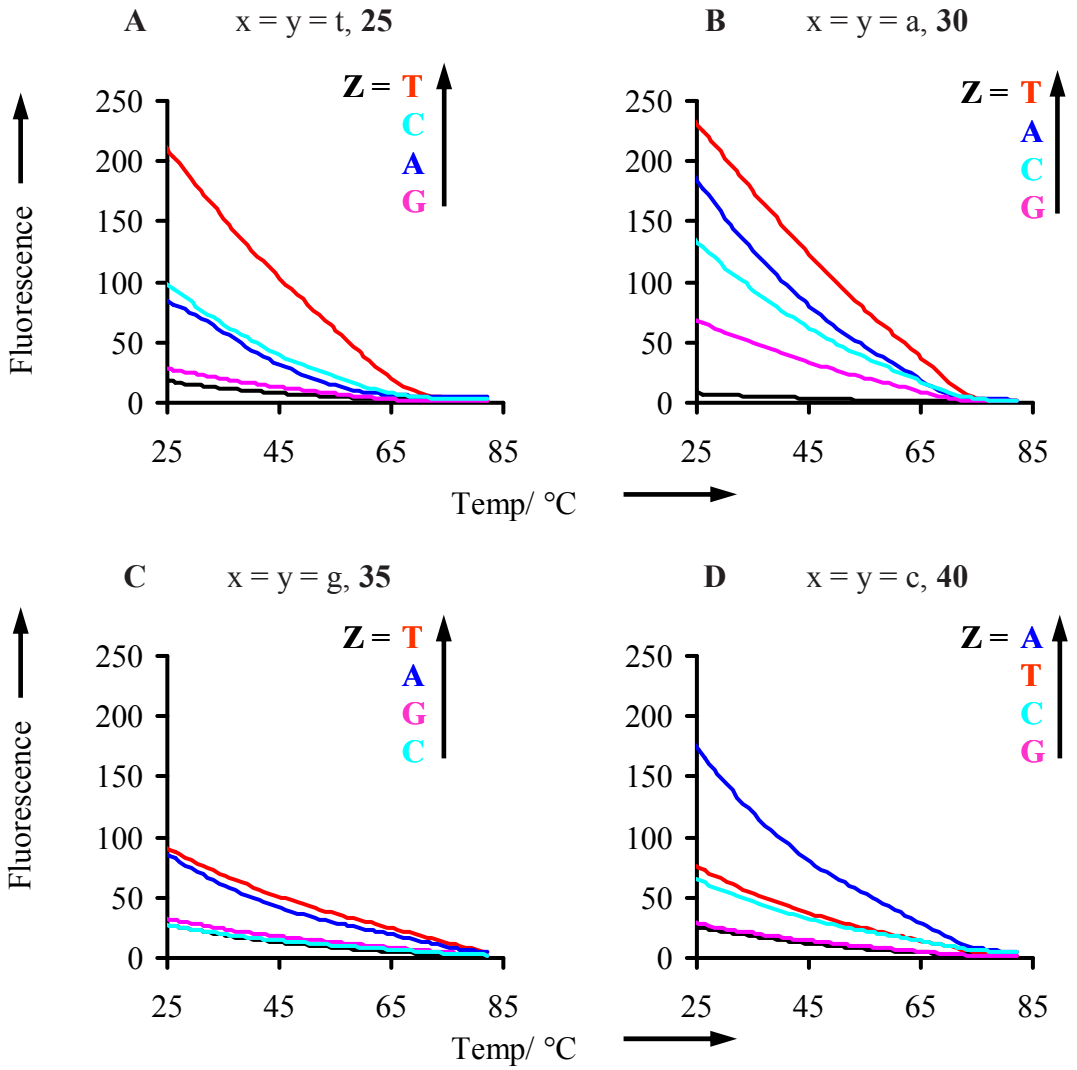

Figure 93: Fluorescence emission of D-Orn-PNA plotted against temperature before (black), after addition of equimolar amount of matched DNA (TO vs T = red, TO vs A = blue, TO vs G = pink and TO vs C = turquoise). M and N are always complementry to x and y, A) **25** (t-TO-t), B) **30** (a-TO-a), C) **35** (g-TO-g) and D) **40** (c-TO-c). [Measurement conditions: 1 µM FIT-PNA or 1 µM FIT-PNA•DNA duplex in degassed buffer (100 mM NaCl, 10 mM NaH_2PO_4 at pH 7.0, Ex. 510 nm, Em. 530 nm, rate of heating 1°C/ min.)].

11.2.3 Experimental part for Section 4

Preparation of TO-PRO-1 solution: The stock solution of TO-PRO-1 was prepared in methanol. The concentration was determined using the molar extinction coefficient (in aqueous buffer) of $\varepsilon_{506} = 63000\ M^{-1}cm^{-1}$.

Fluorescence measurements: The fluorescence measurements were performed Fluorescence emission measurements were performed by applying procedures described in section **11.2.1** except for calculation of quantum yield.

Fluorescence titration: The fluorescence titration experiments were performed with samples prepared for absorbance titration. Fluorescence spectra were recorded at 25°C with excitation at 485 nm (excitation slit width: 5 nm; emission slit width: 2.5 nm). Solvent background signals were subtracted.

Absorbance titration: Solutions of duplexes of DNA•DNA and PNA•DNA were prepared by mixing equimolar amounts of corresponding oligonucleotides to a final duplex concentration of 70-80 μM. In titration experiments TO-PRO1 was added from the stock solution to a fluorescence quartz cuvette (4 x 10 mm) and diluted with aq. degassed buffer (100 mM NaCl, 10 mM NaH_2PO_4 at pH 7.0) to a final concentration of 0.5 μM. The absorbance spectrum was recorded at 25°C. Duplexes from stock solutions were added as required for obtaining the specified duplex concentration. To secure homogeneous binding of dye to duplexes, after each addition the solution was heated at 85°C for ten minutes and cooled to room temperature (5°C/ min). After 20 minutes the spectra were recorded at 25°C. The spectra were corrected for dilution.

Absorbance measurements: Stock solutions of FIT-PNA (140-250 μM in H_2O) and DNA (140-250 μM in H_2O) were prepared. FIT-PNA solution was added into a fluorescence quartz cuvette (4 x 10 mm) and diluted with aq. degassed buffer (100 mM NaCl, 10 mM NaH_2PO_4 at pH 7.0) to a final concentration of 3 μM. The absorbance spectrum was recorded at 25°C. DNA-target solution (3 nmol) was added to give a total volume of 1 mL and the absorbance spectrum was recorded after 20 min. The spectra were corrected for dilution.

Quantum Yield: Quantum yields were determined relative to fluorescein in 0.1N sodium hydroxide as described.[112] Fluorescence spectra were recorded at 25°C with excitation at 485 nm. Emission was integrated between 495 and 750 nm. Solvent background signals were subtracted and fluorescence quantum yields were obtained using the following equation.

$$\Phi_{Sam} = \left(\frac{A_{Sam}}{A_{Ref}}\right) \times \left(\frac{a_{Ref}}{a_{Sam}}\right) \times \left(\frac{n_{Sam}^{2}}{n_{Ref}^{2}}\right) \times \Phi_{Ref}$$

Where A_{Sam} and A_{Ref} are the area under the fluorescence spectrum, a_{Sam} and a_{Ref} are the absorbance at the wavelength of the excitation (485 nm), n_{Sam} and n_{Ref} are the refractive indices of the respective solvents for the sample and reference, respectively.

CD measurements: TO-PRO1 with **4'AT•4'TA** and **4at•4'TA** duplexes: Solutions (52 μM) of DNA•DNA duplexes **4'AT•4'TA** and PNA•DNA duplexes **4at•4'TA** in degassed buffer (100 mM NaCl, 10 mM NaH_2PO_4 at pH 7.0) were prepared. Varying amounts of TO-PRO1 was added from the stock solution. The solution was heated at 85°C for ten minutes and cooled to room temperature (5°C/minute). After 20 minutes, the spectra were recorded at 15°C.

FIT-PNA: FIT-PNA was added into a quartz cuvette (4 x 10 mm) and diluted with aq. degassed buffer to a final duplex concentration of 3 μM. An equimolar amount of DNA target was added to give a total volume of 1 mL CD spectra were recorded after 20 min at 15°C.

Fluorescence decay: Time resolved fluorescence study reported in this thesis have been carried out by Nils Krebs and Sebastian Tannert in the working group of Prof. Beate Röder (Institut für Physik, Humboldt-Universität zu Berlin. Newtonstr. 15, D-12489 Berlin, Germany). Fluorescence lifetimes were measured by time-correlated single photon counting (TCSPC) technique, using the frequency doubled pulses of a Ti: Sapphire laser (Coherent Mira 900, 405 nm, FWHM 200 fs) for excitation. The instrument response function was 60 ps, as measured at excitation wavelength with Ludox. The set up was previously described.[44] The excitation wavelength was 532 nm. Samples were measured in magic angle configuration. Time dependent fluorescence was monitored at different wavelengths in a range from 545-645 nm. A self-made routine was applied to minimize the least square error

between the model function convoluted with instrument response function (IRF) and the measured data set.

11.2.4 Experimental part for Section 5

^{AcHN}gccgta-Aeg (TO)-hagccgGly^{CONH2}, 41

7 mg (≈ 2 μmol) of resin **4a** was used. The PNA was synthesised by linear solid phase synthesis using automated solid phase PNA synthesis and alloc group was removed manually using palladium chemistry.

Yield: OD_{260} = 38.8, 340 nmol, 17.0 %

ε_{260}	114.000 L•mol^{-1}•cm^{-1}
MALDI-TOF/MS; *m/z*	3678 $[M+H]^+$, calc.: 3675
HPLC	t_R = 6.9 min (Gradient A)
$C_{156}H_{189}N_{76}O_{40}S^+$	3674.5

Optical measurements: Fluorescence emission, absorbance, CD, Time resolved fluorescence and T_M measurements were carried out applying procedures described in **11.2.3** and **11.2.1**.

11.2.5 Experimental part for Section 6

TO-$(CH_2)_5$-CONH-$(CH_2)_5$-gccgtaaatagccgGly^{CONH2}, 42

7 mg (≈ 2 μmol) of resin **4a** was used. The PNA was synthesised by linear solid phase synthesis using automated solid phase PNA synthesis and terminal TO coupling was carried out manually using PyBop, NMM and DMF.

Yield: OD_{260} = 23.22, 168 nmol, 8.4 %

ε_{260}	138.000 L•mol^{-1}•cm^{-1}
MALDI-TOF/MS; *m/z*	4378 $[M+H]^+$, calc.: 4375
HPLC	t_R = 14.3 min (Gradient B)
$C_{156}H_{189}N_{76}O_{40}S^+$	4374.8

TO-$(CH_2)_5$-CONH-$(CH_2)_5$-gccgta-Aeg (TO)-aatagccgGly^{CONH2}, 43

7 mg (≈ 2 μmol) of resin **4a** was used. The PNA was synthesised by linear solid phase synthesis using automated solid phase PNA synthesis and terminal TO coupling was carried out manually using PyBop, NMM and DMF.

Yield: OD_{260} = 10.5, 77 nmol, 3.9 %

ε_{260}	136.000 L•mol^{-1}•cm^{-1}
MALDI-TOF/MS; *m/z*	4523 $[M+H]^+$, calc.: 4515
HPLC	t_R = 12.1 min (Gradient B)
$C_{156}H_{189}N_{76}O_{40}S^+$	4514.8

TO-$(CH_2)_5$-$(CH_2)_5$-acaccgccggcGly^{CONH2} 44

7 mg (≈ 2 μmol) of resin **4a** was used. The PNA was synthesised by linear solid phase synthesis using automated solid phase PNA synthesis and terminal TO coupling was carried out manually using PyBop, NMM and DMF.

Yield: OD_{260} = 20.7, 194 nmol, 9.7 %

ε_{260}	99.000 L•mol^{-1}•cm^{-1}
MALDI-TOF/MS; *m/z*	3507 $[M+H]^+$, calc.: 3503
HPLC	t_R = 12.05 min (Gradient B)
$C_{156}H_{189}N_{76}O_{40}S^+$	3503.4

^{ACHN}acacc-Aeg (TO)-ccggcGly^{CONH2}, 45

7 mg (≈ 2 μmol) of resin **4a** was used. The PNA was synthesised by linear solid phase synthesis using automated solid phase PNA synthesis.

Yield: OD_{260} = 24.71, 254 nmol, 12.7 %

ε_{260}	97.000 L•mol^{-1}•cm^{-1}
MALDI-TOF/MS; *m/z*	3190 $[M+H]^+$, calc.: 3186
HPLC	t_R = 8.8 min (Gradient A)
$C_{156}H_{189}N_{76}O_{40}S^+$	4186.3

Optical measurements: Fluorescence emission, absorbance, CD, Time resolved fluorescence and T_M measurements were carried out applying procedures described in **11.2.3** and **11.2.1**.

11.2.6 Experimental part for Section 7

^{AcHN}gccgt-Aeg (TO)-a-Aeg (TO)-tagccgGly^{CONH2}, 48

7 mg (≈ 2 μmol) of resin **4a** was used. The PNA was synthesised by linear solid phase synthesis using automated solid phase PNA synthesis.

Yield: OD_{260} = 10.7, 79 nmol, 3.9 %

ε_{260}	134.000 L•mol^{-1}•cm^{-1}
MALDI-TOF/MS; *m/z*	4232 $[M+H]^+$, calcd for: 4230
HPLC	t_R = 8.4 min (Gradient A)
$C_{156}H_{189}N_{76}O_{40}S^+$	4229.6

Optical measurements: Fluorescence emission, absorbance and T_M measurements were carried out applying procedures described in **11.2.3** and **11.2.1**.

11.2.7 Experimental part for Section 8

^{AcHN}gccgta-Aeg (BO)-atagccgGly^{CONH2}, 49

7 mg (≈ 2 μmol) of resin **4a** was used. The PNA was synthesised by divergent solid phase synthesis using Fmoc/Alloc-protected aminoethylglycine monomer using automated solid phase PNA synthesis. The removal of alloc group using palladium chemistry and subsequent, BO coupling was carried out manually using PyBop, NMM and DMF.

Yield: OD_{260} = 31.00, 227 nmol, 11.3 %

ε_{260}	136.000 L•mol^{-1}•cm^{-1}
MALDI-TOF/MS; *m/z*	4027 $[M+H]^+$, calc.: 4022
HPLC	t_R = 6.8 min (Gradient B)
$C_{156}H_{189}N_{76}O_{40}S^+$	4021.6

Optical measurements: Fluorescence emission, absorbance and T_M measurements were carried out applying procedures described in **11.2.3** and **11.2.1**.

11.2.8 Experimental part for Section 9

^{ACHN}ttcgtat-Aeg (TO)-acatttcLys^{CONH2,} 50

19.48 mg (≈ 5 µmol) of resin **4a''** was used. The PNA was manually synthesised by divergent solid phase synthesis.

Yield: OD_{260} = 22.10, 148 nmol, 2.96 %

ε_{260}	147.000 L•mol^{-1}•cm^{-1}
MALDI-TOF/MS; *m/z*	4357 $[M+H]^+$, calc.: 4351
HPLC	t_R = 13.8 min (Gradient B)
$C_{156}H_{189}N_{76}O_{40}S^+$	4350.

^{ACHN}ttcgtat-L-Orn (TO)-acatttcLys^{CONH2,} 51

19.48 mg (≈ 5 µmol) of resin **4a''** was used. The PNA was manually synthesised by divergent solid phase synthesis.

Yield: OD_{260} = 99.06, 668 nmol, 13.0 %

ε_{260}	147.000 L•mol^{-1}•cm^{-1}
MALDI-TOF/MS; *m/z*	4370 $[M+H]^+$, calc.: 4365
HPLC	t_R = 14.1 min (Gradient B)
$C_{156}H_{189}N_{76}O_{40}S^+$	4364.7

^{ACHN}ttcgtat-D-Orn (TO)-acatttcLys^{CONH2,} 52

19.48 mg (≈ 5 µmol) of resin **4a''** was used. The PNA was manually synthesised by divergent solid phase synthesis.

Yield: OD_{260} = 49.83, 334 nmol, 6.6 %

ε_{260}	147.000 L•mol^{-1}•cm^{-1}
MALDI-TOF/MS; *m/z*	4371 $[M+H]^+$, calc.: 4365
HPLC	t_R = 14.2 min (Gradient B)
$C_{156}H_{189}N_{76}O_{40}S^+$	4364.7

^{ACHN}aacacc-Aeg (TO)-atttacLys^{CONH2,} 53

15.58 mg (≈ 4 µmol) of resin **4a''** was used. The PNA was manually synthesised by divergent solid phase synthesis.

Yield: OD_{260} = 34.26, 256 nmol, 6.4 %

ε_{260}	131.000 L•mol^{-1}•cm^{-1}
MALDI-TOF/MS; *m/z*	3802 $[M+H]^+$, calc.: 3797

HPLC	t_R = 14.3 min (Gradient B)
$C_{156}H_{189}N_{76}O_{40}S^+$	3796.5

^{ACHN}aacacc-L-Orn (TO)-atttacLys^{CONH2,} 54

15.58 mg (≈ 4 µmol) of resin **4a''** was used. The PNA was manually synthesised by divergent solid phase synthesis.

Yield: OD_{260} = 108.07, 805 nmol, 20.0 %.

ε_{260}	131.000 L•mol^{-1}•cm^{-1}
MALDI-TOF/MS; *m/z*	3814 $[M+H]^+$, calc.: 3811
HPLC	t_R = 14.4 min (Gradient B)
$C_{156}H_{189}N_{76}O_{40}S^+$	3810.6

^{ACHN}aacacc-D-Orn (TO)-atttacLys^{CONH2,} 55

15.58 mg (≈ 4 µmol) of resin **4a''** was used. The PNA was manually synthesised by divergent solid phase synthesis.

Yield: OD_{260} = 63.17, 472 nmol, 11.7 %.

ε_{260}	131.000 L•mol^{-1}•cm^{-1}
MALDI-TOF/MS; *m/z*	3815 $[M+H]^+$, calc.: 3811
HPLC	t_R = 14.4 min (Gradient B)
$C_{156}H_{189}N_{76}O_{40}S^+$	3810.6

Optical measurements: Fluorescence emission, absorbance and T_M measurements were carried out applying procedures described in **11.2.3** and **11.2.1**.

11.3 References

[1] Larsson, A.; Carlsson, C.; Jonsson, M. and Albinsson, N. (1994), J. Am. Chem. Soc. (vol. 116), p. 8459.

[2] Netzel, Thomas L.; Nafisi, Kambiz; Zhao, Min; Lenhard, Jerome R. and Johnson, Iain (1995): Base-Content Dependence of Emission Enhancements, Quantum Yields, and Lifetimes for Cyanine Dyes Bound to Double-Strand DNA: Photophysical Properties of Monomeric and Bichromomphoric DNA Stains, Journal of Physical Chemistry (vol. 99), No. 51, pp. 17936-47.

[3] Cosa, G.; Focsaneanu, K. S.; McLean, J. R. N.; McNamee, J. P. and Scaiano, J. C. (2001): Photophysical properties of fluorescent DNA-dyes bound to single- and double-stranded DNA in aqueous buffered solution, Photochemistry and Photobiology (vol. 73), No. 6, pp. 585-599.

[4] Petty, Jeffrey T.; Bordelon, Jason A. and Robertson, Mary E. (2000): Thermodynamic Characterization of the Association of Cyanine Dyes with DNA, Journal of Physical Chemistry B (vol. 104), No. 30, pp. 7221-7227.

[5] Watson, J. D. and Crick, F. H. C. (1953): Molecular Structure of Deoxypentose Nucleic Acids, Nature (vol. 171), pp. 737-738.

[6] www.ncbi.nlm.nih.gov/disease.

[7] Zöller, B. and Dahlbäck, B. (1994): Linkage between inherited resistance to activated protein C and factor V gene mutation in venous thrombosis, The Lancet (vol. 343), pp. 1536-1538.

[8] Strittmatter, W. J. and Roses, A. (1995): Apolipoprotein E and Alzheimer Disease, Proce. Nat. Acad. Sci.USA (vol. 92), No. 11, pp. 4725-4727.

[9] Aubert, Y.; Perrouault, L.; Helene, C.; Giovannangeli, C. and Asseline, U. (2001): Synthesis and Properties of Triple Helix-Forming Oligodeoxyribonucleotides containing 7-Chloro-7-deaza-2'-deoxyguanosine, Bioorganic & Medicinal Chemistry (vol. 9), No. 6, pp. 1617-1624.

[10] Fukui, K.; Morimoto, M.; Segawa, H.; Tanaka, K. and Shimidzu, T. (1996): Synthesis and properties of an oligonucleotide modified with an acridine derivative at the artificial abasic site, Bioconjugate Chemistry (vol. 7), No. 3, pp. 349-355.

[11] Yamana, K.; Aota, R. and Nakano, H. (1995): Oligonucleotides having covalently linked anthracene at specific sugar residue - differential binding to dna and rna and fluorescence properties, Tetrahedron Letters (vol. 36), No. 46, pp. 8427-8430.

[12] Yamana, K.; Kumamoto, S. and Nakano, H. (1997): Homopyrimidine oligonucleotides modified by a pyrenylmethyl group at the terminal position - enhanced fluorescence upon binding to double helical dna, Chemistry Letters (vol. 11), pp. 1173-1174.

[13] Aubert, Yves; Bourgerie, Sylvain; Meunier, Laurent; Mayer, Roger; Roche, Annie-Claude; Monsigny, Michel; Thuong, Nguyen T. and Asseline, Ulysse (2000): Optimized synthesis of phosphorothioate oligodeoxyribonucleotides substituted with a 5'-protected thiol function and a 3'-amino group, Nucleic Acids Research (vol. 28), No. 3, pp. 818-825.

[14] Gryaznov, S. M. and Letsinger, R. L. (1993): Template controlled coupling and recombination of oligonucleotide blocks containing thiophosphoryl groups, Nucleic Acids Research (vol. 21), No. 6, pp. 1403-8.

[15] Zhou, Y. and Ts'o, P. O. P. (1996): Solid-phase synthesis of oligo-2-pyrimidinone-2'-deoxyribonucleotides and oligo-2-üyrimidinone-2'-deoxyriboside methylphosphonates, Nucleic Acids Res. (vol. 24), No. 14, pp. 2652-2659.

[16] Nielsen, P. E.; Berg, R. and Buchardt, O. (1991), Science (vol. 254), p. 1497.

[17] Egholm, M.; Buchardt, O.; Christensen, L.; Behrens, C.; Freier, S.; Driver, D.; Berg, R.; Kim, S.; Nordén, B. and Nielsen, P. (1993), Nature (vol. 365), pp. 566-568.

[18] Nielsen, Peter E.; Egholm, Michael and Buchardt, Ole (1994): Peptide nucleic acid (PNA). A DNA mimic with a peptide backbone, Bioconjugate Chemistry (vol. 5), No. 1, pp. 3-7.

[19] Smulevitch, S. V.; Simmons, C. G.; Norton, J. C.; Wise, J. W. and Corey, D. R. (1996): Enhanced strand invasion by oligonucletotides through manipulation of backbone charges, Nature Biotechnology (vol. 14), pp. 1700-1704.

[20] Bentin, Thomas and Nielsen, Peter E. (2002): PNA-mediated immobilization of supercoiled DNA, Methods in Molecular Biology (Totowa, NJ, United States) (vol. 208), No. Peptide Nucleic Acids, pp. 111-118.

[21] Demidov, V. V.; Potaman, V. N.; Frank-Kamenetskii, M. D.; Egholm, M.; Buchard, O.; Sonnichsen, S. H. and Nielsen, P. E. (1994): Stability of peptide nucleic acids in human serum and cellular extracts, Biochemical pharmacology (vol. 48), No. 6, pp. 1310-3.

[22] Gryaznov, S. M. and Chen, J.-K. (1994), J. Am. Chem. Soc. (vol. 116), pp. 3143.

[23] Hyrup, B. and Nielsen, P. E. (1996): Peptide nucleic acids (PNA): synthesis, properties and potential applications, Bioorganic & Medicinal Chemistry (vol. 4), No. 1, pp. 5-23.

[24] Uhlmann, E.; Peyman, A.; Breipohl, G. and Will, D. W. (1998): Pna - synthetic polyamide nucleic acids with unusual binding properties, Angew. Chem. Int. Ed., 37, 20, 2797-2823.

[25] R. B. Merrifield (1963), J. Am. Chem. Soc. (vol. 85), pp. 2149-2154.

[26] Thomson, Stephen A.; Josey, John A.; Cadilla, Rodolfo; Gaul, Micheal D.; Hassman, C. Fred; Luzzio, Michael J.; Pipe, Adrian J.; Reed, Kathryn L.; Ricca, Daniel J. and et al. (1995): Fmoc mediated synthesis of peptide nucleic acids, Tetrahedron (vol. 51), No. 22, pp. 6179-94.

[27] Brown, Stephen C.; Thomson, Stephen A.; Veal, James M. and Davis, Donald G. (1994): NMR solution structure of a peptide nucleic acid complexed with RNA, Science (Washington, DC, United States) (vol. 265), No. 5173, pp. 777-7.

[28] Eriksson, M. and Nielsen, P. E. (1996): Solution structure of a peptide nucleic acid-DNA duplex, Nature structural biology (vol. 3), No. 5, pp. 410-3.

[29] Betts, Laurie; Josey, John A.; Veal, James M. and Jordan, Steven R. (1995): A nucleic acid triple helix formed by a peptide nucleic acid-DNA complex, Science (Washington, D. C.) (vol. 270), No. 5243, pp. 1838-41.

[30] Rasmussen, H.; Kastrup, J. S.; Nielsen, J. N.; Nielsen, J. M. and Nielsen, P. E. (1997): Crystal structure of a peptide nucleic acid (PNA) duplex at 1.7 A resolution, Nature structural biology (vol. 4), No. 2, pp. 98-101.

[31] Thomson, J. ; Josey, J.; Cadilla, R.; Gaul, M.; Hassman, F.; Luzzio, M.; Pipe, A.; Reed, K.; Ricca, D.; Wiethe, R. and Noble, S. (1995), Tetrahedron (vol. 22), pp. 6179-6194.

[32] Sanger, H.; Nicklen, S. and Coulson, A. R. (1974): DNA Sequencing with Chain-Terminating Inhibitors, Proc. Natl. Acad. Sci. USA (vol. 74), No. 12, pp. 5463-5467.

[33] Huber, M.; Mündlein, A.; Dornstauder, E.; Schneeberger, C.; Tempfer, C. B.; Mueller, M. W. and Schmidt, W. M. (2002): Accessing Single Nucleotide Polymorphisms in Genomic DNA by Direct Multiplex Polymerase Chain Reaction Amplification on Oligonucleotide Microarrays, Analytical Biochemistry (vol. 303), pp. 25-33.

[34] Niemeyer, C. M. and Blohm, D. (1999): DNA microarrays, Angewandte Chemie Int. Ed., 38, 19, 2865.

[35] microarray.ucdavis.edu/.

[36] Tapp, I.; Malmberg, L.; Rennel, E.; Wik, M. and Syvanen, A. C. (2000): Homogeneous scoring of single-nucleotide polymorphisms: Comparison of the 5 '-nuclease TaqMan (R) assay and molecular beacon probes, Biotechniques (vol. 28), No. 4, pp. 732-734.

[37] Tyagi, S. and Kramer, F. R. (1996), Nature Biotechnol. (vol. 12), pp. 303-307.

[38] Tyagi, S.; Bratu, D. P. and Kramer, F. R. (1998): Multicolor molecular beacons for allele discrimination, Nature Biotechnology (vol. 16), No. 1, pp. 49-53.

[39] Yamane, A. (2002): MagiProbe: a novel fluorescence quenching-based oligonucleotide probe carrying a fluorophore and an intercalator, Nucleic Acids Res. (vol. 30), No. 19, p. e97.

[40] Whitcombe, D.; Theaker, J.; Guy, S. P.; Brown, T. and Little, S. (1999): Detection of PCR products using self-probing amplicons and fluorescence, Nature Biotechnology (vol. 17), No. 8, pp. 804-807.

[41] French, D. J.; Archard, C. L.; Brown, T. and McDowell, D. G. (2001): HyBeacon (TM) probes: a new tool for DNA sequence detection and allele discrimination, Molecular and Cellular Probes (vol. 15), No. 6, pp. 363-374.

[42] Marks, A. H. R. ; Bhadra, P. K. ; McDowell, D. G. ; French, D. J. ; Douglas, K. T. ; Bichenkova, E. V. and Bryce, R. A. (2005), J. Biomol. Struct. Dyn. (vol. 23), No. 1, pp. 49-62.

[43] Saito, Isao; Okamoto, Akimitsu and Yoshida, Yasuko (2004): Pyrene-labeled base-discriminating nucleotide derivatives as fluorescent DNA probes for

homogeneous SNP typing, Application: WO, (NGK Insulators, Ltd., Japan). 76, 20031224., 2003-JP16602, 2004058793, AN 2004:566636,

[44] Yamana, Kazushige; Ohtani, Yusuke; Nakano, Hidehiko and Saito, Isao (2003): Bis-pyrene labeled DNA aptamer as an intelligent fluorescent biosensor, Bioorganic & Medicinal Chemistry Letters (vol. 13), No. 20, pp. 3429-3431.

[45] Valis, Linda; Amann, Nicole and Wagenknecht, Hans-Achim (2005): Detection of single base mismatches and abasic sites using phenanthridinium as an artificial DNA base and charge donor, Organic & Biomolecular Chemistry (vol. 3), No. 1, pp. 36-38.

[46] Englund, E. A. and Appella, D. H. (2005), Organic Letters (vol. 7), No. 16, pp. 3465-3467.

[47] Isacsson, J.; Cao, H.; Ohlsson, L.; Nordgren, S.; Svanvik, N.; Westman, G.; Kubista, M.; Sjoback, R. and Sehlstedt, U. (2000): Rapid and specific detection of PCR products using light-up probes, Molecular and Cellular Probes (vol. 14), No. 5, pp. 321-328.

[48] Svanvik, Nicke; Stahlberg, Anders; Sehlstedt, Ulrica; Sjoback, Robert and Kubista, Mikael (2000): Detection of PCR Products in Real Time Using Light-up Probes, Analytical Biochemistry (vol. 287), No. 1, pp. 179-182.

[49] Svanvik, Nicke; Westman, Gunnar; Wang, Dongyuan and Kubista, Mikael (2000): Light-up probes: thiazole orange-conjugated peptide nucleic acid for detection of target nucleic acid in homogeneous solution, Analytical Biochemistry (vol. 281), No. 1, pp. 26-35.

[50] Svanvik, Nicke; Nygren, Jan; Westman, Gunnar and Kubista, Mikael (2001): Free-probe fluorescence of light-up probes, Journal of the American Chemical Society (vol. 123), No. 5, pp. 803-809.

[51] Wolffs, Petra; Knutsson, Rickard; Sjoback, Robert and Radstrom, Peter (2001): PNA-based light-up probes for real-time detection of sequence-specific PCR products, BioTechniques (vol. 31), No. 4, pp. 766,769-771.

[52] Asseline, Ulysse; Chassignol, Marcel; Aubert, Yves and Roig, Victoria (2006): Detection of terminal mismatches on DNA duplexes with fluorescent oligonucleotides, Organic & Biomolecular Chemistry (vol. 4), No. 10, pp. 1949-1957.

[53] Asseline, U. (2006): Development and applications of fluorescent oligonucleotides, Current Organic Chemistry (vol. 10), No. 4, pp. 491-518.

[54] Koehler, Olaf and Seitz, Oliver (2003): Thiazole orange as fluorescent universal base in peptide nucleic acids, Chemical Communications, No. 23, pp. 2938-2939.

[55] Koehler, Olaf (2003), Ph.D., University of Dortmund, Dortmund.

[56] Röglin, Lars (2002), Diploma, Organische Chemie III, University of Dortmund, Dortmund.

[57] Kricka, L. J. (2002): Stains, labels and detection strategies for nucleic acids assays, Ann. Clin. Biochem. (vol. 39), pp. 114-129.

[58] Jenkins, Yonchu and Barton, Jacqueline K. (1992): A Sequence-Specific Molecular Light Switch: Tethering of an Oligonucleotide to a Dipyridophenazine Complex of Ruthenium (II), J. Am. Chem. Soc. (vol. 114), pp. 8736-8738.

[59] Ishiguro, T.; Saitoh, J.; Yawata, H.; Otsuka, M.; Inoue, T. and Sugiura, Y. (1996): Fluorescence detection of specific sequence of nucleic acids by oxazole yellow-linked oligonucleotides - homogeneous quantitative monitoring of in vitro transcription, Nucleic Acids Research (vol. 24), No. 24, pp. 4992-4997.

[60] Seitz, Oliver and Kohler, Olaf (2001): Convergent strategies for the attachment of fluorescing reporter groups to peptide nucleic acids in solution and on solid phase, Chemistry-A European Journal (vol. 7), No. 18, pp. 3911-3925.

[61] Coull, J. M.; Egholm, M.; Hodge, R.P.; Ismail, M. and Rajur, S.B. (1996): Improved Synthons for the synthesis and deprotection of peptide nucleic acids under mild conditions, WO96/40685, USA, Perseptive Biosystems, Inc., 7 June 1995

[62] Coste, J.; Le-Nguyen, D. and Castro, B. (1990): Pybop - a New Peptide Coupling Reagent Devoid of Toxic by- Product, Tetrahedron Letters (vol. 31), No. 2, pp. 205-208.

[63] Ciommer, M. and Kunz, H. (1991), Synlett, p. 593–595.

[64] Ficht, Simon; Roeglin, Lars; Ziehe, Matthias; Breyer, David and Seitz, Oliver (2004): Direct carbodiimide-mediated conjugation of carboxylates using

pyridinium p-toluenesulfonate and tertiary amines as additives, Synlett, No. 14, pp. 2525-2528.

[65] Ross, Philip L.; Lee, Katherine and Belgrader, Phillip (1997): Discrimination of Single-Nucleotide Polymorphisms in Human DNA Using Peptide Nucleic Acid Probes Detected by MALDI-TOF Mass Spectrometry, Analytical Chemistry (vol. 69), No. 20, pp. 4197-4202.

[66] Glazer, A. N. and Rye, H. S. (1992): Stable dye-DNA intercalation complexes as reagents for high-sensitivity fluorescence detection, Nature (vol. 359), No. 6398, pp. 859-61.

[67] Lee, Linda G.; Chen, Chia Huei and Chiu, Laura A. (1986): Thiazole orange: a new dye for reticulocyte analysis, Cytometry (vol. 7), No. 6, pp. 508-17.

[68] Tyagi, S. and Kramer, F. R. (1996): Molecular beacons - probes that fluoresce upon hybridization, Nature Biotechnology (vol. 14), No. 3, pp. 303-308.

[69] Orlando, C.; Pinzani, P. and Pazzagli, M. (1998): Developments in quantitative pcr, Clinical Chemistry & Laboratory Medicine (vol. 36), No. 5, pp. 255-269.

[70] Weiler, J.; Gausepohl, H.; Hauser, N.; Jensen, O. N. and Hoheisel, J. D. (1997): Hybridisation based dna screening on peptide nucleic acid (pna) oligomer arrays, Nucleic Acids Research (vol. 25), No. 14, pp. 2792-2799.

[71] Uhlmann, Eugen; Peyman, Anusch; Breipohl, Gerhard and Will, David W. (1998): PNA: synthetic polyamide nucleic acids with unusual binding properties, Angewandte Chemie, International Edition (vol. 37), No. 20, pp. 2796-2823.

[72] Braasch, Dwaine A. and Corey, David R. (2002): Novel Antisense and Peptide Nucleic Acid Strategies for Controlling Gene Expression, Biochemistry (vol. 41), No. 14, pp. 4503-4510.

[73] Rye, H. S.; Yue, S.; Wemmer, D. E.; Quesada, M. A.; Haugland, R. P.; Mathies, R. A. and Glazer, A. N. (1992): Stable Fluorescent Complexes of Double-Stranded DNA with Bis- Intercalating Asymmetric Cyanine Dyes - Properties and Applications, Nucleic Acids Research (vol. 20), No. 11, pp. 2803-2812.

[74] Schneeberger, C.; Speiser, P.; Kury, F. and Zeillinger, R. (1995), PCR Methods & Applications (vol. 4), p. 234.

[75] Jin, X.; Yue, S.; Wells, K. S. and Singer, V. L. (1994), FASEB Journal (vol. 8), p. A1266.

[76] Carlsson, C.; Larsson, A.; Jonsson, M.; Albinsson, B. and Norden, B. (1994), Journal of Physical Chemistry (vol. 98), p. 10313.

[77] Nygren, Jan; Svanvik, Nicke and Kubista, Mikael (1998): The interactions between the fluorescent dye thiazole orange and DNA, Biopolymers (vol. 46), No. 1, pp. 39-51.

[78] Bunkenborg, Jakob; Gadjev, Nikolai I.; Deligeorgiev, Todor and Jacobsen, Jens Peter (2000): Concerted Intercalation and Minor Groove Recognition of DNA by a Homodimeric Thiazole Orange Dye, Bioconjugate Chemistry (vol. 11), No. 6, pp. 861-867.

[79] Schweitzer, Claude and Scaiano, J. C. (2003): Selective binding and local photophysics of the fluorescent cyanine dye PicoGreen in double-stranded and single-stranded DNA, Physical Chemistry Chemical Physics (vol. 5), No. 21, pp. 4911-4917.

[80] Spielmann, H. P.; Wemmer, D. E. and Jacobsen, J. P. (1995), Biochemistry (vol. 34), p. 8542.

[81] Jacobsen, Jens Peter; Pedersen, Jeanette B.; Hansen, Lene F. and Wemmer, David E. (1995): Site selective bis-intercalation of a homodimeric thiazole orange dye in DNA oligonucleotides, Nucleic Acids Research (vol. 23), No. 5, pp. 753-60.

[82] Johansen, F. and Jacobsen, JP. (1998): 1H NMR studies of the bis-intercalation of a homodimeric oxazole yellow dye in DNA oligonucleotides, Journal of Biomolecular Structure and Dynamics (vol. 16), pp. 205-222.

[83] Petersen, Michael; Hamed, Atef A.; Pedersen, Erik B. and Jacobsen, Jens Peter (1999): Bis-Intercalation of Homodimeric Thiazole Orange Dye Derivatives in DNA, Bioconjugate Chemistry (vol. 10), No. 1, pp. 66-74.

[84] Bunkenborg, Jakob; Stidsen, Maria Munch and Jacobsen, Jens Peter (1999): On the Sequence Selective Bis-Intercalation of a Homodimeric Thiazole Orange Dye in DNA, Bioconjugate Chemistry (vol. 10), No. 5, pp. 824-831.

[85] Seitz, Oliver; Bergmann, Frank and Heindl, Dieter (1999): A convergent strategy for the modification of peptide nucleic acids: novel mismatch-specific PNA-hybridization probes, Angewandte Chemie, International Edition (vol. 38), No. 15, pp. 2203-2206.

[86] Privat, Eric; Melvin, Tracy; Asseline, Ulysse and Vigny, Paul (2001): Oligonucleotide-conjugated thiazole orange probes as \"light-up\" probes for messenger ribonucleic acid molecules in living cells, Photochemistry and Photobiology (vol. 74), No. 4, pp. 532-541.

[87] Privat, Eric and Asseline, Ulysse (2001): Synthesis and Binding Properties of Oligo-2'-deoxyribonucleotides Covalently Linked to a Thiazole Orange Derivative, Bioconjugate Chemistry (vol. 12), No. 5, pp. 757-769.

[88] Privat, Eric; Melvin, Tracy; Merola, Fabienne; Schweizer, Gerd; Prodhomme, Sylvie; Asseline, Ulysse and Vigny, Paul (2002): Fluorescent properties of oligonucleotide-conjugated thiazole orange probes, Photochemistry and Photobiology (vol. 75), No. 3, pp. 201-210.

[89] Wang, X. F. and Krull, U. J. (2002), Analytical Chimica Acta (vol. 470), p. 57.

[90] Wang, Xiaofeng and Krull, Ulrich J. (2005): Synthesis and fluorescence studies of thiazole orange tethered onto oligonucleotide: development of a self-contained DNA biosensor on a fiber optic surface, Bioorganic & Medicinal Chemistry Letters (vol. 15), No. 6, pp. 1725-1729.

[91] Fechter, E. J.; Olenyuk, B. and Dervan, P. B. (2005), Journal of the American Chemical Society (vol. 127), p. 16685.

[92] Lartia, Remy and Asseline, Ulysse (2006): New cyanine-oligonucleotide conjugates: relationships between chemical structures and properties, Chemistry-A European Journal (vol. 12), No. 8, pp. 2270-2281.

[93] Fukui, K. and Tanaka, K. (1996): The acridine ring selectively intercalated into a dna helix at various types of abasic sites - double strand formation and photophysical properties, Nucleic Acids Research (vol. 24), No. 20, pp. 3962-3967.

[94] Karlsson, H. Jonas; Eriksson, Maja; Perzon, Erik; Akerman, Bjoern; Lincoln, Per and Westman, Gunnar (2003): Groove-binding unsymmetrical cyanine dyes for staining of DNA: syntheses and characterization of the DNA-binding, Nucleic Acids Research (vol. 31), No. 21, pp. 6227-6234.

[95] Karlsson, H. Jonas; Lincoln, Per and Westman, Gunnar (2003): Synthesis and DNA binding studies of a new asymmetric cyanine dye binding in the minor groove of [poly(dA-dT)]2, Bioorganic & Medicinal Chemistry (vol. 11), No. 6, pp. 1035-1040.

[96] Prodhomme, Sylvie; Demaret, Jean-Philippe; Vinogradov, Sergei; Asseline, Ulysse; Morin-Allory, Luc and Vigny, Paul (1999): A theoretical and experimental study of two thiazole orange derivatives with single- and double-stranded oligonucleotides, polydeoxyribonucleotides and DNA, Journal of Photochemistry and Photobiology, B: Biology (vol. 53), No. 1-3, pp. 60-69.

[97] Wittung, P.; Kim, S. K. ; Buchardt, O. ; Nielsen, P. and B., Norden (1994), Nucleic Acids Res. (vol. 22), pp. 5371-5377.

[98] Smith, Jeffrey O.; Olson, Darren A. and Armitage, Bruce A. (1999): Molecular Recognition of PNA-Containing Hybrids: Spontaneous Assembly of Helical Cyanine Dye Aggregates on PNA Templates, Journal of the American Chemical Society (vol. 121), No. 12, pp. 2686-2695.

[99] Garoff, R. A. ; Litzinger, E. A.; Connor, R. E. ; Fishman, I. and Armitage, B. A. (2002), Langmuir (vol. 18), p. 6330.

[100] Asseline, U.; Thuong, Nguyen T. and Helene, C. (1997): Synthesis and properties of oligonucleotides covalently linked to intercalating agents, New Journal of Chemistry (vol. 21), No. 1, pp. 5-17.

[101] Kubista, Mikael and Svanvik, Nicke (1997): Nucleic acid hybridization using probes labeled with a reporter group with spectroscopic properties sensitive to hybrid formation, Application: WO, (Kubista, Mikael, Swed.; Svanvik, Nicke). 57, 19970530., 97-SE953, 9745539, AN 1997:805833.

[102] Kubista, Mikael; Stalberg, Anders and Bar, Tzachi (2001): Light-up-probe-based real-time Q-PCR, Proceedings of SPIE-The International Society for Optical Engineering (vol. 4264), No. Genomics and Proteomics Technologies, pp. 53-58.

[103] Zhou, X. F.; Peng, Z. H.; Geise, H.; Peng, B. X.; Li, Z. X.; Yan, M. ; Dommisse, R.; Carieer, R. and Claeys, M. (1995): Blue Sensitizing Dyes: Synthesis, Spectroscopy, and Performance in Photographic Emulsions, J. Imag. Sci. Tech. (vol. 39), pp. 244-252.

[104] D. A. Vourloumis; M. Takahashi; K. B. Simonsen; B. K. Ayida; S. Barluenga; G. C. Wintersa and Hermannb, T. (2003): Solid-phase synthesis of benzimidazole libraries biased for RNA targets, Tetrahedron Letters (vol. 44), pp. 2807-2811.

[105] Ahn, S. J.; Costa, J. and Emanuel, J. R. (1996), Nucleic Acids Res. (vol. 24), p. 2623.

[106] Rye, Hays S. and Glazer, Alexander N. (1995): Interaction of dimeric intercalating dyes with single-stranded DNA, Nucleic Acids Research (vol. 23), No. 7, pp. 1215-22.

[107] Karlsson, H. Jonas; Bergqvist, Mattias H.; Lincoln, Per and Westman, Gunnar (2004): Syntheses and DNA-binding studies of a series of unsymmetrical cyanine dyes: structural influence on the degree of minor groove binding to natural DNA, Bioorganic & Medicinal Chemistry (vol. 12), No. 9, pp. 2369-2384.

[108] Sovenyhazy, Kristine M.; Bordelon, Jason A. and Petty, Jeffrey T. (2003): Spectroscopic studies of the multiple binding modes of a trimethine-bridged cyanine dye with DNA, Nucleic Acids Research (vol. 31), No. 10, pp. 2561-2569.

[109] Zhang, Lande; Liang, Feng; Sun, Lingzhi; Hu, Yuefei and Hu, Hongwen (2000): A novel and practical synthesis of 3-unsubstituted indolizines, Synthesis, No. 12, pp. 1733-1737.

[110] Venter, C. and et al. (2001): The Sequence of the Human Genome, Science (vol. 291), pp. 1304-1351.

[111] Saiki, R. K.; Gelfand, D. H.; Stoffel, S.; Scharf, S.; Higuchi, R.; Horn, G. T.; Mullis, K. B. and Erlich, H. A. (1998): Primer-Directed Enzymatic Amplification of DNA with a Themostable DNA Polymerase, Science (vol. 239), pp. 487-491.

[112] Demas, J. N. and Crosby, G. A. (1971), Journal of Physical Chemistry (vol. 75), p. 991.

Abbrevations

a/ A	(Adenine PNA/ DNA)
Alloc	Allyloxycarbonyl
Aeg	Aminothylglycine
Boc	Tert. butyloxycarbonyl
Bhoc	Benzhydryloxycarbonyl
BO	Pyridinium benzothiazole
c/ C	Cytosine (PNA/ DNA)
Cbz	Benzyloxy carbonyl
CD	Circular dichroism
dA	Deoxy adenine
DCM	Dichloromethane
DHB	2, 5-Dihydroxybenzoic acid
DMF	N, N-Dimethylformamide
DMSO	Dimethylsulfoxide
DNA	Desoxyribonucleic acid
D-Orn	D-ornithine
ds	Double stranded
Fmoc	9-Fluorenylmethoxycarbonyl
FRET	Fluorescence Resonance Energy Transfer
FAB	Fast atom bombardment
g/ G	Guanine (PNA/ DNA)
Gly	Glycine
HPLC	High Performance Liquid Chromatography
HPSF®	High-Purity Salt Free
L-Orn	L-ornithine
MALDI-TOF	Matrix Assisted Laser Desorption and Ionisation- Time of Flight
MM	Mismatch
MT	Match
NMM	*N*-Methylmorpholin
NMP	*N*-Methylpyrrolidon

Orn	Ornithine
PCR	Polymerase Chain Reaction
PNA	Peptide nucleic acid
Pip	Piperidin
PPTS	Pyridinium-*p*-toluolsulfonic acid
Py	Pyridin
PyBOP	Benzotriazol-1-yloxy-tris-pyrrolidinophosphonium Hexafluorophosphate
RNA	Ribonucleic acid
RP	Reversed Phase
ss	Single strand
t/ T	Thymine (PNA/ DNA)
TFA	Trifluoro acetic acid
TG	Tentagel
TO	Thiazolorange
U	Uracil
WT	Wildtype
Z	Benzyloxycarbonyl
ΔT_M	Melting temperature (matched duplex-single base mismatched duplex)

11.4 Spectral Data

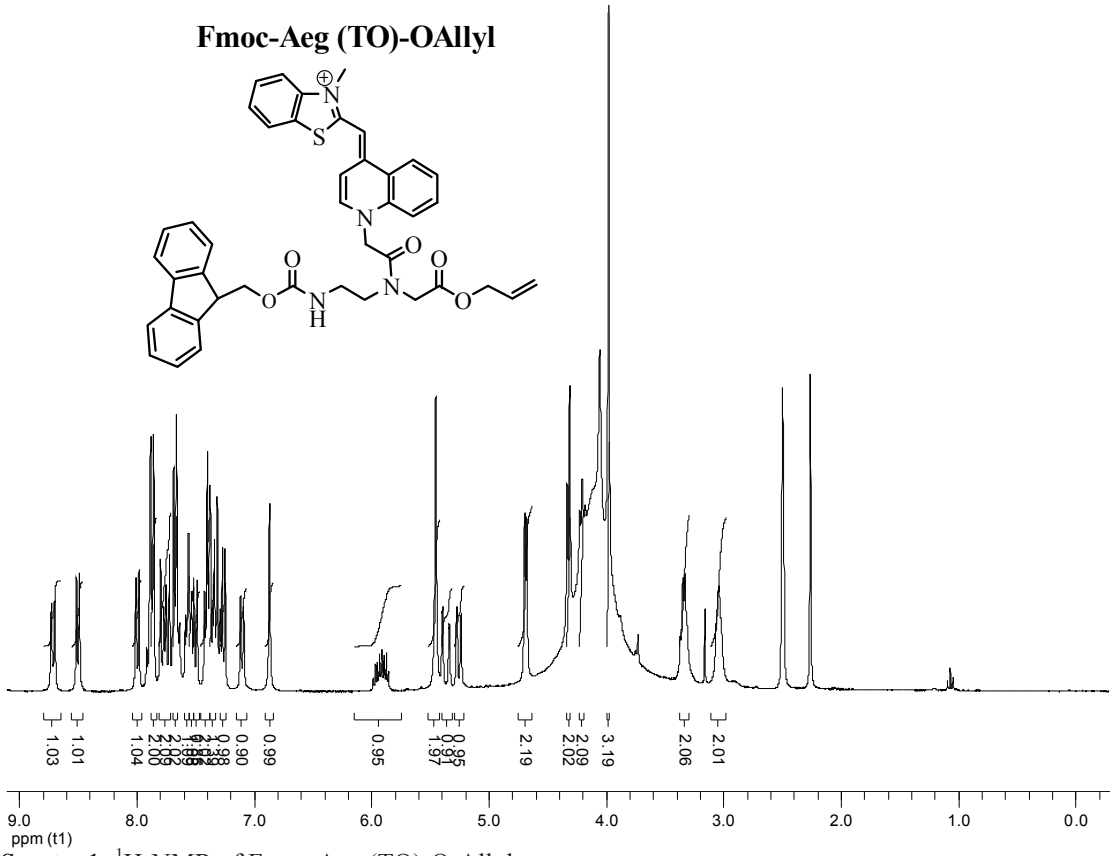

Spectra 1: ^{1}H-NMR of Fmoc-Aeg (TO)-O-Allyl

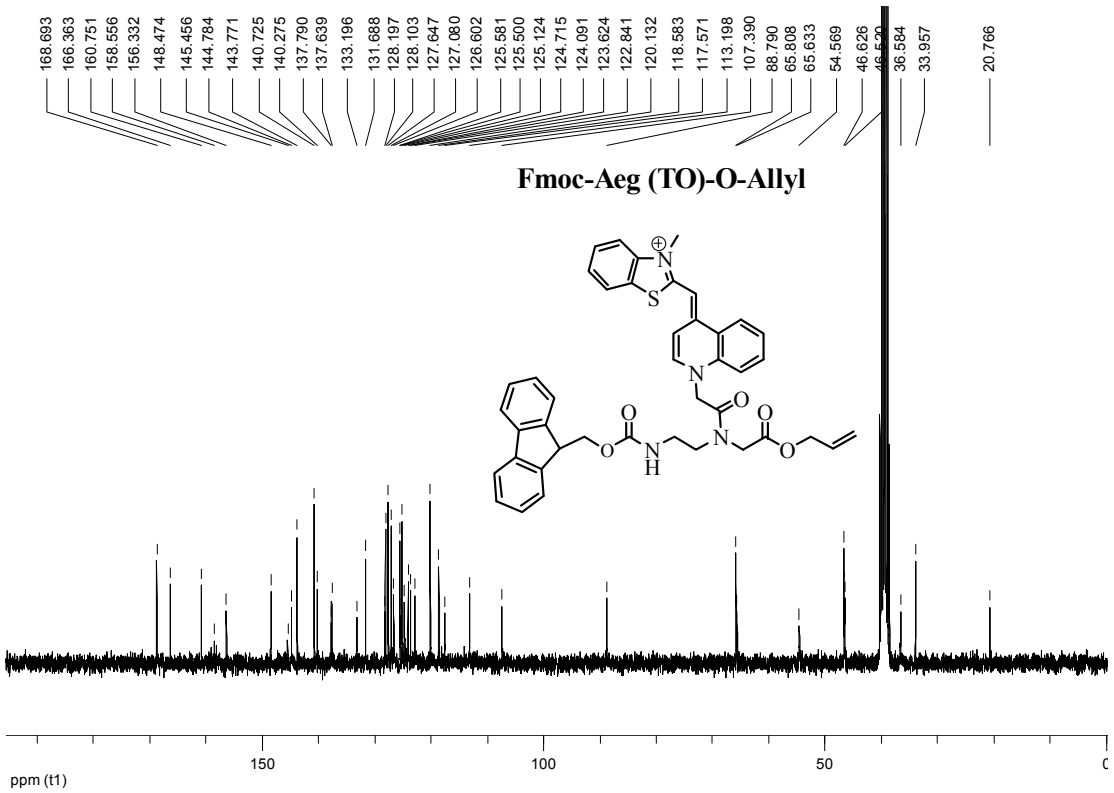

Spectra 2: ^{13}C-NMR of Fmoc-Aeg (TO)-O-Allyl

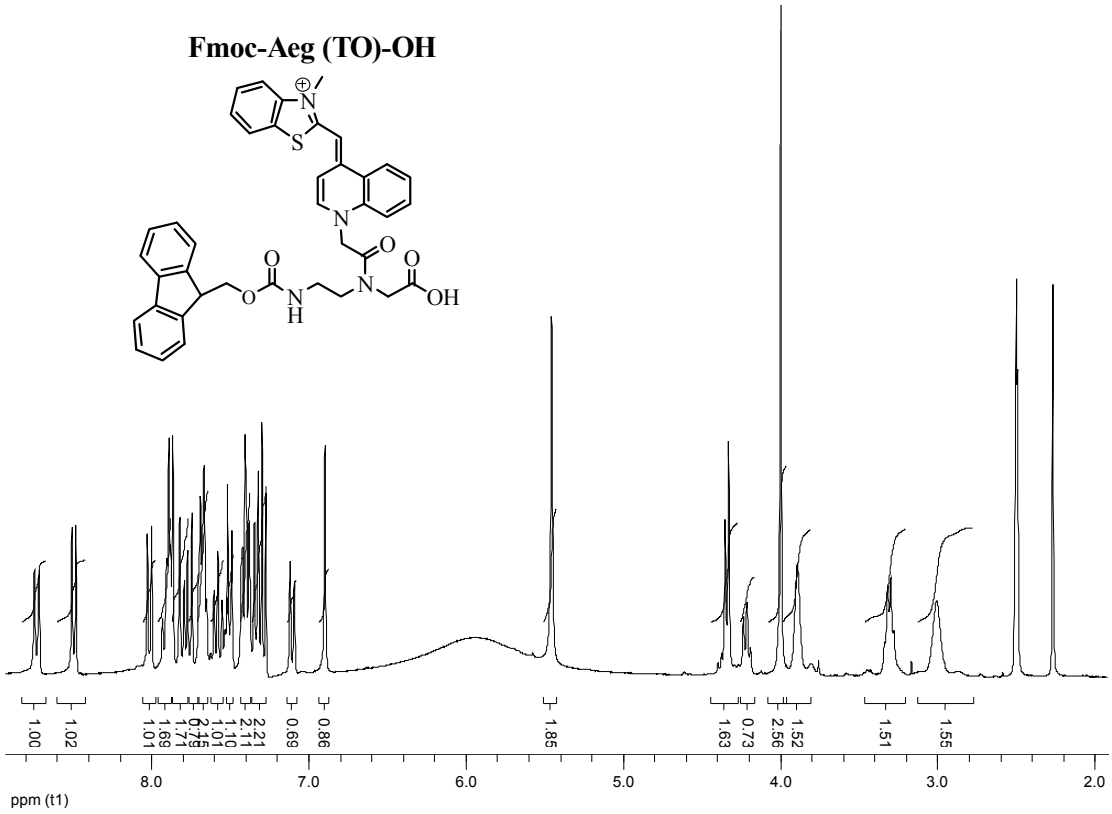

Spectra 3: ^{1}H-NMR of Fmoc-Aeg (TO)-OH

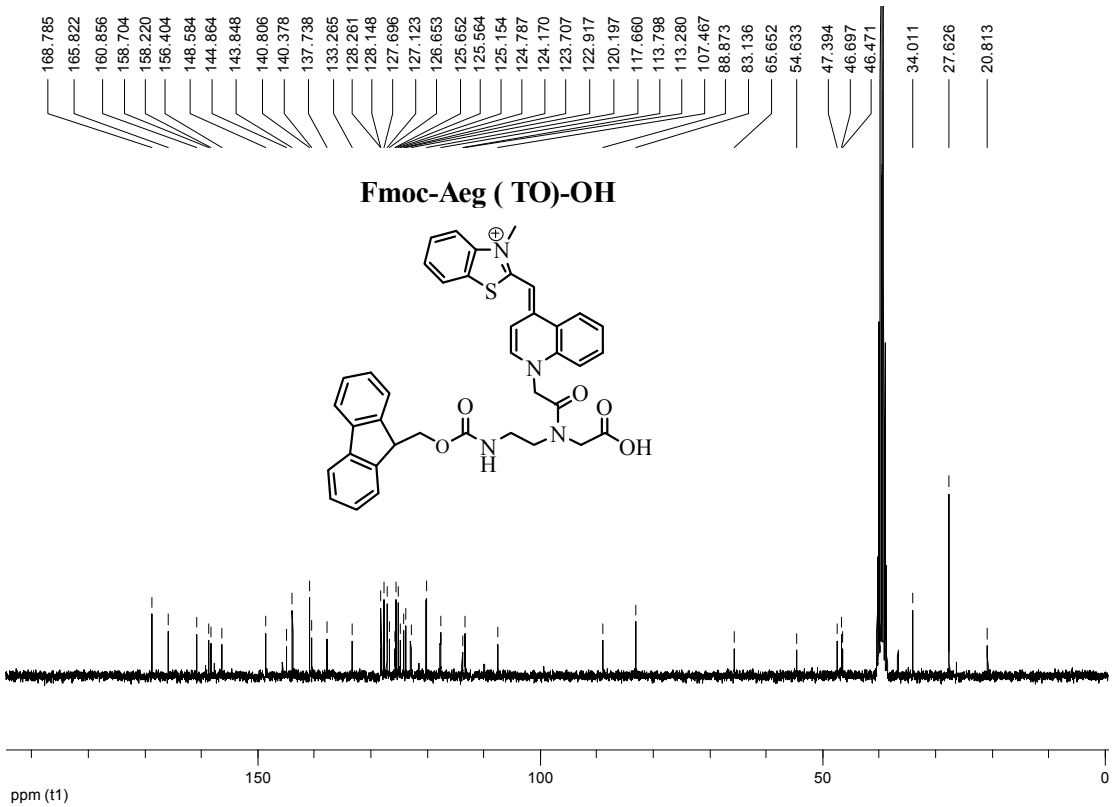

Spectra 4: ^{13}C-NMR of Fmoc-Aeg (TO)-OH

^{AcHN}gccgta-Aeg (TO)-tagccgGly^{CONH2}, 4

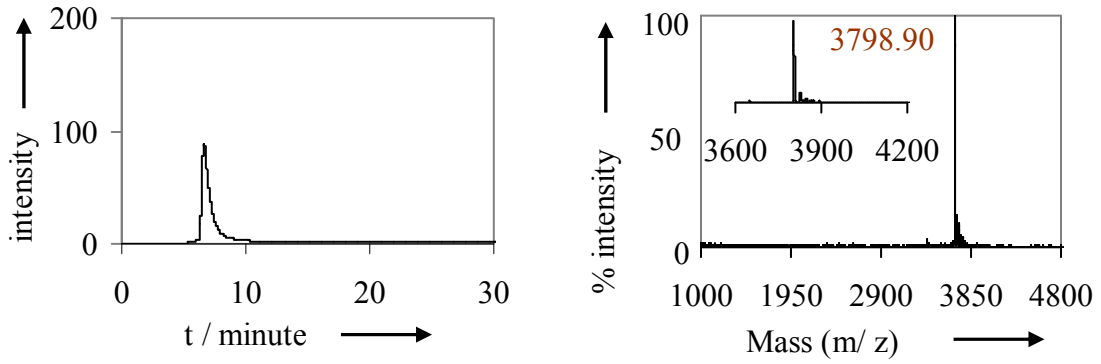

Figure 94: Analytical HPLC ($UV_{\lambda = 260\ nm}$) and MALDI-TOF/MS spectrum of probe **4** (HPLC conditions: gradient A: 0–1 min: 3 %; gradient A; 1–20 min: 3–30 %).

^{AcHN}gccgtaatagccgGly^{CONH2}, 4at

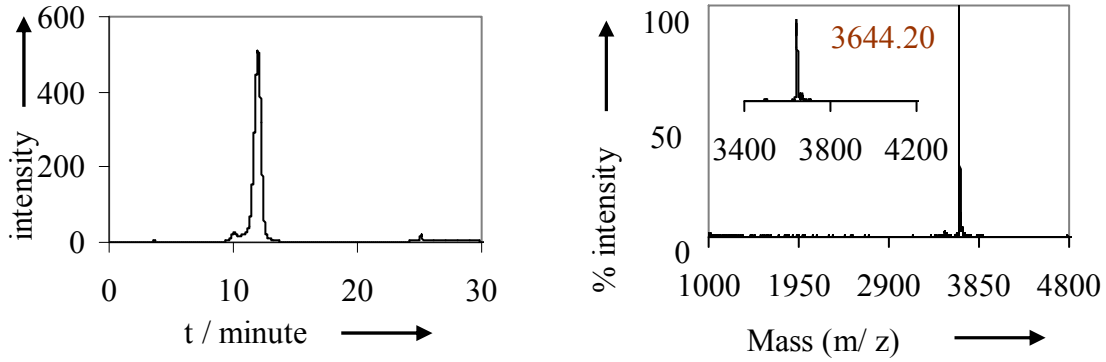

Figure 95: Analytical HPLC ($UV_{\lambda = 260\ nm}$) and MALDI-TOF/MS spectrum of probe **4at** (HPLC conditions: gradient A: 0–1 min: 3 %; gradient A; 1–20 min: 3–30 %).

***AcHN*gccgtt-Aeg (TO)-ttagccgGly*CO*NH2, 5**

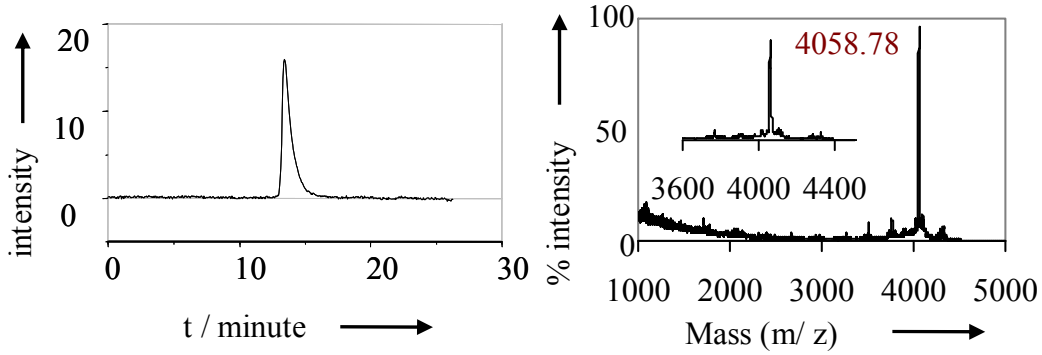

Figure 96: Analytical HPLC ($UV_{\lambda = 260\ nm}$) and MALDI-TOF/MS spectrum of probe **5** (HPLC conditions: gradient A: 0–1 min: 3 %; gradient A; 1–25 min: 3–30 %).

^{AcHN}gccgta-Aeg (TO)-ttagccgGly^{CONH2}, 6

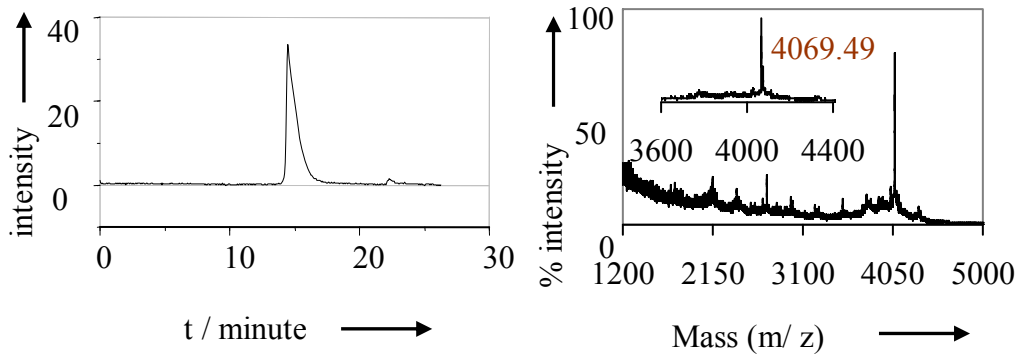

Figure 97: Analytical HPLC ($UV_{\lambda = 260\ nm}$) and MALDI-TOF/MS spectrum of probe **6** (HPLC conditions: gradient A: 0–1 min: 3 %; gradient A; 1–25 min: 3–30 %).

^{AcHN}gccgtg-Aeg (TO) ttagccgGly^{CONH2}, 7

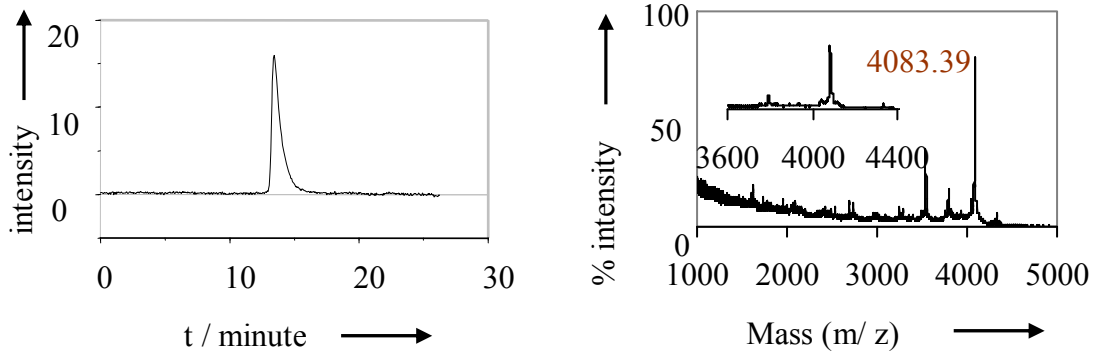

Figure 98: Analytical HPLC ($UV_{\lambda = 260\ nm}$) and MALDI-TOF/MS spectrum of probe **7** (HPLC conditions: gradient A: 0–1 min: 3 %; gradient A; 1–25 min: 3–30 %).

^{AcHN}gccgtc-Aeg (TO)-ttagccgGly^{CONH2}, 8

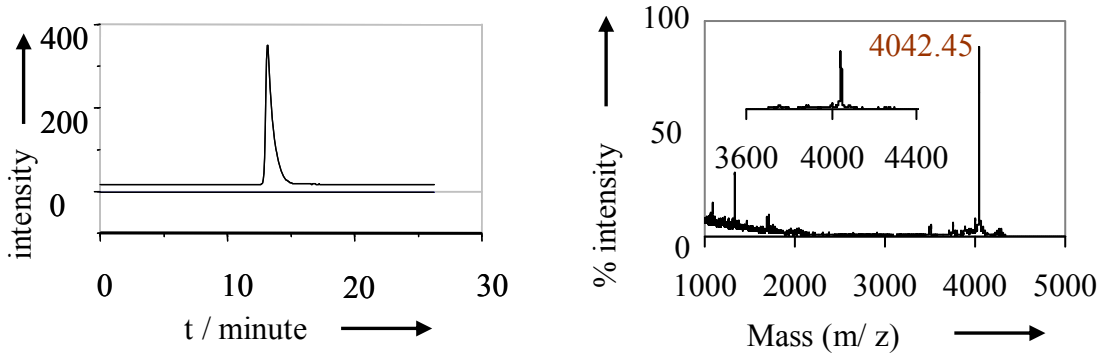

Figure 99: Analytical HPLC ($UV_{\lambda = 260\ nm}$) and MALDI-TOF/MS spectrum of probe **8** (HPLC conditions: gradient A: 0–1 min: 3 %; gradient A; 1–25 min: 3–30 %).

^{AcHN}gccgtt-Aeg (TO)-atagccgGly^{CONH2}, 9

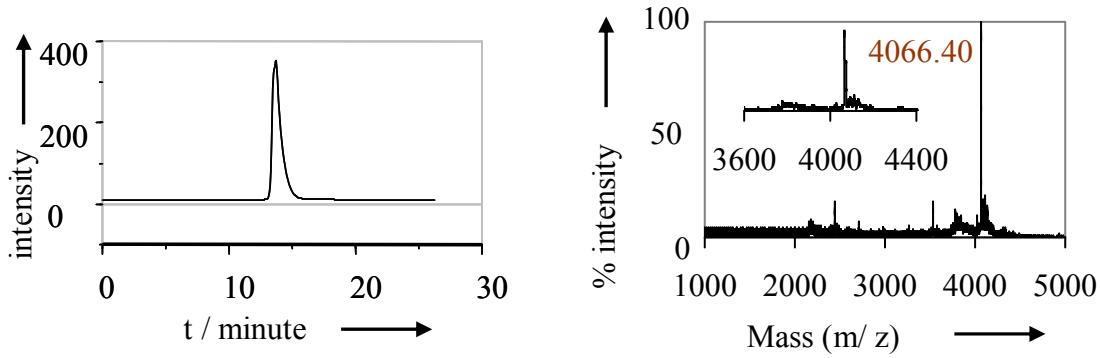

Figure 100: Analytical HPLC ($UV_{\lambda = 260\ nm}$) and MALDI-TOF/MS spectrum of probe **9** (HPLC conditions: gradient A: 0–1 min: 3 %; gradient A; 1–25 min: 3–30 %).

^{AcHN}gccgta-Aeg (TO)-atagccgGly^{CONH2}, 10

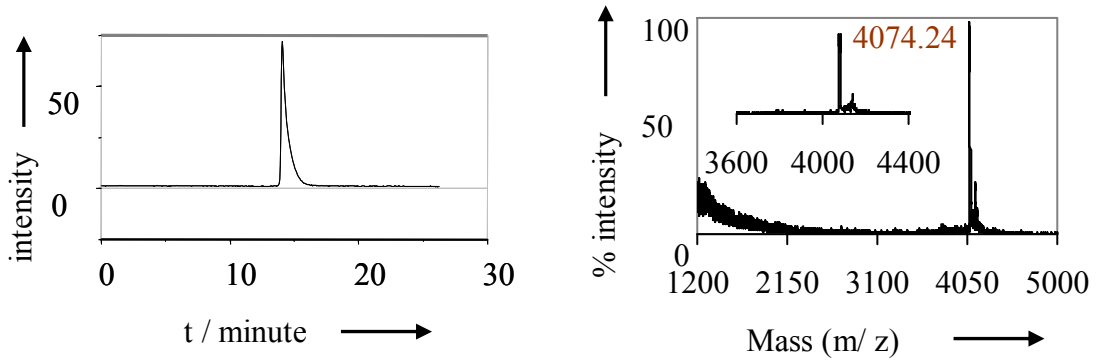

Figure 101: Analytical HPLC ($UV_{\lambda = 260\ nm}$) and MALDI-TOF/MS spectrum of probe **10** (HPLC conditions: gradient A: 0–1 min: 3 %; gradient A; 1–25 min: 3–30 %).

^{AcHN}gccgtg-Aeg (TO)-atagccgGly^{CONH2}, 11

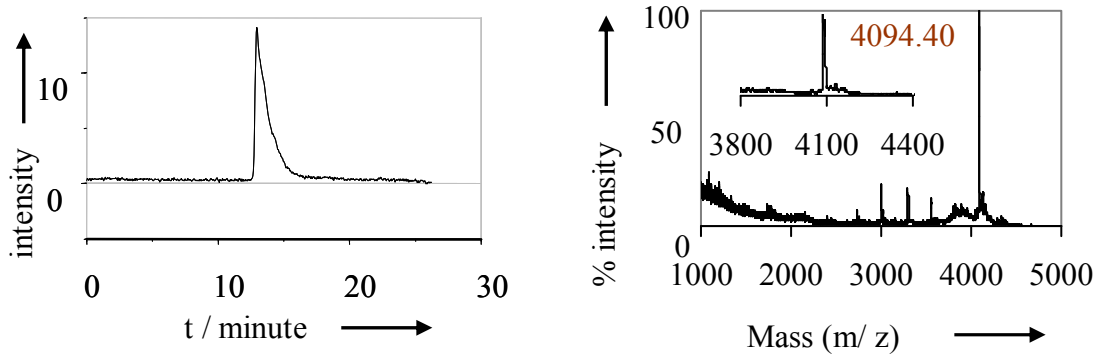

Figure 102: Analytical HPLC ($UV_{\lambda = 260\ nm}$) and MALDI-TOF/MS spectrum of probe **11** (HPLC conditions: gradient A: 0–1 min: 3 %; gradient A; 1–25 min: 3–30 %).

^{AcHN}gccgtc-Aeg (TO)-atagccgGly^{CONH2}, 12

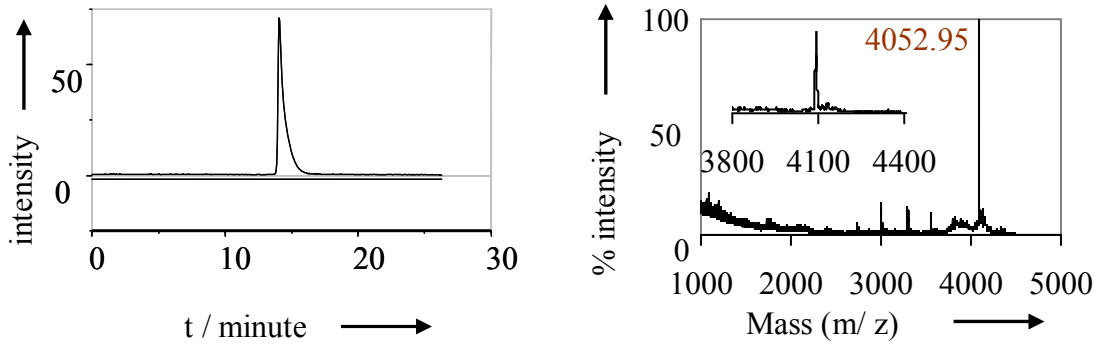

Figure 103: Analytical HPLC ($UV_{\lambda = 260\ nm}$) and MALDI-TOF/MS spectrum of probe **12** (HPLC conditions: gradient A: 0–1 min: 3 %; gradient A; 1–25 min: 3–30 %).

^{AcHN}gccgtt-Aeg (TO)-gtagccgGly^{CONH2}, 13

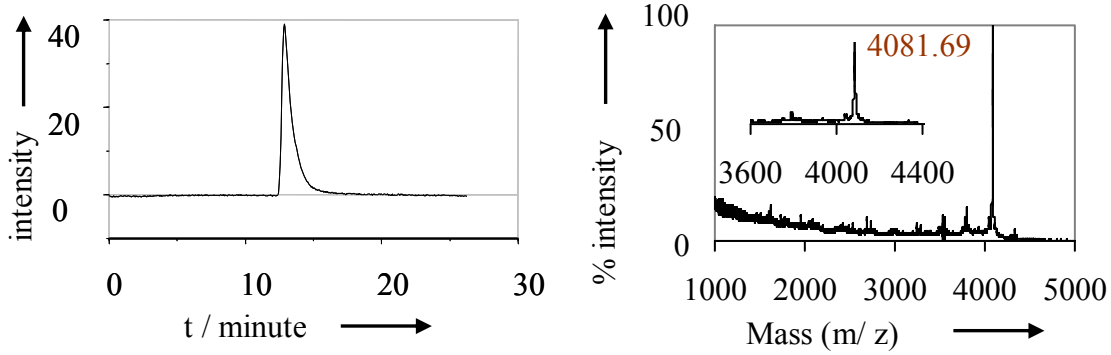

Figure 104: Analytical HPLC ($UV_{\lambda = 260\ nm}$) and MALDI-TOF/MS spectrum of probe **13** (HPLC conditions: gradient A: 0–1 min: 3 %; gradient A; 1–25 min: 3–30 %).

^{AcHN}gccgta-Aeg (TO)-gtagccgGly^{CONH2}, 14

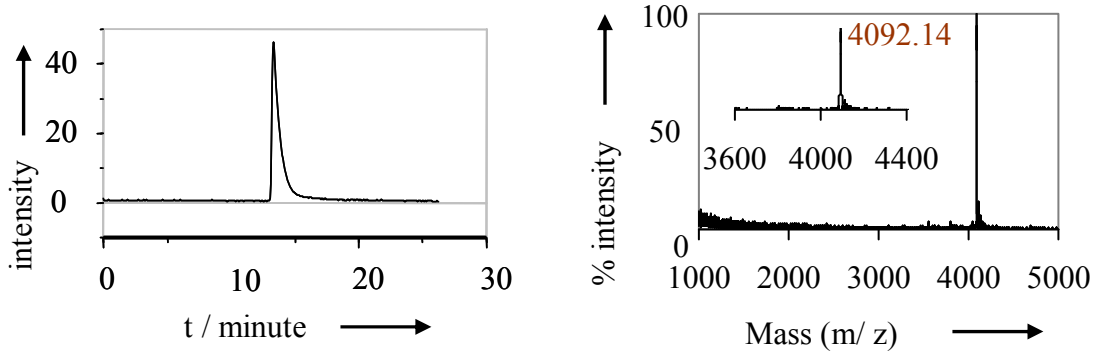

Figure 105: Analytical HPLC ($UV_{\lambda = 260\ nm}$) and MALDI-TOF/MS spectrum of probe **14** (HPLC conditions: gradient A: 0–1 min: 3 %; gradient A; 1–25 min: 3–30 %).

^{AcHN}gccgtg-Aeg (TO)-gtagccgGly^{CONH2}, 15

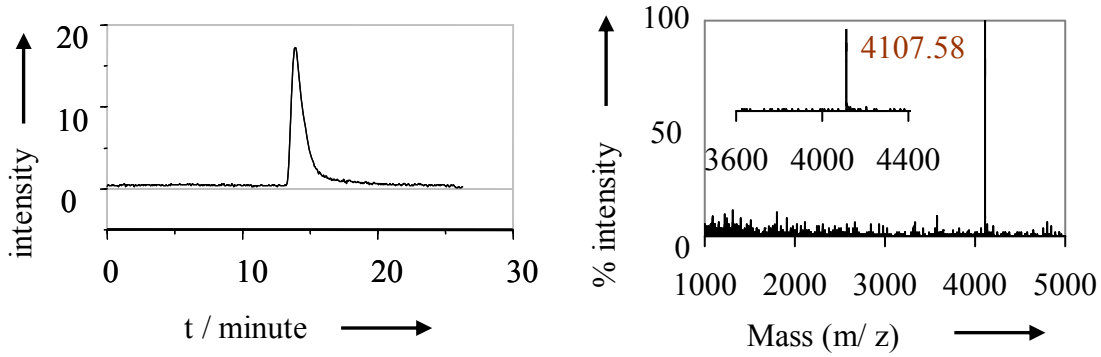

Figure 106: Analytical HPLC ($UV_{\lambda = 260\ nm}$) and MALDI-TOF/MS spectrum of probe **15** (HPLC conditions: gradient A: 0–1 min: 3 %; gradient A; 1–25 min: 3–30 %).

^{AcHN}gccgtc-Aeg (TO)-gtagccgGly^{CONH2}, 16

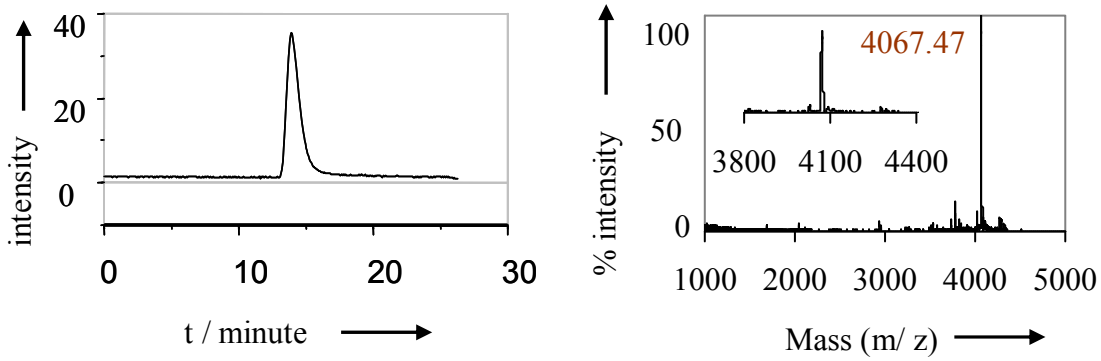

Figure 107: Analytical HPLC ($UV_{\lambda = 260\ nm}$) and MALDI-TOF/MS spectrum of probe **16** (HPLC conditions: gradient A: 0–1 min: 3 %; gradient A; 1–25 min: 3–30 %).

^{AcHN}gccgtt-Aeg (TO)-ctagccgGly^{CONH2}, 17

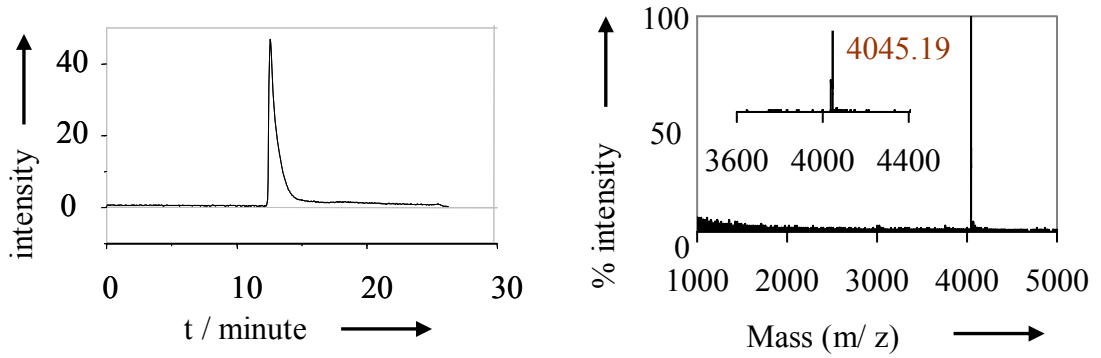

Figure 108: Analytical HPLC ($UV_{\lambda = 260\ nm}$) and MALDI-TOF/MS spectrum of probe **17** (HPLC conditions: gradient A: 0–1 min: 3 %; gradient A; 1–25 min: 3–30 %).

^{AcHN}gccgta-Aeg (TO)-ctagccgGly^{CONH2}, 18

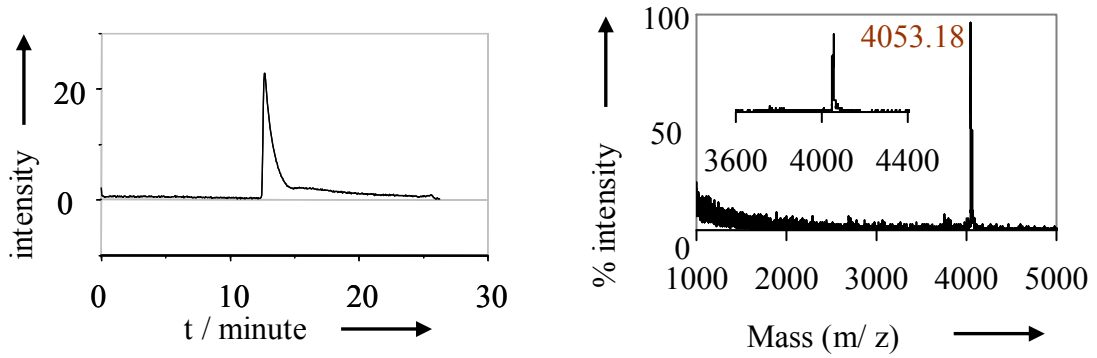

Figure 109: Analytical HPLC ($UV_{\lambda = 260\ nm}$) and MALDI-TOF/MS spectrum of probe **18** (HPLC conditions: gradient A: 0–1 min: 3 %; gradient A; 1–25 min: 3–30 %).

^{AcHN}gccgtg-Aeg (TO)-ctagccgGly^{CONH2}, 19

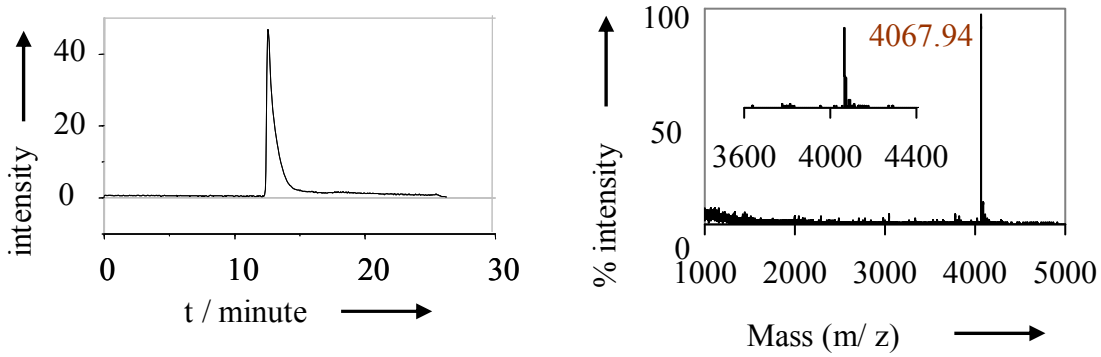

Figure 110: Analytical HPLC ($UV_{\lambda = 260\ nm}$) and MALDI-TOF/MS spectrum of probe **19** (HPLC conditions: gradient A: 0–1 min: 3 %; gradient A; 1–25 min: 3–30 %).

^{AcHN}gccgtc-Aeg (TO)-ctagccgGly^{CONH2}, 20

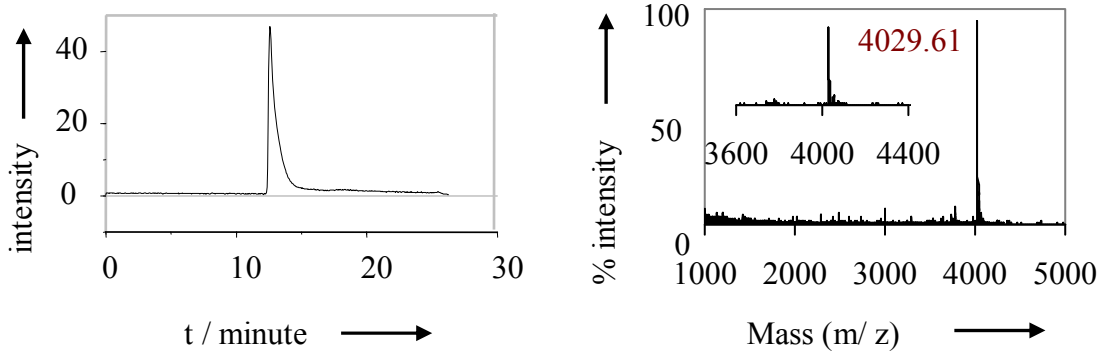

Figure 111: Analytical HPLC ($UV_{\lambda = 260\ nm}$) and MALDI-TOF/MS spectrum of probe **20** (HPLC conditions: gradient A: 0–1 min: 3 %; gradient A; 1–25 min: 3–30 %).

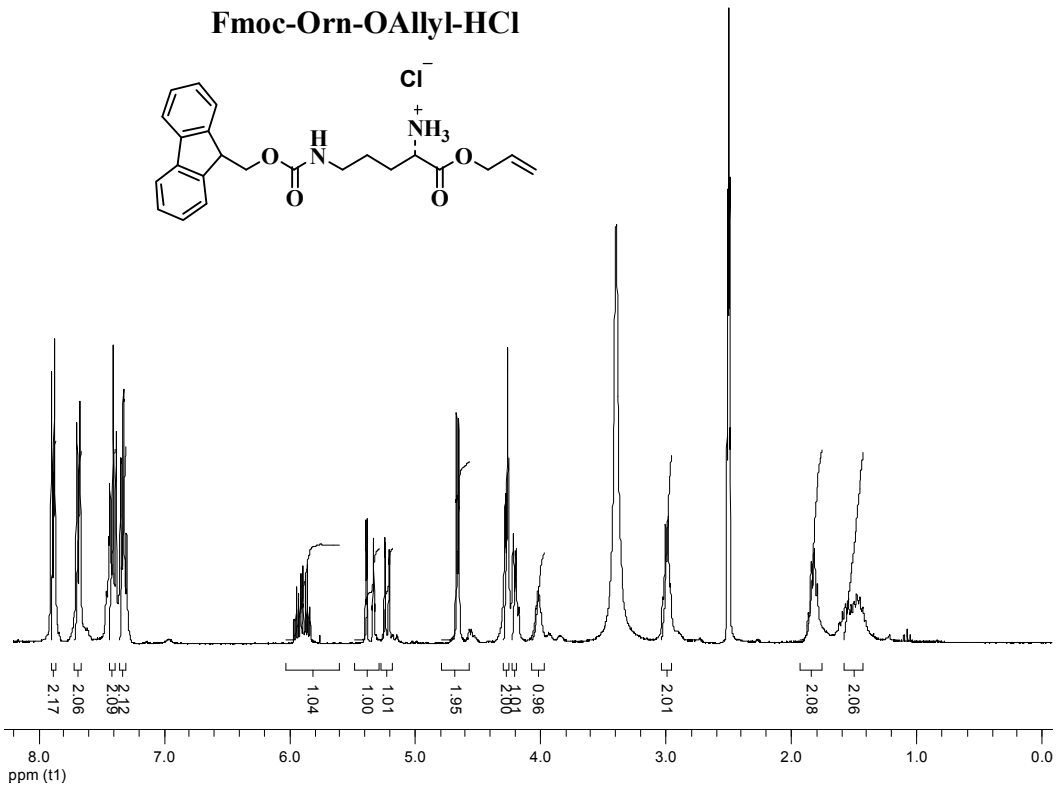

Spectra 5: ^{1}H-NMR of Fmoc-Orn-O-Allyl•HCl

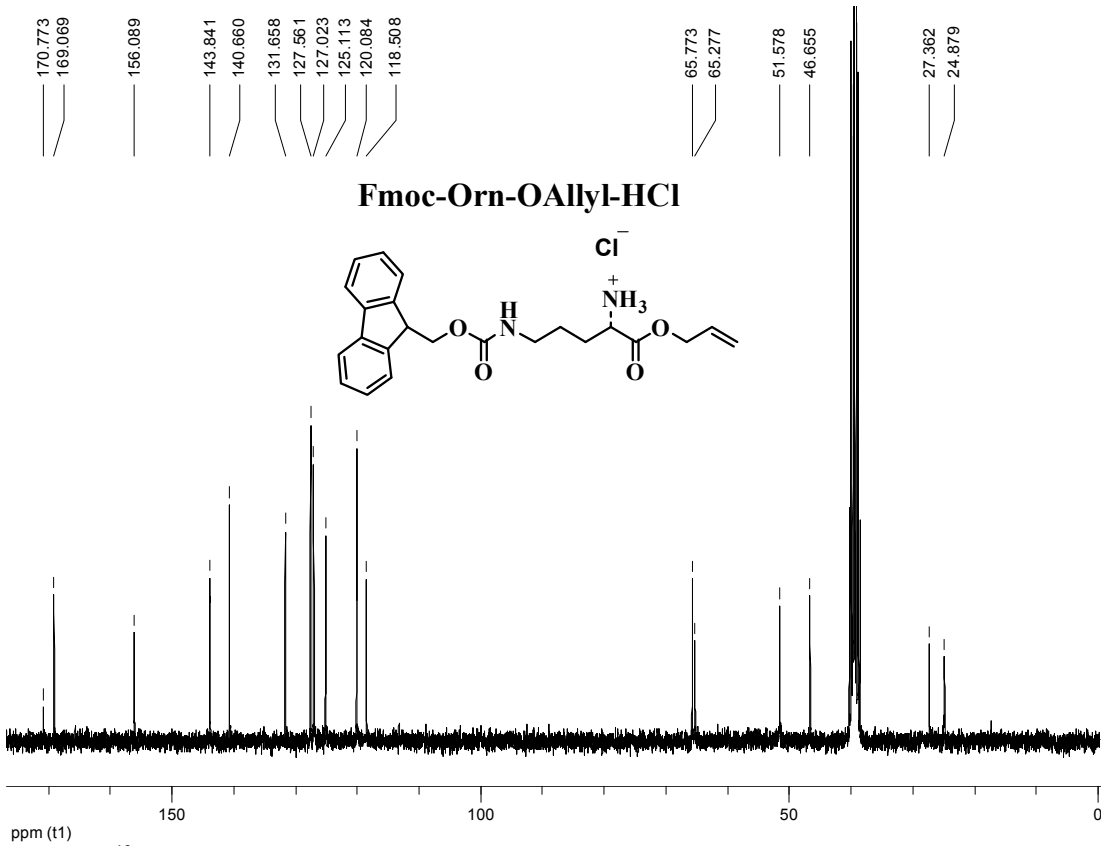

Spectra 6: ^{13}C-NMR of Fmoc-Orn-O-Allyl•HCl

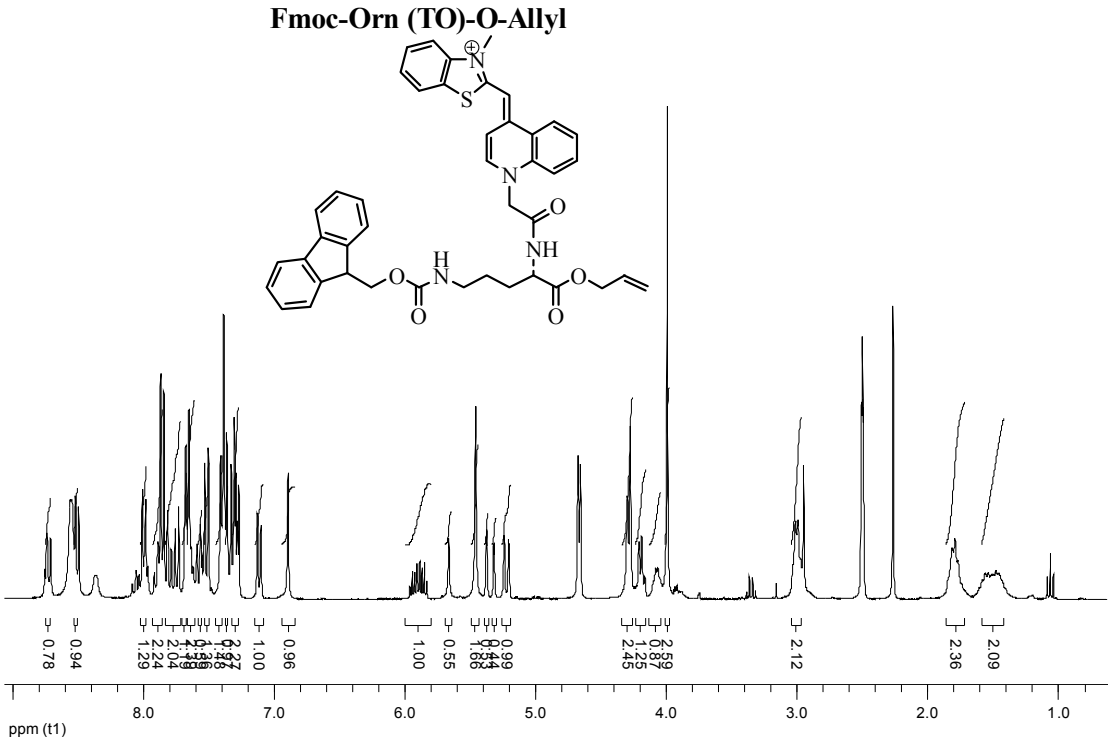

Spectra 7: ^{1}H-NMR of Fmoc-Orn (TO)-O-Allyl

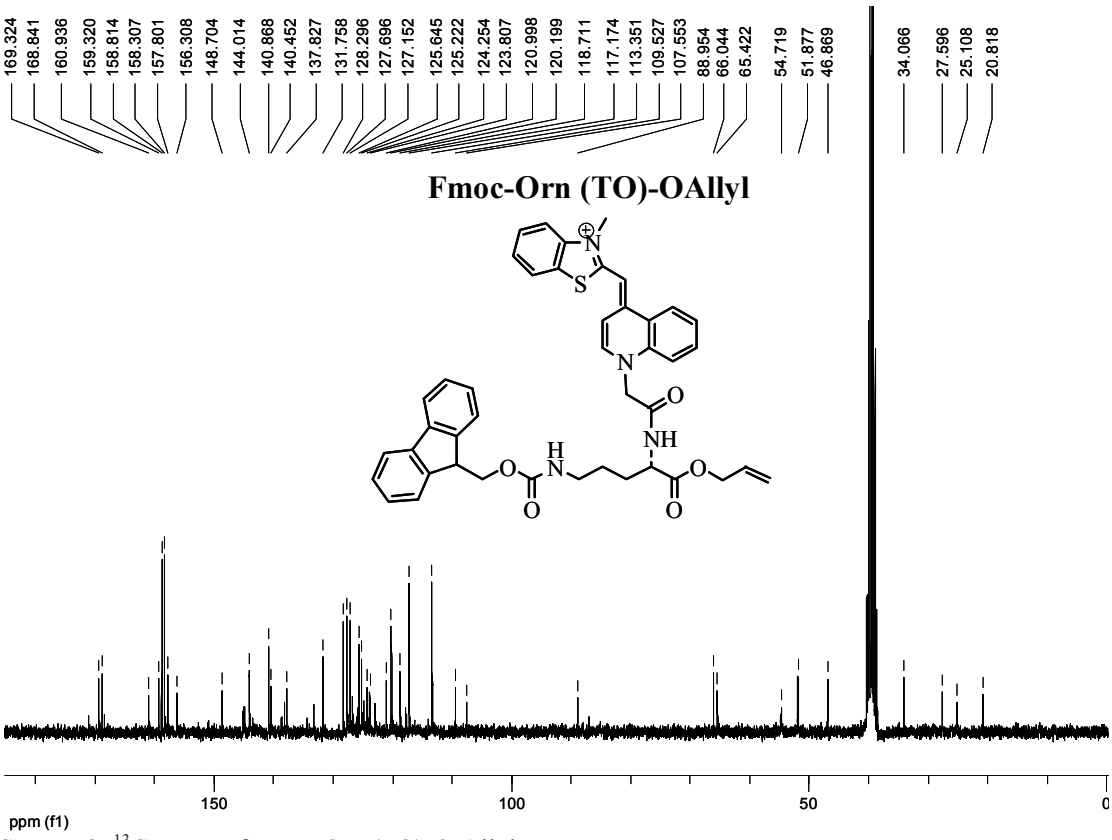

Spectra 8: ^{13}C-NMR of Fmoc-Orn (TO)-O-Allyl

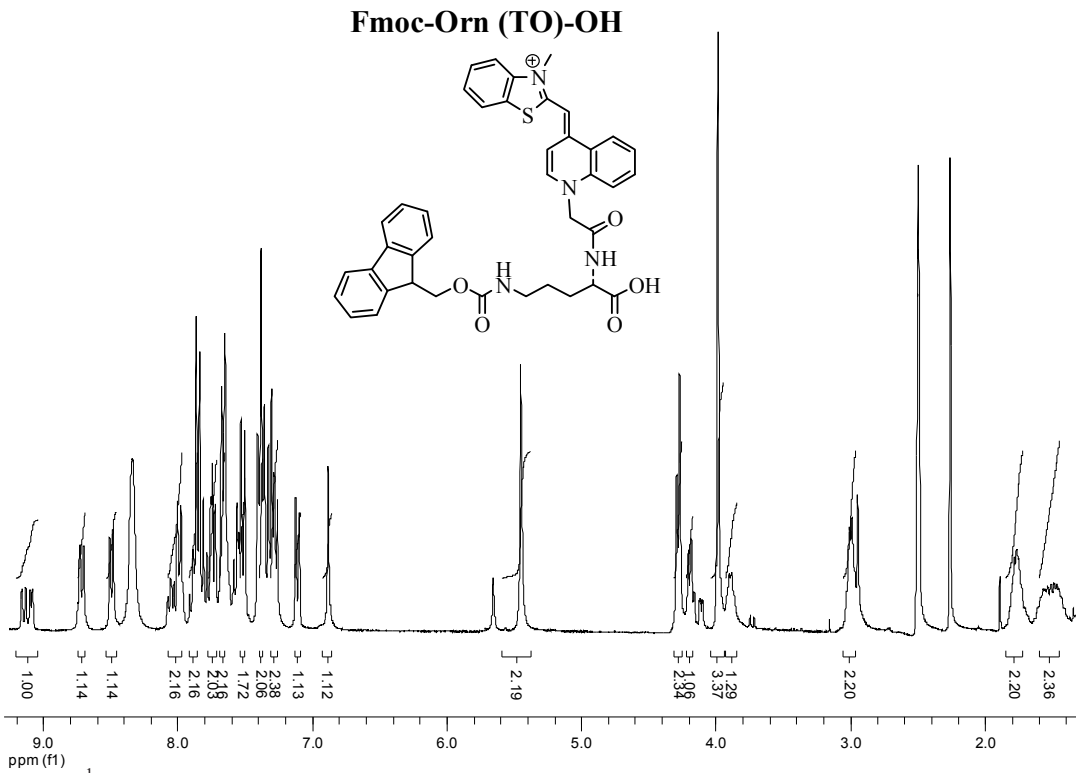

Spectra 9: ^{1}H-NMR of Fmoc-Orn (TO)-OH

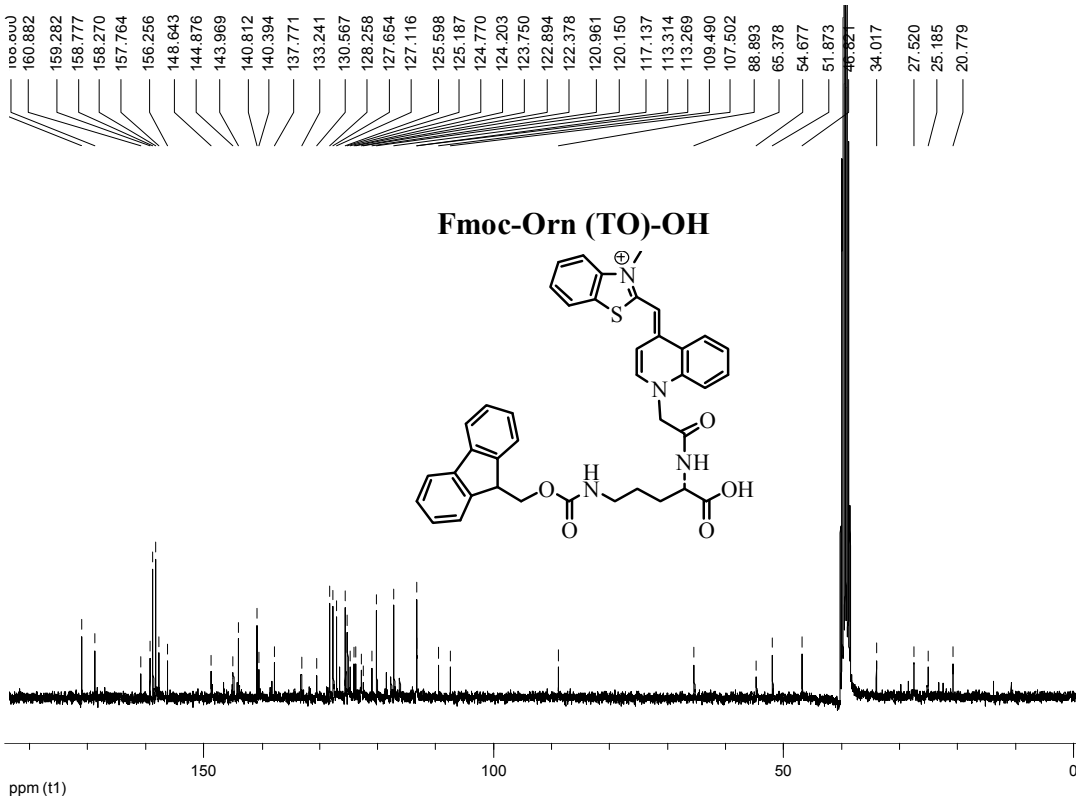

Spectra 10: ^{13}C-NMR of Fmoc-Orn (TO)-OH.

^{AcHN}gccgtt-D-Orn (TO)-ttagccgGly^{CONH2}, 25

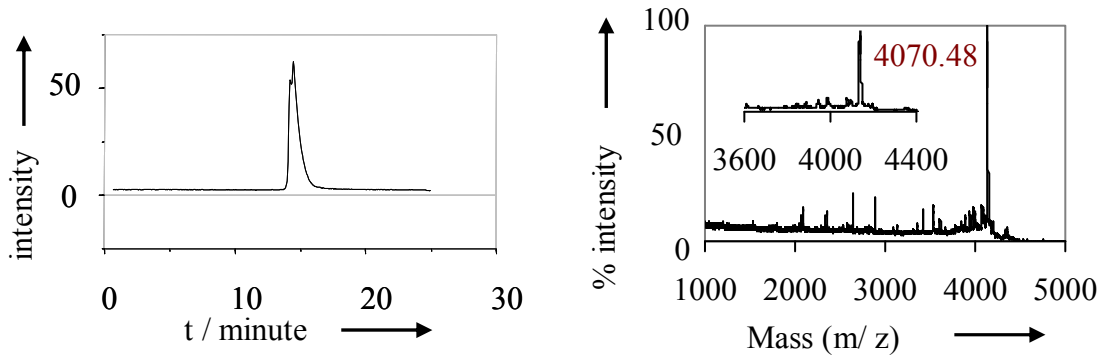

Figure 112: Analytical HPLC ($UV_{\lambda = 260\ nm}$) and MALDI-TOF/MS spectrum of probe **25** (HPLC conditions: gradient A: 0–1 min: 3 %; gradient A; 1–25 min: 3–30 %).

^{AcHN}gccgta-D-Orn (TO)-ttagccgGly^{CONH2}, 26

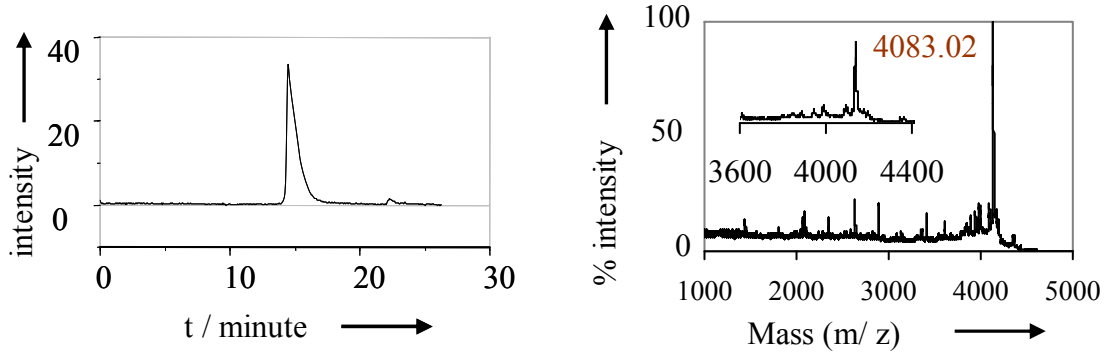

Figure 113: Analytical HPLC ($UV_{\lambda = 260\ nm}$) and MALDI-TOF/MS spectrum of probe **26** (HPLC conditions: gradient A: 0–1 min: 3 %; gradient A; 1–25 min: 3–30 %).

^{AcHN}gccgtg-D-Orn (TO)-ttagccgGly^{CONH2}, 27

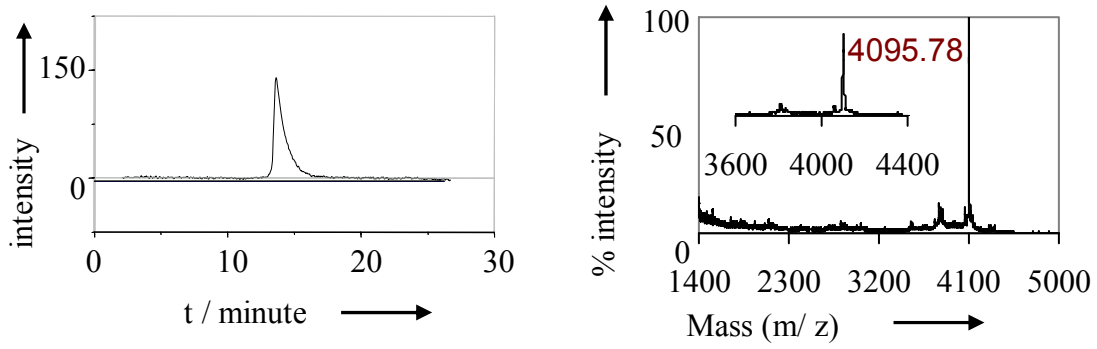

Figure 114: Analytical HPLC ($UV_{\lambda = 260\ nm}$) and MALDI-TOF/MS spectrum of probe **27** (HPLC conditions: gradient A: 0–1 min: 3 %; gradient A; 1–25 min: 3–30 %).

^{AcHN}gccgtc-D-Orn (TO)-ttagccgGly^{CONH2}, 28

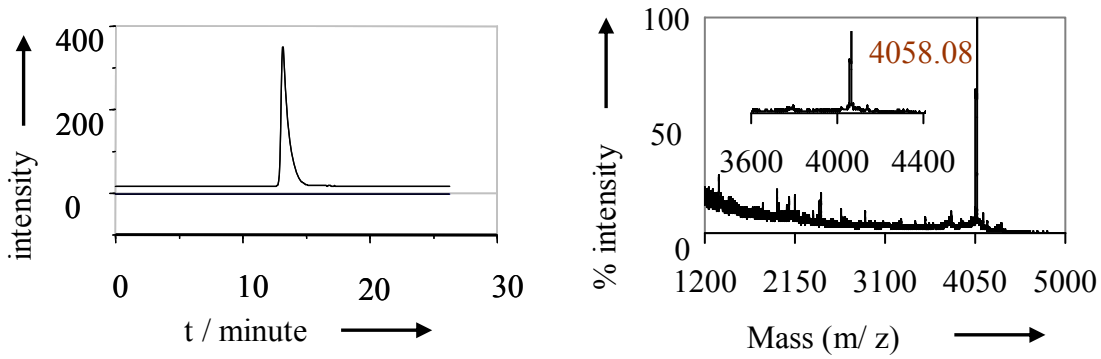

Figure 115: Analytical HPLC ($UV_{\lambda = 260\ nm}$) and MALDI-TOF/MS spectrum of probe **28** (HPLC conditions: gradient A: 0–1 min: 3 %; gradient A; 1–25 min: 3–30 %).

^{AcHN}gccgtt-D-Orn (TO)-atagccgGly^{CONH2}, 29

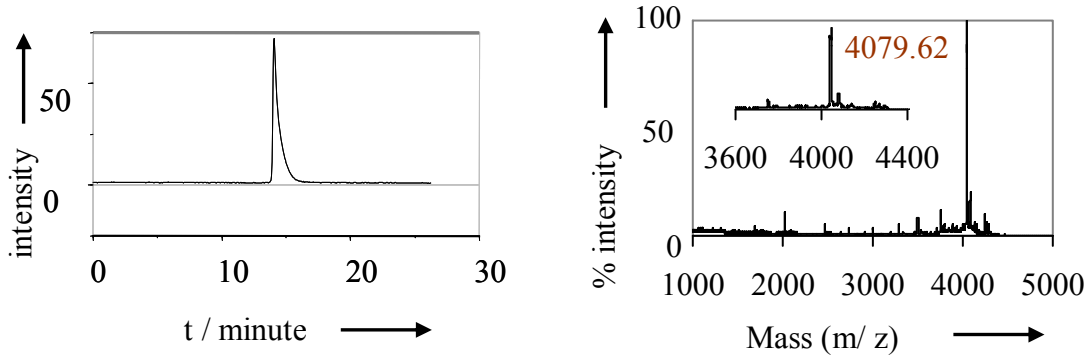

Figure 116: Analytical HPLC ($UV_{\lambda = 260\ nm}$) and MALDI-TOF/MS spectrum of probe **29** (HPLC conditions: gradient A: 0–1 min: 3 %; gradient A; 1–25 min: 3–30 %).

^{AcHN}gccgta-D-Orn (TO)-atagccgGly^{CONH2}, 30

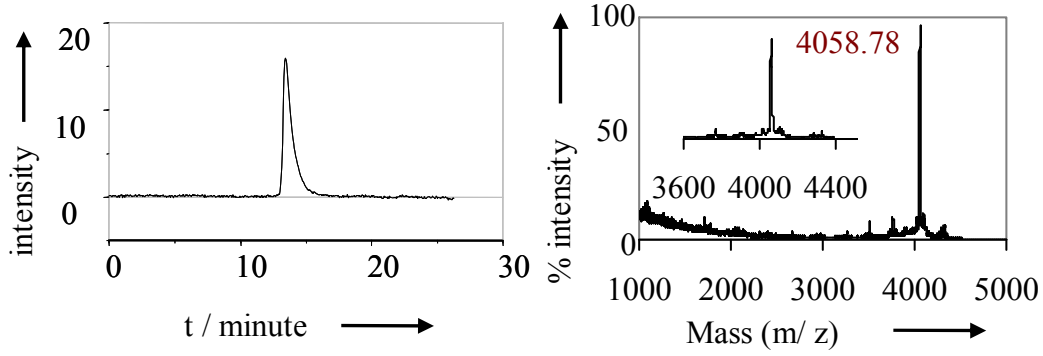

Figure 117: Analytical HPLC ($UV_{\lambda = 260\ nm}$) and MALDI-TOF/MS spectrum of probe **30** (HPLC conditions: gradient A: 0–1 min: 3 %; gradient A; 1–25 min: 3–30 %).

^{AcHN}gccgtg-D-Orn (TO)-atagccgGly^{CONH2}, 31

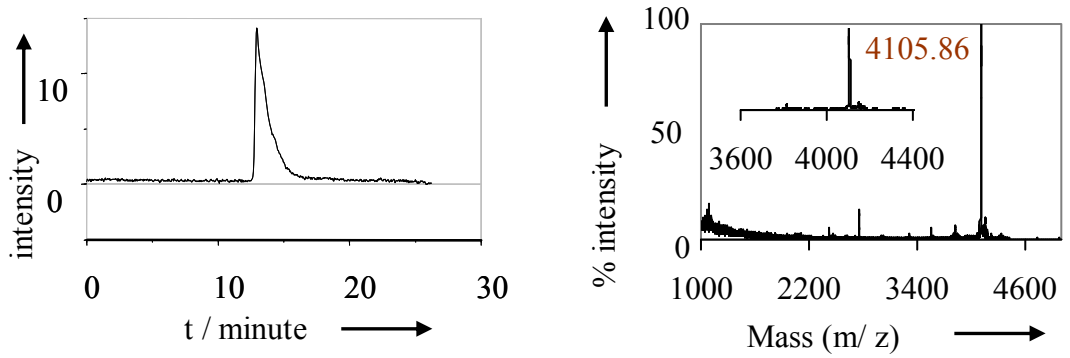

Figure 118: Analytical HPLC ($UV_{\lambda = 260\ nm}$) and MALDI-TOF/MS spectrum of probe **31** (HPLC conditions: gradient A: 0–1 min: 3 %; gradient A; 1–25 min: 3–30 %).

^{AcHN}gccgtc-D-Orn (TO)-atagccgGly^{CONH2}, 32

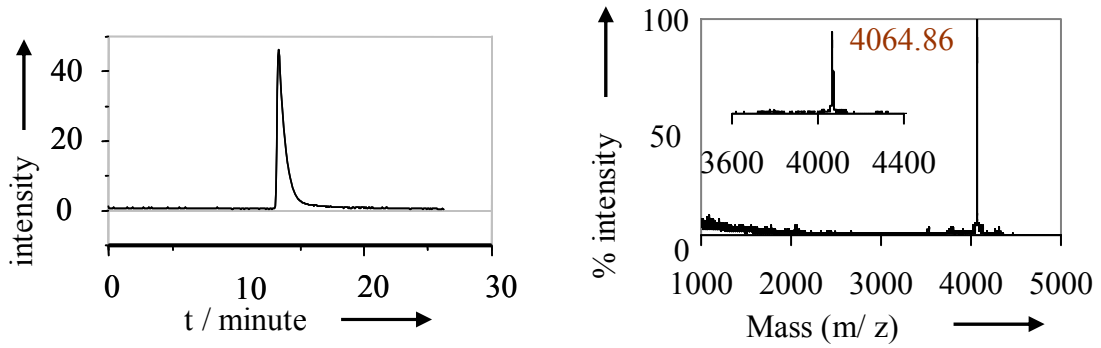

Figure 119: Analytical HPLC ($UV_{\lambda = 260\ nm}$) and MALDI-TOF/MS spectrum of probe **32** (HPLC conditions: gradient A: 0–1 min: 3 %; gradient A; 1–25 min: 3–30 %).

^{AcHN}gccgtt-D-Orn (TO)-gtagccgGly^{CONH2}, 33

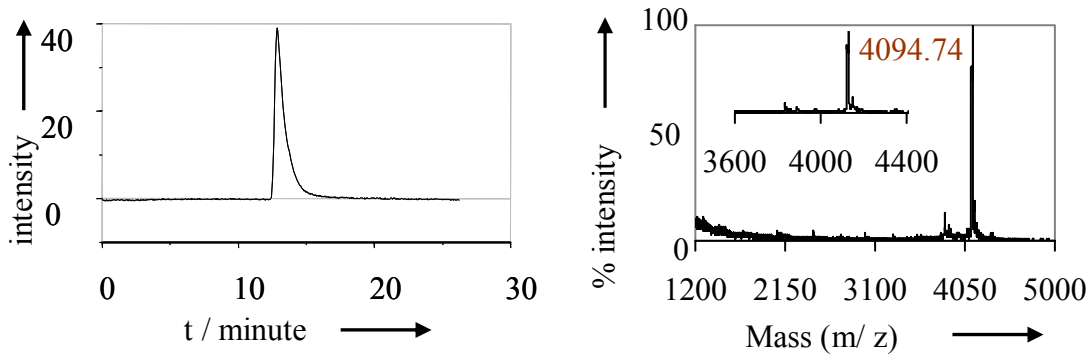

Figure 120: Analytical HPLC ($UV_{\lambda = 260\ nm}$) and MALDI-TOF/MS spectrum of probe **33** (HPLC conditions: gradient A: 0–1 min: 3 %; gradient A; 1–25 min: 3–30 %).

^{AcHN}gccgta-D-Orn (TO)-gtagccgGly^{CONH2}, 34

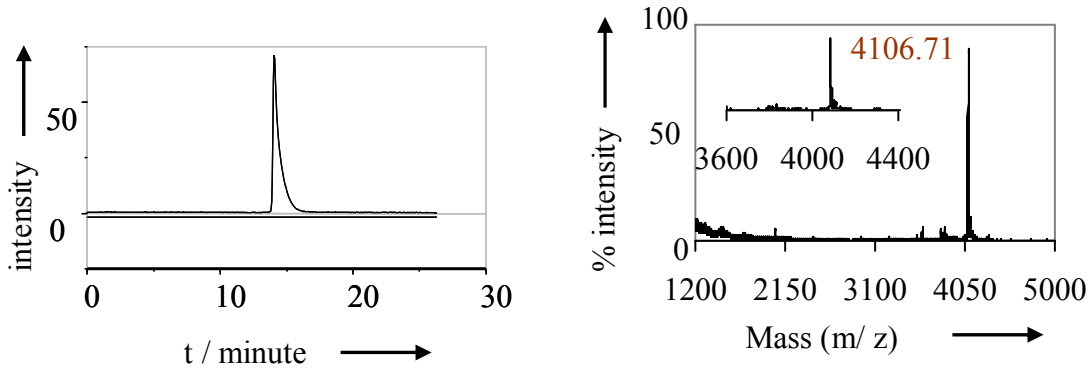

Figure 121: Analytical HPLC ($UV_{\lambda = 260\ nm}$) and MALDI-TOF/MS spectrum of probe **34** (HPLC conditions: gradient A: 0–1 min: 3 %; gradient A; 1–25 min: 3–30 %).

^{AcHN}gccgtg-D-Orn (TO)-gtagccgGly^{CONH2}, 35

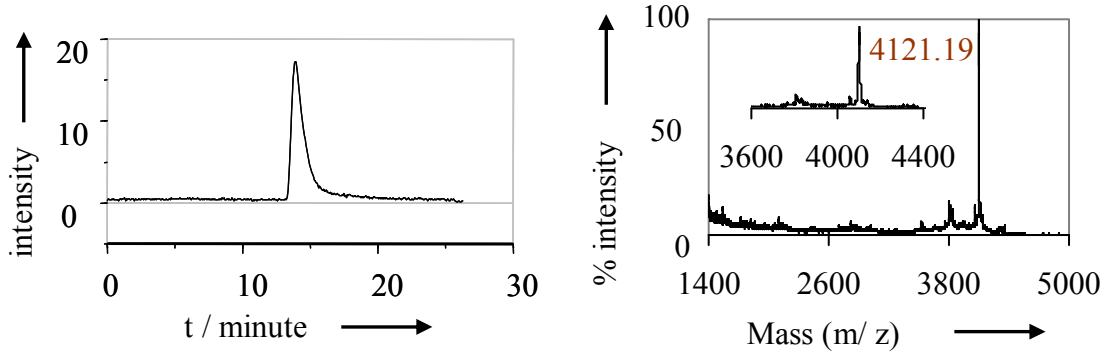

Figure 122: Analytical HPLC ($UV_{\lambda = 260\ nm}$) and MALDI-TOF/MS spectrum of probe **35** (HPLC conditions: gradient A: 0–1 min: 3 %; gradient A; 1–25 min: 3–30 %).

^{AcHN}gccgtc-D-Orn (TO)-gtagccgGly^{CONH2}, 36

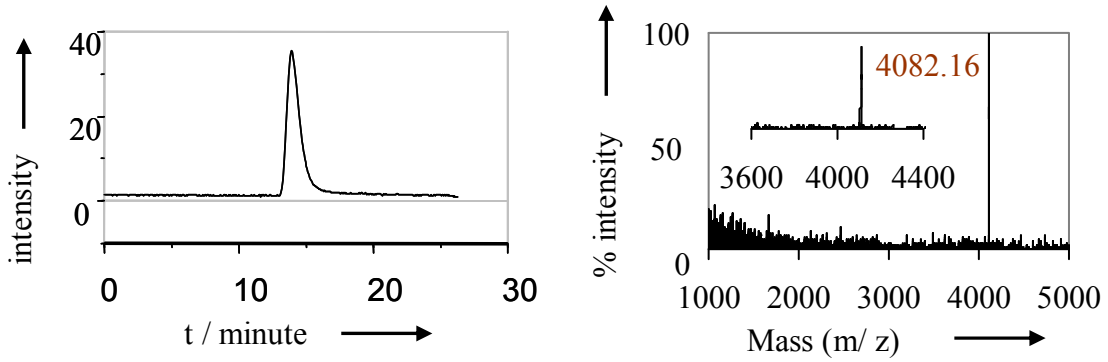

Figure 123: Analytical HPLC ($UV_{\lambda = 260\ nm}$) and MALDI-TOF/MS spectrum of probe **36** (HPLC conditions: gradient A: 0–1 min: 3 %; gradient A; 1–25 min: 3–30 %).

^{AcHN}gccgtt-D-Orn (TO)-ctagccgGly^{CONH2}, 37

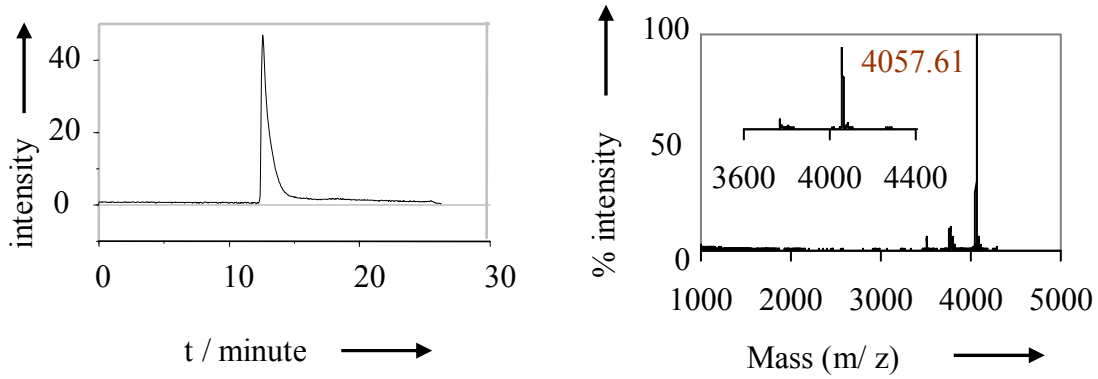

Figure 124: Analytical HPLC ($UV_{\lambda = 260\ nm}$) and MALDI-TOF/MS spectrum of probe **37** (HPLC conditions: gradient A: 0–1 min: 3 %; gradient A; 1–25 min: 3–30 %).

^{AcHN}gccgta-D-Orn (TO)-ctagccgGly^{CONH2}, 38

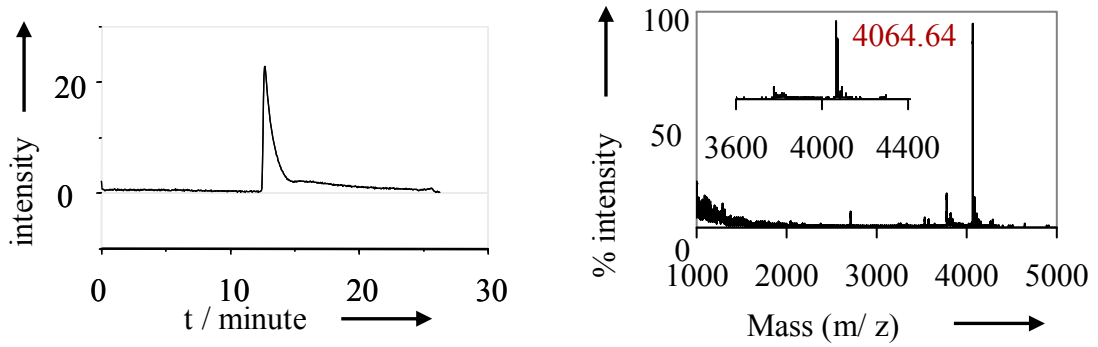

Figure 125: Analytical HPLC ($UV_{\lambda = 260\ nm}$) and MALDI-TOF/MS spectrum of probe **38** (HPLC conditions: gradient A: 0–1 min: 3 %; gradient A; 1–25 min: 3–30 %).

^{AcHN}gccgtg-D-Orn (TO)-ctagccgGly^{CONH2}, 39

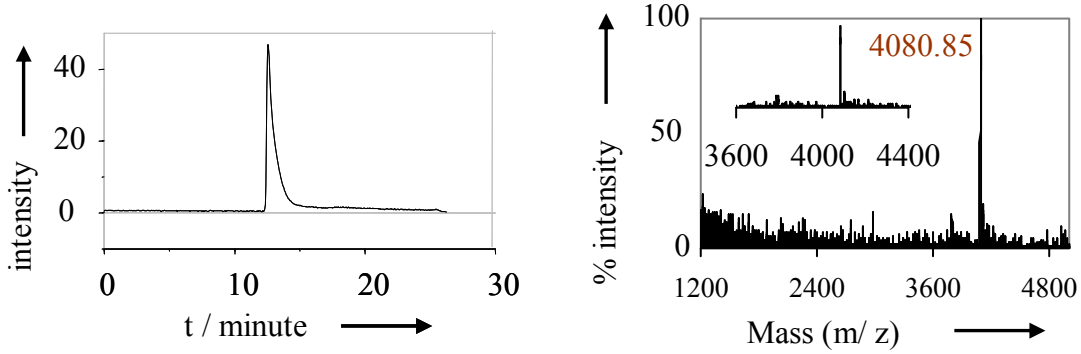

Figure 126: Analytical HPLC ($UV_{\lambda = 260\ nm}$) and MALDI-TOF/MS spectrum of probe **39** (HPLC conditions: gradient A: 0–1 min: 3 %; gradient A; 1–25 min: 3–30 %).

^{AcHN}gccgtc-D-Orn (TO)-ctagccgGly^{CONH2}, 40

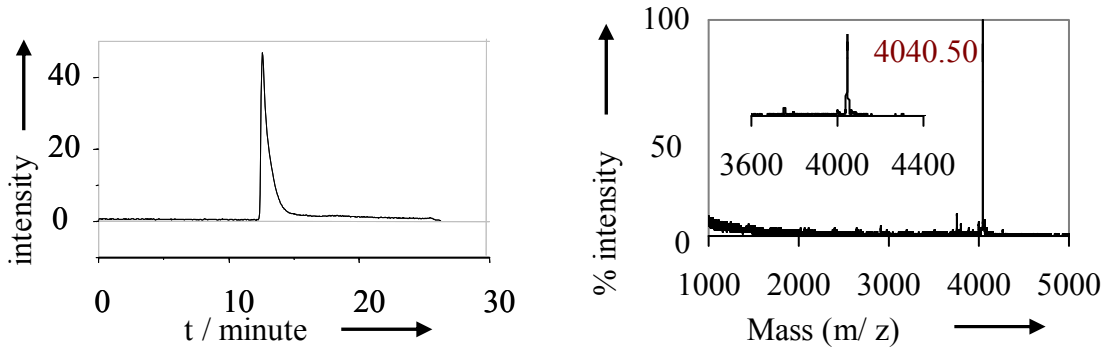

Figure 127: Analytical HPLC ($UV_{\lambda = 260\ nm}$) and MALDI-TOF/MS spectrum of probe **40** (HPLC conditions: gradient A: 0–1 min: 3 %; gradient A; 1–25 min: 3–30 %).

^{AcHN}gccgta-Aeg (TO)-hagccgGly^{CONH2}, 41

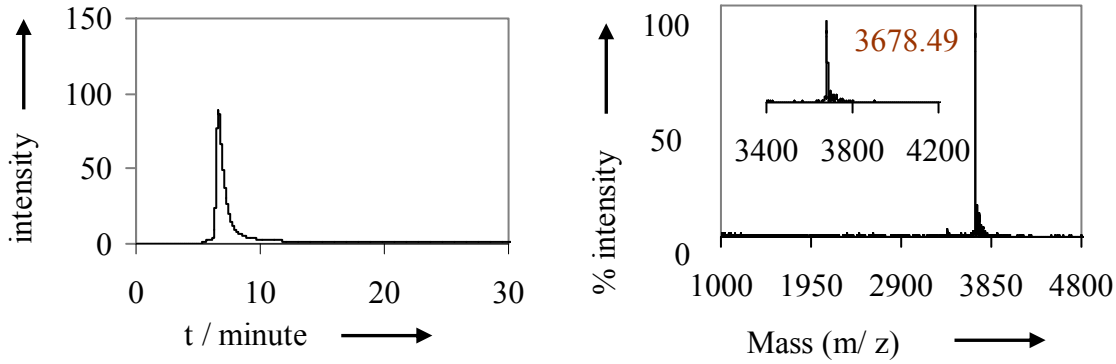

Figure 128: Analytical HPLC ($UV_{\lambda = 260\ nm}$) and MALDI-TOF/MS spectrum of probe **41** (HPLC conditions: gradient A: 0–1 min: 3 %; gradient A; 1–20 min: 3–30 %).

TO-$(CH_2)_5$-CONH-$(CH_2)_5$-gccgtaaatagccgGly^{CONH2}, 42

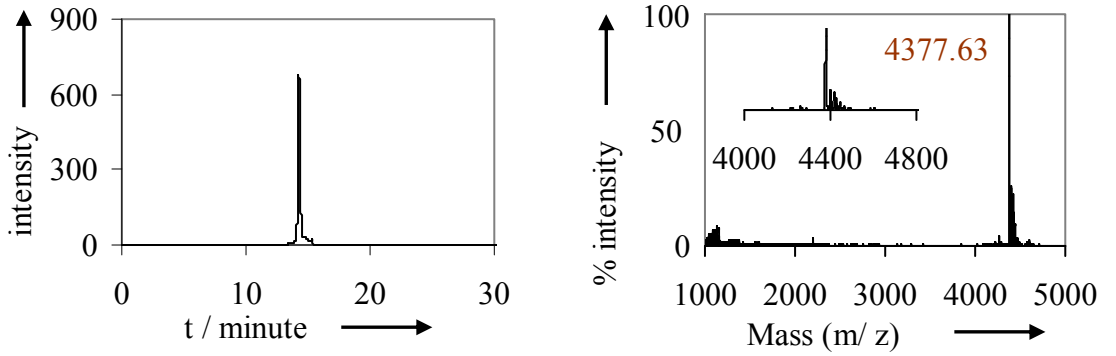

Figure 129: Analytical HPLC ($UV_{\lambda = 260\ nm}$) and MALDI-TOF/MS spectrum of probe **42** (HPLC conditions: gradient A: 0–1 min: 3 %; gradient A; 1–20 min: 3–30 %).

TO-$(CH_2)_5$-CONH-$(CH_2)_5$-gccgta-Aeg (TO)-atagccgGly^{CONH2}, 43

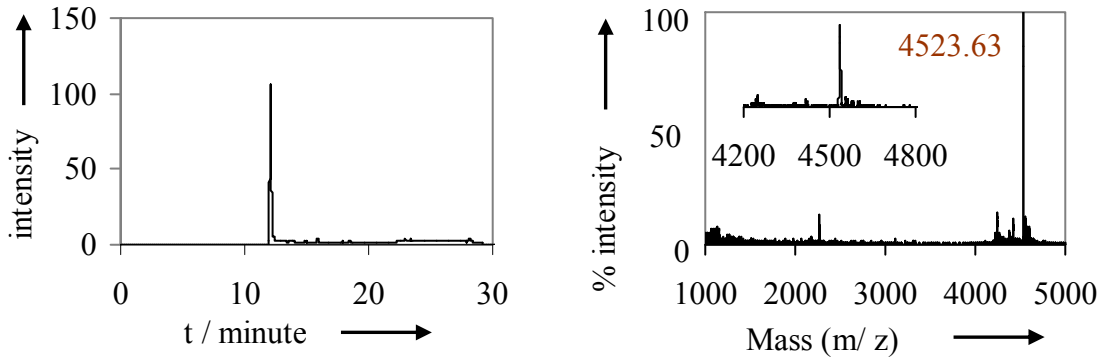

Figure 130: Analytical HPLC ($UV_{\lambda = 260\ nm}$) and MALDI-TOF/MS spectrum of probe **43** (HPLC conditions: gradient A: 0–1 min: 3 %; gradient A; 1–20 min: 3–30 %).

TO-$(CH_2)_5$-$(CH_2)_5$-acaccgccggcGly^{CONH2} 44

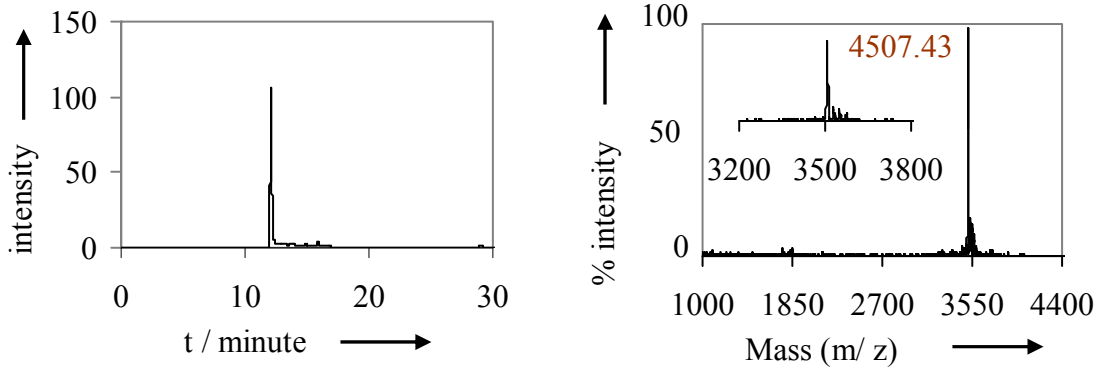

Figure 131: Analytical HPLC ($UV_{\lambda = 260\ nm}$) and MALDI-TOF/MS spectrum of probe **44** (HPLC conditions: gradient A: 0–1 min: 3 %; gradient A; 1–20 min: 3–30 %).

^{ACHN}acacc-Aeg (TO)-ccggcGly^{CONH2}, 45

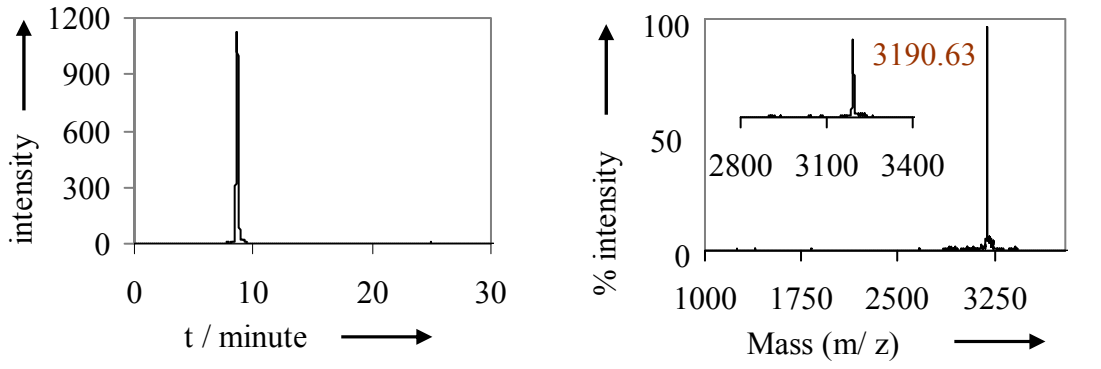

Figure 132: Analytical HPLC ($UV_{\lambda = 260\ nm}$) and MALDI-TOF/MS spectrum of probe **45** (HPLC conditions: gradient A: 0–1 min: 3 %; gradient A; 1–20 min: 3–30 %).

^{AcHN}gccgt-Aeg (TO)-a-Aeg (TO)-tagccgGly^{CONH2}, 48

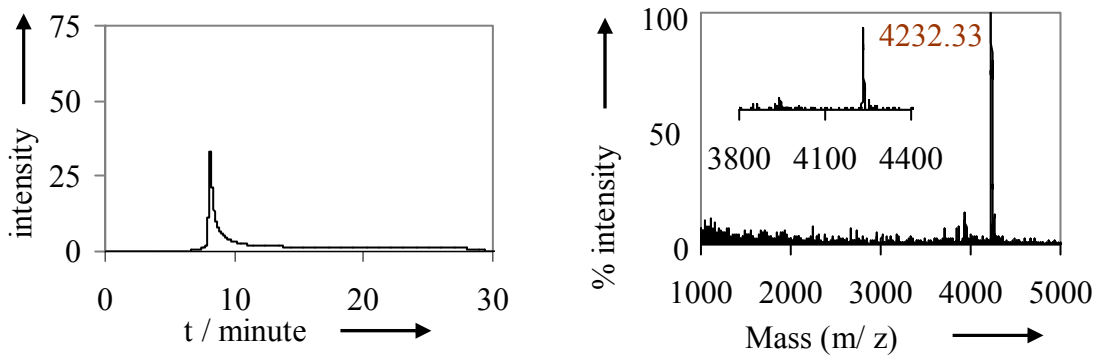

Figure 133: Analytical HPLC ($UV_{\lambda = 260\ nm}$) and MALDI-TOF/MS spectrum of probe **48** (HPLC conditions: gradient A: 0–1 min: 3 %; gradient A; 1–20 min: 3–30 %).

^{AcHN}gccgta-Aeg (BO)-atagccgGly^{CONH2}, 49

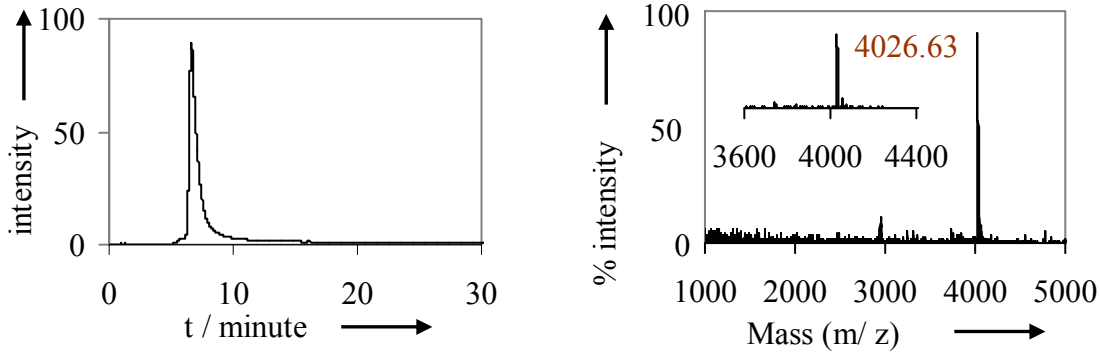

Figure 134: Analytical HPLC ($UV_{\lambda = 260\ nm}$) and MALDI-TOF/MS spectrum of probe **49** (HPLC conditions: gradient A: 0–1 min: 3 %; gradient A; 1–20 min: 3–30 %).

^{ACHN}ttcgtat-Aeg (TO)-acatttcLys^{CONH2,} 50

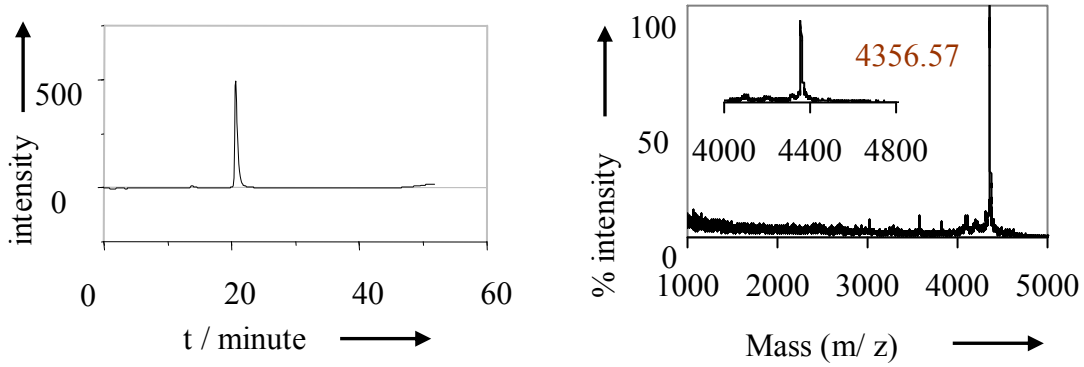

Figure 135: Analytical HPLC ($UV_{\lambda = 260\ nm}$) and MALDI-TOF/MS spectrum of probe **51** (HPLC conditions: gradient A: 0–1 min: 3 %; gradient A; 1–25 min: 3–30 %).

^{ACHN}ttcgtat-L-Orn (TO)-acatttcLys^{CONH2,} 51

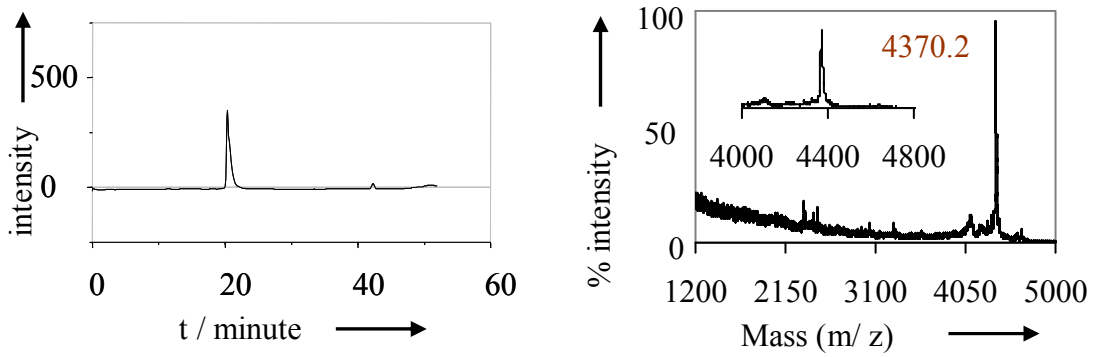

Figure 136: Analytical HPLC ($UV_{\lambda = 260\ nm}$) and MALDI-TOF/MS spectrum of probe **52** (HPLC conditions: gradient A: 0–1 min: 3 %; gradient A; 1–25 min: 3–30 %).

^{ACHN}ttcgtat-D-Orn (TO)-acatttcLys^{CONH2,} 52

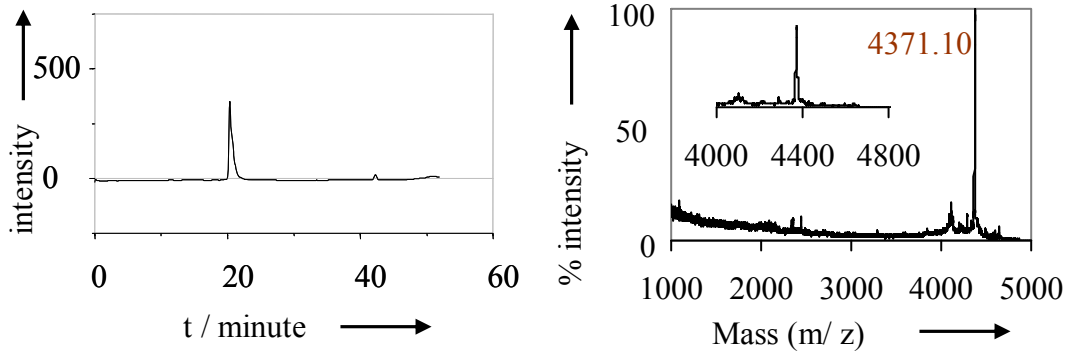

Figure 137: Analytical HPLC ($UV_{\lambda = 260\ nm}$) and MALDI-TOF/MS spectrum of probe **53** (HPLC conditions: gradient A: 0–1 min: 3 %; gradient A; 1–25 min: 3–30 %).

^{ACHN}aacacc-Aeg (TO)-atttacLys^{CONH2,} 53

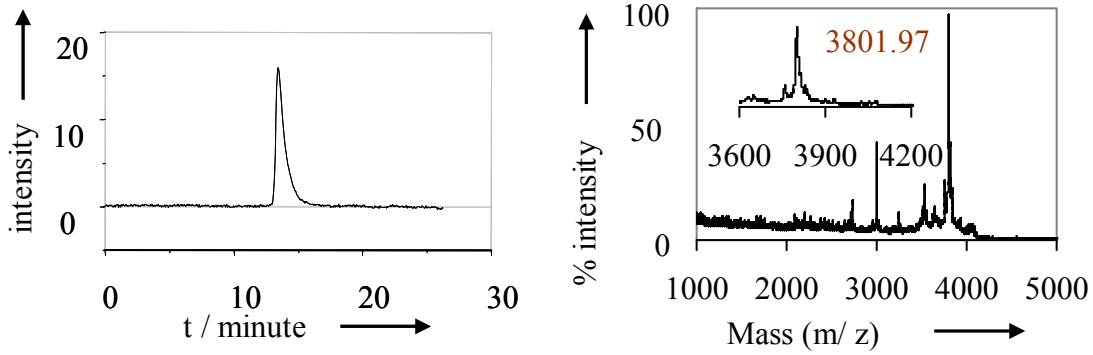

Figure 138: Analytical HPLC ($UV_{\lambda = 260\ nm}$) and MALDI-TOF/MS spectrum of probe **54** (HPLC conditions: gradient A: 0–1 min: 3 %; gradient A; 1–25 min: 3–30 %).

^{ACHN}aacacc-L-Orn (TO)-atttacLys^{CONH2,} 54

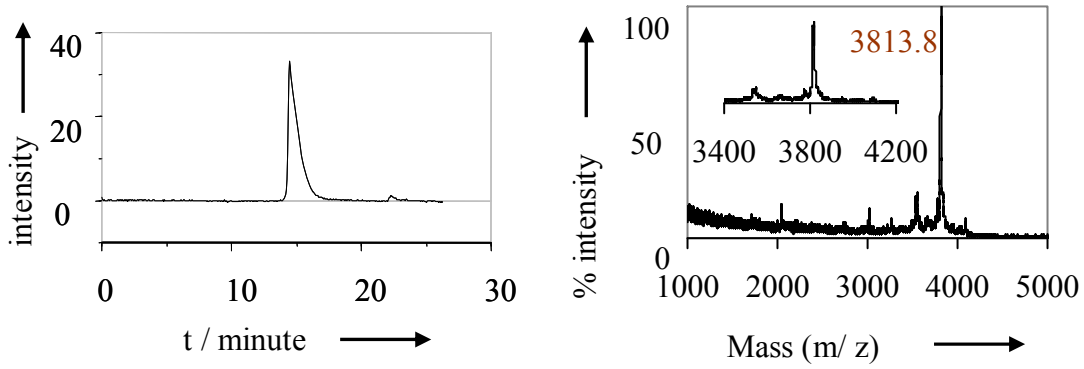

Figure 139: Analytical HPLC ($UV_{\lambda = 260\ nm}$) and MALDI-TOF/MS spectrum of probe **55** (HPLC conditions: gradient A: 0–1 min: 3 %; gradient A; 1–25 min: 3–30 %).

^{ACHN}aacacc-D-Orn (TO)-atttacLys^{CONH2,} 55

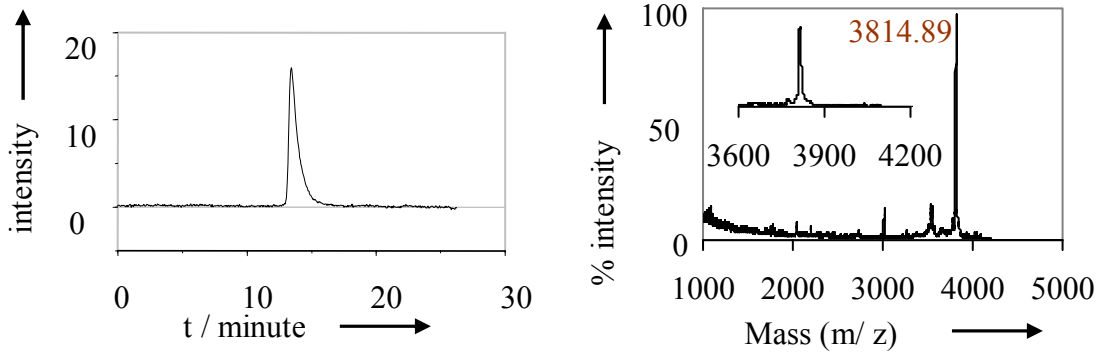

Figure 140: Analytical HPLC ($UV_{\lambda = 260\ nm}$) and MALDI-TOF/MS spectrum of probe **56** (HPLC conditions: gradient A: 0–1 min: 3 %; gradient A; 1–25 min: 3–30 %).

Acknowledgements

The work towards this thesis was carried out during the period of December 2002-May 2003 in the Max Planks Institute of Molecular Biology, Dortmund, Germany and June 2003-May 2006 in the Department of Chemistry, Humboldt University Berlin, Germany.

First of all I would like to thank Prof. Dr. Oliver Seitz for giving opportunity to work with him, his continuous scientific advice and financial support. His experience and knowledge has helped me to understand the aspects of bioorganic-chemistry and helped me to overcome lot of obstacles that appeared in the course of the work.

I would like to specially thank Dr. Andrea Knoll and Elke Socher for corrections and suggestions for this thesis, useful discussion and helping me all time during the work. Special thanks to Dr. Olaf Köhler, Dr. Simon Ficht, Dr. Christian Dose and Lars Röglin for being available whenever I needed their help and keeping laboratory environment always alive. I am very much thankful to Sabine Heinz for helping me in all administrative work and becoming translator (German to English) for me.

I thank to Prof. Beate Röder, Nils Krebs and Sebastian Tannert (Institute for Physics, Humboldt-University zu Berlin) for fruitful collaboration. I wish to acknowledge Brigitte Redlich for synthesis of PNA on synthesiser, Simon, Christian for HPLC, Lars Röglin for all computer related work, Franziska Mende for chemical ordering, Dr. Andera Knoll for translating English 'summary' to german 'zusammenfassung' and Lucas Bethge for useful discussion. Thanks to Dr. Ishwar Singh and Brian Davies for useful discussions. I gratefully thank all the members of the group of Prof. Seitz and Prof. Arenz for their help in different ways during the course of this work.

My sincere thank to Dr. U. R. Kalkote, Dr. S. R. Bhusare, Dr. K. V. Srinivasan, Dr. R. J. Lahoti, Dr. W. N. Jadhav and Dr. R. P. Pawar for encouragement, understanding and suggestions whenever I needed. I wish to thank the many friends and former colleagues who have helped in one way or other, especially Sharad, Shapi, Nilesh, Dr. Rajkumar, Dr. Rajgopal, Dr. Ravindra, Dr. Atul, Amit, Vijay, Sunil, and many in and out of NCL (National Chemical Laboratory, Pune, India) who are not named in person, for their valuable friendship and helping hand.

I cannot end without thanking my parents, my brother and his family members for their love and support relied through out my time in Germany.

Hiermit versichere ich, Dilip Venkatrao Jarikote, die vorliegende Dissertation selbstständig erarbeitet und verfasst zu haben. Es wurden keine weiteren Quellen und Hilfsmittel als die hier angegebenen verwendet.

.....

Unterschrift